Planktonic foraminifera transfer function approach to Red Sea paleoceanography

Dissertation

zur Erlangung des Grades eines Doktors der Naturwissenschaften

der Geowissenschaftlichen Fakultät
der Eberhard Karls Universität Tübingen

Vorgelegt von
Michael Georg Siccha Rojas
aus Rio de Janeiro

2009

Tag der mündlichen Prüfung: 15.10.2009

Dekan: Prof. Dr. Peter Grathwohl

1. Berichterstatter: Prof. Dr. Michal Kucera

2. Berichterstatter: Prof. Dr. Gerhard Schmiedl

Abstract

This study examines the potential of using the assemblage composition of planktonic foraminifera in the Red Sea as a quantitative proxy for paleoclimate reconstructions. To this end, a new surface sediment sample dataset was generated to evaluate the environmental control on foraminifera assemblages and to serve as the calibration dataset for the subsequent development of planktonic foraminifera transfer functions. Gradient analysis was employed to investigate the effect of temperature, salinity, primary productivity, water column stratification and the properties of the oxygen minimum zone on the foraminifera fauna of the Red Sea. Because of the high mutual correlation among all environmental parameters along the basin axis, no unambiguous identification of the controlling parameter could be achieved by statistical analyses of the calibration dataset alone. A comparison with published studies on the ecology of planktonic foraminifera, however, lead to the working hypothesis that primary productivity determines the distinct gradient in the foraminifera community in the Red Sea. Transfer functions were then generated by four mathematical methods to characterise the relationship between foraminifera assemblages and chlorophyll *a* concentration as a proxy for productivity. The transfer functions appear highly efficient in capturing the modern productivity gradient in the Red Sea, with an average root mean squared error of prediction of 0.124 mg/m³, corresponding to 10.3 % of the observed gradient. The working hypothesis was then tested and on two newly generated Holocene faunal records from the central and northern Red Sea. Apart from the impact of sea level on the hydrography of the Red Sea, these records showed a strong influence of the dominant regional climatic system, the Indian monsoon. The reconstructed chlorophyll *a* concentrations indicate low productivity for the early Holocene, which can be ascribed to lowered sea level and a strong SW monsoon. An earlier postglacial recovery of the fauna in the northern Red Sea than in the central Red Sea time is explained by a local additional freshwater source. During the Mid-Holocene, environmental conditions in the Red Sea shifted gradually towards higher productivity, reaching a maximum between 3.5 and 2 ka BP. This distinct event can be explained by a strengthened NE monsoon and generally higher aridity, leading to dominant winter circulation mode in the basin. After 2 ka BP, the modern circulation and climatic conditions became established. The developed transfer functions were also applied on existing Red Sea faunal records covering several glacial and interglacial periods. While non-analogue conditions to present day for fauna and environment were to be expected during the glacials, it became apparent that also for large intervals of interglacial periods, the analogy of the fauna and/or the analogy of the relationship between the fauna and the environment was not given. As a consequence, the applicability of the developed transfer functions is limited to portions of the interglacial intervals with high and stable sea level and atmospheric forcing similar to that during the Holocene.

Zusammenfassung

Diese Studie untersucht das Potenzial der Vergesellschaftung planktonischer Foraminiferen im Roten Meer als Proxy für quantitative Paläoklimarekonstruktionen. Zu diesem Zweck wurde ein neuer Sedimentoberflächendatensatz erstellt, der sowohl der Evaluierung der die Foraminiferen kontrollierenden Umweltparameter als auch später der Kalibration der auf planktonischen Foraminiferen basierenden Transfer-Funktionen dienen sollte. Gradientenanalyse wurde verwandt um die Auswirkungen von Temperatur, Salzgehalt, Primärproduktion, Stratifizierung der Wassersäule und den Eigenschaften der Sauerstoff-Minimum-Zone auf die Foraminiferenfauna des Roten Meeres zu untersuchen. Aufgrund der hohen Korrelation von allen Umweltparametern entlang der Beckenachse war keine eindeutige Identifizierung des kontrollierenden Parameters allein durch statistische Analysen des Kalibrationsdatensatzes möglich. Ein Vergleich mit veröffentlichten Studien über die Ökologie planktonischer Foraminiferen führte jedoch zu der Arbeitshypothese, dass die Primärproduktion die ausgeprägte Zonierung der planktonischen Foraminiferenfauna im Roten Meer bestimmt. Mittels vier verschiedener mathematischer Methoden wurden daraufhin Transfer-Funktionen entwickelt um die Beziehung zwischen Foraminiferengemeinschaften und der Chlorophyll *a*-Konzentration, als Indikator für Primärproduktion, zu charakterisieren. Die Transfer-Funktionen erwiesen sich als höchst effizient in der Erfassung der modernen Produktivitätsverteilung im Roten Meer; der effektive Vorhersagefehler liegt bei 0,124 mg/m³, was 10,3 % des beobachteten Gradienten entspricht. Die Arbeitshypothese wurde an zwei neu erstellten Faunendatensätzen für das Holozän aus dem zentralen und nördlichen Roten Meer getestet. Neben den Auswirkungen von Meeresspiegelveränderungen auf die Hydrographie des Roten Meeres zeigten diese Archive einen starken Einfluss des vorherrschenden regionalen Klimasystems, des indischen Monsun. Die rekonstruierten Chlorophyll *a* Konzentrationen für das frühe Holozän deuten auf eine niedrige Produktivität hin, die dem abgesenkten Meeresspiegel und einem starken SW Monsun zugeschrieben werden kann. Eine im Norden früher als im zentralen Roten Meer einsetzende postglaziale Erholung der Fauna erklärt sich durch einen lokalen zusätzlichen Frischwassereintrag. Im mittleren Holozän verändern sich die Umweltbedingungen im Roten Meer schrittweise in Richtung höherer Produktivität, bis hin zu einem Produktivitätsmaximum zwischen 3,5 und 2 Tausend Jahren vor Heute. Dieses ausgeprägte Maximum lässt sich durch einen verstärkten Winterzirkulationsmodus im Becken erklären, hervorgerufen durch einen verstärkten NO Monsun und generell höhere Trockenheit in der Region. Seit 2 Tausend Jahren vor Heute, haben sich das moderne Zirkulationssystem und heutige klimatische Bedingungen etabliert. Die entwickelten Transfer-Funktionen wurden auch auf bereits publizierte Faunendatensätze aus dem Roten Meer, die mehrere Eis-und Warmzeiten überspannen, angewandt. Während nicht-analoge Bedingungen zu Heute für Eiszeiten erwartet wurden, ist weiterhin deutlich geworden, dass auch für große Zeiträume innerhalb von Warmzeiten, die Analogie der Fauna und/oder die Analogie der Fauna-Umwelt-Beziehung zu Heute nicht bestand. In Folge dessen, beschränkt sich die Anwendbarkeit der entwickelten Transfer-Funktionen auf Zeitabschnitte mit hohem und stabilem Meerspiegel und atmosphärischen Bedingungen, ähnlich denen des Holozäns.

Table of contents

1. Introduction

The Red Sea can undoubtedly be regarded as an exceptional ocean basin. For example, its complex and unique circulation system has been investigated by numerous oceanographers [e.g. Neumann and McGill 1962; Cember 1988; Quadfasel and Baudner 1993; Eshel et al. 1994; Smeed 1997; Tragou and Garrett 1997; Sofianos and Johns 2002; Sofianos and Johns 2003; Manasrah et al. 2004; Biton et al. 2008], but despite their intense efforts it is until now not fully understood in all details. Due to its unique geographic and topographic setting the Red Sea is even more interesting to paleoceanographers. Located within an arid climate belt between Africa and Asia the Red Sea and its circulation system are sensitive to changes in main climate regimes affecting the region. The limited exchange of water with the open ocean [Siddall et al. 2004] causes an almost unparalleled amplification of paleoclimatic and sea-level signals in the sediment archives of the Red Sea. As a consequence of the large eustatic changes in sea level on glacial/interglacial timescales, dramatic changes in water chemistry as recorded by geochemical proxies [Thunell et al. 1988; Rohling 1994] as well as the composition of microfossil assemblages have been observed in records from the Red Sea [e.g. Reiss et al. 1980; Almogi-Labin 1982; Winter 1982; Almogi-Labin et al. 1986; Locke and Thunell 1988; Hemleben et al. 1996; Fenton 1998; Fenton et al. 2000; Badawi et al. 2005; Legge et al. 2006].

At times of stable sea level, the microfossil assemblages of the Red Sea can be expected to reflect environmental forcing driven by the regional climate systems. Indeed, a strong gradient along the basin axis in the recent distribution of planktonic foraminifera [Auras-Schudnagies et al. 1989] as well as distinct variations in their assemblage composition during the Holocene have been observed [e.g. Halicz and Reiss 1981; Locke and Thunell 1988; Edelman 1996; Schmelzer 1998]. Until now, however, the mechanism generating these distribution patterns has remained elusive. The analysis of the distribution of recent planktonic foraminifera with the aim to identify the forcing environmental factors was thus the primary motivation for this study. A detailed understanding of the factors controlling the distribution of modern foraminifera could then be used to alleviate the lack of quantitative paleoenvironmental reconstructions from the Red Sea; a consequence of the difficulties to use and interpret most standard geo- or biochemical proxies in this basin. Unlike the chemistry of their calcite shells, the species composition of microfossil assemblages remains unaffected by anomalous conditions of water chemistry and can by the use of transfer functions be turned into quantitative paleoenvironmental reconstructions. This work presents the first planktonic foraminifera transfer function approach for paleoclimate reconstructions in the Red Sea based on a taxonomically consistent calibration dataset from the Red Sea itself, analysed with advanced statistical methods and considering an array of environmental parameters.

2.1 Geology and bathymetry

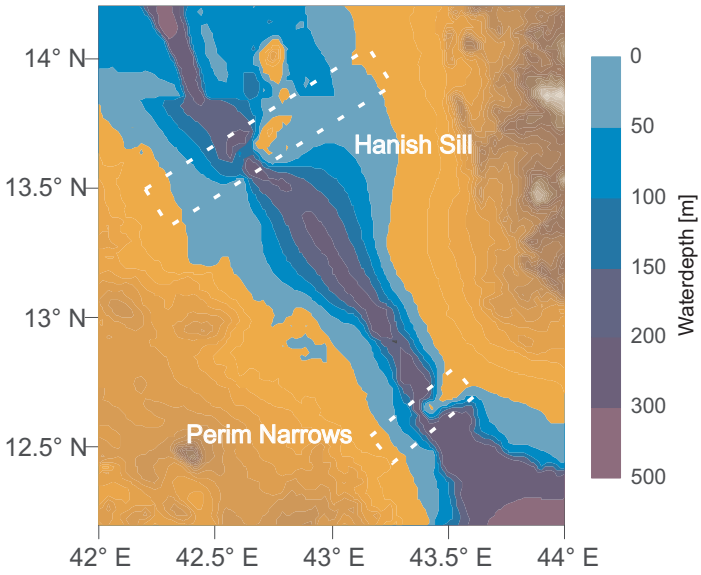

Figure 2 Bathymetry of the Bab el Mandab region with marked areas of special interest. Modified *ETOPO1 Global Relief Model* data [Amante and Eakins 2008] after Werner and Lange [1975]

The Red Sea is a marginal sea of the Indian Ocean. The development of the basin began in the upper Eocene/lower Oligocene with the first major rift movements in the region when the Arabian and African plates started to separate. In a first stage, a rifting process propagating from south to north formed the principal Red Sea graben [Girdler and Styles 1974]. Already before the onset of continental rifting, large parts of the region were below sea level [Bayer et al. 1989]. Subsidence of the Sinai area and transgressions of the Mediterranean Sea led to the deposition of mighty evaporite sequences in the shallow basin. Subsequently, with increasing rift activity in the middle Miocene, sedimentary facies in the basin changed with increasing water depth to deepwater limestones [Bayer et al. 1989]. At the Miocene/Pliocene boundary, the active rifting of the northernmost Red Sea fault in the Gulf of Suez ceased and the Aqaba/Levant fault became active [Lyberis 1988]. The horizontal movement of the Arabian plate in this second (recent) stage of development led to a passive opening of the Red Sea with sea floor spreading rates of 0.6 to 1 cm/a [Roeser 1975]. A detailed review of the geological development of the Red Sea region has been published by Bosworth et al. [2005].

Today, the Red Sea (Figure 1, Figure 13) is a desert-enclosed, narrow basin of 1932 km length, with an average breadth of 280 km. The average depth of the Basin is 491 m, but the axial depression is rather deep with a maximum depth of 2190 m. In the north, the Red Sea divides into the Gulf of Suez, which is 250 km long and 32 km wide, and the Gulf of Aqaba with a length of 160 km and a width of only 16 km. While the former is very shallow (< 90 m), the Gulf of Aqaba has a maximum depth of 1829 m. It is separated from the main body of the Red Sea by the Strait of Tiran with a sill depth of 340 m [Morcos 1970]. The only connection of the Red Sea basin to the open ocean is the Strait of Bab al Mandab in the south, opening into the Gulf of Aden and the Indian Ocean. Within the Bab al Mandab region (Figure 2), while less suspicious than the just 18 km wide Perim Narrows, Hanish Sill is with a maximum depth of only 137 m [Werner and Lange 1975] the critical point for inter ocean exchange.

Four physiographic regions can be recognised within the Red Sea (Figure 13) [Morcos 1970]: the coral reef zone, the coastal shelves, the main trough and the deep axial trough. The up to 50 m deep coral reef zone and the coastal shelves (sensu Morcos [1970]) with a depth of around 400 m increase dramatically in breadth south of 19° N and are generally more extensive on the Arabian side of the basin. The main trough, with depths between 600 and 1100 m and an irregular, broken sea floor, extends from 15° N to the tip of the Sinai Peninsula. The axial trough with depths larger than 1100 m lies between 17° N and 23° N; being continuously deeper than 1500 m between 19° N and 22° N [Morcos 1970]. A hot brine region has been discovered in the axial trough between 21° 10′ and 21° 30′ N. Three depressions greater than 2000 m in this region hold brine pools with anomalously high temperatures, salinities and mineral concentrations [Degens and Ross 1969].

2.2 Climatology

The Red Sea lies between two climatic systems: the Indian monsoon and the northern hemisphere climate controlled by the North Atlantic Oscillation. The Indian monsoon subjects the Red Sea to a bi-modal annual wind regime (Figure 3) [Pedgley 1974]. The pronounced relief at both shores forces the winds to follow the Red Sea's axis. During the Indian winter monsoon, from October to April, NNW winds prevail over the entire Red Sea. In the Indian summer monsoon season, from May to September, NE winds from the Indian Ocean become entrained in the topography and blow from south-east over the southern Red Sea, to collide with the NNW winds at 18° N. Wind speeds are generally higher over the northern Red Sea and reach maximum values of 7 m/s during summer (Figure 3 a). Rainfall over the Red Sea region is generally low (Figure 4 a). The southern part of the Red Sea below 18° N receives an increased amount of

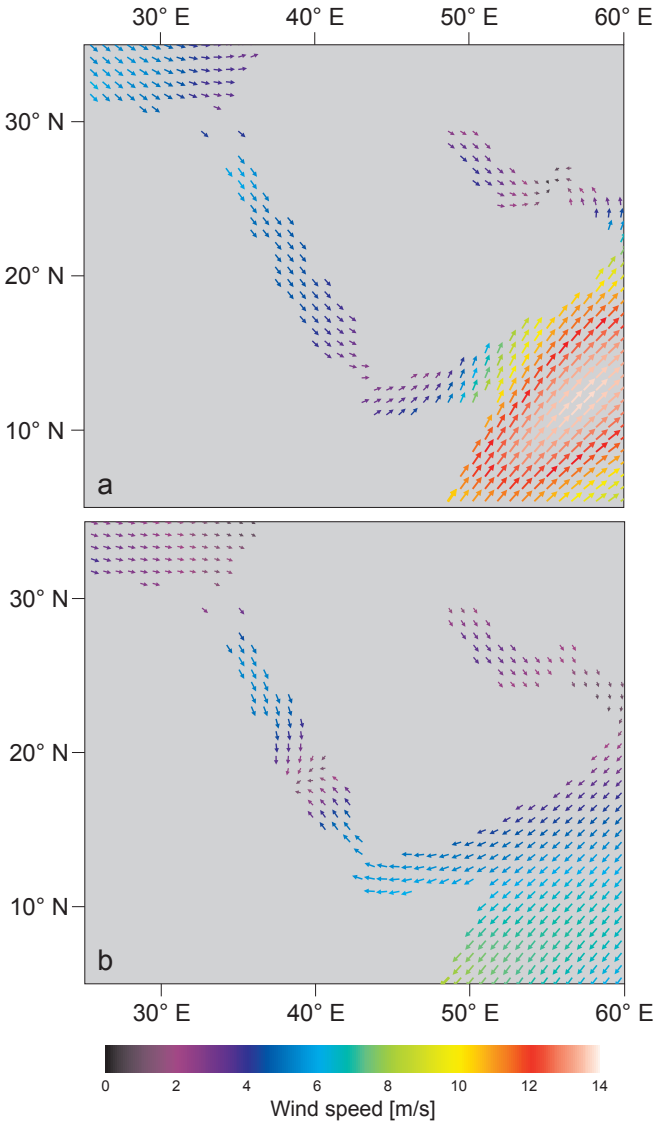

Figure 3 Windfields over the sea surface in the Red Sea region for summer (a) and winter (b). Source: *Atlas of Surface Marine Data* [da Silva et al. 1994]

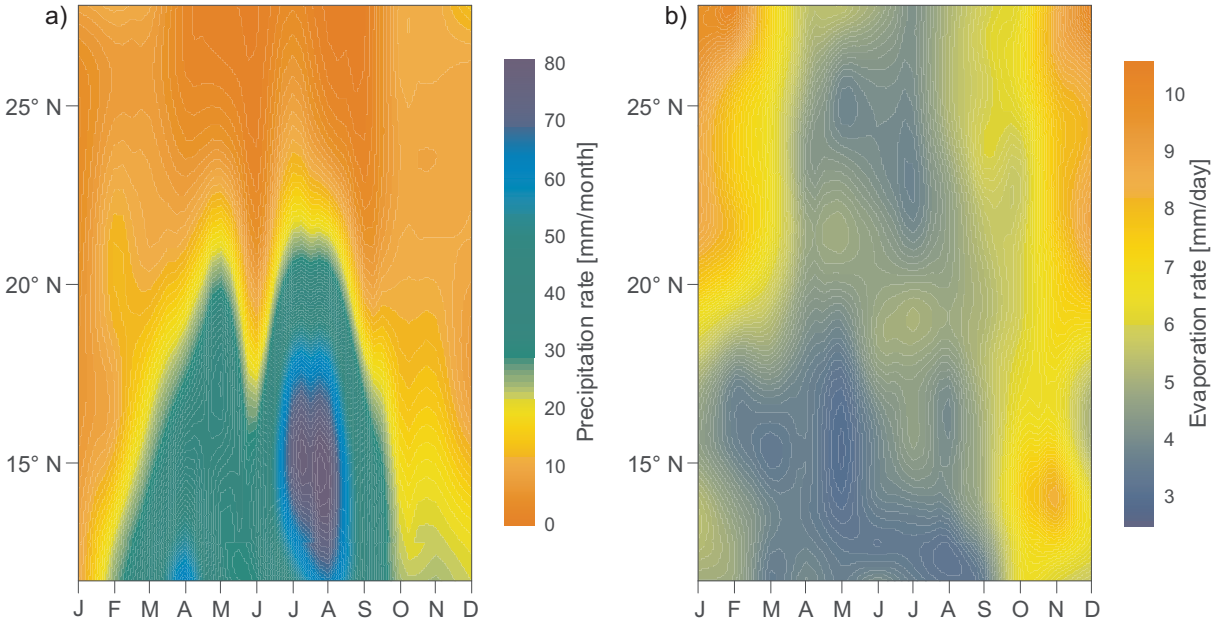

Figure 4 Precipitation rates (a) and unconstrained evaporation rates (b) along the Red Sea's central axis over the course of one year. Source: (a) *CAMS-OPI* [Janowiak and Xie 1999], (b) *Atlas of Surface Marine Data* [da Silva et al. 1994]

precipitation during the months July to August, when the Inter Tropical Convergence Zone (ITCZ) reaches its northernmost position. Other than during this period, precipitation rates do not exceed 40 mm/month anywhere over the Red Sea. River runoff is negligible and most freshwater input occurs through wadis (ephemeral streams) draining seasonal rainfall on the slopes of the bordering mountain ranges.

Air temperatures in the region range between minimally 13 °C at the tip of the Sinai Peninsula in winter and 40 °C in the Bab al Mandab region during summer (Table 1). Summer temperatures are almost balanced along the Red Sea with small gradients of 2-3 °C, while in winter the temperature gradient reaches as much as 9 °C (Table 1). The combination of the described climatic factors causes high evaporation rates, which drive the circulation of the Red Sea. Evaporation rates are highest during winter in the northern Red Sea (Figure 4 b) and can reach annual values of up to 2.1 m/a [Sofianos et al. 2002]. Evaporation and winds cause a difference in sea level of 35 cm [Lisitzin 1965] between the tip of the Sinai Peninsula and the Perim Narrows, which is larger than the tidal amplitude of only 30 cm [Grace 1930].

		January		August	
	Latitude	Min	Max	Min	Max
Sharm el Sheikh	27° 54' N	13	22	27	38
Jiddah	21° 30' N	17	27	27	37
Bur Sudan	19° 37' N	20	27	28	40
Al Hudaydah	14° 48' N	24	27	32	34
Assab	13° N	21	31	30	40

Table 1 Air temperatures in °C at stations along the Red Sea coast. Source: *MADIS* [NOAA]

2.3 Oceanography

2.3.1 General circulation system and deep water properties

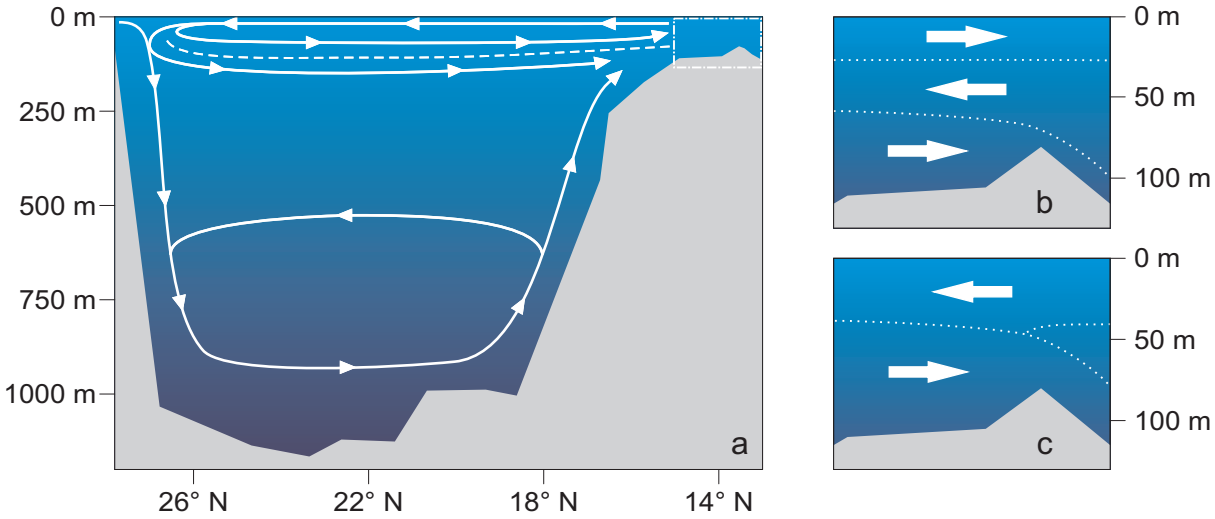

Figure 5 Circulation system of the Red Sea reproduced after *Eshel et al.* [1994] and *Smeed* [1997]. Main basin circulation (a) and circulation pattern at Bab el Mandab (framed area) in summer (b) and winter (c). The pycnocline is indicated by a dashed line. All depths levels are approximate values.

The circulation system of the Red Sea is basically antiestuarine (Figure 5 a). It is primarily driven by thermohaline forcing and only secondarily by winds [Eshel et al. 1994; Sofianos and Johns 2002]. The sea level difference pulls surface water from the Gulf of Aden into the Red Sea, while dense Red Sea deep water flows out of the basin. The entering surface water flows northward, increasing in density on its way due to the intense evaporation. North of 25° N the density of the surface water has increased to a level that allows ventilation of water above the pycnocline. The water body above the pycnocline, consisting of inflowing surface water and the southward flow of ventilated deep water has a short residence time of about 20 years [Rohling et al. 2008a]. In the very north of the basin, at around 27° N, deep water is formed isopycnally. This type of Red Sea deep water flows southwards at a depth of around 160 m, just below the pycnocline. The main part of the Red Sea deep water, residing

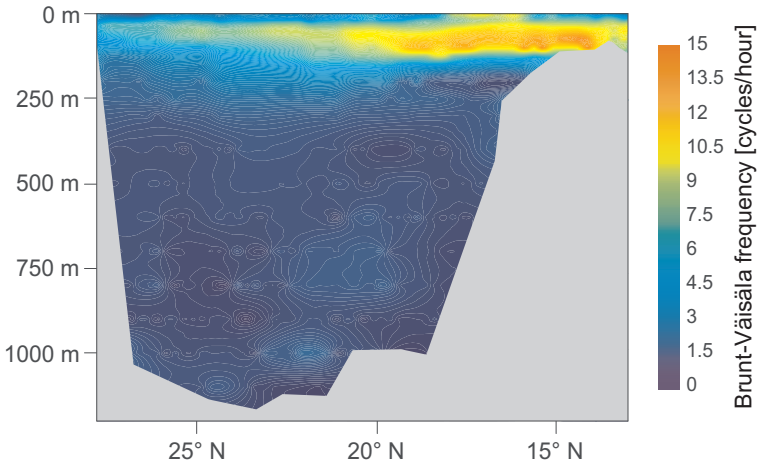

Figure 6 Profile of water column stratification (annunal mean values) in the Red Sea along its central axis. Source : *World Ocean Atlas 2001* [Levitus and NODC]

below 300 m depth with a uniform temperature and salinity of 21.6 °C and of 40.6 (Figure 7 a and b), is generated by convection of water from the adjoining Gulf of Suez and Gulf of Aqaba [Cember 1988; Eshel et al. 1994]. The water leaving the Red Sea over Hanish Sill into the Gulf of Aden is mixture of all deep water types [Naqvi and Fairbanks 1996] and can be recognised as warm, saline and oxygen depleted water in the Indian Ocean at depths of around 700 m [Morcos 1970]. The circulation pattern of the deep water masses within the basin and the mass contributions of different deep water sources in the north of the Red Sea and the adjoining Gulf of Aqaba and Gulf of Suez are due to the lack of actual measurements still under debate [Cember 1988; Eshel et al. 1994; Woelk and Quadfasel 1996; Eshel and Naik 1997; Manasrah et al. 2004; Eshel and Heavens 2007].

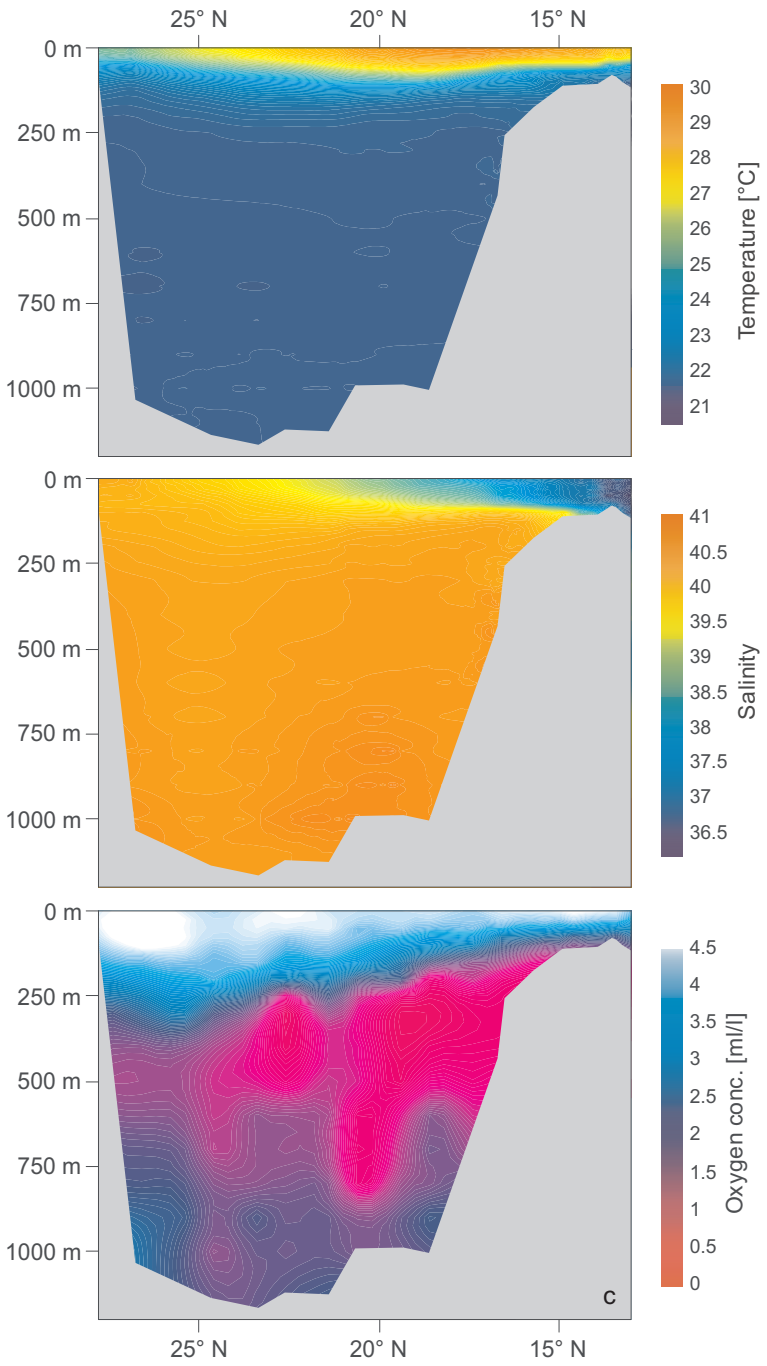

Figure 7 Profiles of annual mean values of temperature (a), salinity (b) and dissolved oxygen concentration (c) in the Red Sea along its central axis. Source : *World Ocean Atlas 2001* [Levitus and NODC]

While the principal circulation system of the Red Sea is constant throughout the year, the secondary forcing by the seasonal monsoonal winds results in strong seasonal differences in the circulation at Bab al Mandab and the southernmost Red Sea [Patzert 1974; Murray and Johns 1997; Smeed 1997; Siddall et al. 2004]. During the Indian NE Monsoon (October to April), the circulation pattern over the Hanish Sill is two-layered (Figure 5 c): a layer of surface water enters the Red Sea, while a layer of deep water leaves it. From May to September, during the Indian SW Monsoon, the circulation pattern over the Hanish Sill is three-layered (Figure 5 b). NW winds force a thin layer of surface water to leave the Red Sea and thus the inflow of water is displaced to deeper

levels. At intermediate water depths, above the weaker outflow of Red Sea deep water, a layer of nutrient-rich water, upwelled by the Monsoon in the Gulf of Aden, enters the Red Sea. The increased nutrient levels in the intruding intermediate water fuel productivity in the surface layer in the very southern Red Sea (cf. Figure 9 c). As a result of the formation of deep water in the north and the stratification of the water column in the south of the Red Sea, an oxygen minimum zone (OMZ) develops south of 20° N, with oxygen concentrations as low as 0.5 ml/l in its core (Figure 7 c). The 2 ml/l oxycline lies at 75 m depth in the south (< 16° N) and deepens continuously to the north until it reaches depths of around 300 m at 25° N [Levitus and NODC; Neumann and McGill 1962].

2.3.2 Surface water circulation and properties

The surface water circulation in the Red Sea (Figure 8) shows a complex and seasonal array of boundary currents and permanent or semi-permanent gyres [Quadfasel and Baudner 1993; Sofianos and Johns 2003; Biton 2006]. South of 18° N, the seasonal variability is strongest due to the seasonality of the wind field and the exchange flow at Bab al Mandab. An example for this is an mesoscale gyre located between 15° and 16° N, which reverses from an anticyclonic rotation during winter to a cyclonic rotation during the summer [Sofianos and Johns 2003] (cf. Figure 8). The surface inflow during winter takes the form of a strong boundary current along the western coast of Saudi Arabia. The circulation field in the northern Red Sea is dominated by two permanent eddies; a small

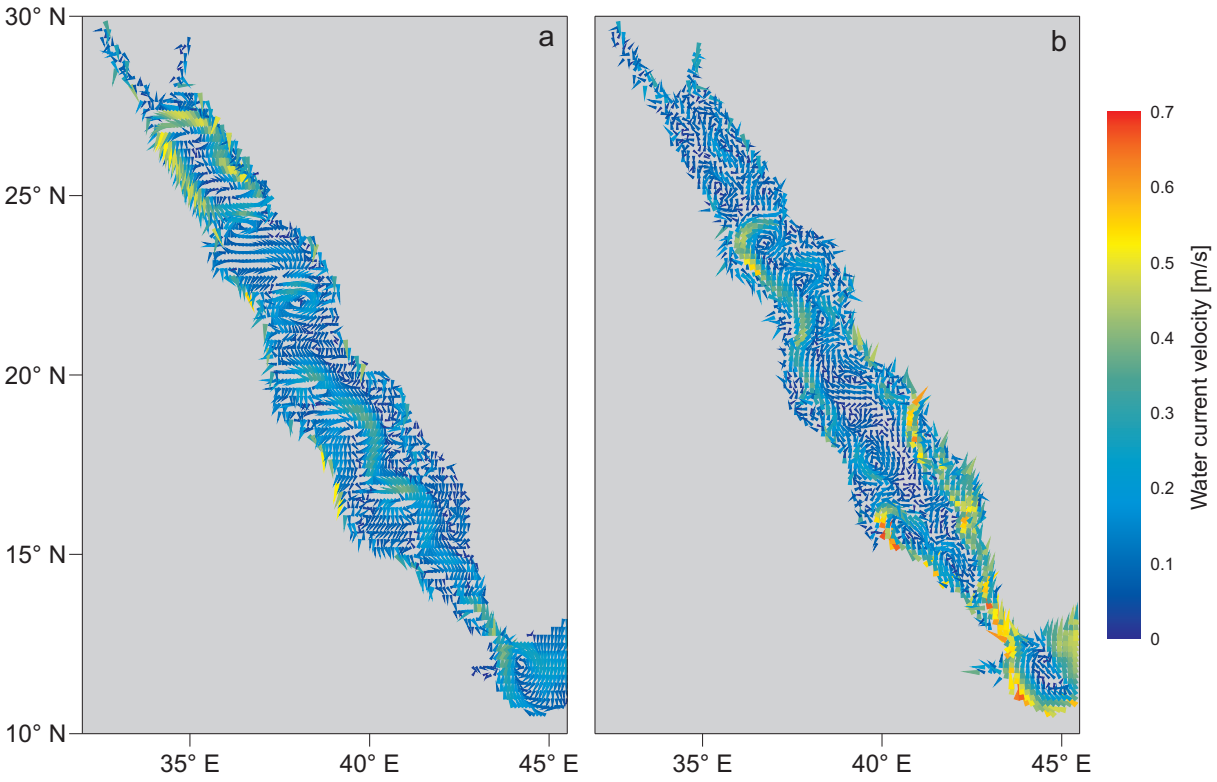

Figure 8 Modelled surface circulation pattern in the Red Sea during summer JJA (a) and winter DJF (b). Source: *Biton* [2006]

anticyclonic gyre centered around 23.5° N and a larger, more elongated cyclonic gyre centered around 25° N [Morcos 1970; Sofianos and Johns 2003]. Actual measurements of the Red Sea surface water circulation are sparse but the published general circulation models [Sofianos and Johns 2002; Sofianos and Johns 2003; Biton 2006] agree reasonably well with the available data [Morcos 1970; Sofianos and Johns 2007].

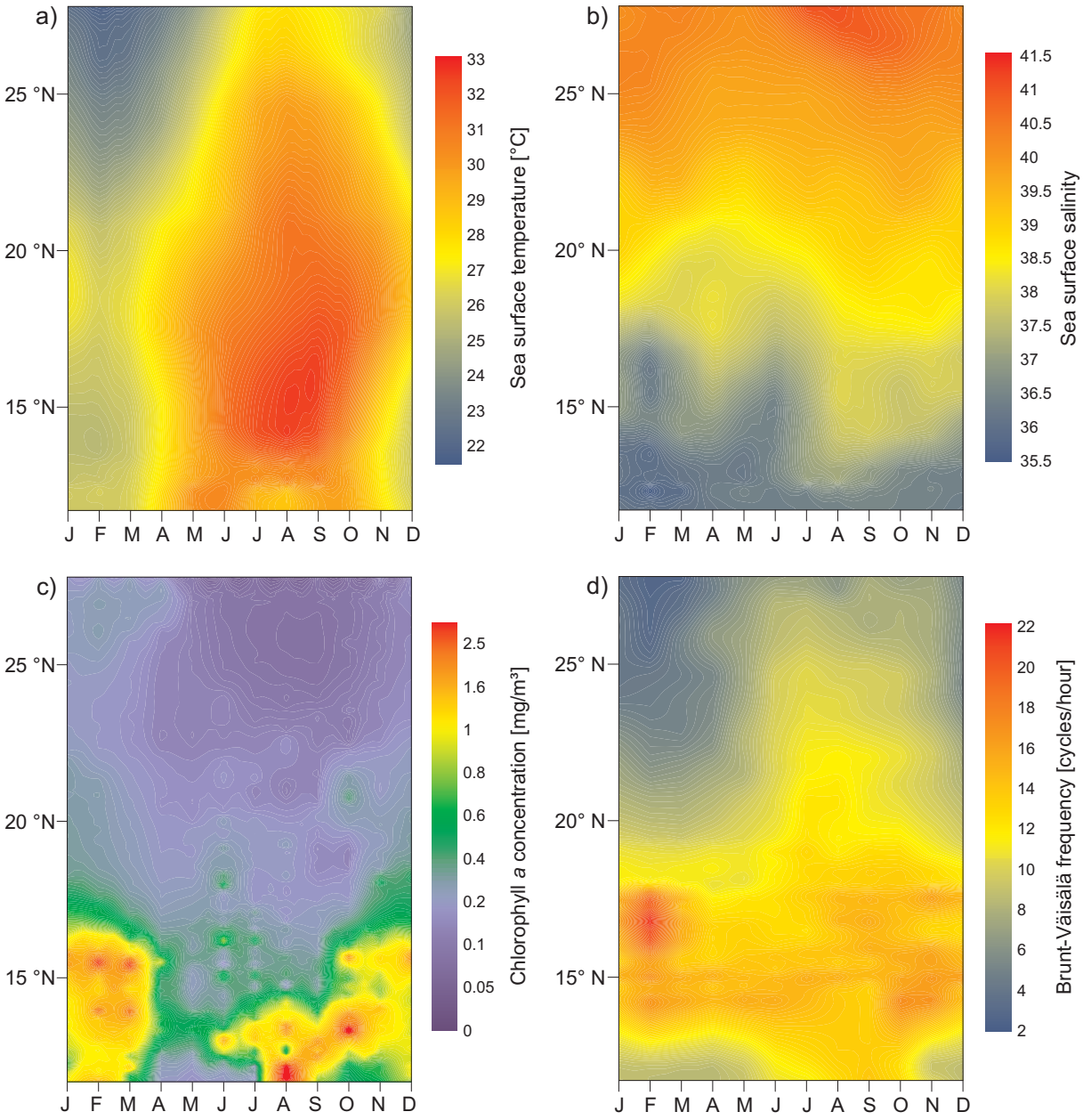

Figure 9 Sea surface temperature (a), sea surface salinity (b), remote-sensed chorophyll *a* concentration (c) and stratification in form of the maximum Brunt-Väisälä-frequency of the top 250 m water column (d) along the Red Sea's central axis over the course of one year. Source: (a, b, d) *World Ocean Atlas 2001* [Levitus and NODC], (c) *Ocean Color Web, Merged AQUAModis / SEAWIFS* [Feldman and McClain 2006]

In pace with the circulation pattern, the properties of the surface waters show a strong seasonality (Figure 9). Similar to the pattern of air temperatures, the seasonal variability of sea surface temperature (SST) is larger in the south than in the north of the Red Sea (Figure 9 a). The highest SSTs reach more than 32 °C in the southern Red Sea during summer and the lowest SSTs of around 22 °C are observed in the very north of the basin in winter. The SST gradient in the basin remains approximately 6 °C during all seasons. Sea surface salinity changes most dramatically in the southern Red Sea, where the alternating circulation system produces seasonal differences of almost 2 (Figure9 b). The highest salinities with values greater than 41 are reached in the very north during the late summer.

The pattern of primary productivity, approximated by surface water chlorophyll *a* concentration, features the most pronounced seasonality of all investigated parameters (Figure 9 c). During summer, the inflow of nutrient rich intermediate water from the Gulf of Aden induces patches of high primary productivity south of 18° N. Winter is the productive season for the entire Red Sea, when the inflow of Gulf of Aden surface waters and vertical overturning promote primary productivity up to 22° N. The absolute values of chlorophyll *a* concentrations are still very low, maximally 0.5 at 18° N and 0.3 mg/m³ at 21° N. The origin of the weak productivity maximum in the very north of the basin during the winter is most probably connected to mixing processes in the water column during deep water formation. The stratification of the top 250 m of the water column shows maximal values in the south during winter; the density difference between inflowing Gulf of Aden surface water and outflowing Red Sea bottom water is apparently larger than between Red Sea surface, bottom and Gulf of Aden intermediate water (Figure 9 d). The stratification minimum in the north of the Red Sea during winter marks the time and place of bottom water formation.

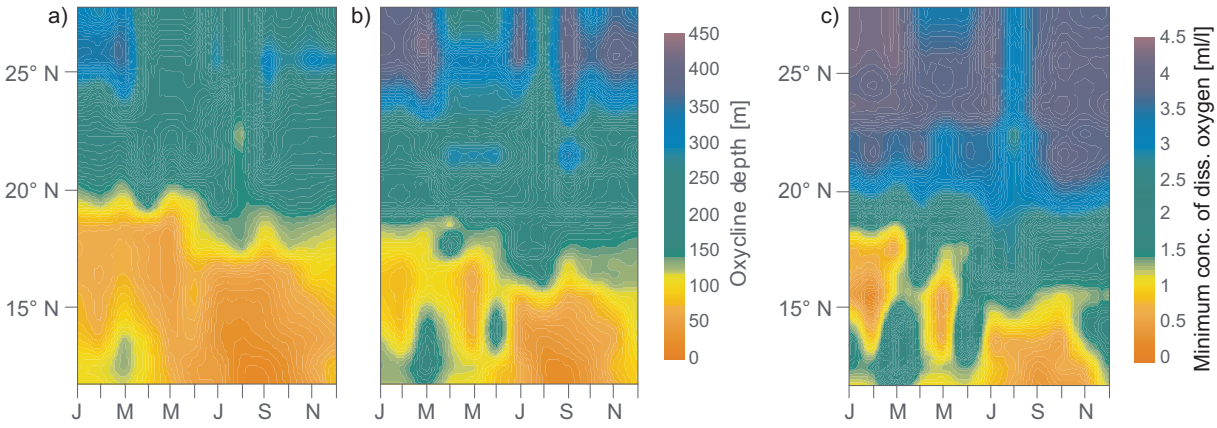

Figure 10 Depth levels of the 3 ml O_2/l oxycline (a), the 2 ml O_2/l oxycline (b) and the minimum concentration of dissolved oxygen in the top 150 m water column (c) along the Red Sea's central axis over the course of one year. Source: *World Ocean Atlas 2001* [Levitus and NODC]

The oxygen concentration of subsurface water layers is also affected by the seasonal pattern of circulation and productivity (Figure 10). Over the course of a year the depth levels of the 3 and 2 ml/l oxyclines vary most distinctively between 18° and 20° N and north of 24° N. In the central part the oxyclines rise during winter and spring, while in the northern part of the basin they deepen during autumn and winter. Thus, the strongest gradient of oxycline depths in the Red Sea occurs in winter and the weakest in summer. The pattern of minimum concentrations of dissolved oxygen in the upper 150 m water layer shows the same behaviour as the oxycline depth gradients (Figure 10 c).

In summary the north-south orientation of the Red Sea in combination with restricted water exchange only at its southern end, results in strong and mutually correlated gradients of most oceanographic parameters along the basins axis. The strong seasonality of the Red Sea causes an amplification of the gradients of most environmental variables during the winter season.

3. Red Sea paleoceanography

Paleoceanography in the Red Sea is in many cases confronted with difficulties as the exceptional environment of the Red Sea entails ranges of environmental parameters that lie outside those encountered in the global oceans and are often outside the calibration ranges of established reconstruction methods. This chapter aims at giving a short overview of previous research, methodological approaches and the restrictions and modifications, which apply to standard paleoceanographic proxies under the special conditions of the Red Sea. In general, research so far has clearly focused on glacial/interglacial timescales and for political/logistical reasons on material from the northern part of the Red Sea.

3.1 Geochemical proxies

- The **isotopic composition of oxygen** in seawater is a measure of global ice volume [Shackleton 1987] and if analysed in the tests of foraminifera also of temperature [Emiliani 1955] and local evaporation (salinity) [e.g. Thunell and Williams 1989; Duplessy et al. 1991]. In the Red Sea however, the isotopic composition of oxygen in the tests of planktonic foraminifera was found to be a proxy for global sea level [Siddall et al. 2003; Siddall et al. 2004]. This extraordinary relationship bases on the restricted water exchange through the shallow Strait of Bab al Mandab and the high evaporation rates. The principle is that the isotopic composition of the entering seawater from the Gulf of Aden is altered by evaporation in the Red Sea; as the light isotope is preferentially removed during evaporation, the remaining seawater becomes progressively isotopically heavier. The degree of alteration is a thus a function of the residence time of waters within the basin, which in turn is predominantly depending on the sea-level controlled water exchange at the Strait of Bab al Mandab. With a postulated accuracy of ± 12 m [Siddall et al. 2003], this method provides at present the only means that allows continuous reconstructions of past global sea level. Rohling et al. [2008a; 2008b; 2009] employed this method on the records of cores KL11 and KL9 from the central Red Sea to reconstruct past sea level, exposing the tight coupling of Antarctic climate and global sea level, both on glacial/interglacial timescales and for millennial scale climate variability during marine isotope stage (MIS) 3.

- The **magnesium/calcium ratio in foraminifera tests** was found to be dependant on ambient water temperature during calcification [Chave 1954]. Scores of culture, sediment trap and core top studies have subsequently been undertaken to validate this finding and calibrate the species-specific relationship of Mg/Ca ratio and temperature. Later, researchers found that salinity also influences the Mg/Ca ratio, both under laboratory conditions [Nürnberg et al. 1996], and in the natural environment [Ferguson et al. 2008]. A study on material from the Red Sea [own unpublished results; Groeneveld et

al. 2008; Hoogakker et al. 2009] revealed that the Mg/Ca ratio in foraminifera from plankton tow samples match the expected values of temperature and salinity calibrations, but the encountered values in core tops from the northern Red Sea are in some cases more than four times higher than expected. Such a large difference could only be explained by diagenetic precipitation of high magnesium calcite, which is in its scale unprecedented and apparently starts already in the water column. Recent methodological approaches in spatially highly resolved analysis of the Mg/Ca ratio in foraminifera tests can circumvent some of the difficulties regarding the diagenetic alteration [see supplementary material in Rohling et al. 2008b] and will in future probably lead to the successful application of this proxy in the Red Sea [Hoogakker et al. 2009].

- **Sediment properties** have so far only sparsely been employed for paleoceanographic research in the Red Sea. The magnetic susceptibility of sediment samples from the central Red Sea was found to be highly correlated to titanium concentration [Rohling et al. 2008a], and can therefore be employed as a proxy for eolian dust input as demonstrated in other regions by Larrasoana et al. [2003]. The study of Rohling et al. [2008a] showed that sea level changes during MIS 3 were out of phase with dust input peaks, contradicting the proposed northern hemisphere climate control over millennial-scale glacial sea-level variability [Arz et al. 2006a]. In another study, the strontium isotope ratios of sediment were used to infer the sources of terrestrial input over glacial/interglacial timescales [Stein et al. 2007]. Furthermore, grain size measurements have been employed as an index for aridity in the northern Red Sea [Arz et al. 2003a] and XRF elemental counts of manganese in brine sediments have been used to infer changes in bottom water ventilation [Arz et al. 2006b].

3.2 Biochemical proxies

- **Alkenones** with 37 carbon atoms and different degrees of unsaturation are synthesised by the globally distributed coccolithophorid algae and are well preserved in marine sediments. The functional role of these molecules in the living organism is still under debate [Rosell-Melé and McClymont 2007]. It was however found that the level of unsaturation is related to ambient water temperature [Marlowe et al. 1984] and this relationship was formulated as the alkenone unsaturation index $U^{K'}_{37}$ [Brassell et al. 1986]. Alkenone paleothermometry operates accurately in global oceans in the temperature range of 0 to 29 °C [Sikes et al. 1991; Müller et al. 1998; Conte et al. 2006]. Attempts to employ this method on a record from the central Red Sea have so far been thwarted by too low concentrations of alkenones in the sediment [own unpublished results; Trommer et al. 2009a]. A single alkenone paleotemperature record of a core in the northern Red Sea (present - 22 ka BP) has been published by Arz et al. [2003a; 2003b]. This record shows a monotonously increasing temperature trend for the Holocene of 2 °C, and minimal temperatures of 16 °C at 16 ka BP, implying a glacial-interglacial SST contrast of 8 °C.

- The **TEX_{86}** (TetraEther indeX of tetraethers consisting of 86 carbon atoms) is a paleothermometry method based on the ratio of different components in the membranes of a group of marine bacteria (Archaea). These Crenarchaeota are common extremophiles, but also form a significant proportion of the marine bacterioplankton [DeLong 1992; Sinninghe Damsté et al. 2002]. They synthesize mono-layered membranes consisting of several species of membrane lipids (glycerol dialkyl glycerol tetraethers), whose composition was found to be correlated with temperature [Schouten et al. 2002]. The membrane lipids are readily preserved in marine sediments and could be found and analysed in samples dating back to the cretaceous [Schouten et al. 2003]. A study attempting to calibrate this paleothermometer in Red Sea sediments [Trommer et al. 2009b] discovered an endemic Crenarchaeota population, with a different relationship of membrane composition and temperature than the global population [Kim et al. 2008]. To date only two TEX_{86} paleotemperature records from the Red Sea exist, both covering the Holocene. They show warmer SST during the early Holocene and a significant temperature variability of 3 °C related to alterations in the circulation system over the Holocene period [Trommer et al. 2009a].

3.3 Microfossil assemblages

- **Coccolithophorida** are unicellular planktonic algae and an important constituent of oceanic nannophytoplankton**.** The algae cells are covered by minute calcareous scales (3-15 µm), the coccoliths, which are readily preserved in marine sediments. An investigation of living coccolithophorida in the Gulf of Aqaba showed that the assemblage composition is indicative for productivity regimes and water column stratification [Winter et al. 1979]. Studies on fossil assemblages of coccolithophorida in the northern Red Sea and the Gulf of Aqaba reported that the assemblages do not only differ between glacials and interglacials [Winter 1982] but also record northern hemisphere climate events (Heinrich events, Younger Dryas, Bølling-Allerød) during the last glaciation [Legge et al. 2006; Legge et al. 2008].

- **Thecosomate pteropods** are planktonic ophistobranch molluscs with aragonitic shells. Due to selective dissolution of aragonite in the deep ocean, the preservation of their shells is limited to shallow seas or marginal basins with carbon saturated bottom waters, like the Red Sea. Most thecosomate pteropods are herbivorous and live either in the epipelagial or conduct diel migrations into the upper mesopelagial (up to 600 m depth) [Bé and Gilmer 1977]. For these reasons, the relative abundances of pteropods species in fossil assemblages have been used to reconstruct productivity and the extent of oxygen minimum zones in the Arabian Sea [e.g. Singh et al. 2006]. In studies from the Red Sea, these parameters were expanded by water column stratification [Almogi-Labin 1982; Almogi-Labin et al. 1991; Edelman-Furstenberg et al. 2009] and properties of the carbonate system inferred from pteropod shell preservation [Almogi-Labin et al. 1986; Almogi-Labin et al. 1998].

Paleoclimatic studies connected the dominance of epipelagic species and a good preservation of pteropod shells during glacials with a poorly aerated and stratified water body in the Red Sea; dominance of mesopelagic species and poor preservation of pteropod shells during interglacials were related to a well-aerated water body [Almogi-Labin 1982; Almogi-Labin et al. 1986; Almogi-Labin et al. 1998]. A study concerning thecosomate pteropods with focus on the Holocene inferred a gradual transition from a humid regional climate in the early Holocene to an arid climate in the late Holocene [Almogi-Labin et al. 1991].

- **Benthic foraminifera** are epi- or endobenthic marine unicellular amoeboid protozoa, which build a test of either secreted organic tectin, calcite, aragonite or silica or of agglutinated particles. They are highly diverse and form a vital part of the benthic fauna, particularly in the deep sea. Due to the preservation of their tests, the benthic foraminifera with calcitic tests are widely used in paleoceanography as indicators of organic matter fluxes to the sea floor and bottom water oxygenation. The reconstructions of these parameters on glacial/interglacial timescales have been used to assess the influences of different climatic regimes on the Red Sea circulation and productivity [Badawi 2003; Badawi et al. 2005], suggesting a dominance of the NE monsoon system during glacials. Furthermore, changes in the extent of the Red Sea OMZ and bottom water ventilation events during the late Holocene have been inferred from the composition of benthic foraminifera assemblages [Edelman-Furstenberg et al. 2001; Arz et al. 2006b].

- **Planktonic foraminifera** are marine planktonic unicellular amoeboid protozoa, which build exclusively calcitic shells. This group is less diverse than their benthic counterparts and today only 40 to 50 different species are recognised. Most planktonic foraminifera live in the photic zone; species inhabiting deeper waters can be found in depths of 1000 m or more [Bé and Hutson 1977]. The food spectrum ranges from minute phytoplankton to copepod-sized zooplankton. Many species harbour algal symbionts, predominantly dinoflagellates, within their cytoplasma [Lee and Anderson 1991]. Although planktonic foraminifera constitute only a minor percentage of the biomass of the plankton, the sedimentation of their calcitic tests form the so-called foraminifera oozes, which cover about 30 % of the ocean floors [Hemleben et al. 1989]. In global oceans, fossil assemblages of planktonic foraminifera have been employed for reconstructions of temperature [e.g. Kucera et al. 2005b] and productivity [e.g. Watkins and Mix 1998]. In the Red Sea the distinct recent distribution of species has been attributed to salinity [Berggren and Boersma 1969], productivity (dietary preferences) [Auras-Schudnagies et al. 1989], water column stratification [Edelman-Furstenberg et al. 2009] and the extent of the OMZ [Fenton et al. 2000]. Using different ecological preferences of individual foraminifera species, investigations of the composition of fossil assemblages in the Red Sea during the Holocene have resulted in divergent reconstructions of past circulation regimes [Edelmann 1996; Badawi 1997; Schmelzer 1998; Edelman-Furstenberg et al. 2009; Trommer et al. 2009a]. On glacial/interglacial

timescales the planktonic foraminifera fauna was found to reflect mainly the sea-level driven changes in hydrography [Hemleben et al. 1996; Fenton 1998; Geiselhart 1998; Schmelzer 1998; Fenton et al. 2000; Braun 2009; Trommer et al. in preparation], but also the impact of the Indian monsoon system [e.g. Hemleben et al. 1996] or the northern hemisphere Heinrich events [Schmelzer 1998]. A single investigation attempted to derive quantitative information from planktonic foraminifera assemblages in the Red Sea by the application of a transfer functions for paleotemperature calibrated in the Indian Ocean [Ivanova 1985]. For planktonic foraminifera are sensitive to various environmental parameters and foraminifera based transfer functions are major paleoclimate proxies in open ocean settings, the potential of this approach is clearly not exploited in the Red Sea.

4. Transfer function theory

4.1 General transfer function methodology

4.1.1 Theoretical transfer function prerequisites

The basic principle of any transfer function is the translation of a set of known variables into a related unknown variable. In paleoceanography, the known variables are usually the abundances of species present in the fossil record and the unknown variable is an environmental factor, which one wants to reconstruct. Typical pairs of species assemblage and environmental factor for a transfer function in this field are planktonic foraminifera and temperature [e.g Kucera et al. 2005b], diatoms and pH-value [e.g. Birks et al. 1990] or pollen and precipitation rate [e.g. Seppa et al. 2004].

The application of transfer functions in paleoceanograhpy, which combines climatic and ecological data, requires certain theoretical prerequisites and assumptions [compare review in Birks 1995]:

- Causality - Climate in general and the reconstructed environmental variable in particular is the ultimate cause for the observed changes of the faunal assemblages in the fossil record.
- Uniformitarianism - The ecological optima and requirements of the species employed in the transfer functions are the same in the present time and the period to be analysed.
- Analogy - Observations in the present time contain all the necessary information to interpret the fossil data.

The criterion of causality results from the ecological niche concept [Hutchinson 1957], which states that each species occupies a ecological niche, a combination of environmental factors in a multi-dimensional ecospace, for which it is adapted best and where it accordingly outcompetes all other species. For simple single-celled organisms like planktonic foraminifera the properties of the water body in which they live determine the ecospace, where the different species coexist. The generally considered most important properties of a water body are temperature, salinity, and food availability. Changes in these properties of a water body result in changes of the faunal assemblage, which can occur spatially, in form of the global distribution of species, or temporally in form of changes in the faunal record of a sediment core. Morey et al. [2005] analysed the impact of a score of environmental parameters on the global distribution of planktonic foraminifera and found temperature to be the dominant factor controlling the composition of assemblages.

The criterion of uniformitarianism is more difficult to assess. It states that the ecological requirements of a species or a taxonomic unit are constant over time. While this assumption is certainly correct for short time spans, it can in general not be reconciled with the concept of ecological adaptation [e.g.

Schluter 2000]. This concept states that species can change their ecological preferences for reasons of resource availability, predation or competition without speciating. For simplicity, one can assume that the divergence of ecological preferences of a species from their recent ones increases monotonously with time. For the application of transfer functions, this leads to a loss of reliability of estimates with time (Figure 11). The use of ecological or functional units instead of species as input for transfer functions should then lead to a comparatively slower decrease in reliability at the cost of initial accuracy.

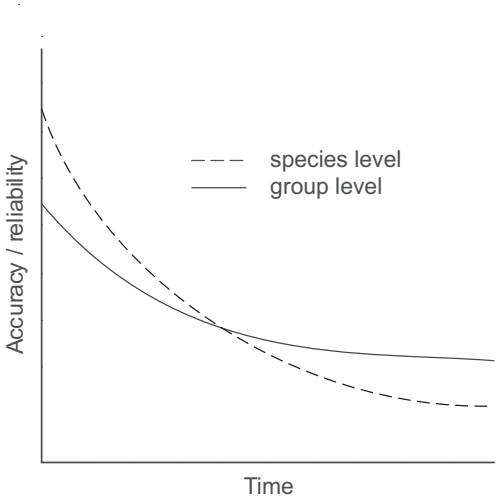

Figure 11 Conceptual model for the development of reconstruction accuracy in time by use of different taxonomic levels.

What remains is the criterion of analogy, which involves, unlike the other prerequisites, much more practical aspects of transfer function development. All transfer function approaches need a calibration dataset, on which the transfer function is established. The validity of any transfer function requires the analogy of the calibration dataset and the fossil record in both the faunal assemblages and the environmental conditions. While the latter cannot be checked for as the environmental conditions are usually to be reconstructed by the transfer function, the analogy of the faunal assemblage can be assessed by various mathematical methods. These methods calculate a measure of similarity between the fossil assemblages and those from the recent calibration dataset. If all fossil assemblages find a counterpart in the calibration dataset the faunae can be considered analogous. It is often overlooked, that the analogy of faunal assemblages does not automatically imply analogy of environmental conditions. Different environmental conditions, that are different combinations of environmental parameters, can translate into similar or identical equilibria in the fauna. In practice, environmental conditions are generally considered analogous, if other climatic proxies do not indicate otherwise.

4.1.2 Transfer function development

The first of typically two steps in the development of a transfer function is the generation of the calibration dataset. Ideally, this dataset consists of many hundred of recent faunal samples, all processed and counted in an identical manner, and covers large ranges of environmental parameters and all possible combinations of parameter values. Unsurprisingly, these ideal conditions are never met in scientific reality. A more manageable issue is the choice of taxonomic level to employ. The definition of taxonomic groups on morphological or ecological criteria and their use instead of species trades accuracy of reconstruction for reliability. The use of all data on the highest taxonomic level available entails an increased error due to probability or misclassification, resulting in a greater

volatility of reconstructions and in the worst case ecological insensibility of the generated transfer functions. The attention to confidence intervals of faunal census data and the use of a threshold for minimal abundance are simple and effective measures for the generation of sensible transfer function input data.

The second step in transfer function development is the predictive regression. In this step, the pairs of environmental variable and faunal assemblage of the calibration dataset are mathematically identified to obtain an equation, the "transfer function", with the faunal data as input and the environmental variable as output. The mathematical procedures employed for this task are manifold, and range from simple multiple regression to artificial neural network techniques. Certain methods allow or require the transformation of input data, e.g. square root or logarithmic, and most include a certain level of "noise reduction".

4.1.3 Assessment of transfer functions

Probably the most important characteristic of any transfer function in terms of its usability is the error of prediction. The calibration process already produces a first estimate, when the samples used for calibration are estimated by the developed transfer function. The RMSE (Root Mean Squared Error) is a measure of the transfer function's ability to fit the calibration dataset. The error of prediction, the RMSEP (Root Mean Squared Error of Prediction), however, must be calculated on an independent dataset. A common approach is to exclude a subset of the data from the calibration process to serve as

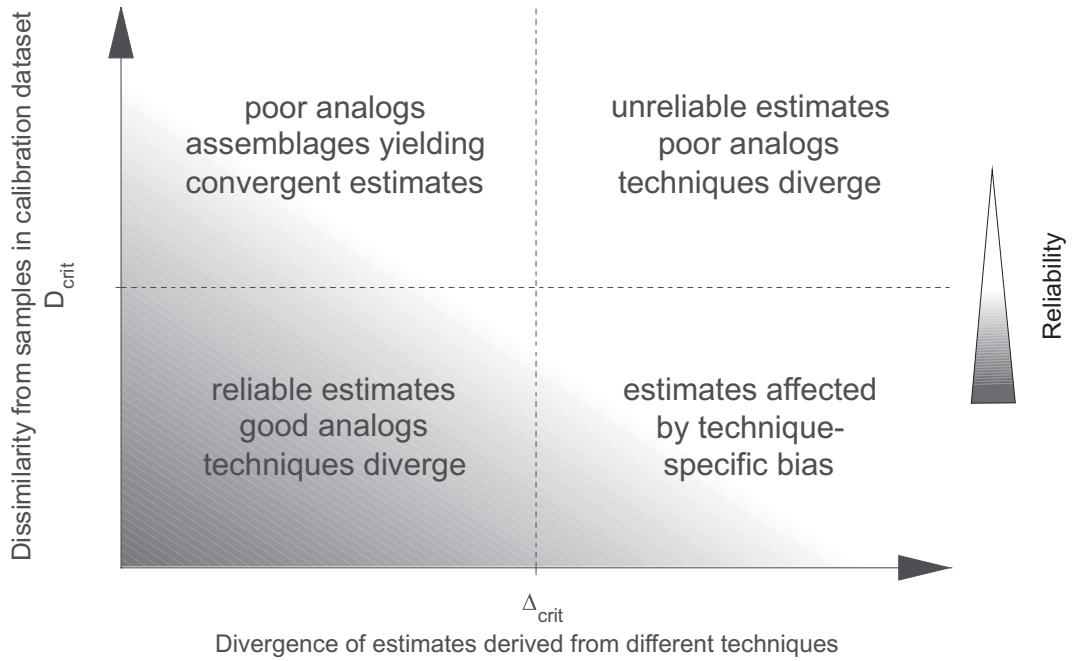

Figure 12 Conceptual model for the assessment of reliability of paleoreconstructions, modified after *Kucera et al.* [2005b].

a verification dataset on which the RMSEP can be calculated. However, as any reduction of the calibration dataset removes valuable information from the calibration of fauna and environment during transfer function development, methods that do not require a separate verification dataset are more commonly employed. These cross-validation methods calibrate the transfer function over many iterations, always excluding a part of the dataset for verification purposes, finally averaging the RMSEP. Another approach is the bootstrapping method, where the calibration dataset is randomly subsampled (allowing duplicates) from the full dataset in each iteration, leading to a robust error estimate when a high number of iterations are employed.

All verification methods are affected by spatial autocorrelation of samples in both the calibration and verification dataset. This intrinsic property of ecological data is the tendency of sites close to each other being more similar than randomly selected sites. In most cases, spatial autocorrelation conflicts with the statistical requirement of the verification dataset to be independent from the calibration dataset. This leads to the calculation of incorrect prediction errors, which are then generally underestimated [Telford et al. 2004; Telford and Birks 2005].

As a transfer function will always produce an estimate of any given faunal assemblage, it is recommendable to assess not only the prediction error but also the reliability of these estimates in general. The two main reasons for incorrect results of transfer function reconstructions are the violation of analogy and method-specific bias [Hutson 1977; Kucera et al. 2005b] (Figure 12). While there are many methods to assess the analogy of samples, a distinction between analogue and non-analogue samples on basis of a continuous measure of similarity is ultimately arbitrary. The definition of a critical value of similarity is therefore rather difficult. Method-specific bias on the other hand can be easily detected by the employment of several transfer function methods on the same dataset [Kucera et al. 2005b]. The definition of a critical value for the divergence of estimates can be based on the prediction errors of the individual transfer function methods.

4.2 Transfer function methods

4.2.1 Imbrie and Kipp method

The method of Imbrie and Kipp (IKM) [Imbrie and Kipp 1971] was the first paleoceanographic transfer function as such. It is a straightforward approach and stands close to the purest form of a predictive regression; a simple multiple regression of the species data on the environmental factor. It includes two measures to exclude or minimize the noise in the assemblage data. The first is a principal component (PCA) or factors analysis of the assemblage data, which reduces the number of variables, in this case species, in the data by extraction of a number of factors that retain the largest amount of

variance of the original data. The number of factors to use in the regression is usually determined by either the use of the Kaiser-Guttman-criterion [Guttman 1954], which requires a factor to have an eigenvalue of at least 1, or the inspection of the Scree-plot, termed Scree-test [Cattell 1966]. This plot of factor eigenvalues against factor number shows typically a sharp decrease in eigenvalue after the first few factors and the occurrence of this drop determines the number of factors to use. A second and not always used method to reduce the noise in the data further is the individual removal of species that explain only a negligible amount of the total variance from the factors. In the ensuing step, the environmental parameter to be reconstructed is regressed on the obtained factors, usually including cross products and quadratic terms. The strength and at the same time weakness of this approach is the ability/tendency to extrapolate out of the ranges of the calibration dataset. Where a relatively rare species with a high loading in a factor with a strong and positive weight in the regression increases in abundance, the predictions of the environmental parameter can easily surpass the ranges of the parameter in the calibration dataset.

4.2.2 Weighted averaging partial least squares

The Weighted Averaging Partial Least Squares method (WA-PLS) [ter Braak and Juggins 1993] is a combination of two methods, which are full transfer function methods by themselves. The first half, weighted averaging, bases on the ecological niche concept, assuming that different species occupy different niches in ecospace. Motivated by the assumption that a species will be most abundant at a site where the environmental parameters are close to its optimum, the method calculates species optima by weighted averaging of the species abundances. The environmental parameters are then estimated by weighted averaging of the obtained species optima. The repeated use of averages requires a subsequent deshrinking, where the environmental parameter is regressed on its estimate. The final prediction formula includes the coefficients of the deshrinking regression and the calculated species optima. The second half, the partial least squares method, is a combination of component extraction and regression similar to the approach of Imbrie and Kipp [1971]. One difference is that the environmental parameter to be reconstructed is involved in the process of component extraction. In contrast to components obtained by PCA, the PLS components yield the maximum covariance with the environmental parameter. In addition, the regression is inserted into the component extraction; the regression for all components after the first is calculated on the residuals of the last regression. The combination of these two approaches results in a method more accurate than any of the two constituent approaches alone. The WA-PLS method suffers from “noisy” datasets and has usually a larger RMSEP than the ANN or MAT approaches, but is also the method most robust to autocorrelation in the calibration dataset [Telford and Birks 2005]. It is important to stress that this approach bases on the assumption that species in the calibration dataset are most abundant where the controlling environmental parameter is close to the species’ optimum. This approach is therefore not well suited to

datasets where species live under extreme environmental conditions or the controlling environmental parameter is a limited resource.

4.2.3 Artificial neural networks

Artificial Neural Networks (ANN) are a "black box" approach which allows a close data fitting but only a limited analysis of causality between the input and output variables. The use of ANNs for reconstructions in the field of paleoceanography was introduced by Malmgren and Nordlund [1997]. In case of the usually employed back-propagating ANN, the network consists of several interconnected layers; the first consisting of the input variables, followed by a variable number of hidden layers containing the processors called neurons, and terminated by one neuron producing the output variable. Each neuron is linked with all neurons or variables of the preceding layer. The information of the input variables passes along these links through the network layers and is modified at each neuron by a predetermined function before being sent to the next layer. The coefficients of the function of each neuron are iteratively tuned to produce the best fit of output variable and calibration data. Several hundred iterations are required for the process of estimating the adjustable coefficients, called network training, which is continued until no further reduction in estimation error is recorded within a defined number of iterations. Due to its non-linearity and efficient fitting process ANN are prone to overfitting, that is fitting the training dataset including the inherent noise uncorrelated to environmental forcing. To avoid this effect the training dataset is split into a training and a test subset. The ANN is calibrated to the training set but the prediction error is calculated on the test set, thus disregarding an error reduction due to noise-fitting in the training set. As the functions of the individual neurons have to be predefined before training, an unlimited number of artificial neural networks exits, which are able to handle the given problem. An evolutionary approach was found to be suited best to solve the issue of finding the best network for a problem in a limited amount of time [Malmgren et al. 2001]. In this approach a population of randomly (within certain specifications) generated networks is for a given number of generations subjected to training, mutation and selection for performance. The result is a number of structurally potentially very different networks that all reproduce the calibration data with superior performance.

4.2.4 Modern analogue technique

The Modern Analogue Technique (MAT) [Hutson 1980] is based on the similarity between samples from the calibration dataset and the fossil record. Consequently, the development step of predictive regression is replaced by the calculation of similarity during the application of the transfer function. Any method for the calculation of similarity between multivariate data can be employed; since a comparative study of Prell [1985], squared chord distance is commonly used. For application of the

modern analogue technique, the similarity of the sample to be investigated with each sample of the calibration dataset is calculated. The average or weighted average of the environmental variables of a given number of the most similar samples is the reconstruction result. The actual number of samples to be used for this average is dependent on the size and spatial distribution of the calibration dataset. The modern analogue benefits most of all methods from a large calibration dataset with high spatial resolution, spanning a broad range of assemblages and environmental conditions, since it cannot reconstruct environmental parameter values outside the ranges of the calibration dataset.

5. Material and methods

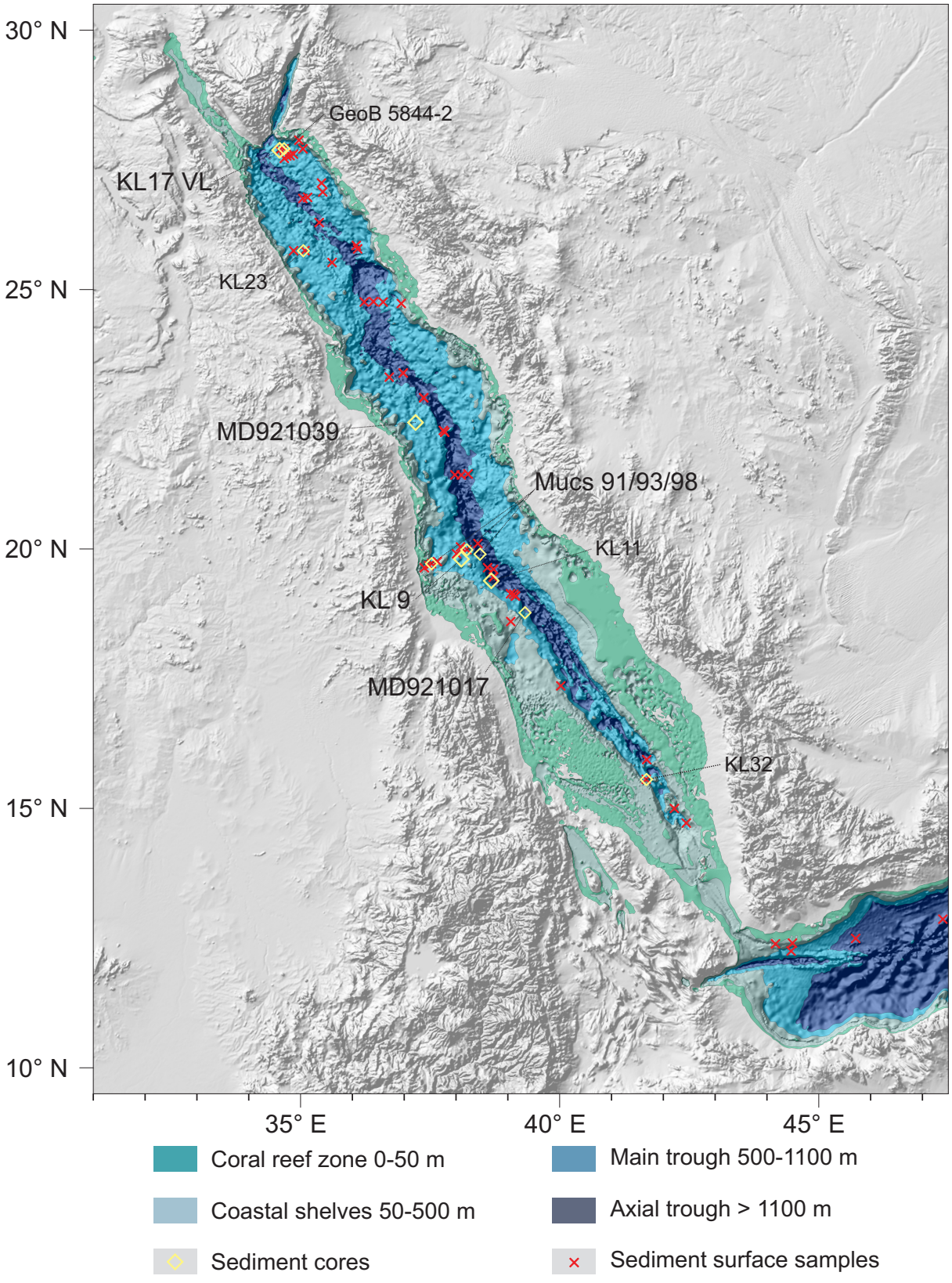

Figure 13 Combined topographic and bathymetric map showing the distribution of sediment surface samples and cores used in this study. Physiographic regions modified after *Morcos* [1970]. Source: *ETOPO1 Global Relief Model* [Amante and Eakins 2008]

5.1 Samples

5.1.1 Surface samples

The distribution pattern of planktonic foraminifera species was determined by analysis of 60 surface sediment samples from the Red Sea and the Gulf of Aden, collected during three cruises. This sample set included all Red Sea samples available in the core repository of the University of Tübingen, and represents, even though comparatively small, the largest set of surface sediment samples from the Red Sea to date investigated by a consistent methodology (details in the Appendix). Apart from eight boxcorer samples, already investigated and published in the study of Auras-Schudnagies et al. [1989], all other sediment surface samples were taken from multicorer tubes from the top 1 cm or the top 0.5 cm. None of the included surface samples showed any signs of carbonate dissolution, precluding any dissolution related modification of the assemblages [Hutson 1977].

5.1.2 Downcore samples

The two investigated cores of this study are piston core M5/KL143-2 [Nellen et al. 1996], referred to as KL9, from the central Red Sea and the trigger core of piston core M31/KL78-2 [Hemleben et al. 1995], referred to as KL17 VL from the northern Red Sea (Table 2). Both cores were opened shortly before or during the conduct of this work and had been stored at 4 °C at the core repository Tübingen Sand, Tübingen, Germany. The primary core KL9 was chosen for investigation for its excellent condition and location close to the key Red Sea record from core KL11, which is no longer available for continuous sampling. The study was later supplemented by the trigger core KL17 VL to validate the conclusions drawn from central Red Sea on a record from a different position along the Red Sea axis. The radiocarbon ages of all available and comparable faunal records from the Red Sea, i.e. the record of piston core KL11 [Schmelzer 1998] and the multicores MC91, MC93 and MC98 [Edelmann 1996; Edelman-Furstenberg et al. 2009] were used for the construction of age models. Additionally, data of piston cores KL23, KL32 [Schmelzer 1998] and GeoB 5844-2 [Arz et al. 2003b] were used for comparative purposes. The developed transfer functions were applied to the only other published faunal records of the same size class, the records of cores MD921017 and MD921039 [Fenton et al. 2000] and the multicores MC91, MC93 and MC98 [Edelman 1996].

	Lon [° E]	Lat [° N]	Depth [m]
KL9	38.103	19.804	814
KL17 VL	34.596	27.686	1014
KL11	39.332	18.772	810
MC91	38.463	19.900	1782
MC93	38.210	19.987	934
MC98	37.528	19.717	585
KL23	35.055	25.748	702
KL32	41.675	15.557	598
GeoB 5844-2	34.682	27.713	1235
MD921017	38.681	19.387	570
MD921039	37.219	22.437	1050

Table 2 Positions of sediment cores used in this study.

5.2 Sample processing

5.2.1 Sediment sample processing

To obtain workable and continuous subsections, the sediment cores were subsampled by use of U-channels, with a height and width of 1.8 cm. The sediment string from the U-channels was cut into 0.5 or 1 cm long pieces, temporarily stored in plastic bags and dried at 60 °C for 48 hours. The dried samples were weighed before and after washing over a 63 µm sieve. For counting purposes, the samples were dry-sieved over 150 µm mesh and split with an *ASC Scientific* microsplitter into successively smaller aliquots.

5.2.1 XRF and Colour scanner measurements

Sub-samples of KL17 VL and the Holocene section of KL9 were analysed with an XRF core scanner to obtain information about the elemental composition of the sediments. Measurements were performed at the National Oceanography Centre Southampton (Southampton, United Kingdom) in 0.5 mm resolution following the recommendations of Croudace et al. [2006]. Luminescence measurements (0.5 mm resolution) and core images were obtained with a *DMT Slab-CoreScan© Colour* scanner on undisturbed core halves intended for storage. The recorded raw data were manually checked for artefacts resulting from small cracks in the dried out sediment.

5.2.2. Stable isotope analysis

Oxygen and carbon isotope measurements for the construction of an age model were performed for the full length of KL9 (17.09 m) in a 10 cm resolution. A larger number of measurements (32) from a high-resolution oxygen isotope study [Rohling et al. 2009] complemented the measurements (15) of the Holocene section. The trigger core KL17 VL was measured in resolution of at least 4 cm, increasing to 2 cm in key intervals. For each measurement 10-15 tests of the planktonic foraminifera *Globigerinoides ruber* were picked from the 250-315 µm size fraction and ultrasonically cleaned. The isotopic composition of the calcite tests was analysed with a *Europa Scientific Geo 2020* mass spectrometer at the National Oceanographic Centre Southampton (Southampton, United Kingdom). To obtain information about productivity and nutrient cycling the stable isotope of nitrogen were analysed in 5 cm intervals for KL 9 at the Royal Netherlands Institute for Sea Research (Den Burg, Texel, The Netherlands). For each measurement 40 to 50 mg of sediment were homogenised, decalcified (2N HCl), and finally freeze-dried. The nitrogen isotopic composition of organic matter was determined by a *Thermofinnigan Delta Plus* isotope ratio mass spectrometer connected on-line to a *Carlo Erba Instruments Flash 1112* elemental analyzer.

5.3 Data collection and processing

5.3.1 Faunal data

A minimum of 300 individual planktonic foraminifera were counted and determined to species level under the binocular in each investigated sediment sample. For counts of this size, the 95 % confidence level for the detection limit of a species corresponds to an observed abundance of 1 % [Dryden 1931; Revets 2004]. Therefore, the faunal data of each sample was purged of species not reaching 1 % relative abundance in order to eliminate any influence of rare species, which might or might not have been recorded by chance. The purged data were then recalculated to 100 %. The individual variables in compositional data are not linearly independent. This property may lead to overestimation of similarity between samples. Therefore, log-ratio transformed data was used in certain analyses concerning the similarity of faunal assemblages [Aitchison 1999; Aitchison et al. 2000]. Following the recommendations of Pollard and Blockley [2006], the transformation was performed on raw count data of the taxonomic units in question.

5.3.2. Environmental data

As there exist several candidates of environmental parameters for control of the planktonic foraminifera distribution in the Red Sea, a wider range of parameters than usual for planktonic foraminifera transfer functions was investigated, including temperature, salinity, primary productivity, water column stratification and oxygen concentration. Adopting the definitions of the MARGO project group [Kucera et al. 2005a], the temperature and salinity values used in all analyses represent the annual average of the 10 m depth level of the World Ocean Atlas 2001 [Levitus and NODC]. Satellite derived surface water chlorophyll *a* concentration data from the Ocean Color Web [Feldman and McClain 2006] were used as proxy for primary productivity. All data used from this source were averaged over the four-year period, July 2002 to June 2006. Although there exist model estimates of primary productivity [Behrenfeld and Falkowski 1997], these include certain generalised parameters which make them unsuited for the Red Sea. (e.g. parts of the Red Sea lie outside the temperature range of 1 to 29 °C). Nevertheless, for the Red Sea the correlation coefficients for the model-derived productivity estimates [Ocean Productivity Homepage] and the satellite-based chlorophyll *a* concentrations for the positions of the surface samples used in this study (n = 60) are 0.89 for annual values, 0.19 for the summer (JJA) and 0.93 for the winter season (DJF). The concept of water column stratification is difficult to condense into single number suitable for mathematical analysis. For the Red Sea, the estimates for the depth of the mixed layer are very shallow, ranging from 30 m in the south to around 70 m in the north of the basin [NODC WOA94]. These estimates reflect the first boundary, a stepwise increase in temperature or density, encountered in the water column and can neither indicate a second boundary nor differentiate between different strengths of the detected

boundary. Therefore, a more sophisticated index, the Brunt-Väisälä frequency (BVF), was employed as a measure of water column stratification. The BVF is the frequency with which a packet of water will oscillate when it is vertically displaced from its original position in the water column. High frequencies correspond to large density differences found typically in a stratified water column, whereas low frequencies will be found in a homogenous water column. The BVF values were calculated with the *Ocean Data View* software [Schlitzer 2007] for all depth intervals available in the World Ocean Atlas 2001 [Levitus and NODC]. The minimum, maximum and average of the BVF are highly correlated (average r = 0.95; n = 443) for any geographical position in the Red Sea, so that the maximum BVF of the top 250 m water column was chosen as the stratification parameter for use in the analyses. It holds no information about the depth of the mixed layer but has the considerable advantage that it is a measure of the intensity of any pycnocline present and the overall water column stability. To investigate possible effects of the OMZ in the southern Red Sea on the planktonic foraminifera assemblages, a measure of oxygen concentration was also included in the analyses. Oxygen concentration data was taken from the World Ocean Atlas 2001 [Levitus and NODC] and the depths of .the 3 ml, 2 ml and 1 ml O_2/l oxyclines were calculated by linear interpolation. The comparison of the values with oxygen concentration minima led to the choice of the minimal oxygen concentration of the top 150 m water column as the final variable to assess the influence of the oxygen minimum zone. Values of environmental parameters for the exact sample positions were extracted from a grid of the respective variable produced by the surface mapping software *Surfer 8.05* [Golden Software, Inc. 2004] using a kriging algorithm. In all cases, if not otherwise indicated, the annual average value of an environmental parameter was considered. Values for the summer season are the average of the months June to August, the winter season as the average of the months December to February.

5.4 Environmental gradient analysis

Since the environmental parameters in the Red Sea are mutually correlated, gradient analysis was employed to assist in their deconvolution. Gradient analysis is a family of statistical techniques that assist the interpretation of community composition in terms of species responses to environmental gradients [ter Braak and Prentice 1988]. These techniques base on the niche theory and concepts of ecological continua and gradients [Hutchinson 1957; Austin 1985]. Basically, gradient analysis combines species data and environmental data into one ordination space, thus showing the interrelations of these variables and offering the possibility of mathematically supported interpretations of species-environment-relations. Here, the analysis was performed using the *Canoco 4.5* software package [ter Braak and Smilauer 1997]. An initial detrended canonical correspondence analysis of the calibration dataset showed a gradient length of 1.89, suggesting that a linear species response model is appropriate for the analysis of the dataset [Leps and Smilauer 2003]. The shown

redundancy analysis was conducted with untransformed percentage data and scaling focus on species-correlations. Species and samples were centred and samples also standardised.

5.5 Taxonomy

Following the taxonomy of Hemleben et al. [1989] and Brummer and Kroon [1988], 30 species of planktonic foraminifera were identified in the > 150 µm size fraction of the surface sample set (Table 3, cf. Chapter 6.1 Design of a transfer function input matrix for explanation of the grouping). Scanning electron microscopy images were taken with a *LEO Model 1450 VP* Microscope at the University of Tübingen. As a measure of comparison for the absolute numbers mentioned in the following section, a total of 23,818 planktonic foraminifera were counted in the surface sample set.

included	excluded
Globigerina bulloides	*Beella digitata*
Globigerinella calida	*Gallitellia vivans*
Globigerinella siphonifera	*Globigerina falconensis*
Globigerinoides ruber	*Globigerinita minuta*
Globigerinoides sacculifer	*Globigerinita uvula*
Globigerinita glutinata	*Globigerinoides conglobatus*
Globorotalia menardii	*Globoquadrina conglomerata*
Globoturborotalita tenella	*Globorotalia anfracta*
Neogloboquadrina dutertrei	*Globorotalia inflata*
Neogloboquadrina incompta	*Globorotalia scitula*
Neogloboquadrina pachyderma	*Globorotalia truncatulinoides*
	Globorotaloides hexagonus
	Globoturborotalita rubescens
	Hastigerina digitata
	Hastigerina pelagica
	Orbulina universa
	Pulleniatina obliquiloculata
	Turborotalita humilis
	Turborotalita quinqueloba

Table 3 Species of planktonic foraminifera found in the surface sediment sample set and their employment in the developed transfer functions.

Species list:

Globigerina bulloides d'Orbigny, 1826 Plate I a

This species is abundant in the very south of the Red Sea and in the Gulf of Aden.

Globigerinella calida (Parker), 1962 Plate I b, c

This species is common in low numbers throughout the area of investigation and in morphology similar to *G. siphonifera* (cf. Plate I c and f). The distinctive morphotype b on Plate I was rarely encountered.

Globigerinella siphonifera (d'Orbigny), 1839 Plate I d-f

This species is abundant throughout the area of investigation and occurred in different morphotypes.

Globigerinoides sacculifer (Brady), 1877 Plate I g-i

This species was the most abundant one in this study. It occurs with a strong declining gradient from north to south in the Red Sea, but also with very low numbers in the Gulf of Aden. No differentiation between morphotypes (*sacculifer* vs. *trilobus*) was made, as their occurrence is related to the

reproductive cycle [Bijma and Hemleben 1994] and no significant differences in the ecology of the types could be demonstrated [e.g. Ravelo and Fairbanks 1990].

Globigerinoides ruber (d'Orbigny), 1839 Plate II a-d

This species occurs abundantly throughout the area of investigation. No differentiation between morphotypes was attempted due to the difficulty of the definition of reliable and objective criteria for their separation [Parker 1962]. No pink specimens were found in the surface sample set.

Globigerinita glutinata (Egger), 1893 Plate II e, f

This species is abundant and showed a gradient of increasing occurrence from north to south in the Red Sea.

Globorotalia menardii (Parker, Jones and Brady), 1865 Plate II g-i

This species occurs only in the very southern Red Sea and Gulf of Aden. Auras-Schudnagies et al. [1989] showed that this and other species reflect the advection of water masses from the Gulf of Aden into the Red Sea. Its abundance increases when larger size fractions are investigated, but in the 150 µm size fraction it is extremely rare in the Red Sea. For the small number of specimen found, *G. menardii* showed a great amount of morphological variability.

Globoturborotalita tenella (Parker), 1958 Plate III b, c

This species is common in low numbers throughout the area of investigation with a higher abundance in the northern Red Sea.

Neogloboquadrina dutertrei (d'Orbigny), 1839 Plate III d

N. dutertrei is subject to the same issues concerning abundance pattern and size as *G. menardii*.

Neogloboquadrina incompta (Cifelli), 1961 Plate III e

This species is common in low numbers throughout the area of investigation with higher abundances in the northern Red Sea.

Neogloboquadrina pachyderma (Ehrenberg), 1861 Plate III f, g

This species is common in low numbers throughout the area of investigation with higher abundances in the northern Red Sea. The occurrence of this species could possibly reflect advection of the small population of the *N. pachyderma* form that thrives in the upwelling cells of the western Arabian Sea [Schiebel et al. 2004], as the abundance of sinistral *Neogloboquadrina* individuals is much higher than what would be expected of the known anomalously sinistral specimens of *N. incompta* [Darling et al. 2006].

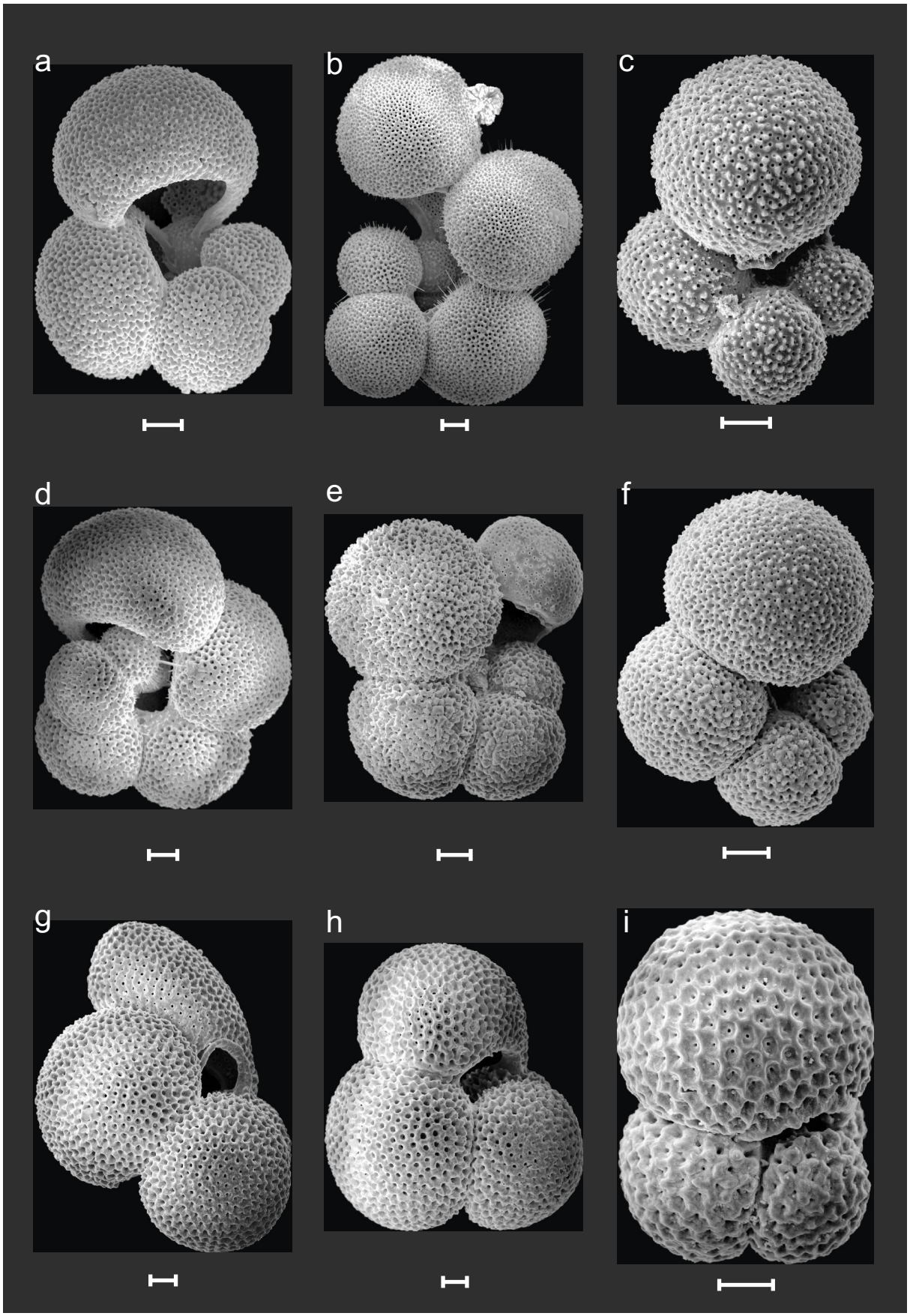

Plate I (a) *Globigerina bulloides* (b), (c) *Globigerinella calida* (d)-(f) *Globigerinella siphonifera* (g)-(i) *Globigerinoides sacculifer*. All scales are 50 µm.

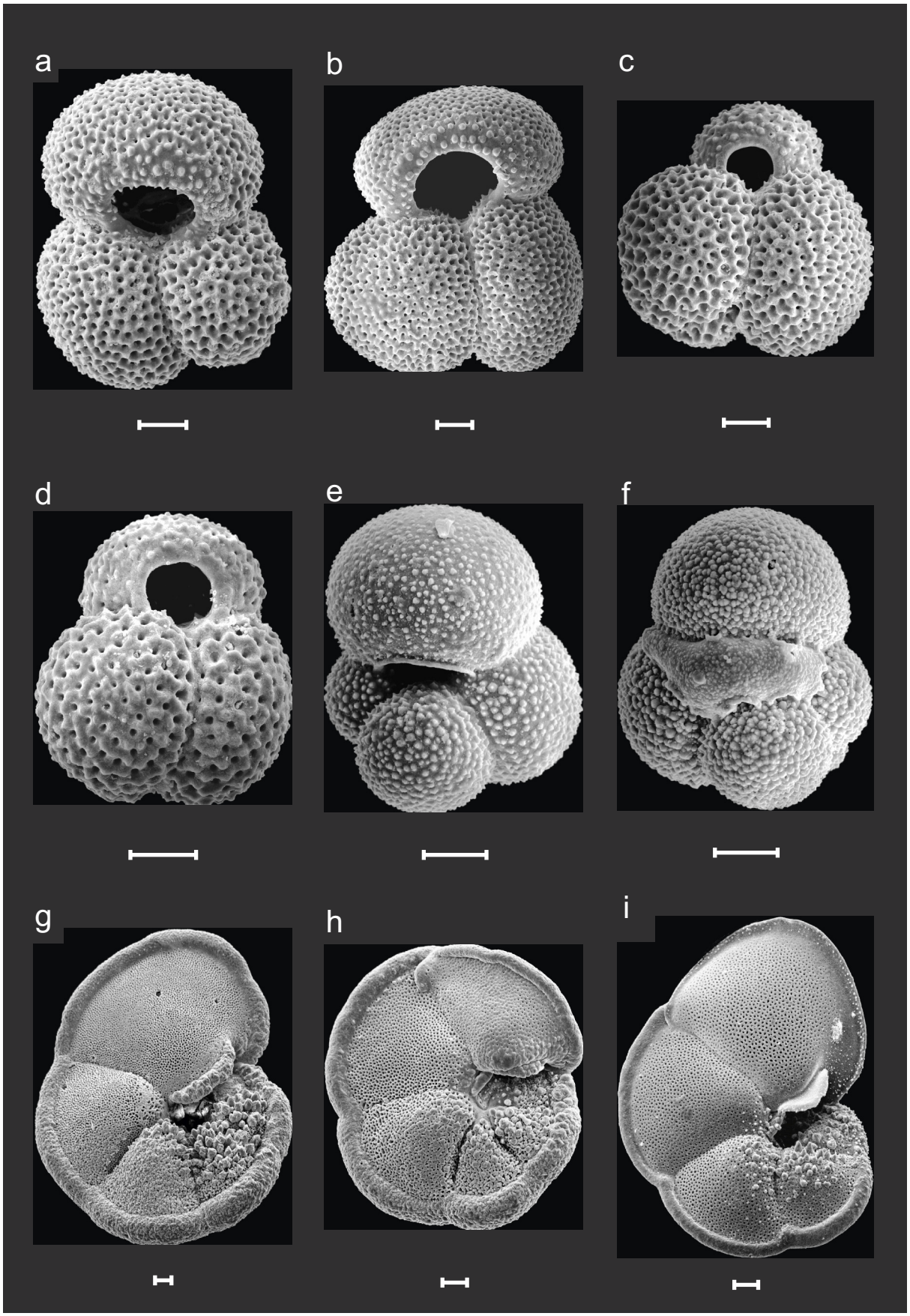

Plate II (a)-(d) *Globigerinoides ruber* (e), (f) *Globigerinita glutinata* (g)-(i) *Globorotalia menardii*. All scales are 50 µm.

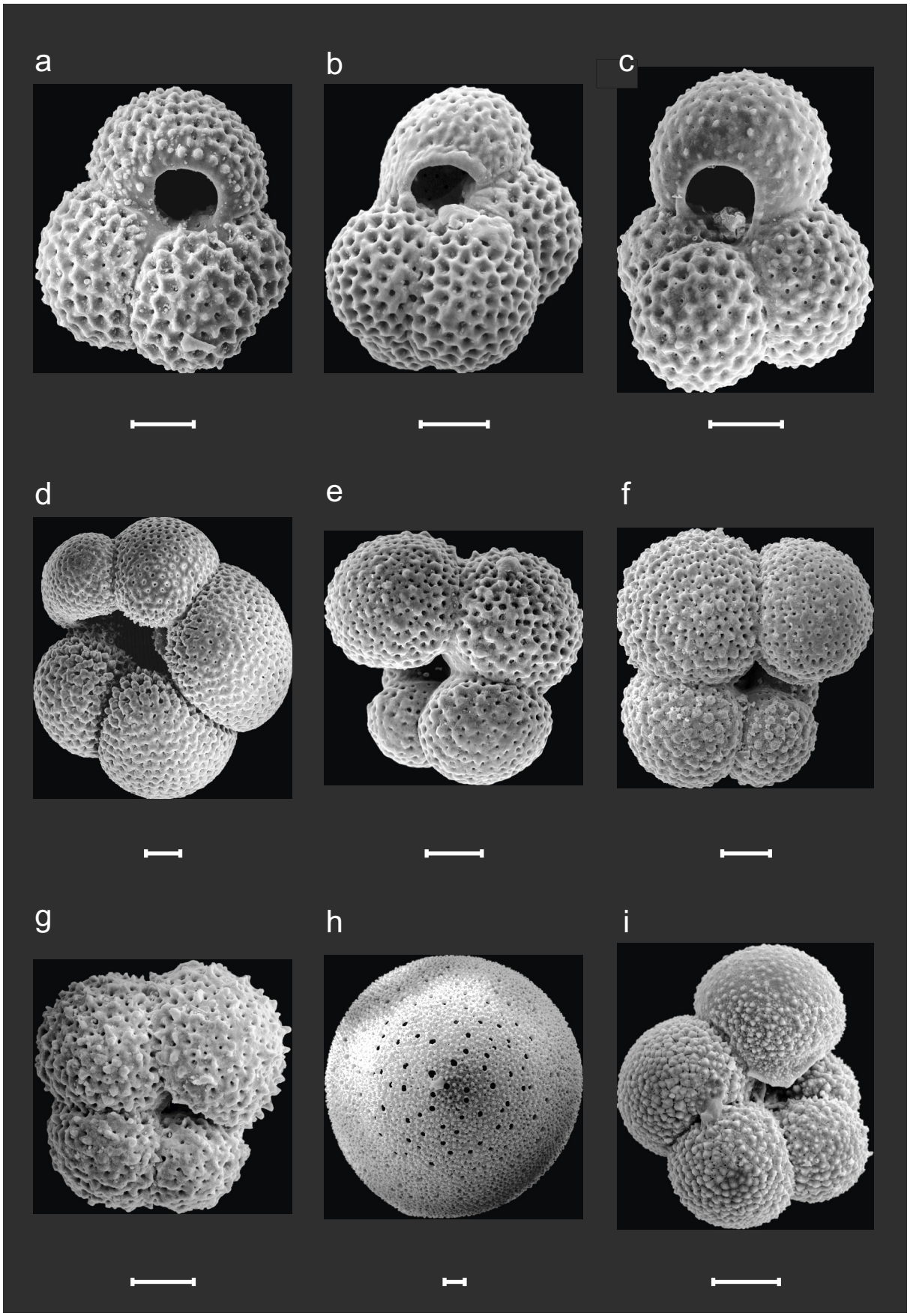

Plate III (a) *Globoturborotalita rubescens* (b), (c) *Globoturborotalita tenella* (d) *Neogloboquadrina dutertrei* (e) *Neogloboquadrina incompta* (f), (g) *Neogloboquadrina pachyderma* (h) *Orbulina universa* (i) *Turborotalita quinqueloba*. All scales are 50 µm.

Beella digitata (Brady), 1879
Eight individuals were identified, seven of these in the Gulf of Aden.

Gallitellia vivans (Cushman), 1934
Thirteen individuals were identified, eleven of these were found in a single sample from the southern Red Sea.

Globigerina falconensis Blow, 1959
Twelve individuals were identified, eight of these in the Gulf of Aden.

Globigerinita minuta (Natland), 1938
This species occurred in very low numbers throughout the area of investigation.

Globigerinita uvula (Ehrenberg), 1861
Eight individuals of this species were identified.

Globigerinoides conglobatus (Brady), 1879
Seven individuals were identified.

Globoquadrina conglomerata (Schwager), 1866
One individual was found in the northern Red Sea.

Globorotalia anfracta (Parker), 1967
This species occurred in very low numbers mostly in the southern Red Sea and the Gulf of Aden.

Globorotalia inflata (d'Orbigny), 1839
One individual was found in the central Red Sea.

Globorotalia scitula (Brady), 1882
This species occurred in very low numbers in the southern Red Sea and Gulf of Aden.

Globorotalia truncatulinoides (d'Orbigny), 1839
One individual was found in the central Red Sea.

Globorotaloides hexagonus (Natland), 1938
Five individuals were identified in the Gulf of Aden.

Globoturborotalita rubescens Hofker, 1956 Plate III a
This species occurs in low numbers throughout the area of investigation. The majority of the individuals show the typical pink colouration.

Hastigerina digitata (Rhumbler), 1911
Fourteen individuals of this species were identified.

Hastigerina pelagica (d'Orbigny), 1839
This species occurs in low numbers throughout the area of investigation.

Orbulina universa d'Orbigny, 1839 Plate III h
This species occurs in low numbers throughout the area of investigation.

Pulleniatina obliquiloculata (Parker and Jones), 1865
Three individuals were identified in the Gulf of Aden.

Turborotalita humilis (Brady), 1884
Three individuals were identified in the Gulf of Aden.

Turborotalita quinqueloba (Natland), 1938 Plate III i
This species appeared sporadically in about a quarter of the samples, more often in the southern Red Sea and the Gulf of Aden. Most individuals of this species were below 150 µm in size and appeared in the larger 150 µm size fraction as attachments to larger particles and other foraminifera. This made a representative count impossible. In samples were quantification was attempted, the abundance of this species never exceeded 12 %; the average abundance was 1.3 %.

5.6 Transfer functions

The surface sample dataset used for calibration of the transfer functions is with 60 samples comparatively small and therefore vulnerable to a method-specific bias [Kucera et al. 2005b]. Additionally, the foraminifera distribution data in the Red Sea can be expected to show a high measure of autocorrelation [Auras-Schudnagies et al. 1989], which is known to lead to the underestimation of error rates in certain methods [Telford et al. 2004]. These undesirable conditions led to the approach of employing a range of different transfer function methods with different sensitivities to the potential sources of error. The limited number of recent surface samples and their uneven distribution made the random selection of a validation subset impossible; instead the bootstrap approach (1000 cycles) was chosen for cross-validation of all methods except artificial neural networks. Due to the high time-demand for the training of artificial neural networks, no attempt was made to validate their results by bootstrapping. The estimated prediction error, the RMSEP, was calculated as the average RMSE of the bootstrapping cycles.

5.6.1 Analogy analysis

Three approaches for the identification of non-analogue samples were used in this study. The first was a joint principal component analysis of log-transformed downcore and calibration set faunal counts. In the subsequent plot of the factor scores of the samples as Cartesian coordinates, the axes have been scaled for their explained variance in the PCA (e.g. Figure 22). The distance between samples in this plot then becomes a more accurate measure of their similarity and thus analogy. This type of visualization also allows the quick identification of groups of samples sharing a certain type of fauna. Regarding the importance of sea level for the circulation and as such for all oceanographic parameters in the Red Sea, the oxygen isotope values as proxy for the exchange with the open ocean were taken into account in a second approach. A cross-plot of the first principal component of the log-transformed planktonic foraminifera abundance data of the four dominant species (Chapter 6.1 Design of a transfer function input matrix, Table 6) and the oxygen isotope values of the respective samples from the calibration dataset show a linear relationship (Figure 14), reflecting the fact that both variables capture the north-south gradient in the Red Sea. Samples from outside the Red Sea were omitted in this plot, as they do not follow this linear relationship. This type of analogy cross-plot can be utilised to assess the joint variation of fauna and environment. Analogue fossil samples will plot close to the regression line, as they should represent similar faunal assemblages (ordinate), which lived under similar circulation system conditions (abscissa). Fossil samples that plot outside the ranges of the PCA component (non-analogue fauna) or oxygen isotope values (non-analogue environment) of the calibration dataset can be identified as non-analogue even without this type of diagram. However, the advantage of this cross-plot is the ability to identify samples that are analogue in terms of the fauna but apparently stem from circulation (environmental) conditions different from those associated with this type of assemblage at present. These fossil samples will plot distant to the regression line but within the range of parameters encountered in the calibration dataset. The transfer function reconstructions of these samples should not be principally dismissed but considered to have a larger

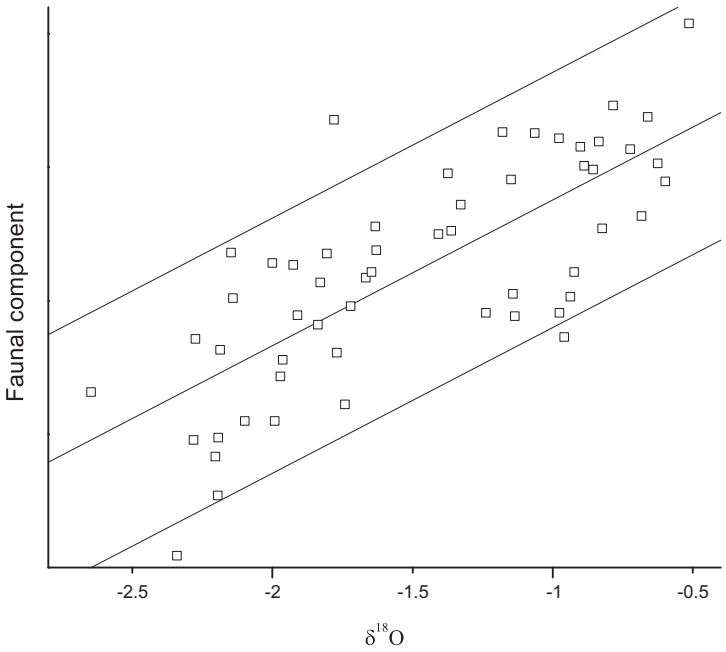

Figure 14 Environmental analogy plot of the calibration datset (Red Sea samples only). Lines represent the linear regression and the upper and lower margin of the 95 % confidence interval for values around the regression line.

uncertainty and be handled cautiously. The last, most simple and most practical approach is the plot of the minimal Bray-Curtis dissimilarity values between a fossil samples and its nearest analogue in the calibration dataset (see Chapter 5.6.2 Transfer function method configuration parameters) together with the reconstruction results.

5.6.2 Transfer function method configuration parameters

The Imbrie and Kipp method [IKM; Imbrie and Kipp 1971] was conducted using the *C2* software [Juggins 2003]. The Kaiser-Guttman criterion (Eigenvalue > 1) [Guttman 1954] was employed to limit the number of factors to three. Quadratic terms and cross products of the extracted factors were included in the regression.

The weighted averaging partial least squares method [WA-PLS; ter Braak and Juggins 1993] was performed by use of the *C2* software [Juggins 2003]. The decision on how many components to use was based on the respective RMSEP; in most cases two components yielded the lowest error.

Artificial neural networks (ANN) were constructed using the *NeuroGeneticOptimizer*© software [BioComp Systems 1997]. The developed back propagation networks consisted of a maximum of four neurons in one hidden layer. A population of 50 networks was trained over 25 generations. In a single generation a network was trained between minimally 50 and maximally 1000 times, depending on RMSE improvement. The software allows the application of a genetic algorithm to optimise the network structure (number of neurons and type of neuron function). After each generation the best quartile of networks was selected for further training, while the remainder was replaced by new randomly generated networks. Network fitness was based solely on the test set, consisting of 50 % of the surface sample set. The test set samples were randomly chosen by the software and each partition was manually checked for consistency in the coverage of the environmental gradient. Due to the high amount of contingency involved in the development of ANNs, the reported ANN results are the average of the five best networks obtained from five different training set partitions for any single factor.

The modern analogue technique [MAT; Hutson 1980] was conducted using the *C2* software [Juggins 2003]. Prell [1985] found that the squared chord distance performs best as the measure of similarity between samples. For this work the Bray-Curtis-dissimilarity [Bray and Curtis 1957] (Equation 1) was

Equation 1

$$BC_{ij} = 1 - \sum_{k=1}^{n} \frac{\left| x_{ik} - x_{jk} \right|}{x_{ik} + x_{jk}}$$

where x_{ik} is the abundance of the k^{th} species in sample i and n the total number of species

employed as similarity measure for it includes in contrast to the squared chord distance no square root transformation of the abundance data. The weighted average of the three most similar samples, which equals 5 % of the samples of the calibration dataset, was used as the reconstruction result.

5.6.3 Assessment of uncertainties on reconstructions

As outlined in chapter 4.1.3 Assessment of transfer functions (cf. Figure 12), the similarity between fossil samples and those in the calibration dataset as well as inter-method deviations of estimates can be employed to assess the reliability of transfer function reconstructions. The definition of a critical value for similarity, which objectively decides whether a downcore sample is similar to a samples from the calibration dataset is, no matter how sophisticated the arguments for or calculations of it may be, ultimately arbitrary. A commonly employed critical value of similarity is 0.25 [e.g. Gersonde et al. 2005]. De Vernal et al. [2005] considered the variance of their calibration dataset and used the average similarity of randomly picked sample pairs minus the corresponding standard deviation as the critical similarity value. For the calibration dataset of this study, the latter method would have resulted in a critical value of 0.1. For this study, a quarter of the maximal dissimilarity within the calibration sample set, that is incidentally also the dissimilarity between the northernmost sample from the Red Sea and the easternmost sample from the Gulf of Aden, was chosen as critical similarity value (D_{crit} = 0.74 / 4 = 0.185). The standard deviation of the RMSEP values for the IKM, MAT and WA-PLS approaches was used as a critical value for the detection of method-specific bias. This definition can be considered as a mild criterion, for the fact that ANN, the method with the perhaps lowest estimation error, is not included in the calculation.

5.7 Dating of samples

The special circulation system of the Red Sea complicates the calibration of sample ages obtained by radiocarbon dating. Different rates of water exchange through Bab al Mandab, caused by either changes in sea level and/or the forcing of the antiestuarine circulation system, alter the local radiocarbon reservoir ages. The effect of this becomes apparent when Holocene faunal census data from different cores along the basin axis are compared to each other. The construction of age models for the cores KL9 and KL17 VL solely on basis of the calibrated accelerator mass spectrometry (AMS) radiocarbon dates results always in a strong temporal incongruity of the faunal records. Modelling experiments and oceanographic observations, however, show that the Red Sea surface water behaves as one water body with a short residence time of around 20 years [Rohling et al. 2008a]. It is thus highly reasonable to assume that faunal variations throughout the Red Sea were in phase, reflecting changes in the oceanographic settings affecting the entire basin. Therefore, the radiocarbon AMS dates of several cores together with the respective faunal records were combined into one age model for the entire Red Sea. The different age models obtained are shown and discussed in chapter 7.1 Generalised Holocene age model.

5.7.1 Radiocarbon accelerator mass spectrometry dating

The ages for ten samples (Table 4) from cores KL9 and KL17 VL were obtained by radiocarbon AMS dating of hand-picked tests of the planktonic foraminifera *Globigerinoides sacculifer* (250-315 µm size fraction). The analyses were performed at the Leibniz Labor für Altersbestimmung und Isotopenforschung Kiel, Germany. Calibration of radiocarbon dates was performed with the program *Calib 5.0.2* [Stuiver and Reimer 1993], using the *Marine04* calibration [Hughen et al. 2004] with a ΔR of 170 years and a ΔR uncertainty of 64 years. These values are the basin-wide averages taken from the *Marine Reservoir Correction Database* [Reimer and Reimer 2001]. In the literature, cores from the northern Red Sea and the Gulf of Aqaba were calibrated with this value [Arz et al. 2006a], a ΔR of 180 years [Arz et al. 2006b] or a ΔR of 100 years [Arz et al. 2003a].

Lab.-ID	Depth [cm]	Conventional age [a BP]	± Error [a]	Calibrated age ranges [1σ cal. a BP]		[2σ cal. a BP]	
KL9							
KIA33786	2.25	1315	25	639	761	562	852
KIA33785	24.25	3260	25	2771	2943	2728	3054
KIA36807	30.25	3465	25	3039	3242	2942	3324
KIA36808	50.25	4950	30	4950	5195	4856	5258
KIA33130	60.25	6595	35	6798	6999	6732	7125
KIA33131	84.25	8955	40	9390	9524	9270	9603
KL17 VL							
KIA36802*	0.5	520	25	0	132	0	234
KIA36803	7.5	1495	30	782	933	712	1023
KIA36804	21.5	3455	30	3021	3230	2926	3319
KIA36805	92.5	10340	50	11109	11234	10925	11341

Table 4 Sample ages obtained by radiocarbon accelerator mass spectrometry dating. * A ΔR of 70 was used to avoid a negative calibrated age.

5.7.2 Date synchronisation by correlation of faunal data

The faunal data and radiocarbon datings of cores KL9 and KL17 VL were supplemented with data from four additional records from the Red Sea: the piston core KL11 [Schmelzer 1998] and three multicorers MC91, MC93 and MC98 [Edelman 1996; Edelman-Furstenberg et al. 2009] (Table 2, Figure 13). Using the mid-point of the calibrated 1σ age ranges as a starting configuration, the records were aligned to achieve maximal congruency of the faunal data, while keeping the deviation of sample ages from their radiocarbon datings to a minimum. Where no dated tie points existed but the alignment could be significantly improved, additional control points without reference to a radiocarbon date were inserted into the records (cf. Table 13). Only the four dominant taxa, *G. sacculifer*, *G. ruber*, *G. glutinata* and *G. siphonifera* were used for this alignment. Where age inconsistencies in alignment between different taxa occurred, emphasis was given to the dominant taxon. Next to the faunal data, the sedimentation rates of the records were monitored during the alignment process and checked for unrealistically frequent and large changes.

5.7.3 Orbital tuning

For the determination of sample ages surpassing the reaches of radiocarbon dating, the isotopic record of KL9 was compared to the SPECMAP time scale [Imbrie et al. 1984; Imbrie et al. 1990]. Identified isotopic events were matched and ages between these control points were calculated by linear interpolation.

6 Development of transfer functions for the Red Sea

6.1 Design of a transfer function input matrix

A total of 30 different species of planktonic foraminifera in the size fraction > 150 µm were identified in the surface sample set (Table 3). Species overall abundances were unevenly distributed with the three most abundant species, *G. sacculifer*, *G. ruber* and *G. glutinata* together contributing 73.4 %, while eighteen rare species occurred in overall abundances below 0.5 %. Because of the low signal to noise ratio and due to the low ecological significance of rare species, which can be assumed to be especially pronounced under the oligotrophic conditions of the Red Sea (< 1 individual planktonic foraminifer per m³ in the top 100 m water column of the central Red Sea [Weikert 1982]), the mathematical analyses of the data were based on a filtered dataset. The first criterion for inclusion of a species into the calibration dataset was an overall abundance of at least 0.5 %, translating into a minimum of 119 specimens in the entire calibration dataset. The matrix of the thirteen species fulfilling this requirement (Table 5) was than further modified as following:

	Overall abundance [%]	Occurence [%]
Globigerina bulloides	2.5	17
Globigerinella calida	2.4	73
Globigerinella siphonifera	11.3	100
Globigerinoides ruber	27.1	100
Globigerinoides sacculifer	29.3	97
Globigerinita glutinata	17.0	100
Globoturborotalita rubescens	0.9	49
Globoturborotalita tenella	1.7	63
Hastigerina pelagica	0.6	28
Neogloboquadrina incompta	1.6	63
Neogloboquadrina pachyderma	2.2	70
Orbulina universa	1.1	55
Turborotalita quinqueloba	1.4	27
Globorotalia menardii	0.4	8
Neogloboquadrina dutertrei	0.2	7

Table 5 Overall abundance (percentage of the total of individuals) and occurrence (percentage of samples with species present) of selected planktonic foraminifera species in the calibration dataset.

- **Fusion:** *G. siphonifera* and *G. calida* were combined into one taxonomic unit to avoid the possible error of misidentifications due to the difficulty in differentiation between these species [e.g. Hayes et al. 2005] (cf. Plate I). The species *N. pachyderma* and *N. incompta* were also merged because they differ only in their coiling direction [Darling et al. 2006] and the taxonomic significance of this character outside the polar and subpolar waters could not yet be established. Any reference to *G. siphonifera* from here onwards thus refers to the counts of this species and those of *G. calida*. The same applies to *N. pachyderma* and *N. incompta*.
- **Deletion:** The species *T. quinqueloba* was deleted as most individuals found were below 150 µm in size and appeared in the > 150 µm size fraction only because they were attached to larger particles and other foraminifera. The species *G. rubescens*, *H. pelagica* and *O. universa* were excluded due to their low association with the environmental parameters investigated and thus negligible value as

signal carriers. The first three canonical axes of an initial redundancy analysis could not explain even 10 % of the variance of any of these species (Table 7).

- **Addition:** The species *G. menardii* and *N. dutertrei* were in mathematically reliable numbers only found in samples from the Gulf of Aden and therefore combined into one new taxonomic unit, the Gulf of Aden species. Earlier studies of plankton tows from the Red Sea concluded that these species are advected into the Red Sea and do not reproduce within the basin [Auras-Schudnagies et al. 1989; Ganssen and Kroon 1991]. This group could therefore serve as an indicator of a stronger inflow of waters from outside the Red Sea.

	Axis 1	Axis 2	Axis 3
Eigenvalue	**0.73**	**0.05**	**0.02**
Globigerina bulloides	0.71	0.86	0.89
Globigerinella calida	0.08	0.08	0.08
Globigerinella siphonifera	0.25	0.26	0.42
Globigerinoides ruber	0.03	0.30	0.36
Globigerinoides sacculifer	0.90	0.90	0.90
Globigerinita glutinata	0.89	0.92	0.93
Globoturborotalita rubescens	0.00	0.00	0.01
Globoturborotalita tenella	0.13	0.29	0.38
Hastigerina pelagica	0.01	0.01	0.03
Neogloboquadrina incompta	0.03	0.29	0.29
Neogloboquadrina pachyderma	0.15	0.41	0.41
Orbulina universa	0.01	0.02	0.06
Gulf of Aden species	0.44	0.57	0.85

Table 7 Eigenvalues of the first three canonical axes and cumulative fit per species as fraction of variance of the species in a redundancy analysis of species abundances and annual mean values of environmental parameters for the Red Sea calibration dataset.

The final input matrix for the transfer functions comprises eight taxonomic units encompassing eleven species (Table 6). This matrix is now robust in terms of its mathematical reliability and ecological meaning and comprises 95.4 % of the foraminifera assemblage data. The distribution patterns of these taxonomic units in our new surface sediment dataset (Figure 15) are consistent with the results of the only other study concerning the distribution of planktonic foraminifera in the Red Sea by Auras-Schudnagies et al. [1989]. *G. sacculifer*, the most abundant unit, shows a distinct gradient from north to south with two maxima of around 60 % standing out from the average relative abundance of 40 % in the northern half of the Red Sea. South of 16° N in the Red Sea and in the Gulf of Aden the abundance of *G. sacculifer* decreases to below 2 % and in two samples no specimens of this species were recorded. The distribution pattern of *G. glutinata* is almost perfectly complementary to that of *G. sacculifer*. It shows maximal abundances of almost 50 % in the southern Red Sea and is in the Gulf of Aden with around 30 % slightly more abundant than in the south of the Red Sea. *G. ruber* is abundant throughout the area of investigation with abundances above 20 % and shows an abundance maximum of almost 40 % in the convergence zone around 18° N where the highest SST in the Red Sea is recorded (cf. Figure 3 and 9). *G. siphonifera* is of all units most

Taxonomic unit	Overall abundance [%]	Cumulative overall abundance [%]
G. sacculifer	29.3	29.3
G. ruber	27.1	56.4
G. glutinata	17.0	73.4
G.siphonifera + *G. calida*	13.7	87.1
N. pachyderma + *N. incompta*	3.9	91.0
G. bulloides	2.5	93.5
G. tenella	1.7	95.2
Gulf of Aden species	0.5	95.7

Table 6 Overall abundance of taxonomic units included in the transfer function input matrix.

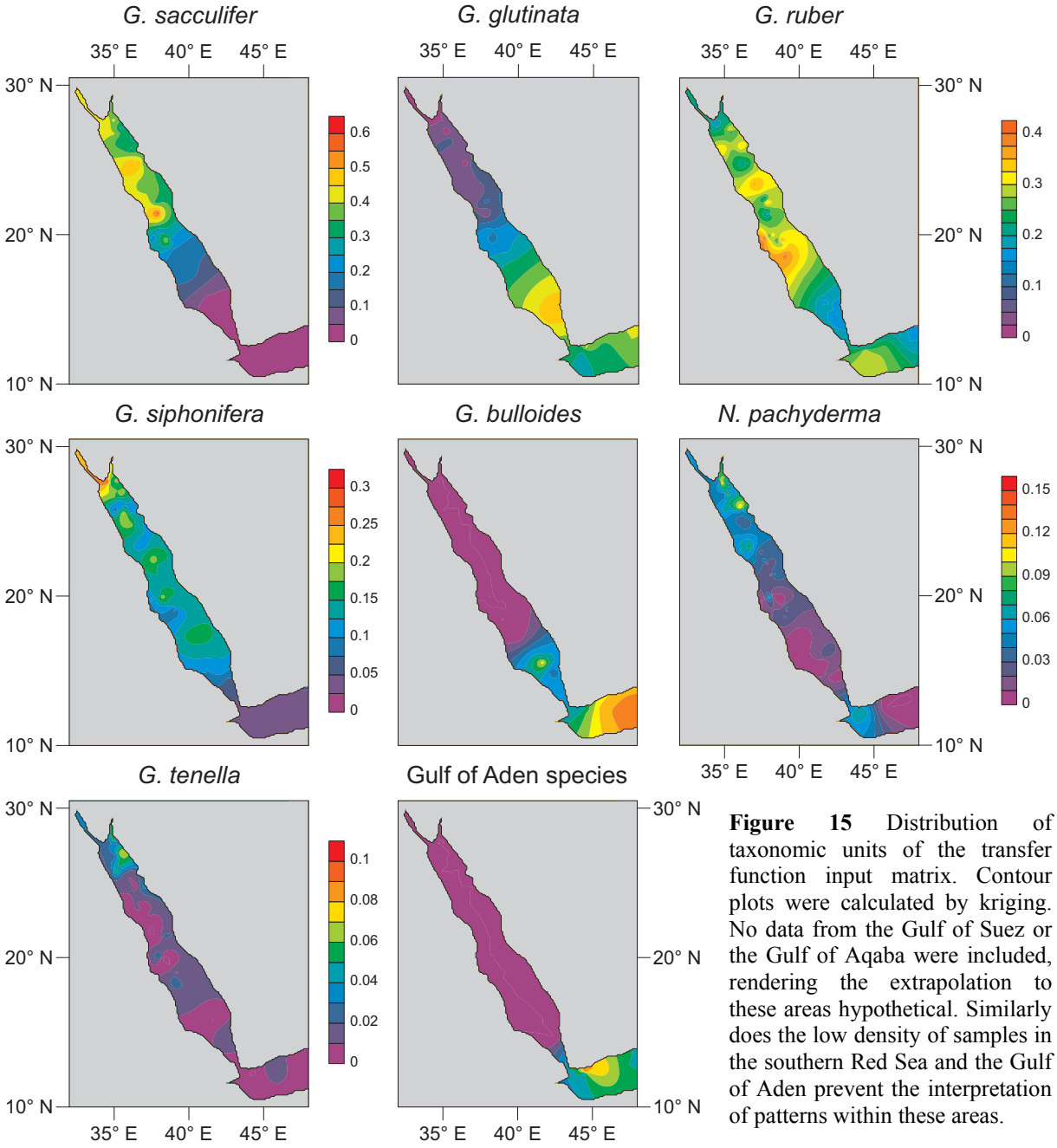

Figure 15 Distribution of taxonomic units of the transfer function input matrix. Contour plots were calculated by kriging. No data from the Gulf of Suez or the Gulf of Aqaba were included, rendering the extrapolation to these areas hypothetical. Similarly does the low density of samples in the southern Red Sea and the Gulf of Aden prevent the interpretation of patterns within these areas.

evenly distributed throughout the Red Sea with abundances of around 15 %. Outside the basin, its abundance decreases to below 5 %. *G. bulloides* is with abundances around 20 % common in the Gulf of Aden, while it is restricted to the area south of 16° N in the Red Sea with abundances below 10 %. A distinct abundance maximum of just above 20 % is recorded in one sample at 15.5° N. The taxonomic unit *N. pachyderma* is with abundances just below 5 % common in the northern half of the Red Sea, reaching abundances above 10 % in two samples in the very north. It also appears in the proximal samples from the Gulf of Aden with abundances just above 5 %. *G. tenella* is typical for the northern Red Sea but attains abundances above 5 % only in a small area. The Gulf of Aden species unit is restricted to its name-giving basin; only singular specimens belonging to this unit were found in samples from within the Red Sea. This finding is in contrast to that of Auras-Schudnagies et al.

[1989], but can be explained by the different size classes under investigation. The mentioned study analysed the > 250 µm size class and accordingly recorded higher relative abundances of these large species, compared to the > 150 µm size fraction analysed in this study.

The question whether the distribution reflects features of the surface circulation is difficult to answer and will not be addressed mathematically within the scope of this work. The low density of only 60 sediment surface samples in combination with the disagreement between different oceanic circulation models and real observations do not allow meaningful conclusions on the influence of surface water circulation features on the spatial distribution of planktonic foraminifera species in Red Sea sediments. The species composition in sediment samples is temporally averaged over many decades as well as spatially by the advection of sinking specimens. However, do the local abundance minima and maxima of *G. sacculifer* in the northernmost part of the basin coincide with modelled (cf. Figure 8) [Sofianos and Johns 2003; Biton 2006] and observed [Morcos 1970; Clifford et al. 1997] cyclonic and anticyclonic features of the surface circulation. The suspicious abundance maximum of *G. bulloides* in the southern Red Sea is in good agreement with the position of a mesoscale gyre between 15° N and 16° N, which reverses its rotation between winter and summer [Sofianos and Johns 2003].

	Temperature	Salinity	Chlorophyll	Stratification	Oxygen
Salinity	-0.689				
Chlorophyll	0.421	-0.773			
Stratification	0.797	-0.809	0.816		
Oxygen	-0.572	0.951	-0.851	-0.818	
Position	-0.725	0.996	-0.751	-0.820	0.939

Table 8 Correlation matrix of environmental parameters (annual mean values) including a measure of the position (N>S) along the axis of the Red Sea.

6.2 Environmental control on planktonic foraminifera distribution

For a study that seeks to relate a faunal assemblage to its environment, the choice of environmental variables is critical. Since the Red Sea is characterised by a range of unusual environmental conditions, a wider range of environmental variables than usually employed in planktonic foraminifera transfer functions was investigated in this study. Additional to the standard paleoceanographical parameters temperature, salinity, and productivity (chlorophyll *a* concentration serves here as the best available proxy), measures of water column stratification and the properties of the oxygen minimum zone were included in the analyses (see Chapter 5.3.2. Environmental data for the definition of these parameters). Due to the combination of the north-south orientation of the Red Sea basin and the restricted water exchange with the open

	annual / summer	annual / winter	summer / winter
Temperature	0.937	0.971	0.842
Salinity	0.994	0.992	0.979
Chlorophyll	0.774	0.984	0.759
Stratification	0.949	0.989	0.897
Oxygen	0.986	0.988	0.949

Table 9 Seasonal autocorrelation matrix of seasonal values of the environmental parameters of the surface sample set.

ocean only at its southern end, all oceanographic parameters in the basin are highly correlated (Table 8, cf. Chapter 2.3.2 Surface water circulation and properties).

Temperature and chlorophyll *a* concentration show the lowest, albeit still highly statistically significant correlation with the north-south gradient. Correlation analysis of the seasonal values of the environmental parameters (Table 9) indicates that the annual values reflect the winter circulation conditions and that even though a strong seasonality in climate over the Red Sea region exists, it does in most cases not significantly affect the shape of the environmental parameter gradients. Standing out in Table 9 is the chlorophyll *a* concentration with the lowest correlation of summer and winter values to the annual average, showing that the pattern of productivity does change seasonally. The high correlation among environmental parameters is clearly seen in the redundancy analysis (Figure 16, Table 10). It shows the dominance of one single parameter, capturing 74.2 % of the variance, underlying the distribution of the planktonic foraminifera taxonomic units. This one parameter is highly correlated with salinity, oxycline depth, stratification and chlorophyll *a* concentration and can be almost equated to the geographical position along the basin's axis (cf. Table 8). The second axis explains only 6.1 % of the

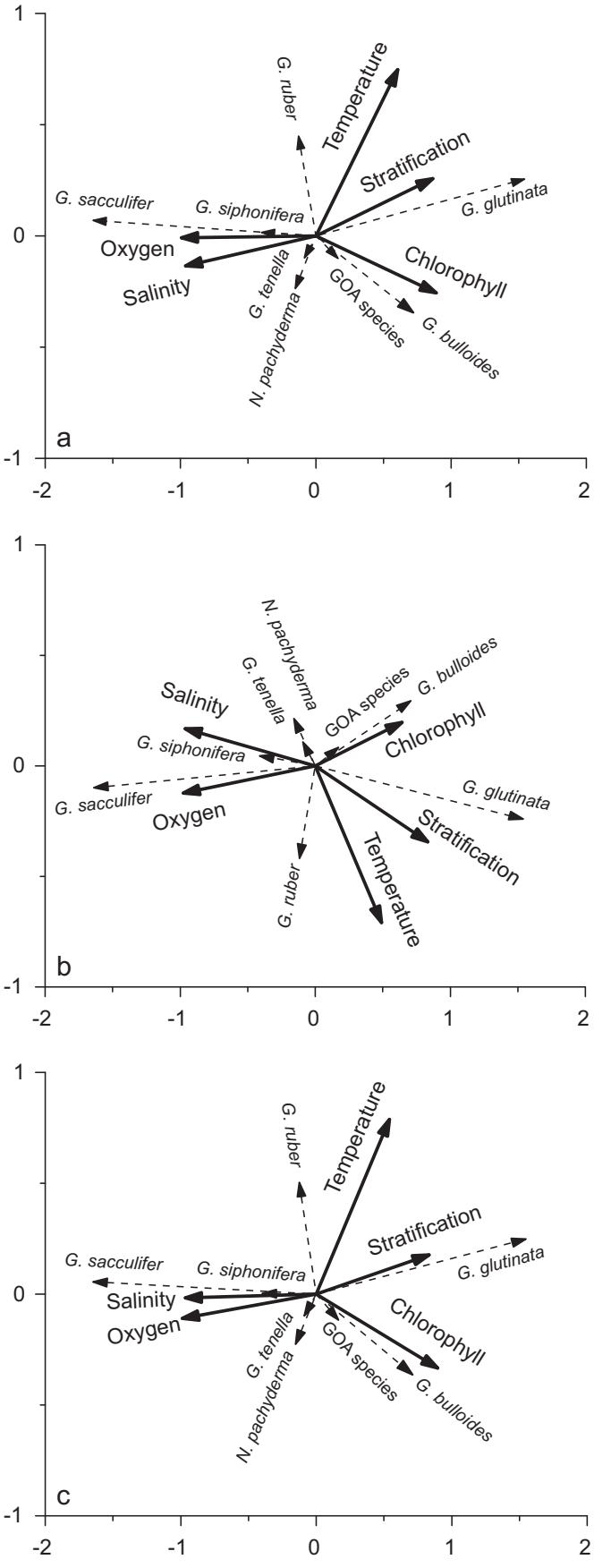

Figure 16 Redundancy analysis plots of the transfer function input matrix with annual (a), summer (b) and winter values (c) of environmental parameters.

	Axis 1			Axis 2			Axis 3					
	annual	summer	winter	annual	summer	winter	annual	summer	winter			
Eigenvalue	0.742	0.735	0.706	0.061	0.051	0.064	0.020	0.023	0.025			
Species-environment correlation	0.978	0.973	0.974	0.780	0.721	0.811	0.622	0.655	0.597			
Cumulative percentage variance												
of species data	74.2	73.5	70.6	80.3	78.5	77.0	82.3	80.9	79.5	captured variance of species data in singular analysis		
of species-environment relation	89.8	90.1	88.4	97.1	96.4	96.4	99.5	99.3	99.4			
Correlation										annual	summer	winter
Temperature	0.593	0.477	0.527	0.582	-0.511	0.633	0.037	-0.270	-0.044	30.7	20.6	25.8
Salinity	-0.940	-0.935	-0.942	-0.106	0.122	-0.014	0.140	-0.122	0.101	68.8	68.1	65.8
Chlorophyll	0.846	0.811	0.813	0.201	-0.248	0.142	0.217	-0.105	0.300	59.3	30.1	57.6
Stratification	0.870	0.626	0.874	-0.200	0.143	-0.268	0.153	-0.287	0.102	56.2	51.7	49.9
Oxygen	-0.970	-0.951	-0.965	-0.006	-0.089	-0.089	0.019	-0.070	-0.022	73.0	67.2	69.1

Table 10 Redundancy analyses results of the transfer function input matrix and the different seasonal values of environmental parameters.

variance and correlates highest with temperature and chlorophyll *a* concentration. Further axes add only negligible amounts to the explained variance of the species distribution (2 % and 0.4 %, data for the fourth axis not shown). The comparison of redundancy analyses for the distinct seasons (Table 10, Figure 16) reveals no significant differences and confirms the conclusion of the correlation analyses. In the following discussion of the individual parameters will therefore focus on the annual values.

- **Temperature** is the dominant controlling factor for the distribution of planktonic foraminifera in global oceans [Morey et al. 2005], yet it appears to have little effect on the fauna of the Red Sea, where it shows the least explanatory power (captured variance, Table 10) for the recent distribution of planktonic foraminifera. This low explanatory power (30.7 % of the species variance) of temperature is supplemented by the fact that the associations of species with temperature trends in the Red Sea contradict open-ocean observations, in which *G. sacculifer* is associated with higher SST than *G. ruber* [e.g. Prell 2003; Lombard et al. 2009]. On the other hand, the taxonomic unit *N. pachyderma*, typical for polar and upwelling regions, is correctly associated with low temperatures.

- **Salinity** shows the second highest explanatory power among the investigated parameters. However, neither analyses of the global distribution of planktonic foraminifera [Morey et al. 2005] nor laboratory experiments [Bijma et al. 1990] indicate a strong influence of salinity on planktonic foraminifera. A valid argument against this factor exerting a primary control on the recent foraminifera distribution in the Red Sea comes from the analysis of species disappearances during sea-level lowstands in the very same basin during the late Pleistocene [Fenton et al. 2000]. Throughout MIS 3, when sea level was approximately 60 m lower than today [Shackleton 1987; Siddall et al. 2003] and salinity in the Red Sea significantly higher [Thunell et al. 1988; Rohling 1994; Hemleben et al. 1996], *G. ruber* remained the dominant species, whereas the species which nowadays seem to be associated with high salinities, *G. sacculifer*, had almost disappeared from the Red Sea at that time.

Therefore the high correlation of the factor salinity with the first axis in the redundancy analysis is not based on ecological control of the species assemblage by this parameter, but rather to the fact that it faithfully reflects the general circulation system of the Red Sea.

- **Chlorophyll *a*** concentration was used as a proxy for primary productivity and ranks third in explanatory power among the investigated parameters. Several studies have demonstrated the response of the planktonic foraminifera community to primary productivity on regional [Thiede 1975; Ortiz et al. 1995; Watkins et al. 1996; Watkins and Mix 1998; Cayre et al. 1999; Ivanova et al. 2003; Zaric et al. 2005; Ishikawa and Oda 2007] and global scale [Morey et al. 2005]. Primary productivity has also already been invoked as an explanation for the faunal gradient in the Red Sea [Auras-Schudnagies et al. 1989; Hemleben et al. 1996]. A number of species of planktonic foraminifera have been consistently associated with different productivity regimes: *G. bulloides* has been recognised as indicator species for upwelling conditions [Thiede 1975; Peeters and Brummer 2002; Schiebel et al. 2004], as has *G. glutinata* [Naidu and Malmgren 1996; Ishikawa and Oda 2007]. Also without upwelling conditions present in the respective study areas, these species have been associated with increased levels of primary productivity [Ortiz et al. 1995; Watkins and Mix 1998; Cayre et al. 1999; Schiebel et al. 2001; Schulz et al. 2002; Zaric et al. 2005]. The species *G. sacculifer*, *G. ruber* and *G. siphonifera* are correspondingly considered as indicators for low productive water masses [Thiede 1975; Watkins et al. 1996; Watkins and Mix 1998; Cayre et al. 1999; Peeters and Brummer 2002]. The RDA results of this study are in perfect agreement with these findings, the species *G. bulloides*, *G. glutinata* are as highly correlated with high productivity levels as *G. sacculifer* and *G. siphonifera* are with low ones. The indiscriminate positioning of *G. ruber* along the productivity axis between these two pairs is supported by the results of Zaric et al. [2005] and Naidu and Malmgren [1996], but conflicts with those of Bé and Hutson [1977]. In accordance with the latter and based on plankton tows with monthly resolution from the Gulf of Aqaba and the northernmost Red Sea, Almogi-Labin [1984] associated *G. ruber* with the least, *G. sacculifer* with intermediate and *G. siphonifera* with the most productive conditions. Different ecophysiological traits of the foraminifera species must be responsible for this clear distribution along gradients of primary productivity, as no simple concurrence model can be invoked for planktonic foraminifera. The harbouring of symbionts (e.g. *G. sacculifer*) provides a species with a certain degree of autotrophy and thus gives it an advantage in oligotrophic conditions compared to non-symbiont bearing species (e.g. *G. bulloides*). The prey spectrum, both in quality and size, is another trait where planktonic foraminifera differ substantially. Non-spinose species (e.g. *G. glutinata*) were reported as generally herbivore and spinose species as omni-(e.g. *G. ruber*) to carnivore (e.g. *G. sacculifer*) [Spindler et al. 1984; Hemleben et al. 1989]. Since zooplankton abundance is highly correlated with phytoplankton abundance [e.g. Lampert and Sommer 1993], differences in food preference alone can hardly introduce any differences in the species composition of planktonic foraminifera with variable productivity. However, distinctions in

prey type are almost invariably connected with distinctions in prey size (phytoplankton being smaller than zooplankton), and thus allow by invoking more complex ecological concepts, like the determination of plankton size by Top-Down or Bottom-Up control of the trophic cascade [e.g. Lampert and Sommer 1993], alterations of the foraminifera species composition along a productivity gradient. Ortiz et al. [1995] proposed that water turbidity, an indirect effect of different productivity regimes, has an influence on the community structure of planktonic foraminifera. This factor would concern symbiont-bearing foraminifera only and promote the survival of shallow-living species compared to deeper dwelling ones. Consequently it requires differences in the depth habitat of foraminifera species, which are covered in the following paragraph about stratification.

- **Stratification** ranks only minimally below the factor chlorophyll in terms of explained variance in the redundancy analysis. Stratification of the water column could affect planktonic foraminifera species selectively and consequently alter the composition of the assemblage as a whole [Edelman-Furstenberg et al. 2009]. An intense and shallow pycnocline could deny a species its preferred depth habitat or prevent it from reaching its preferred depth for reproduction. Reliable direct data on these depths is difficult to obtain as the density of planktonic foraminifera in plankton tows is low and plankton tows are only point observations in space and time. Yet, the literature data on this topic agrees on that the three most abundant species in this study *G. sacculifer*, *G. glutinata* and *G. ruber* are all mixed layer species. *G. sacculifer* is the shallowest living species, occurring mainly in the upper 60 m together with *G. ruber* [Bé and Hutson 1977; Erez and Honjo 1981; Fairbanks et al. 1982; Pujol and Vergnaud Grazzini 1994; Watkins et al. 1996; Schiebel et al. 2001; Peeters and Brummer 2002; Anand et al. 2003; Kuroyanagi and Kawahata 2004; Loncaric et al. 2006], which is also found deeper than 100 m [Loncaric et al. 2006]. *G. glutinata* shows the widest depth range [Watkins et al. 1996; Schiebel et al. 2001; Kuroyanagi and Kawahata 2004] and is reported from depths of up to 200 m [Fairbanks et al. 1982; Pujol and Vergnaud Grazzini 1994] or deeper [Loncaric et al. 2006]. Analyses of the isotopic composition of the foraminifera tests infer slightly shallower depth ranges [Rohling et al. 2004; Farmer et al. 2007] but also detect a signal of gametogenic calcification at depth for the species *G. sacculifer* [Bé 1980; Lohmann 1995; Anand et al. 2003; Spero et al. 2003; Rohling et al. 2004]. These findings are consistent with reproduction depth of around 80 m inferred from plankton tows by Bijma and Hemleben [1994]. In the redundancy analysis, *G. glutinata* is associated with the most and *G. sacculifer* with the least intense stratification. As the employed measure of stratification is highly correlated with the mixed layer depth in the recent Red Sea, this association would not coincide with the observed habitat depth ranges for the respective species. A less successful reproduction of *G. sacculifer* under conditions of intense stratification could be imagined, but this line of argumentation conflicts with the only slightly diminished abundance of *G. siphonifera* in the stratified waters in the southern Red Sea; a species that is generally considered as living deeper than any of the three discussed species [e.g. Erez and Honjo 1981; Fairbanks et al. 1982; Bijma et al. 1992;

Rohling et al. 2004]. Furthermore, a study on stable isotopes from the tropical Atlantic showed that the depth habitat range of *G. sacculifer* populations is adapted to the stratification of the water column, extending deeper with a deep thermocline or staying shallower with a shallow thermocline [Steph et al. 2009]. This adaptability of habitat range is supported by results from plankton tows in the central Red Sea [Weikert 1982], which showed that 91 % of the total planktonic foraminifera individuals were found within the top 100 m of the water column. It also complies with findings from the northernmost Red Sea and the Gulf of Aqaba, which both show almost no stratification of the water column, where *G. sacculifer* was reported from depths of up to 300 m [Almogi-Labin 1984]. The positioning of *G. glutinata* along the stratification gradient does however fit well with its known preference of conditions of nutrient entrainment in depth by an intense pycnocline [Schiebel et al. 2004]. This again would primarily be the result of the pattern of primary productivity in the overlying surface water. While some studies find a dependence of the planktonic foraminifera distribution on the hydrographic structure of the water column [Ravelo et al. 1990; Chen and Prell 1998], most probably by ignoring any other environmental factor than temperature and salinity, our results indicate that stratification appears not to exert a primary control on the foraminifera distribution in the Red Sea.

- **Oxygen** concentration ranked highest in terms of explained variance in the redundancy analysis. The significant differences between epipelagic and mesopelagic zooplankton communities in the central Red Sea have been attributed to the presence and intensity of the oxygen minimum layer [Weikert 1982; Beckmann 1984]. Similarly Fenton et al. [2000] and Edelman-Furstenberg et al. [2009] suggested that the extent and intensity of the oxygen minimum zone in the Red Sea is critical for the ratio of *G. sacculifer* to *G. ruber* and, due to the large abundances of these two species for the foraminifera assemblage as a whole. The oxygen minimum zone could affect the planktonic foraminifera if the dissolved oxygen concentration in their habitat depth attains values low enough to impair foraminifera on an organismic level. So far, there exist no studies concerning the effect of low oxygen concentrations on planktonic foraminifera, but from benthic foraminifera it is known that O_2 concentrations above 1 ml/l do neither affect individual foraminifera nor the community composition [e.g. Bernhard and Gupta 1999]. Bijma et al. [1992] concluded that the oxygen supply provided by photosynthesizing symbionts is the limiting factor for the growth of individual spinose planktonic foraminifera, but could not provide experimental or convincing theoretical (calculation of diffusion rates) proof for their considerations. One should expect that symbiont-bearing foraminifera gain an advantage from their dinoflagellate symbionts in terms of oxygen supply, rather than being limited in growth by their photosynthesis rates. The common non-symbiont-bearing planktonic foraminifer *G. bulloides* actually thrives under upwelling condition with presumably lower oxygen concentrations. An oxygen minimum zone can only develop below the mixed layer and thus should only affect deep dwelling species, which are in fact absent from the Red Sea. A negative effect of the uppermost reaches of the oxygen minimum zone below the pycnocline on the successful reproduction of *G.*

sacculifer could be imagined, but again this argumentation conflicts with the oxygen concentration unaffected, yet supposedly deeper living species *G. siphonifera*. It must be concluded that the large explanatory power of the factor oxygen concentration in the redundancy analysis is not due to the primary control of this factor on the foraminifera assemblage but due to a secondary correlation reflecting the general Red Sea circulation system.

		RMSE			R^2		
		annual	summer	winter	annual	summer	winter
Temperature [°C]	IKM	0.754	0.805	0.707	0.72	0.68	0.73
	MAT	0.517	0.464	0.532	0.87	0.90	0.85
	WA-PLS	0.598	0.517	0.664	0.82	0.87	0.76
	ANN	0.328	**0.287**	0.330	0.91	**0.94**	0.90
Salinity	IKM	0.359	0.359	0.333	0.91	0.91	0.92
	MAT	0.271	0.273	0.310	0.95	0.95	0.94
	WA-PLS	0.278	0.299	0.291	0.95	0.94	0.94
	ANN	**0.150**	0.161	0.166	**0.97**	**0.97**	**0.97**
Chlorophyll *a* concentration [mg/m³]	IKM	0.078	1.824	0.080	0.90	0.61	0.93
	MAT	0.100	1.882	0.100	0.84	0.60	0.89
	WA-PLS	0.090	1.919	0.098	0.87	0.57	0.90
	ANN	0.052	0.561	**0.049**	0.88	0.88	**0.94**
Brunt Väisälä frequency [cycles/hour]	IKM	1.007	1.087	1.413	0.86	0.74	0.84
	MAT	0.608	0.611	0.838	0.95	0.92	0.95
	WA-PLS	0.844	0.887	1.050	0.90	0.83	0.91
	ANN	**0.456**	0.534	0.563	0.95	0.90	**0.96**
Minimum oxygen concentration [ml/l]	IKM	0.187	0.158	0.248	0.97	0.97	0.95
	MAT	0.247	0.181	0.328	0.94	0.96	0.92
	WA-PLS	0.250	0.203	0.321	0.94	0.94	0.92
	ANN	0.146	**0.112**	0.172	0.97	**0.98**	0.96

Table 11 Root mean squared errors and coefficients of determination of transfer functions for the employed environmental parameters, transfer function methods and seasons. The highest value in each block is highlighted.

6.3 Transfer function performance

Since the redundancy analysis failed to identify one of the parameters unambiguously as controlling factor underlying the foraminifera distribution, transfer functions were constructed with the four described methods for three seasonal values of all five environmental parameters (Table 11). All types of transfer functions reproduced the environmental parameters of the surface sample dataset with a high accuracy (average $R^2 = 0.89$). The order of quality of this reproduction resembles the respective parameter's correlation with the first axis of the redundancy analysis. Of the different methods, ANN performs best for all combinations of environmental parameters and seasons (summer stratification is the only exception). In general, MAT performs second best, followed by WA-PLS and IKM. This order does not apply for the parameters stratification and productivity, where the errors of the IKM estimates are smaller than those of WA-PLS and MAT. In terms of seasons the RMSE for annual values is generally the lowest but the corresponding coefficient of determination is surpassed by its winter equivalent.

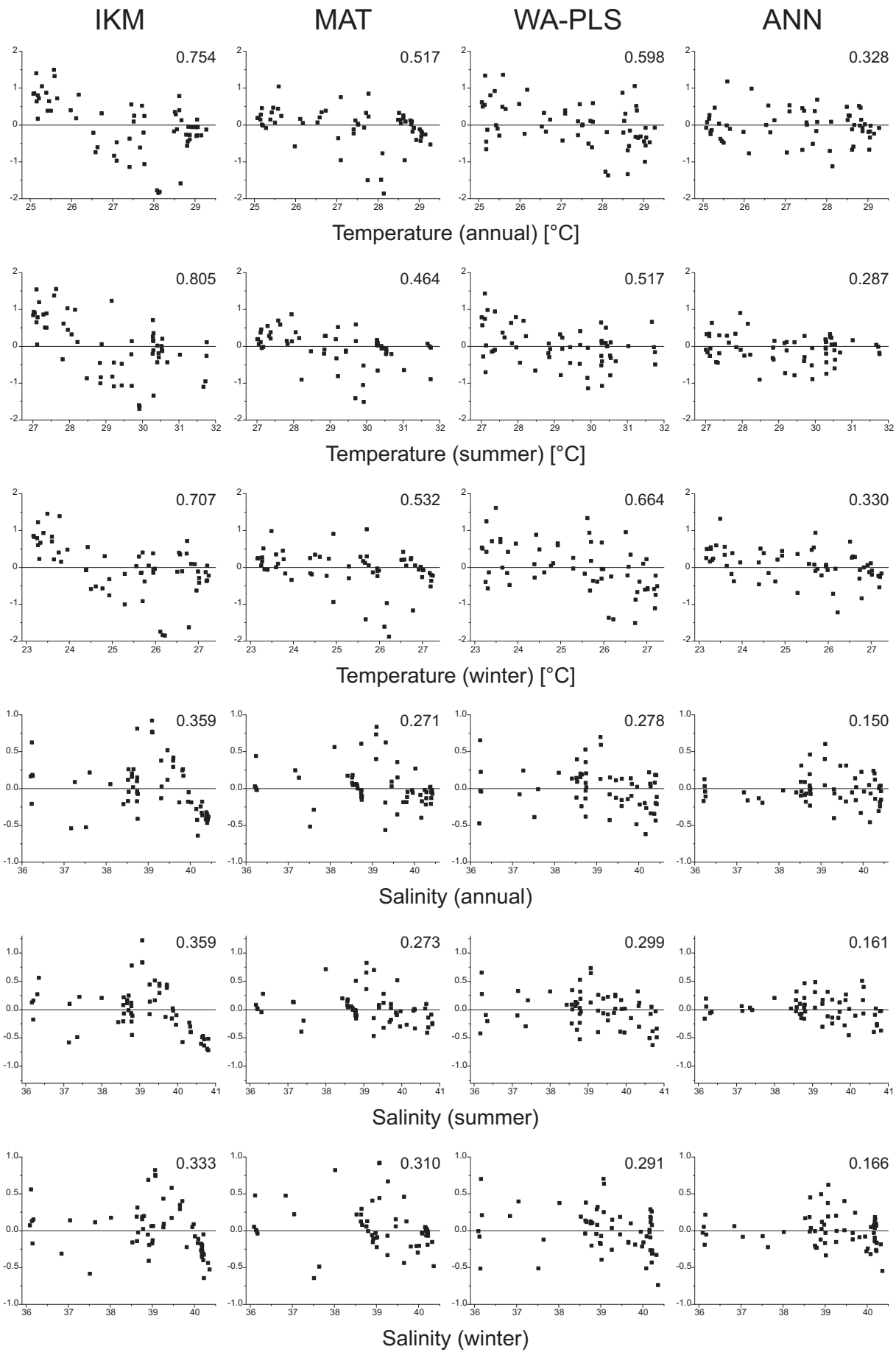
IKM
MAT
WA-PLS
ANN
0.754
0.517
0.598
0.328
Temperature (annual) [°C]
0.805
0.464
0.517
0.287
Temperature (summer) [°C]
0.707
0.532
0.664
0.330
Temperature (winter) [°C]
0.359
0.271
0.278
0.150
Salinity (annual)
0.359
0.273
0.299
0.161
Salinity (summer)
0.333
0.310
0.291
0.166
Salinity (winter)

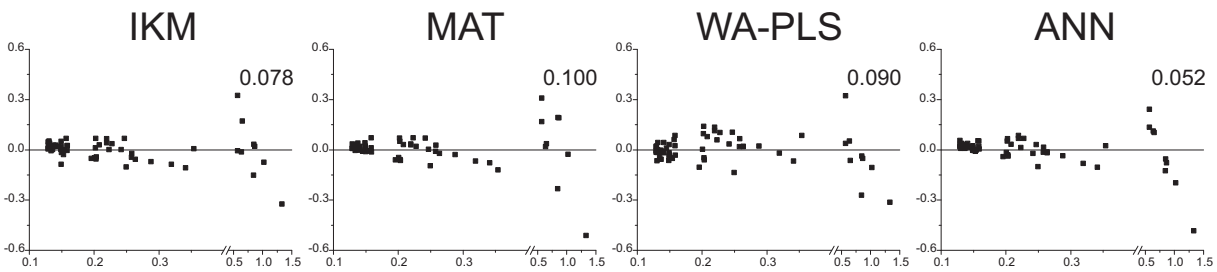

Chlorophyll *a* concentration (annual) [mg/m³]

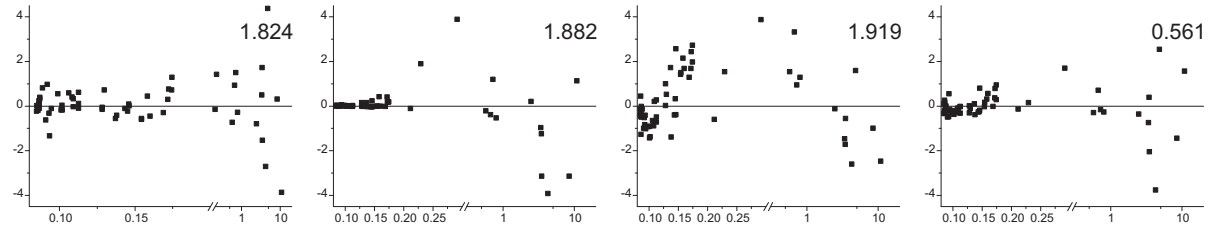

Chlorophyll *a* concentration (summer) [mg/m³]

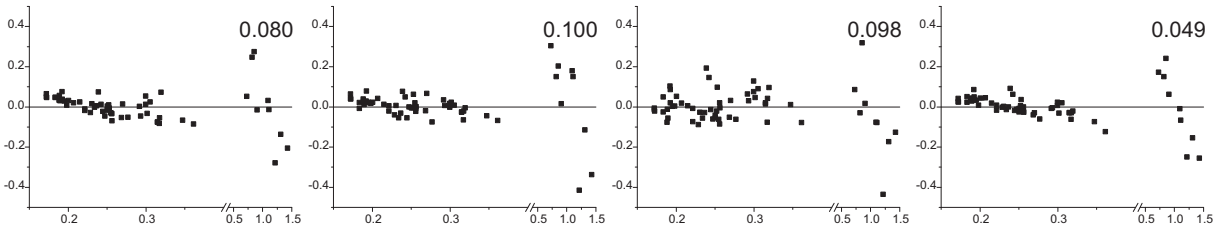

Chlorophyll *a* concentration (winter) [mg/m³]

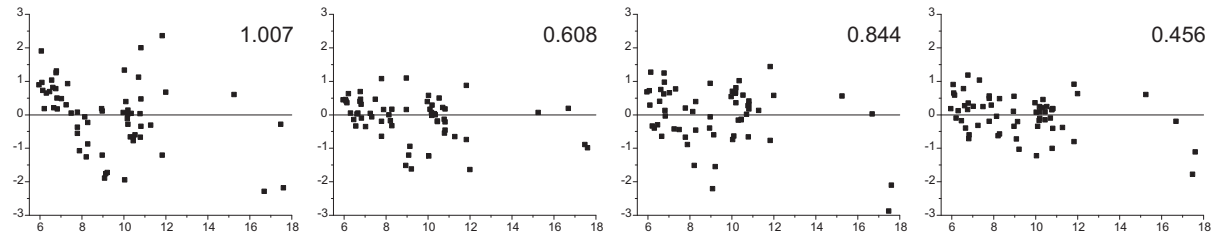

Brunt-Väisälä frequency (annual) [cycles/hour]

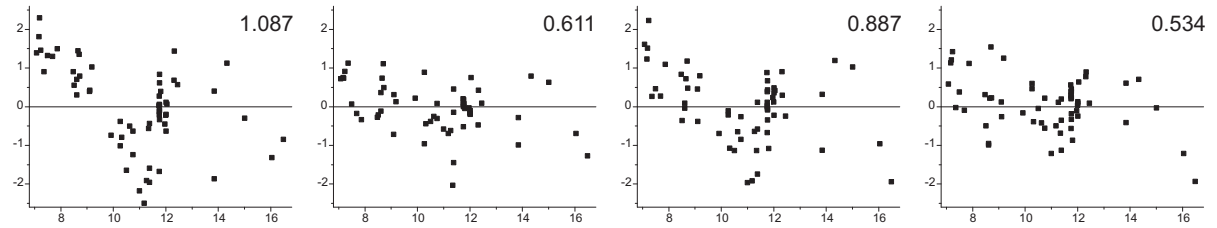

Brunt-Väisälä frequency (summer) [cycles/hour]

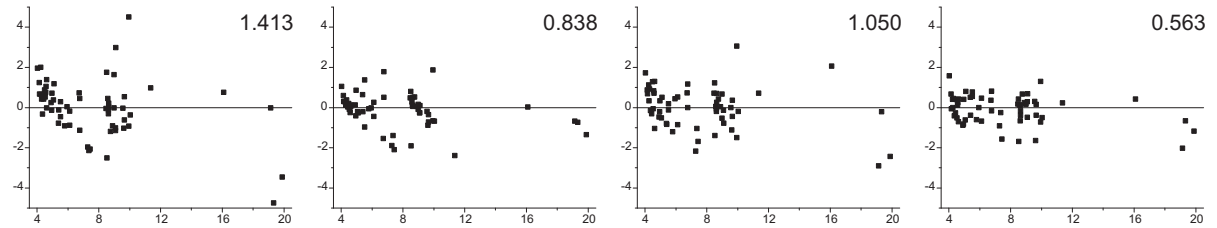

Brunt-Väisälä frequency (winter) [cycles/hour]

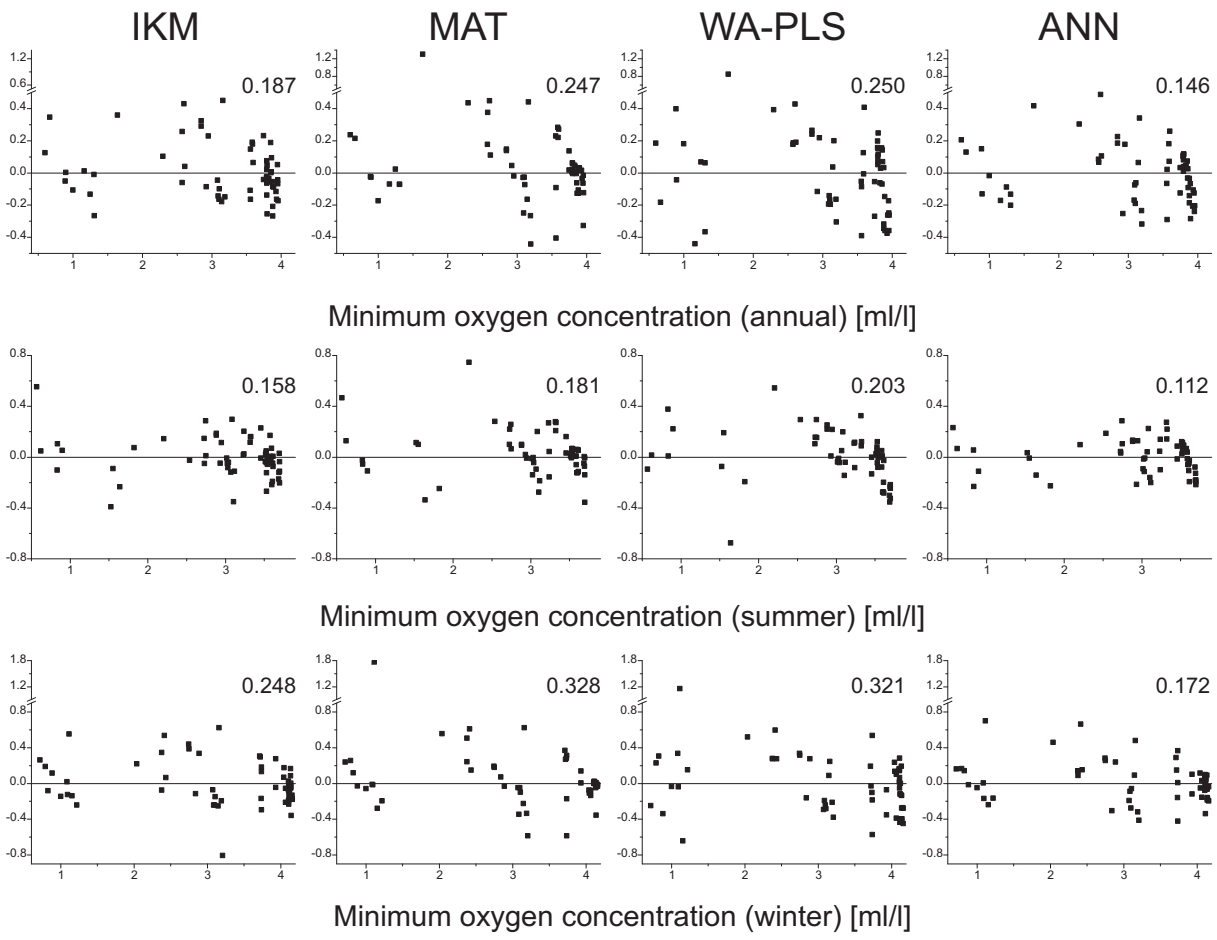

Figure 17 (continuation from the previous two pages) Transfer function residuals for all parameters for the different methods and seasons. The RMSE is denoted in the upper right corner of each plot.

Systematic errors in the fit of the transfer functions to the calibration dataset are revealed in the residual plots (Figure 17). A clear and significant trend in the residuals, that is the underestimation of a certain range of the environmental gradient and the simultaneous overestimation of another range (e.g. temperature by IKM for all seasons), denotes one such a systematic error. This phenomenon reflects a failure of the transfer function to reproduce the relationship between the parameter and the calibration data accurately. The causes for such an error can be manifold: the inadequacy of the employed method, the disturbing influence of a second, possibly unrecognised parameter or in the least desirable scenario it may signify the presence of an incidental rather than systematic relationship between the reconstructed parameter and the calibration data. For the parameter temperature, one can observe a tendency of overestimation of cold temperatures together with an underestimation of warm temperatures across all methods (most pronounced in IKM). In this case, the cause for this systematic error is the incidental correlation of the faunal gradient and the temperature gradient in the Red Sea (cf. Chapter 6.2 Environmental control on planktonic foraminifera distribution). The inadequacy of a method is demonstrated by the conspicuous unimodal distribution of estimates produced by the WA-PLS approach (as exemplified in summer chlorophyll *a* concentrations). The method's assumption that species are most abundant at their optimum value of the respective environmental parameter leads to a

more or less apparent systematic error in the reconstructions. The residuals also demonstratively explain the low fit of certain parameters in particular seasons due to the occurrence of a small set of extreme values. Due to its sensitivity to outliers, the RMSE is extraordinarily high for the parameters chlorophyll *a* concentration (all seasons) and stratification (winter).

Since the RMSE and coefficient of determination are only measures of the transfer function's fit to the calibration data, different representations of the RMSEP calculated by bootstrapping were compared to assess the performance of the different transfer function methods (Table 12, cf. Chapter 4.1.3 Assessment of transfer functions). ANN were due to unavailability of bootstrapped RMSEP excluded from this comparison, but it can be expected that they outperform MAT, and their RMSEP is accordingly smaller [Malmgren et al. 2001]. Considering the general frailty of transfer functions to spatial autocorrelation [Telford et al. 2004; Telford and Birks 2005], which can be expected to be especially pronounced in the Red Sea, it must be assumed that the bootstrapping validation still significantly underestimates the true RMSEP for down-core samples. It is characteristic for this inherent autocorrelation that even the RMSEP of the parameter temperature, which is considered not to have any control on the foraminifera distribution in the Red Sea, is with only 0.33 °C very low and much smaller than the generally expected error of 1-2 °C for foraminiferal transfer functions. In general, the bootstrapped RMSEP values confirm the performance of the individual methods measured by RMSE and the coefficient of determination (Table 11). With ANN not included in the RMSEP comparison, MAT performs best for all environmental parameters, followed by WA-PLS and IKM. The overall mean RMSEP for annual parameter values is 11.4 % of the parameter range. This may appear satisfactory on the first glance, but the high similarity of RMSEP expressed as percent of the range for the different environmental parameters is also very conspicuous and could be attributed to

		RMSEP			RMSEP (% of average)			RMSEP (% of range)		
		annual	summer	winter	annual	summer	winter	annual	summer	winter
Temperature [°C]	IKM	1.018	1.213	0.928	1.9	1.7	1.9	12.5	10.6	11.6
	MAT	0.615	0.675	**0.610**	1.2	**1.1**	1.4	7.8	**7.1**	8.7
	WA-PLS	0.707	0.634	0.798	1.3	1.3	1.5	8.7	8.0	9.6
Salinity	IKM	0.526	0.501	0.472	2.6	3.1	2.4	24.1	26.1	21.7
	MAT	**0.326**	0.335	0.356	**1.6**	1.7	**1.6**	14.6	14.5	14.3
	WA-PLS	0.364	0.381	0.391	1.8	**1.6**	2.0	16.8	**13.7**	18.7
Chlorophyll *a* concentration [mg/m³]	IKM	0.137	2.982	0.136	48.6	264.2	36.7	11.4	16.9	10.8
	MAT	**0.111**	2.098	0.113	39.4	186.0	**30.6**	9.2	11.9	**9.0**
	WA-PLS	0.125	2.456	0.145	44.5	217.7	39.1	10.4	14.0	11.5
Brunt Väisälä frequency [cycles/h]	IKM	1.678	1.643	2.449	18.1	15.2	31.9	14.4	17.5	15.5
	MAT	0.923	**0.847**	1.382	9.9	**7.8**	18.0	**7.9**	9.0	8.7
	WA-PLS	1.044	1.009	1.507	11.3	9.3	19.6	9.0	10.7	9.5
Minimum oxygen concentration [ml/l]	IKM	0.265	0.256	0.350	8.6	8.6	11.0	7.9	8.2	10.2
	MAT	0.262	**0.215**	0.339	8.5	**7.2**	10.6	7.8	**6.9**	9.8
	WA-PLS	0.285	0.225	0.362	9.2	7.6	11.4	8.5	7.2	10.5

Table 12 Root mean squared errors of prediction of transfer functions as absolute values and proportions for all combinations of the investigated environmental parameters, transfer function methods (except ANN) and seasons. The lowest value in each block is highlighted.

their high correlation along the basin axis. An aggravating finding is that the RMSEP of the parameter considered to have significant influence on the foraminifera distribution in the Red Sea, the chlorophyll *a* concentration as proxy for primary productivity, is due to the oligotrophy of the basin very large when compared to the average parameter values.

6.4 Transfer function concept for the Red Sea

Due to the strong mutual correlation of all parameters along the basin's axis, the environmental factor that exerts primary control on the distribution of planktonic foraminifera in the Red Sea cannot be identified unambiguously by any mathematical analysis of the surface sample dataset. The employed statistical methods, however, allow the exclusion of temperature as the controlling factor. Further factors can be excluded by consideration of the ecology of planktonic foraminifera. Literature data yield partially contrasting views on the ecological demands of foraminifera species, but are consistent in attributing low significance to the factor salinity and high significance to primary productivity. The stratification of the water column determines the habitat boundaries and depth preferences of planktonic foraminifera species, yet an effect of this parameter on the distribution of mixed layer dwelling planktonic foraminifera, independent from changes in primary productivity, has so far not been demonstrated. Similar correlation issues affect the parameter oxygen, which has until now been rarely considered, providing limited empirical data and theoretical conclusions.

The synthesis of results from the surface sample dataset and literature data leads to the conclusion, henceforth termed working hypothesis, that primary productivity is the dominant controlling parameter for the recent distribution of planktonic foraminifera in the Red Sea. A secondary influence of the factors stratification and oxygen concentration cannot be completely excluded, but plays according to the published literature only a minor role. An assessment of any of these parameters individually is not possible within the scope of the calibration dataset, as these parameters are tightly interrelated and linked to the Red Sea circulation system. Primary productivity ("water fertility", "nutritional setting") as explanation for the distribution pattern of planktonic foraminifera in the Red Sea or the marginal Gulf of Aqaba has already been

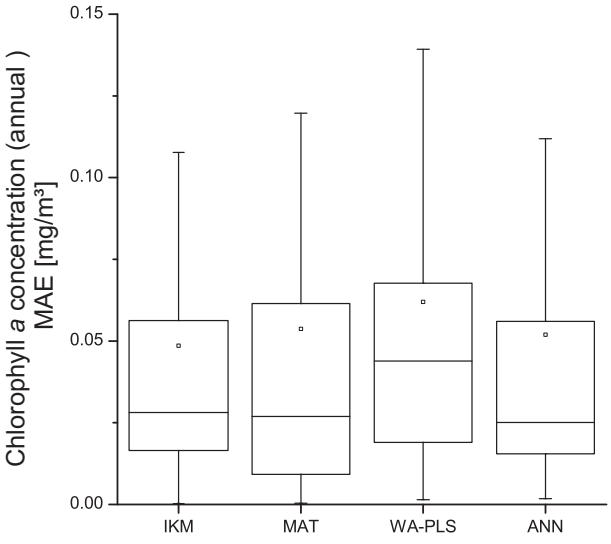

Figure 18 Box chart of mean absolute errors of annual chlorophyll *a* concentration by the different transfer function methods for the calibration dataset. Boxes represent the 75 %, 25 % quantile and median, squares the mean, bars the minimum and maximum values.

invoked by Reiss [1974], Halicz and Reiss [1981], Bjima and Hemleben [1994] and Auras-Schudnagies et al. [1989], although in some cases with a differing attribution of the productive season, reflecting the paucity of empirical data at that time.

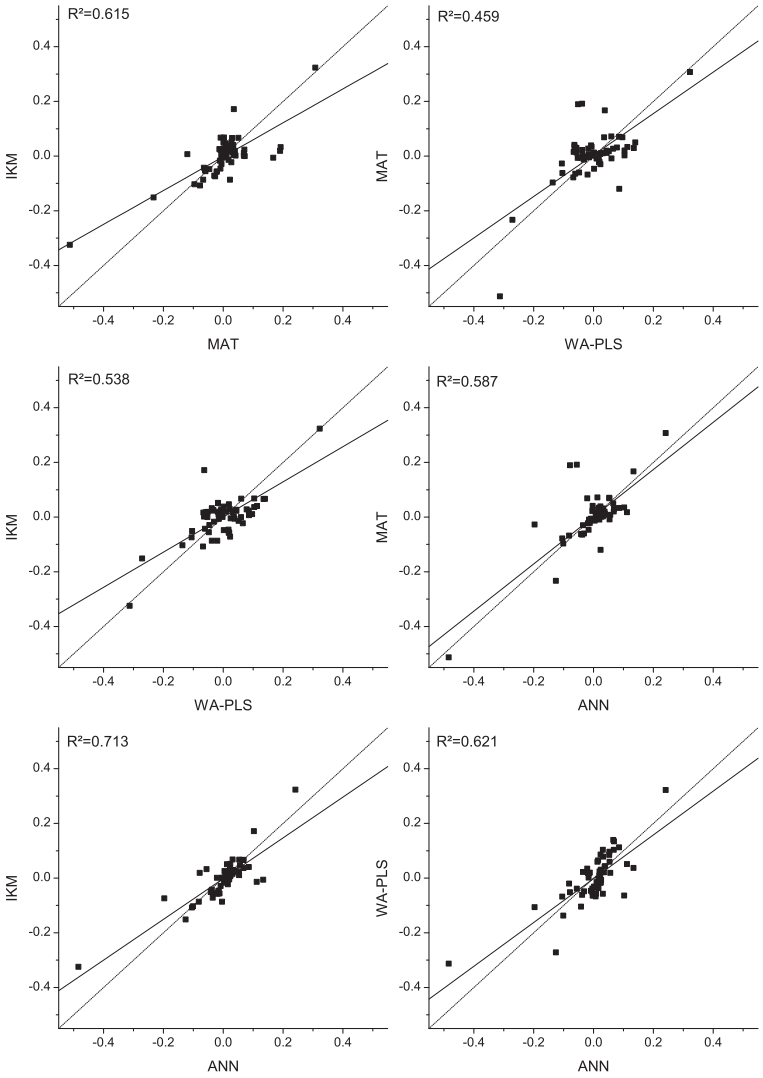

Figure 19 Crossplot of chlorophyll *a* estimate residuals of different transfer function methods for the calibration dataset. The coefficient of determination of the linear fit (solid line) is shown in the upper left corner.

Set into the context of the environmental setting of the Red Sea the working hypothesis implies that the ultimate causes for changes in the distribution of planktonic foraminifera are changes in the circulation pattern. Specifically, changes in the winter circulation pattern are most significant for productivity in the basin, as high primary productivity in the central and northern Red Sea is linked to the winter circulation mode with inflowing surface water from the Gulf of Aden. The perception that the winter circulation controls the primary productivity in the Red Sea is consistent with satellite data (cf. Chapters 2.3.2 Surface water circulation and properties and 6.2 Environmental control on planktonic foraminifera distribution) and part of the existing observational oceanographic studies [Weikert 1987 and ref. therein; Souvermezoglou et al. 1989]. The lower fit of summer chlorophyll *a* concentrations by the transfer function compared to winter and annual values further support this view.

A detailed comparison between the prediction errors regarding the parameter annual chlorophyll *a* concentrations does not reveal any significant differences among transfer function methods (Figure 18). The least accurate reproductions of the calibration dataset by WA-PLS and MAT have also the wider range of mean absolute errors (MAE). The comparison of the residuals (Figure 19) shows no true sign of independency of the different transfer function methods estimates from one

another. Again the WA-PLS method diverges most from all other methods. The noticeable difference of WA-PLS is most probably based on the assumption of an optimum of the estimated parameter for the species in the calibration dataset, which is certainly not true for the distribution of planktonic foraminifera species in the oligotrophic Red Sea, where most likely all species experience sub-optimal nutritional conditions. The results of the WA-PLS approach should therefore be considered with reserve. In summary, all developed transfer functions could potentially reconstruct changes in primary productivity via the proxy chlorophyll *a* concentration correctly. Due to the dependence of primary productivity on the supply of nutrients from outside the Red Sea and circulation-driven vertical mixing, the planktonic foraminifera assemblage will respond indirectly both to changes in sea level and the Indian Monsoon system (cf. Chapters 2.2 Climatology and 2.3 Oceanography). This working hypothesis will be re-evaluated under consideration of the various reconstruction results at the end of the next chapter (Chapter 7.5 Synopsis of Holocene climatic conditions for the Red Sea).

7. The Holocene

7.1 Generalised Holocene age model

The most noticeable feature of the Holocene faunal records from the Red Sea is a faunistic event between 2 and 3 ka BP. During a period of around 1000 years, the most abundant planktonic foraminifera taxa showed a dramatic shift in their relative abundances. The ecological significance of this event is beyond doubt as its occurrence has been documented by several studies of cores from the northern and central Red Sea [Halicz and Reiss 1981; Edelman 1996; Geiselhart 1998; Schmelzer 1998]. Due to the extent of this event, it can be concluded that the underlying environmental forcing was singular and identical for all the faunal records of the different cores. Yet the age models based on radiocarbon dating indicate neither synchrony nor a sensible temporal sequence of this event. Therefore, the construction of a generalised Holocene age model was attempted, which does not only incorporate radiocarbon AMS datings but also the available planktonic foraminifera fauna data. In addition to the data generated in this work, published data of piston core KL11 [Schmelzer 1998] and the three multicores MC91, MC93 and MC98 [Edelman 1996] were included for this approach. The result of the simple though work-intensive alignment process is an age model where the faunal event occurs nearly simultaneously in all records, centred at

	Depth	Calibration range		Tuned age	Deviation
	[cm]	[2σ cal. a BP]		[a BP]	[a]
KL9	*0*	-	-	*450*	
	2.25	562	852	664	in range
	24.25	2728	3054	2675	-53
	30.25	2942	3324	3177	in range
	50.25	4856	5258	5453	195
	60.25	6732	7125	7016	in range
	84.25	9270	9603	9826	223
	89	-	-	*11100*	
KL17 VL	0.5	0	234 *	450	216
	7.5	712	1023	1484	461
	21.5	2926	3319	3471	152
	35.0	-	-	*5240*	
	70.0	-	-	*8175*	
	92.5	10925	11341	10765	-160
	97.5	-	-	*11620*	
KL11	*0*	-	-	*350*	
	27.5	2241	2705	2741	36
	51.5	5996	6452	5912	-84
	78.5	8931	9434	8462	-469
	82.5	10140	10556	10083	-57
	86	12333	12879	12879	in range
MC91	*0*	-	-	*500*	
	5.5	982	1279	1045	in range
	17.5	2887	3293	3046	in range
	27.5	3878	4328	4148	in range
	31.2	4437	4818	4628	in range
MC93	*0*	-	-	*500*	
	5.5	592	871	860	in range
	11.5	1935	2298	2029	in range
	21.5	3937	4522	4138	in range
	29.5	5464	5892	5589	in range
MC98	*0*	-	-	*600*	
	5.5	53	461	566	105
	13.5	1521	1860	2038	178
	23.5	3211	3559	3689	130
	29	-	-	*4500*	

Table 13 Details of the generalised Holocene age model. 2-σ calibration ranges of the radiocarbon datings of the different cores are shown with the tuned ages and the resulting deviation. Inserted control points with no reference to a dating are printed in italics.
* A ΔR of 70 was used, because the standard ΔR allowed no calibration.

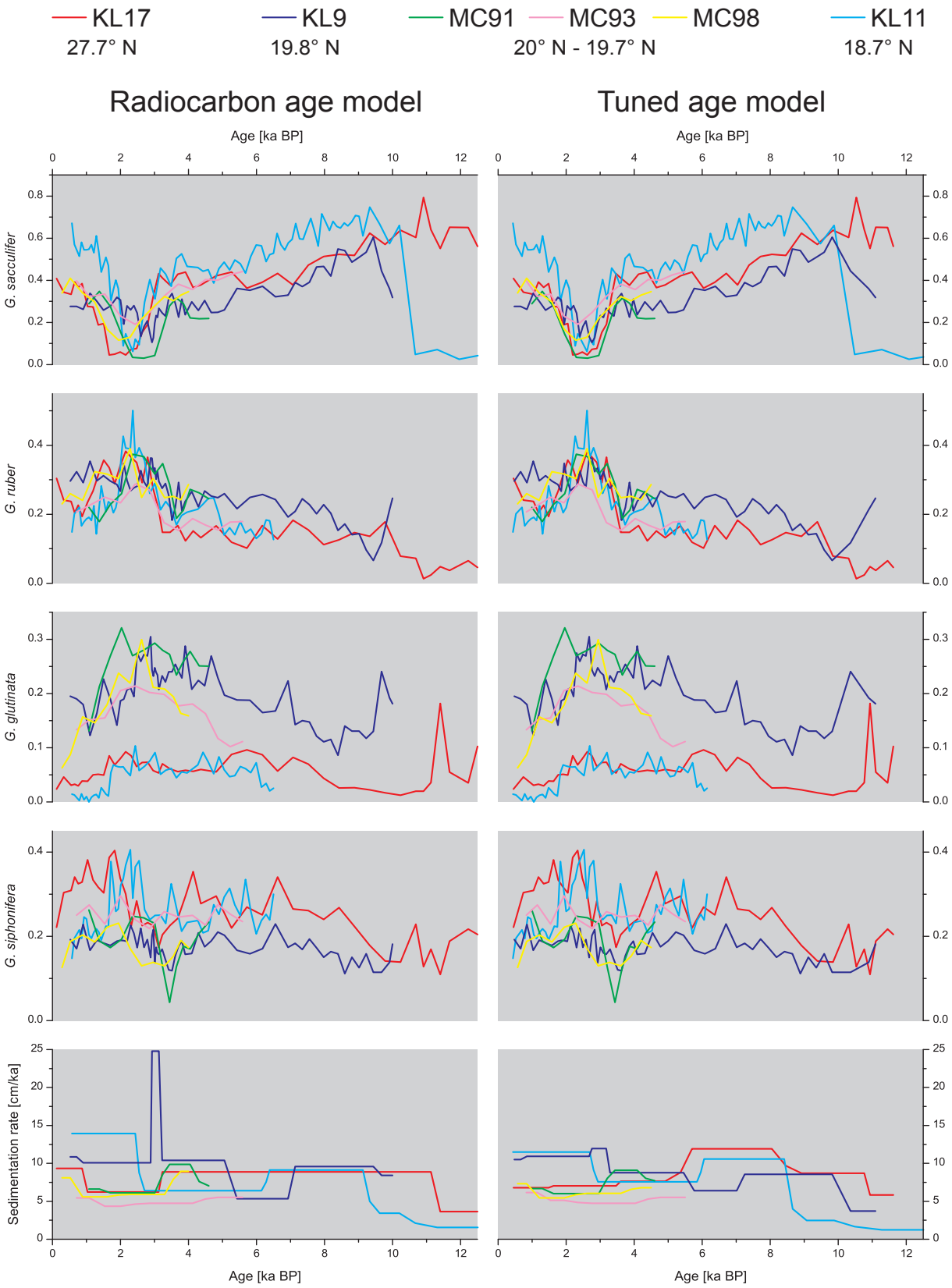

Figure 20 Relative abundances of the four most abundant taxonomic units and sedimentation rates of five different cores from the central and northern Red Sea during the Holocene. The left side shows the Holocene pattern in the framework of an age model based solely on calibrated radiocarbon datings. The right side shows the same data in the framework of the generalised Holocene age model. For KL11 only *G. sacculifer* abundances are shown for the older half of the record due to unresolvable inconsistencies in the original data. Data for KL11 from *Schmelzer* [1998].Data for MC91;MC93 and MC98 from *Edelman* [1996].

around 2.6 ka BP (Table 13, Figure 20). In this generalised tuned age model, the analysed sections of KL9 (89 cm) and KL17 VL (97 cm) reach back to 11.1 and 11.6 ka BP respectively, both containing almost the complete Holocene, except for around 450 years at the top of the records, and short episode after the last glacial. The dating of the older half of the Holocene in the Red Sea is based on only few datings and corresponding faunal census data, which certainly reduces the confidence of the age model for that time period. The obvious differences between KL17 VL on the one hand and KL9 and KL11 before the onset of the Holocene and the early Holocene on the other hand, are not the result of a incorrect alignment, but caused by an actual separation of the environmental conditions between the northern and central Red Sea at that time (see Chapters 7.2.4 Non-faunal proxy resultsand 7.3.4 Non-faunal proxy results). Probably the most demonstrative improvement of the generalised age model concerns the sedimentation rates, which are less variable and show more realistic and uniform values than in the age model based solely on radiocarbon dates. The improved fit of faunal data, however, comes at the price of deviations from the calibrated radiocarbon age ranges. The amount of deviation ranges up to 469 years in KL11, 461 years in KL17 VL and 223 in KL9. In general, the deviations are small and increase the age of the samples, implying a larger reservoir correction than the one used, which is not unreasonable regarding the special circulation system in the Red Sea. The post-depositional precipitation of high-magnesium calcite on foraminifera tests could have lead to the contamination with old carbon from bottom and pore water, thus increased the age of samples dated by radiocarbon chronometry. Two samples are an exception, as the generalised age model suggests a younger age than the radiocarbon dating. In one case (KL17 VL 92 cm) the reduction in age is at the limit of the calibration uncertainty range, and just 10 years short of the applied reservoir correction. In the other case (KL11 78.5 cm) the age reduction is with 469 years difficult to account for. The occurrence of an error of this magnitude is, however, not uncommon or unrealistic as another study that attempted a multiproxy chronostratigraphy encountered even larger age shifts of up to 1000 years [Casford et al. 2007]. That study took place in the eastern Mediterranean, which is in many respects similar to the Red Sea and which suffers from the same problems in terms of reservoir ages.

7.2 Holocene record of KL9

The Holocene section of core KL9 encompasses the top 89 cm. Directly below lies a hard layer caused by microbially mediated post-depositional carbonate precipitation during the last glacial sea level lowstand [Brachert 1999]. Due to the cementation of this interval, micropaleontological sampling and extraction of foraminifera from these sediments were not possible. The faunal record with all twenty identified species as well as the isotope measurements of the Holocene section of core KL9 are given in the appendix.

7.2.1 Faunal record

After a clear increase in the first 20 cm above the cemented layer, the absolute abundance of planktonic foraminifera during the Holocene remained relatively stable (Figure 21). The composition of the planktonic foraminifera fauna, however, showed distinct trends, on which basis the Holocene interval in this core can be divided into five phases (H-I to H-V). A stable Holocene assemblage was first established at the end of the initial post-glacial recovery phase (H-V), characterised by frequent and rapid changes in faunal composition. In the early Holocene phase (H-IV) *G. sacculifer* was the dominant species, showing a declining trend in relative abundances, which was compensated by increasing trend of relative abundances of *G. ruber.* At the end of this phase both species had attained their respective Holocene average. *G. siphonifera* showed a similar trend to *G. ruber* during the early Holocene phase albeit with generally lower relative abundances. *G. glutinata* abundances were low compared to later phases and show no obvious trend during the early Holocene. In the following mid-Holocene phase (H-III) the faunal composition was relatively stable; only *G. glutinata* increased slightly in relative abundance at the expense of *G. sacculifer*. At the end of this phase, the abundances of *G. siphonifera* showed a marked but short-timed decrease. The subsequent faunal shift phase (H-II) shows the most notable change in faunal composition of the entire Holocene record. *G. sacculifer* and *G. ruber* abundances mirrored each other; the first showed a marked decrease in relative abundance centred in this phase and the latter a corresponding increase. This pattern of short timed dominance of *G. ruber* over *G. sacculifer*, henceforth referred to as the faunal shift, is with minor differences universal for the central and northern Red Sea and was found in all records from that region so far [Halicz and Reiss 1981; Locke and Thunell 1988; Edelman 1996; Badawi 1997; Schmelzer 1998; Edelman-Furstenberg et al. 2009]. *G. glutinata* abundances continued their increasing trend, to reach maximal values for the Holocene during this phase. Starting from the preceding low, the abundances of *G. siphonifera* showed an unsteady rising trend. The only conspicuous change in *G. tenella* abundances occurred at the very beginning of the faunal shift phase, when maximum abundances were attained in a peak overlapping with the *G. siphonifera* low. Towards the end of the faunal shift phase, the abundances of all planktonic foraminifera species returned to their respective Holocene averages,

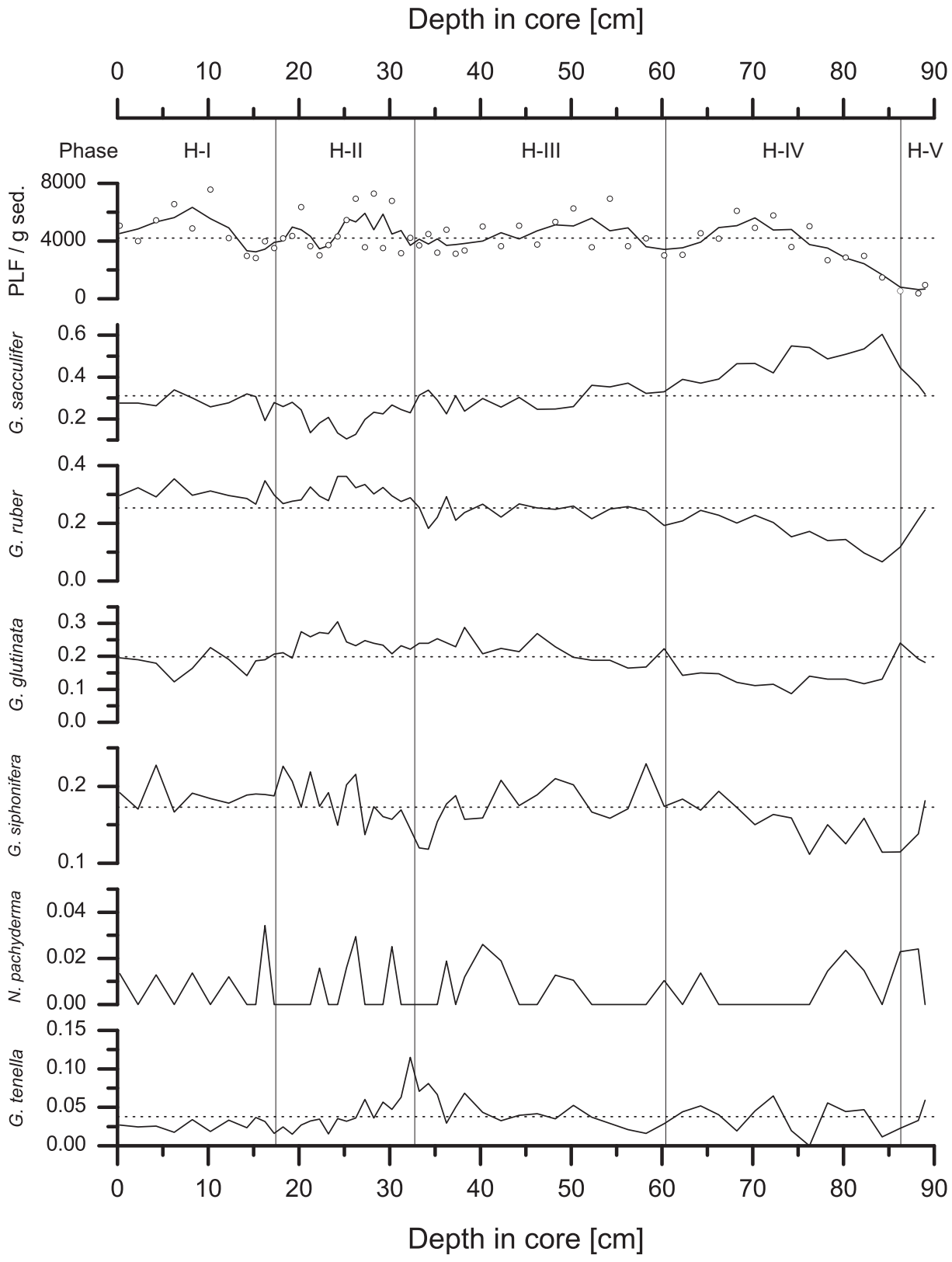

Figure 21 Holocene faunal record of KL9 showing the absolute number of planktonic foraminifera per gram sediment (solid line is the 3-point moving average) and relative abundances of the taxonomic units. Horizontal dotted lines denote the averages for the respective variables. Vertical lines represent the boundaries between the described faunal phases.

G. ruber whose abundances returned to a higher level compared to the preceding mid-Holocene phase being the only exception. During the last phase (H-I), the faunal assemblage composition was steady and relative abundances varied around the level attained after the faunal shift. Specimens belonging to the taxonomic unit *N. pachyderma* occurred only sporadically in the Holocene record, complicating any correlation with the described faunal phases. Virtually no specimens of *G. bulloides* and the Gulf of Aden species group were found in the Holocene section of core KL9, which is the typical situation for the central Red Sea today (Figure 15).

7.2.2 Analogy situation

All of the employed analyses confirm the analogy of planktonic foraminifer faunae in the KL9 Holocene section and the calibration dataset. The analogy plot of the principal components of a PCA of log-transformed faunal data shows an almost perfect overlap (Figure 22). The first component of the PCA contrasts the Gulf of Aden and southern Red Sea assemblages from the northern Red Sea surface sediment samples and all Holocene samples. The second axis broadly captures the faunal gradient from the northern (component 2 more negative) to the central Red Sea (component 2 more positive). The broad overlap between the two datasets clearly indicates that at no time during the Holocene did the planktonic foraminifera fauna deviate significantly from assemblages found in the Red Sea at the present day. As the distance between samples in this diagram is a direct measure of their similarity it is clearly visible that the recent faunal

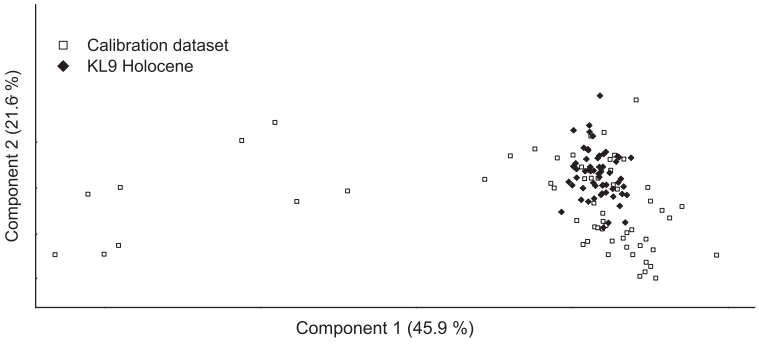

Figure 22 Analogy analysis in form of a scaled plot of a principal component analysis of log-transformed faunal data from the Holocene section of KL9 and the calibration dataset.

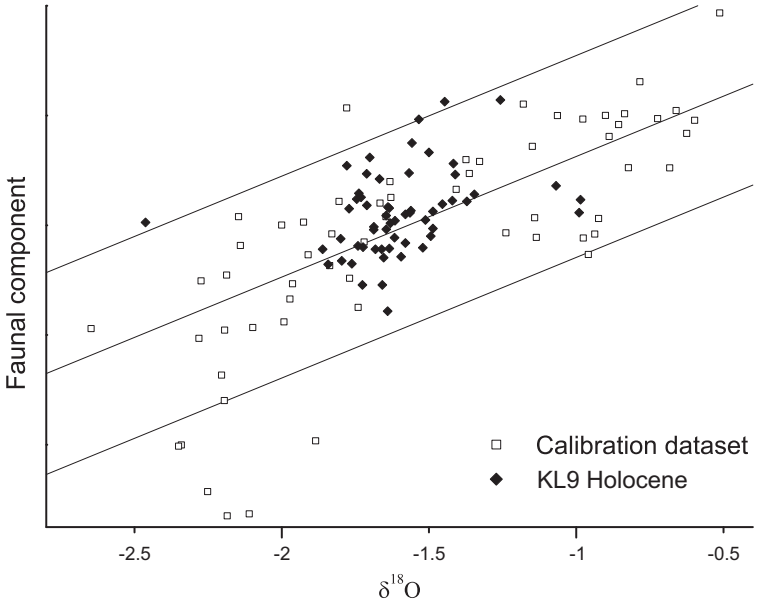

Figure 23 Analogy analysis in form of a cross plot of oxygen isotopes and the first principal component of faunal data from the Holocene section of KL9 and the calibration dataset. Solid lines denote the linear fit through the calibration dataset and the boundaries of the 95 % confidence interval for values around the regression line.

gradient in the Red Sea from south to north spans a much wider range than the Holocene record of KL9. The environmental analogy plot (Figure 23) also shows excellent analogy of all Holocene samples and present-day Red Sea samples. The only samples that deviate slightly from the expected pattern of oxygen isotopic ratio to faunal gradient are one the early Holocene with the highest value of the faunal component and the topmost sample of the record. The latter sample appears to have a too low oxygen isotopic compositions ($\delta^{18}O \sim 1.9$ ‰), which is probably the result of an outlying measurement. The plot of Bray-Curtis dissimilarity (Figure 24) shows higher values for the early Holocene, although the critical value of dissimilarity (cf. Chapter 5.6.3 Assessment of uncertainties on reconstructions) is never reached for the Holocene record of KL9.

7.2.3 Transfer function reconstructions

In order to allow the comparison and discussion of reconstruction results, the transfer functions for all five investigated environmental parameters were employed for the Holocene record of KL9, even though the estimates of certain parameters must *a priori* be regarded as incorrect. The reconstructions of all parameters show a broad similarity between the individual methods and resemble the faunal patterns of the investigated time period. The conspicuous complementarity of the salinity and temperature reconstructions reflects the correlation between these two parameters in the calibration dataset. In an analogous manner, the reconstructions of water column stratification resemble those of temperature and oxygen concentration reconstructions those of salinity. The most obvious feature of all estimates is the early Holocene phase (H-IV) from 10.5 to 7 ka BP, during which the reconstructed salinities and oxygen concentrations are elevated, while reconstructed temperatures, chlorophyll *a* concentrations and the stratification of the water column are lower than at present. The postglacial (H-V), mid-Holocene (H-III) and modern time phases (H-I) are for the majority of the methods and parameters unremarkable with reconstructed values very similar to recent ones. During the faunal shift phase (H-II) centred at 2.6 ka BP, which corresponds to the maximal abundance deflections of *G. sacculifer*, *G. ruber* and *G. glutinata*, transfer functions reconstruct decreased salinity and oxygen concentrations and increased chlorophyll *a* concentrations and water column stratification. The event character of the faunal shift is emphasised in the oxygen concentration reconstructions as a sharp delineated excursion, while it appears as a transition point of a gradual development in the chlorophyll *a* estimates. Next to the distinct faunal shift event, a second excursion is manifested selectively in the environmental parameters. This excursion affects the WA-PLS and ANN temperature and salinity reconstructions and relates to the increased abundance of *G. tenella* at the beginning of the faunal shift phase.

The reconstructions of all environmental parameter are highly correlated (global $R^2 = 0.55$; $n = 190$; $p < 0.05$ for all individual correlations); as expected due to them being the transformations of the same

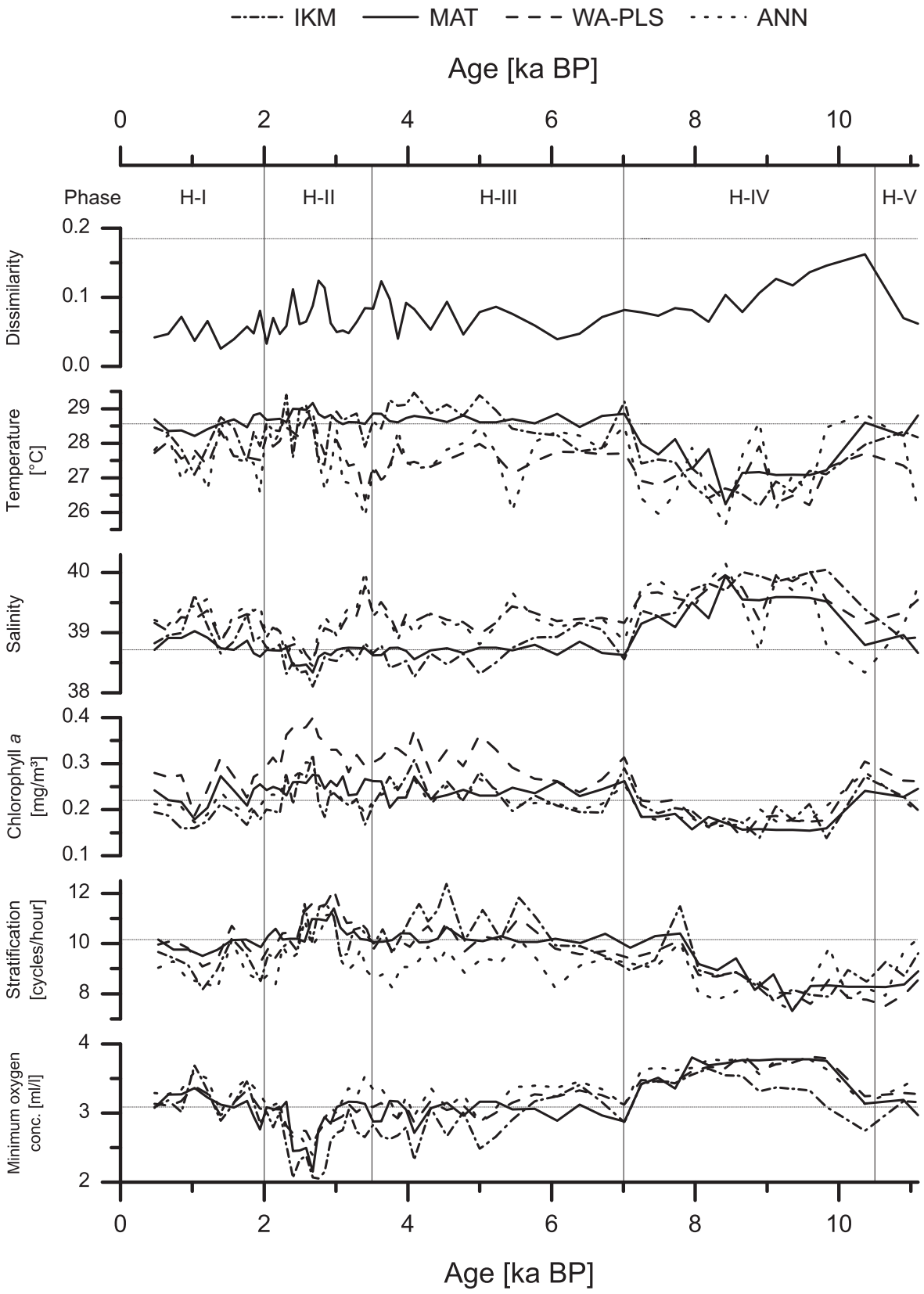

Figure 24 Transfer function reconstruction results for all five investigated environmental parameters in the Holocene record of KL9. Minimal dissimilarity to the calibration dataset is shown as an indicator of sample analogy. Horizontal dotted lines represent present day values of the respective environmental parameter at the core position. In the case of the dissimilarity, the dotted line is the critical value of dissimilarity (cf. Chapter 5.6.3 **Assessment of uncertainties on reconstructions**). Vertical lines represent the boundaries

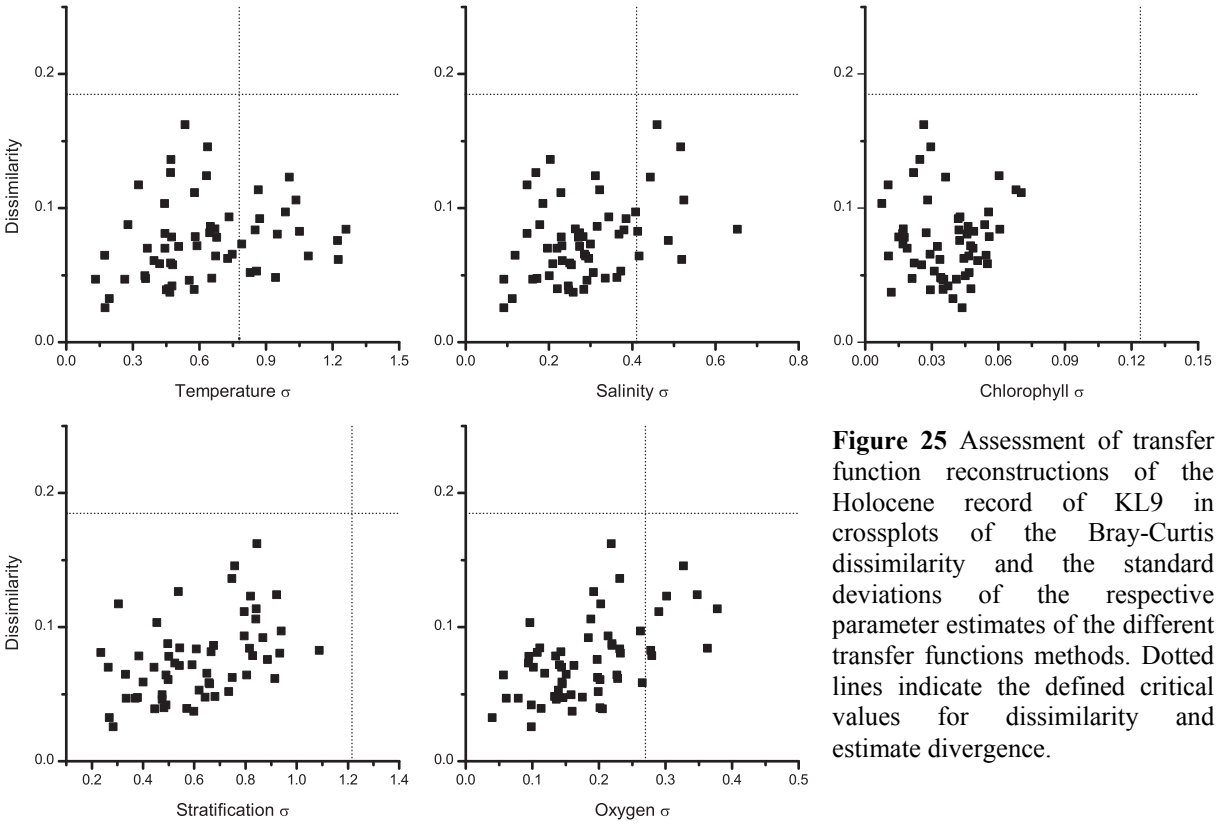

Figure 25 Assessment of transfer function reconstructions of the Holocene record of KL9 in crossplots of the Bray-Curtis dissimilarity and the standard deviations of the respective parameter estimates of the different transfer functions methods. Dotted lines indicate the defined critical values for dissimilarity and estimate divergence.

fauna, which today is in turn highly correlated with the environmental gradient in the Red Sea. The variations in the reconstructions can thus be expressed as variations in the position along the recent environmental gradient. In this interpretation, the distinct early Holocene trend represents a northward shift along the gradient, towards conditions of increased salinity and oxygen concentrations, and decreased temperature, stratification and productivity. Conversely, the reconstructions around the faunal shift indicate an alteration towards conditions found today at a more southernly position in the Red Sea with increased temperature, productivity and stratification in combination with decreased salinity and oxygen concentration.

The assessment of reconstruction reliability (Figure 25) focuses solely on method-specific bias, as the critical similarity value has not been reached in any of the Holocene samples. The parameter temperature shows the largest proportion (28 %) of samples affected by method-specific bias, followed by salinity (15 %) and minimum oxygen concentration (14 %). The reconstructions of the parameters chlorophyll a concentration and stratification include no samples where the divergence of estimates reaches the respective parameter's critical value. Chlorophyll *a* concentration reconstructions appear to be the most reliable estimates (cf. Chapter 5.6.3 Assessment of uncertainties on reconstructions), yet two circumstances underlying this picture have to be considered. Firstly, the critical value of chlorophyll *a* divergence among the estimates of different transfer function methods is relatively high owing to the high RMSEP of the parameter; secondly, a single method is contributing an unproportional large amount of variance (41 %) to the estimated divergence. This method is the

WA-PLS approach, which has already been considered as problematic in its theoretical basis for this study (cf. Chapter 6.4 Transfer function concept for the Red Sea). In summary, the reliability assessment speaks against a controlling influence of the environmental parameters temperature, salinity and oxygen concentration. The unreliable reconstructions of these parameters result from the inability of the transfer functions to extract a potentially non-existing or weak causal relationship between the fauna and the environmental factor.

7.2.4 Non-faunal proxy results

Visual observations and luminescence data (Figure 26) show a blurred sapropel layer with two sections of different intensity at the beginning of the Holocene record of KL9. The first darker section is located in the postglacial phase, ranging from the very beginning to 10.5 ka BP; the second lighter section in the early Holocene phase follows to around 9.2 ka BP. The sharp boundary in the core picture and luminescence data just below 2 ka BP corresponds to the break between two core sections, and the strong difference in visual appearance at this point must be attributed to changes that occurred during storage. Regrettably, this break almost coincides with the end of the faunal shift phase and can also be identified in $\delta^{13}C$ and $\delta^{15}N$ isotope measurements and the amount of organic nitrogen, which could mean that the measurements of these variables at the margins of core sections depict storage related artefacts.

As already described, the boundary between the postglacial phase (H-V) and early Holocene phase (H-IV), which is congruent with the boundary between the sapropel sections, marks a strong change in the planktonic foraminifera fauna. The older, postglacial sapropel section is reflected in the oxygen (heavier), carbon (lighter) and nitrogen (lighter) isotopic composition, in the case of nitrogen the younger, early Holocene section is also manifested with lighter isotopes. Inside the almost complete sapropel, the calcium to iron ratio, a measure of calcitic pelagic sedimentation vs. terrestrial input, is reduced. At the same time the elemental counts of vanadium, an indicator of dysoxic bottom waters [Tribovillard et al. 2006] are significantly higher. The amount of total organic nitrogen is highest in the oldest sample and a small peak coincides with the upper boundary of the sapropel. The faunal shift phase centered around 2.8 ka BP is only weakly expressed in the geo- or biochemical proxy records. Measurements of $\delta^{15}N$ show a poorly developed minimum, indicative for higher primary production [Calvert et al. 1992; Struck et al. 2001], followed by a single measurement of increased total organic nitrogen. The acute lower limit of a region of manganese elemental counts is also found within this phase but should be interpreted as an oxidative front similar to those found in sediments from the Atlantic [Froelich et al. 1979] and Pacific [Berger et al. 1983] rather than a sedimentary signal.

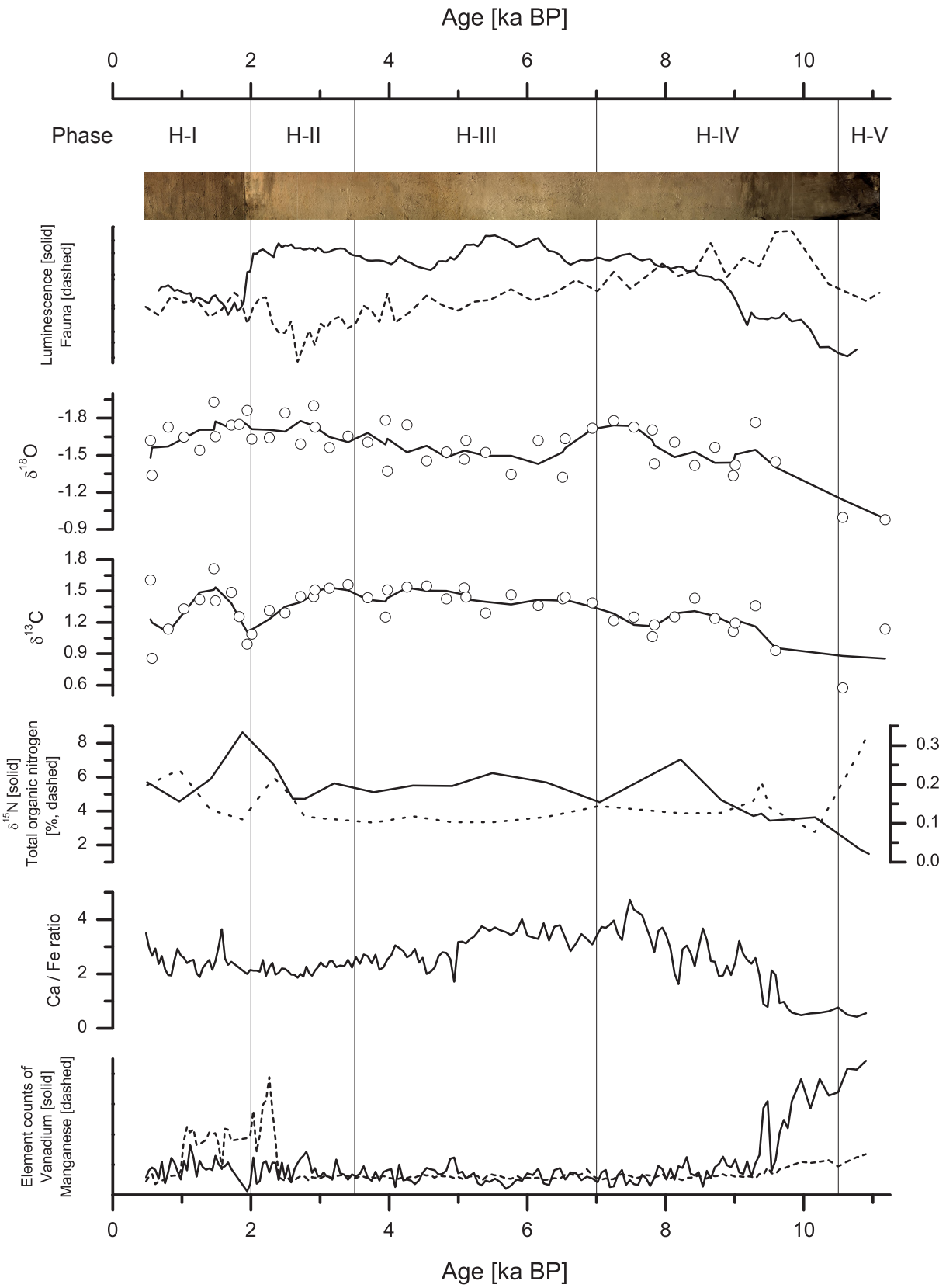

Figure 26 Data from the Holocene section of KL9. Core picture (scaled correctly for age); luminescence data and first principal component of log-tranformed abundance data of the four main species; oxygen and carbon isotopic composition (dots are actual measurements, line is the 3-point moving average, nitrogen isotopic composition and total organic nitrogen content; XRF calcium/iron ratio; XRF element count data of manganese and vanadium. Vertical lines represent the boundaries between described faunal phases.

7.3 Holocene record of trigger core KL17 VL

The analysed section of the trigger core KL17 VL from the very north of the Red Sea spans 97 cm, below which foraminifera are absent from the sediment or the number of planktonic foraminifera is too low for statistically useable analysis. The full faunal record of trigger core KL17 VL with all eighteen identified species as well as the isotope measurements are given in the appendix. Based on the outlined working hypothesis, only the reconstructions of chlorophyll *a*, stratification and minimum oxygen concentration are presented in this context.

7.3.1 Faunal record

The faunal record of KL17 VL bears many similarities to that of KL9; in particular the early Holocene and the faunal shift phase, so accordingly the same division into faunal phases was applied. In general, the absolute abundance of planktonic foraminifera in KL17 VL is much lower than in KL9 (cf. Figure 21 and 27). During the initial postglacial phase (H-V), absolute abundances of planktonic foraminifera rose from almost zero to the Holocene average and remained stable except for a period of decreased abundances during the faunal shift phase. The postglacial phase reveals a conspicuous peak in relative abundance of *G. glutinata*, which coincides exactly with a thin (1.5 cm) sapropel layer at 93 cm core depth (Figure 32). As expected from the recent faunal gradient in the Red Sea *G. sacculifer* completely dominated the assemblage in KL17 VL, in particular during the early Holocene phase (H-IV) when it reached relative abundances of up to 79 %. The early Holocene phase was characterised by gradual change in the abundances of most foraminifera species. Simultaneous to the decrease of *G. sacculifer*, the relative abundances of *G. ruber*, *G. glutinata* and *G. siphonifera* rose to their respective Holocene averages during this phase. As observed in KL9, the planktonic foraminifera assemblage composition was stable through the mid-Holocene phase (H-III). *G. glutinata* abundances showed minor variations, that is a higher relative abundance during the first half of this phase. The abundances of *G. siphonifera* reached a low at the boundary between mid-Holocene and faunal shift phase. An increase of *G. tenella* abundances started already at the end of the mid-Holocene, which is earlier than in KL9, and continued until the end of the faunal shift phase. The faunal shift phase (H-II) of KL17 VL is in general much more strongly delimited and of larger amplitude than that of KL9. During this phase, between 10 and 20 cm depth in core, the *G. sacculifer* abundances dropped dramatically to almost zero, while relative abundances of *G. ruber* mirror this drop and rose from 15 % to nearly 40 %. *G. glutinata* abundances are higher than average, but similar to those during the early mid-Holocene phase. At the end of the faunal shift phase, the relative abundances of *G. sacculifer* and *G. tenella* returned to their respective mid-Holocene level; those of *G. ruber* and *G. siphonifera* reached higher values, whereas those of *G glutinata* reached lower values than during the mid-Holocene. These new abundance levels were retained throughout the modern time phase (H-I). The taxonomic unit

N. pachyderma occurred only sporadically in the Holocene record of KL17 VL and never reached abundances above 5 %.

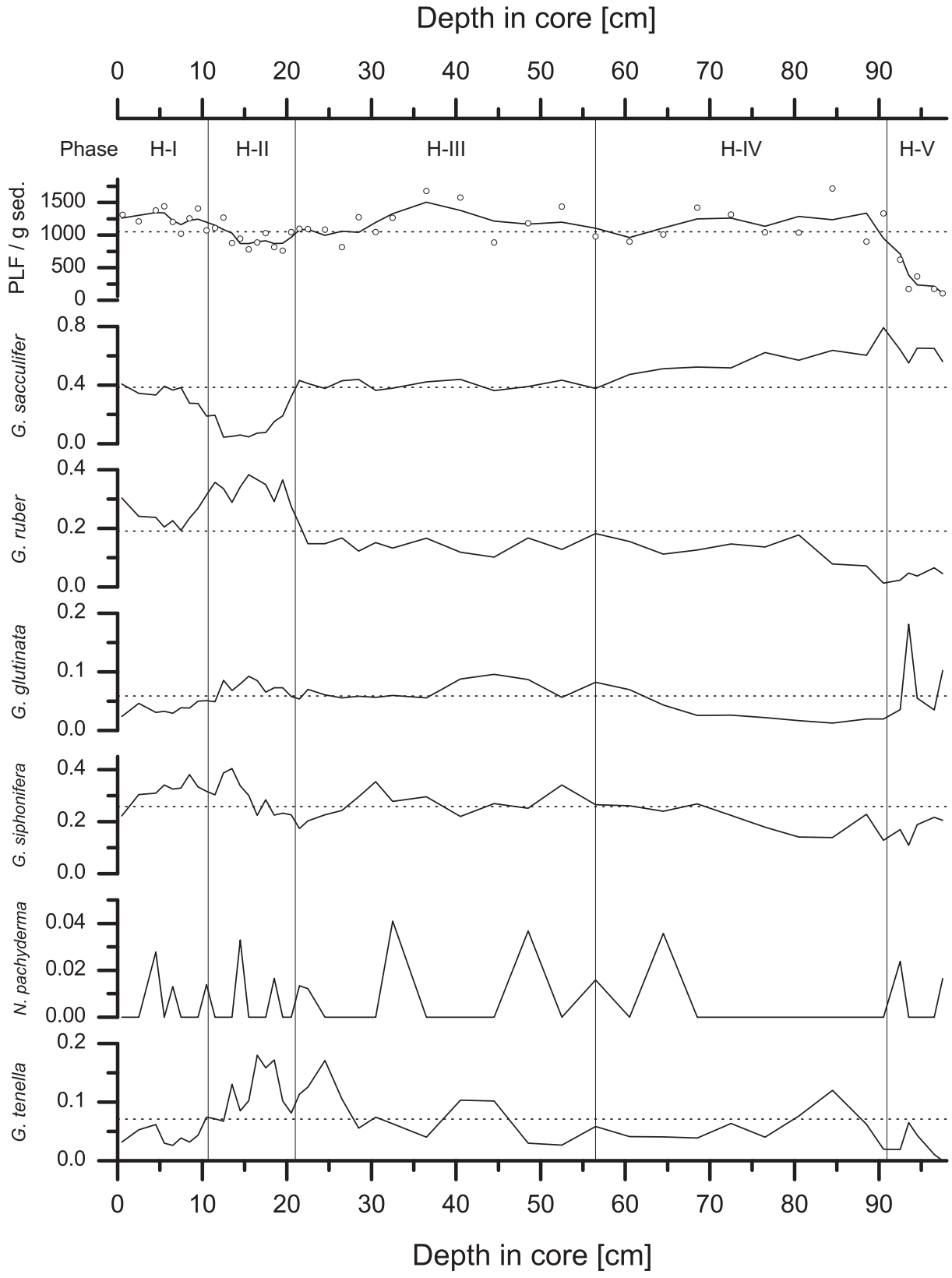

Figure 27 Holocene faunal record of KL17 VL. Absolute number of planktonic foraminifera per gram sediment (solid line is the 3-point moving average) and relative abundances of taxonomic units present. Dotted lines are the averages for the respective variables. Vertical lines represent the boundaries of the described faunal phases.

7.3.2 Analogy situation

As a consequence of the core's position in the north of the Red Sea, the Holocene record of KL17 VL is less analogous to the calibration dataset than that of KL9. The fauna of KL17 VL represents the northern end of the recent Red Sea faunal gradient and so changes in faunal composition beyond the boundaries of the recent gradient lead to a significant decrease in analogy. The overlap of samples from KL17 VL and the calibration dataset in the analogy plot (Figure 28) is minimal to nonexistent. The proximity and relative position of the sample clusters however, indicate that the KL17 VL record represents an extension of the recent Red Sea faunal gradient and downcore samples are still more analogue to northern Red Sea samples than some of the recent samples from the central Red Sea. The analogy crossplot (Figure 29) displays a comparatively higher degree of analogy. Most samples plot at the upper end of the recent faunal gradient but within the 95 % confidence interval. The samples from the postglacial phase (H-V) have the heaviest oxygen isotopic composition and are separated from the remainder of the samples. Samples from the early Holocene phase (H-IV) harbour a fauna, which is outside the northern boundary of the recent faunal gradient but have at the same time an average oxygen isotopic composition. Both these patterns indicate significantly different circulation conditions during these phases. The Bray-Curtis dissimilarity measure (Figure 30) denotes the early Holocene as analogue and only two samples of the postglacial phase as non-analogue. It also classifies the main part of the faunal shift period between 2 and 3 ka BP as non-analogue; a group of samples which has been unsuspicious in the analogy crossplot, where they plotted with an oxygen isotope

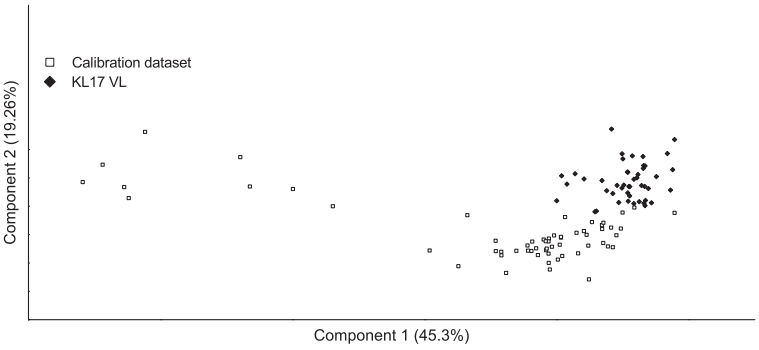

Figure 28 Analogy analysis in form of a scaled plot of a principal component analysis of log-transformed faunal data from KL17 VL and the calibration dataset.

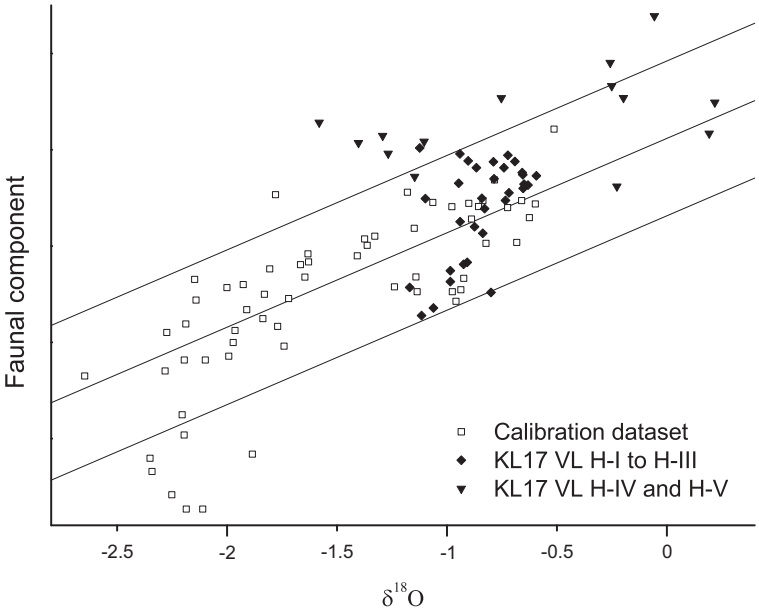

Figure 29 Analogy analysis in form of a cross plot of oxygen isotopes and the first principal component of faunal data from KL17 VL and the calibration dataset. Solid lines denote the linear fit through the calibration dataset and the boundaries of the 95 % confidence interval.

value of ~ -1 between the regression line and the lower 95 % quantile only slightly apart of the main cluster (Figure 29). The differently weighted role of *G. ruber* is responsible for this discrepancy. The species is only of minor importance for the calculation of the faunal component used in the analogy crossplot, as it occurs abundantly throughout the Red Sea. Yet in the calculation of dissimilarity its weight is equal to all other species and high abundances of *G. ruber* paired with very low abundances of *G. sacculifer* lead to high dissimilarity values, as no samples with a similar fauna can be found in the calibration dataset.

7.3.3 Transfer function reconstructions

Motivated by the preliminary conclusion on the environmental control of the planktonic foraminifera assemblages in the Red Sea only the transfer function reconstructions for chlorophyll *a*, stratification and minimum oxygen concentration are presented for the Holocene record of KL17 VL (Figure 30). The reconstructions of these parameters for KL17 VL certainly show much less inter-method similarity than for KL9. Overall, the MAT and ANN transfer functions show very little response to the changes in the faunal composition and their estimates vary very little over time. In contrast to this, the IKM produces estimates of an enormous range and in some cases even values below zero. The behaviour of the MAT can easily be explained by a limitation of the method, which is restricted to produce reconstructions that lie within the ranges of the calibration dataset. The IKM approach on the other hand is subject to the opposed problem; when encountering a non-analogue fauna it extrapolates the environmental parameter values, sometimes to values outside sensible or possible ranges. Significant changes in the reconstructions of primary productivity are only found for the IKM and WA-PLS approaches. The latter reconstructs a similar pattern to that found in the central Red Sea; lower productivity with an increasing trend during in the early Holocene phase and an excursion to more productive conditions during the faunal shift. IKM reconstructions capture predominantly the faunal shift and counter-intuitively estimate chlorophyll *a* concentrations below zero between 1.5 to 3.1 ka BP. MAT and ANN reconstructions show almost no difference to the present-day situation in their estimates for this interval. Stratification reconstructions imply a more intensely stratified water column for the whole period with estimated Brunt-Väisälä frequencies 20 % higher than at modern times in the northern Red Sea. All methods except IKM reconstruct maximal stratification values during the faunal shift. IKM reconstructions have their maxima during the postglacial phase and show values below half the recent annual average and even below zero during the faunal shift. The small peak in reconstructed stratification at 10.9 ka BP coincides with a peak in *G. glutinata* abundances and the deposition of a thin sapropel (cf. Figure 32). For oxygen concentration, it are again only the IKM reconstructions that exhibit any significant variations. According to this method, minimum oxygen levels in the upper 150 m of the water column during the faunal shift would have been as low 1 ml/l or

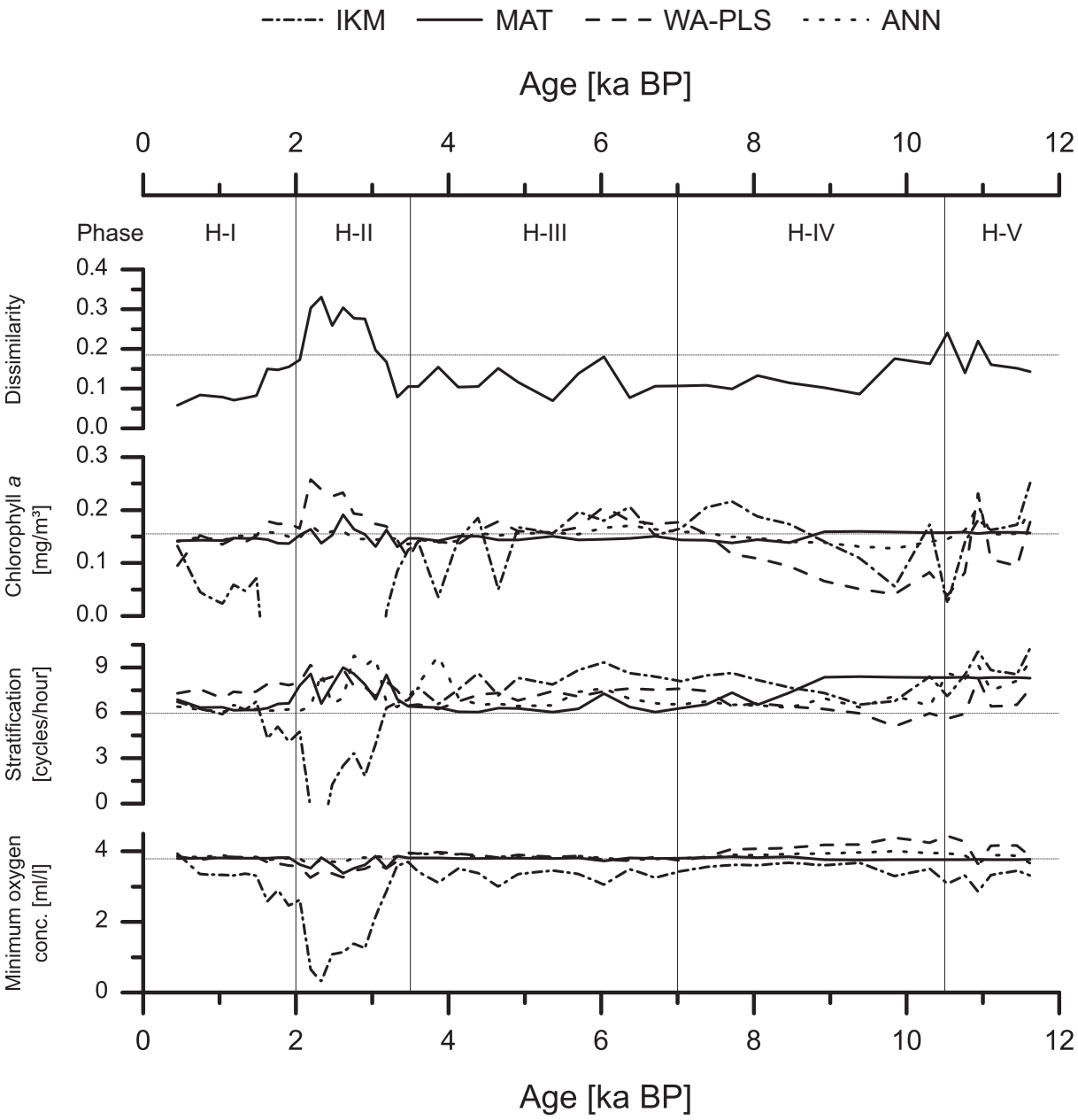

Figure 30 Transfer function reconstruction results for the Holocene record of KL17 VL for three of the investigated environmental parameters. The topmost minimal dissimilarity is shown as an indicator of sample analogy. Horizontal dotted lines represent present day values of the respective environmental parameter at the core position. In case of dissimilarity, the dotted line is the critical value of dissimilarity (cf. Chapter 5.6.3 **Assessment of uncertainties on reconstructions**). Vertical lines represent the boundaries between the described

even close to zero. The reconstructions of the other methods are less spectacular; WA-PLS shows slightly increased oxygen concentrations during the early Holocene phase.

The assessment of reconstruction reliability for chlorophyll *a* indicates good reliability with the estimate divergence of most samples being significantly smaller than the prediction error of the calibration dataset. The reliability of reconstructions decreases from chlorophyll *a* to stratification to oxygen concentration as seen in the increasing number of samples showing a larger divergence among the reconstructions by individual transfer function methods (Figure 31).

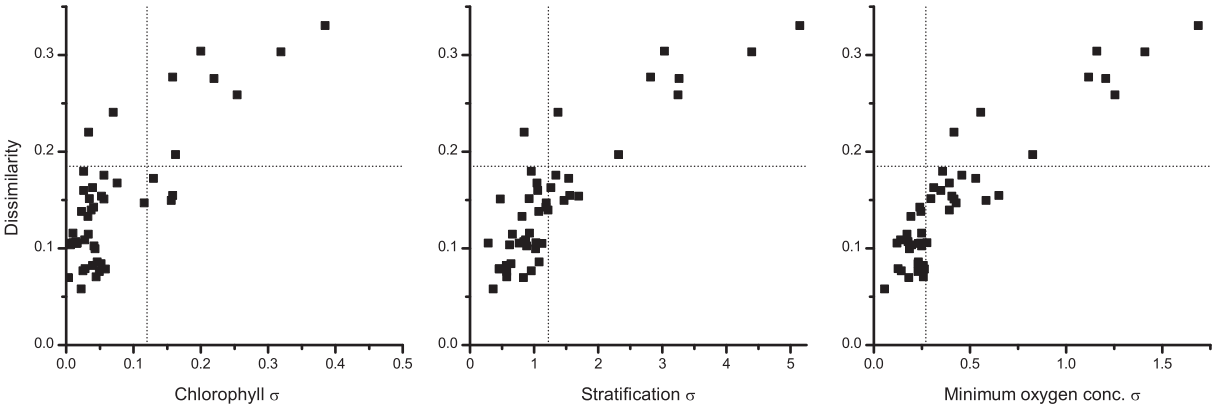

Figure 31 Assessment of transfer function reconstructions of the record of KL17 VL in crossplots of the Bray-Curtis dissimilarity and the standard deviations of the respective parameter estimates of the different transfer functions methods. Dotted lines indicate the defined critical values for dissimilarity and estimate divergence.

7.3.4 Non-faunal proxy results

The luminescence record of KL17 VL and that from the published core GeoB 5844-2 [Arz et al. 2003a; Arz et al. 2003b] are congruent. Consequently, the thin sapropel layer at 93 cm depth in KL17 VL corresponds to the "*Red Sea Sapropel 1b"* in core GeoB 5844-2 [Arz et al. 2003b], which was dated by radiocarbon chronometry to 10.8 ka BP. The age difference for the sapropel deposition between the age model of Arz et al. [2003b] and the generalised age model of this work is only 150 years. Increased vanadium concentrations denote dysoxic bottom water conditions [Tribovillard et al. 2006] during sapropel deposition and dramatically elevated elemental counts of manganese just above the visible upper margin of the sapropel indicate the oxidation of organic rich sediment [De Lange et al. 2008] The oxygen isotopic composition shows a sharp decrease to lighter values during the first 1.6 ka of the record. From 10 ka until around 6.3 ka BP, roughly coinciding with faunal early Holocene phase, the oxygen isotope values are lighter than at modern times, a finding that contradicts the conclusions of Siddall et al. [2004], that oxygen isotopes in the Red Sea reflect predominantly sea level. Arz et al. [2003a] proposed a "humid period" to have a local effect on the northern Red Sea during the early Holocene. The details and implications of this oxygen isotope excursion will be discussed in chapter 7.5 Synopsis of Holocene climatic conditions for the Red Sea. During the faunal shift, the oxygen isotopes were lighter than at present or during the mid Holocene. The carbon isotopes values show an erratic increase from the early Holocene to modern time with the highest values attained during the faunal shift phase. The ratio of calcium to iron is low during the postglacial phase and rises throughout the early Holocene phase. At the end of this phase, a constant level is reached and maintained until modern times. Two distinct iron peaks at 3.6 and 4.3 ka BP, accompanied by increased arsenic concentrations, indicate the presence of pyrite, which may be of detrital or authigenic origin during short anoxic events [Rothwell et al. 2006]. Similar to KL9 a small peak in manganese concentrations just at the end of the faunal shift is interpreted as the signal of an oxidative front [Froelich et al. 1979; Berger et al. 1983].

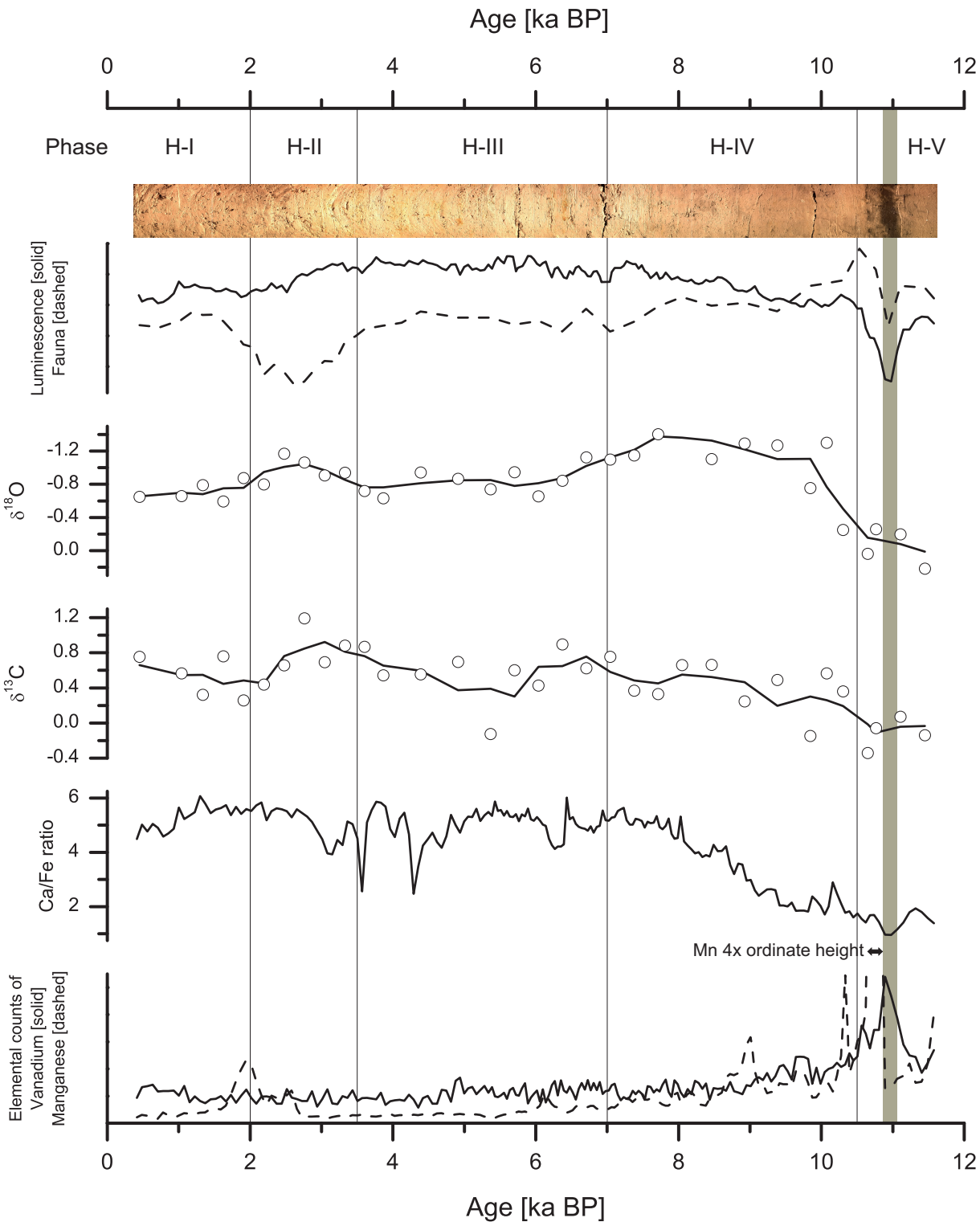

Figure 32 Data from the Holocene section of KL17 VL. Core picture (scaled correctly for age); luminescence data and first principal component of log-tranformed abundance data of the four main species; oxygen and carbon isotopic composition (dots are actual measurements, line is the 3-point moving average), nitrogen isotopic composition and total organic nitrogen content; XRF calcium/iron ratio; XRF element count data of manganese and vanadium. Vertical lines represent the boundaries between the described faunal phases. Coloured area denoted the position of *"Red Sea sapropel 1b"* [Arz et al. 2003b].

7.4 Holocene records of multicorers MC91, MC93 and MC98

The data of these records from the central Red Sea were taken from the master thesis of Y. Edelman [1996]. The results of this thesis are also published as peer-reviewed paper [Edelman-Furstenberg et al. 2009]. The multicorers from the central Red Sea were part of a transect, orthogonal to the basin axis (Figure 13, Table 2). Coretop data of MC93 and MC98 were also included in the calibration dataset of the transfer functions. To avoid redundancy only the chlorophyll *a* reconstructions of the multicorer records are presented. All three multicorers have a length of approximately 30 cm and cover according to the generalised Holocene agemodel a time span of around 4.5 ka (5.5 ka for MC93).

7.4.1 Faunal records

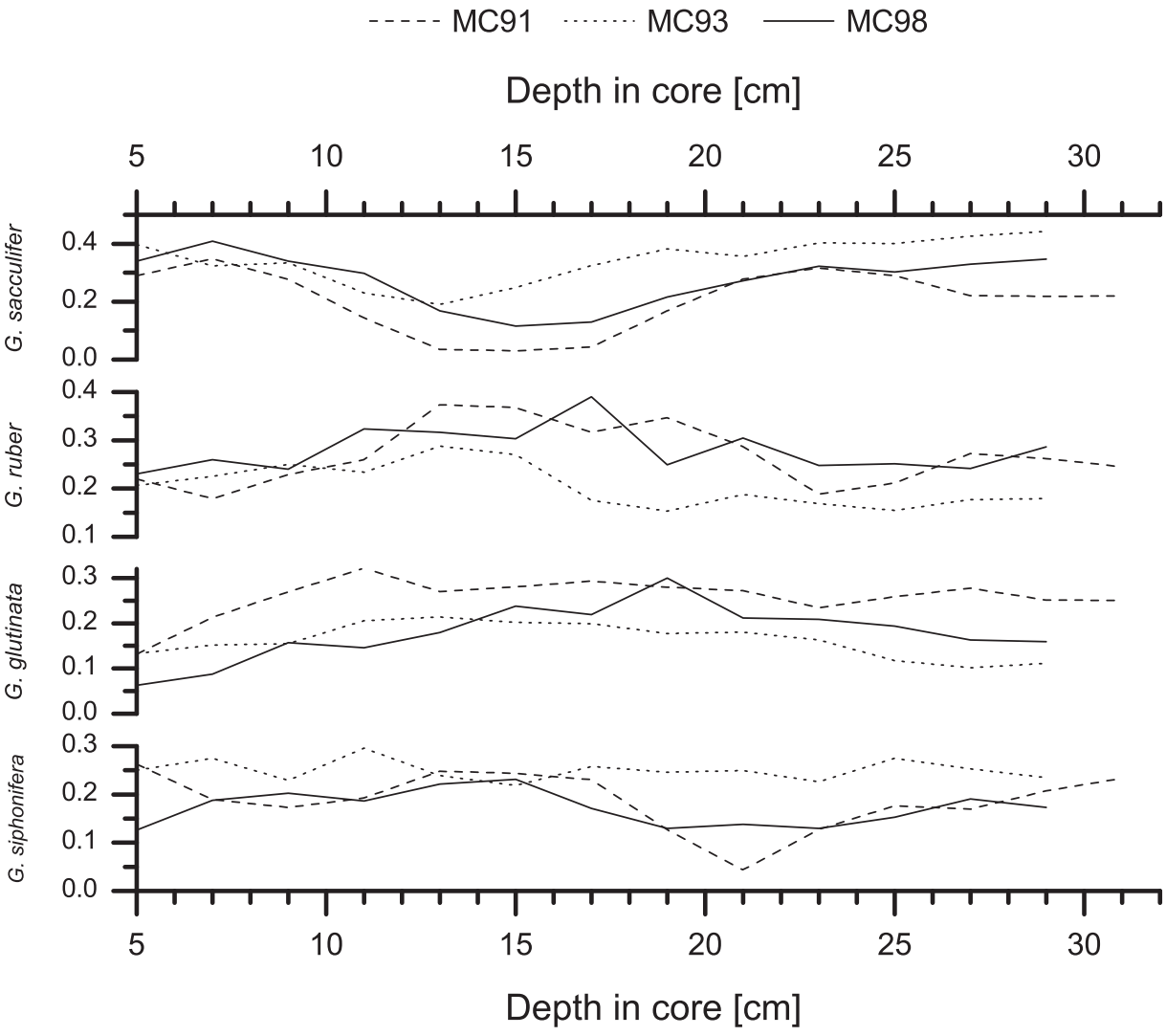

Figure 33 Faunal record of the taxonomic units defined in this work of multicorers MC91 (dashed line), MC93 (dotted line) and MC 98 (solid line). Data from *Edelman* [1996].

The faunal data of these multicorers show major differences to the faunal data produced during this work and to that produced by Fenton et al. [2000]. The species *N. pachyderma*, *N. incompta*, *G. tenella*, *G. rubescens* and *T. quinqueloba*, which together account for 7.8 % of the calibration dataset, are not present in the multicorer counts of Edelman [1996]. On the other hand, the species *T. clarkei* has been identified and recorded with an average and maximal abundance of 2.3 % and 21.9 % respectively. This species is in appearance very similar to *T. quinqueloba* [Hemleben et al. 1989] and a misidentification would fit to the comparable count data of these species. Confusion arises also about the size fraction as this species has been described as being smaller than 149 µm [Edelman 1996], yet appears in the count data of the larger than 149 µm fraction. Data of the five taxonomic units which could be extracted from the census data of Edelman [1996] are in good agreement with other records (Figure 33); all three multicorer records capture the faunal shift, the decrease of *G. sacculifer* abundances compensated by increased abundances of *G. ruber* and *G. glutinata*, at around 15 cm depth. A decreased abundance of *G. siphonifera* before or at the beginning of the faunal shift event, which has been observed in the records of KL9 and KL17 VL, is only noticeable in the record of MC91. Even though the temporal sampling resolution is coarse, the recorded changes in faunal composition are in general rather smooth for all records. Consequently, the boundaries of the faunal shift phase in these records can not as clearly be identified as in those described before.

7.4.2 Analogy situation

According to the analogy plot, MC93 has the most and MC91 the least analogue record to the calibration dataset of the three multicores (Figure 34). The differences lie in the second component of the PCA and are thus only weakly connected to the main faunal gradient along the basin axis in the Red Sea. The dissimilarity values are with around 0.1 on average only slightly higher than those for the Holocene record of KL9 (Figure 35): The defined critical dissimilarity level is only just surpassed in two samples from the faunal shift in MC91. Considering the given differences in the taxonomy, the overlap in the analogy plot and the low dissimilarity is quite surprising and must be ascribed to the dominance of the north south gradient on the faunal assemblage composition. Overall, the analogy of the three multicorer records can be seen as sufficient for the application of the developed transfer functions.

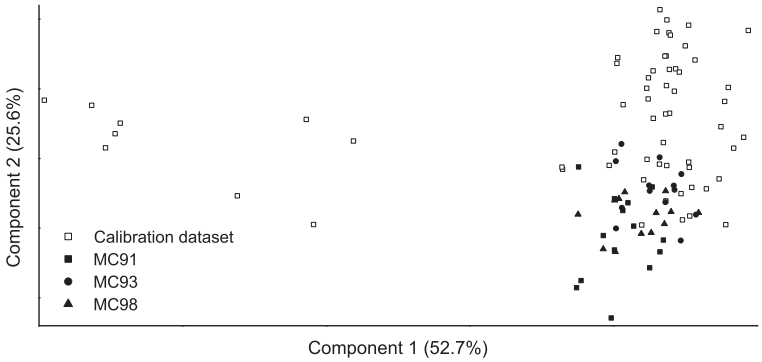

Figure 34 Analogy analysis in form of a scaled plot of a principal component analysis of log-transformed faunal data from the multicorer records MC91, MC93 and MC98 from *Edelman* [1996] and the calibration dataset.

7.4.3 Transfer function reconstructions

The transfer function reconstructions of the multicorer records are in general not as definite as those from the cores already discussed. This is obviously the consequence of the inconspicuous faunal census data, in which the faunal shift is not as distinct as in KL9 or KL17 VL. Reconstructions of MC91 and MC93 for the youngest samples at 1 ka BP are satisfyingly close to the recent average but modern chlorophyll *a* concentrations are underestimated by 20 % in MC98.

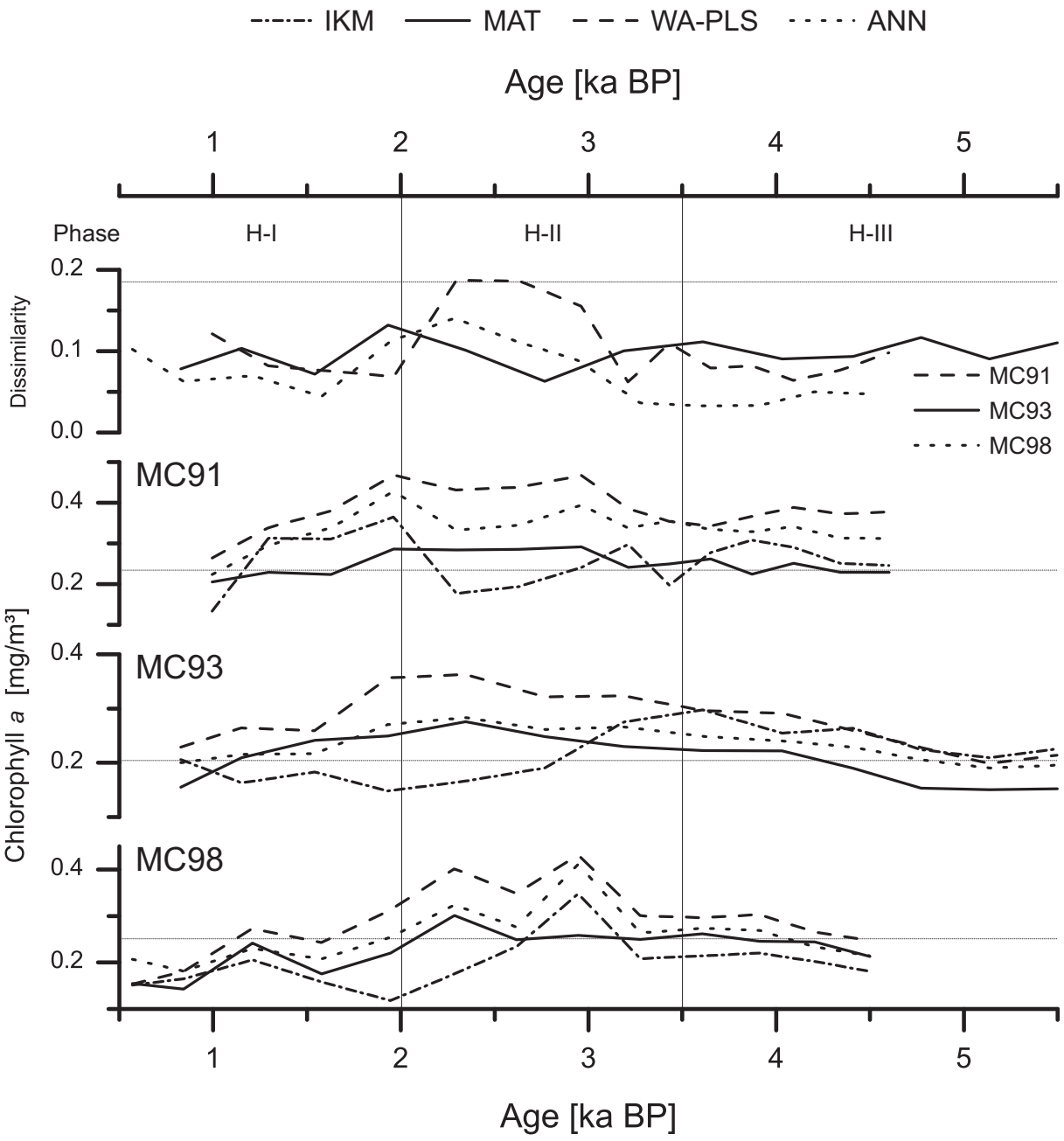

Figure 35 Transfer function chlorophyll *a* reconstruction results for the multicorer records MC91, MC93 and MC98 [Edelmann 1996]. Horizontal dotted lines represent present day values of the respective environmental parameter at the core position. In case of dissimilarity, the dotted line is the critical value of dissimilarity (cf. Chapter 5.6.3 **Assessment of uncertainties on reconstructions**). Vertical lines represent the boundaries between the described faunal phases.

The MAT approach produces the most conservative estimates and shows no significant increase in primary productivity during the faunal shift. The IKM reconstructions are generally lowest and deviate clearly from those of ANN and WA-PLS; maximum reconstructed productivity values for MC93 occur earlier than and at the very beginning of the faunal shift phase, while for MC91 maximal values are attained after the phase. Apart from these inconsistencies, which must be attributed to uncertainties in the age model and the taxonomic comparability, chlorophyll *a* estimates for the faunal shift period are elevated and show absolute values similar to those encountered for KL9. The reconstruction reliability plot (Figure 36) shows that the estimate divergence is lower than the defined critical value for all samples of all three records. The two least similar samples from MC91 have also the largest estimate divergence.

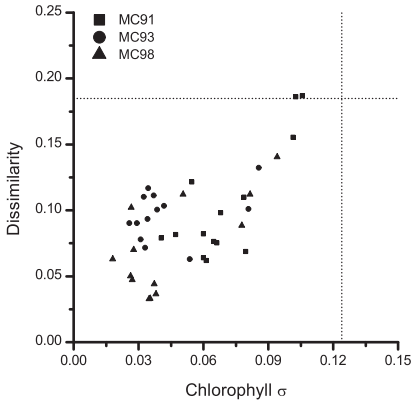

Figure 36 Assessment of transfer function reconstructions of the records of MC91, MC93 and MC98 from *Edelman* [1996] in a crossplot of the Bray-Curtis dissimilarity and the standard deviations of the chlorophyll *a* estimates of the different transfer functions methods. Dotted lines indicate the defined critical values for dissimilarity and estimate divergence.

7.5 Synopsis of Holocene climatic conditions for the Red Sea

Due to the close relationship of primary productivity and the circulation system in the Red Sea, the chlorophyll *a* concentrations reconstructed by the transfer functions can be utilised not only to identify productive or unproductive conditions, but also for a more extensive interpretation of the state of the Red Sea system. For this interpretation, the reconstructions of chlorophyll *a* concentrations will be compared not only within the Red Sea, but also to the well-known climatic conditions for the Holocene in the investigated region. The existence of these independent reconstructions, based on a range of proxies, allow for the re-evaluation and validation of the working hypothesis on the environmental control of planktonic foraminifera in the Red Sea developed in the previous chapter.

Post-glacial phase (Phase H-V, 11.7 to 10.5 ka BP)

The last glacial was the period with the most extreme conditions during the last 500 ka of Red Sea history. Sea level was reduced by more than 100 m [e.g. Rohling et al. 1998] compared to today and accordingly the exchange with the open ocean was diminished. Salinities reached values between 55 [Hemleben et al. 1996] and 57 [Biton et al. 2008], exceeding the tolerance levels of most planktonic organisms. Consequently, an "aplanktonic zone" is found during MIS 2 in most cores from the Red Sea [Fenton et al. 2000]. When sea level rose, the conditions in the Red Sea normalised and the pelagial was re-colonised. According to the generalised age model the Holocene record of KL9 begins at 11.1 ka BP. Prior to this date, continuous sediment sampling and extraction of foraminifera are impossible due to the presence of a hard layer. This phenomenon is well known from the Red Sea and has been attributed to post-depositional carbonate precipitation in bacterial mats [Brachert 1999]. Immediately after this layer, the foraminifer species with the apparently lowest salinity tolerance, *G. sacculifer* [Hemleben et al. 1989], is present and consequently salinities must have dropped below 49 at that time, at least within the mixed layer. The record of KL17 VL starts within the aplanktonic zone of MIS 2 and it is at 11.6 ka BP that planktonic foraminifera reach abundances that allow quantification of the assemblage. Again, *G. sacculifer* is abundant in the very first sample after the aplanktonic zone. This pattern denotes firstly, that salinity changed rapidly during the time of sea level rise and secondly, that the control of salinity on planktonic foraminifera assemblages is enacted not gradually but in form of a threshold.

Even though the analogy analyses show that the fauna was analogous during the post-glacial phase in the central Red Sea, the deposition of sapropel documents that the circulation conditions were very different. This exemplifies the fact that an analogue foraminifera fauna does not necessarily have to live under analogue environmental conditions. Under normal conditions the oxygen in the bottom waters of the Red Sea are replenished by newly formed of deep water in the north of the basin. The deposition of a sapropel during the post-glacial phase implies a lack of oxygen in the bottom water

resulting from diminished deep-water formation. The causes for this situation during the very early Holocene in the Red Sea lay in the lower sea level and therewith limited the water exchange with the open ocean during the last glacial [Siddall et al. 2003]. The post-glacial sea level rise reactivated the circulation, but it most likely required time and a certain sea level to produce the amount of heavy deep waters to replace the brines residing in the Red Sea since MIS 2. For the Red Sea the absence or reduction of deep-water formation entails that the general circulation is weakened dramatically, compared to the present-day situation. Throughout the Red Sea, but especially in the northern part, the water column stratification would increase, both in terms of intensity and in the form of an ascent of the pycnocline. Due to the lack of fresh oxygenated deep water, the OMZ in the central and southern Red Sea would also intensify and rise to shallower water depths. This scenario, essentially the same as proposed by Almogi-Labin et al. [1991] for this period, is incompatible with the view that either stratification or oxygen concentration controls the planktonic foraminifera distribution in the Red Sea, as the species *G. sacculifer*, which has been claimed to be especially sensitive to these parameters [Fenton et al. 2000; Eldeman-Furstenberg et al. 2009], is present abundantly. Reconstructed productivity during the times of sapropel deposition is similar to modern time, a finding that could be explained by a combination of the reduced nutrient supply with a tighter coupling of primary production and remineralisation within the shallow mixed layer. Yet, due to the implied non-analogue environmental conditions associated with the postglacial recovery phase, one of the main assumptions of transfer function is clearly violated and a high uncertainty of the productivity reconstructions must be accepted.

The conspicuous differences in the timing of sapropel deposition between KL17 VL from the northern and KL9 from the central Red Sea during this period (cf. Figure 26 and 32) must be due to their position in the circulation system. The deep-water source for the central Red Sea is the very northern part of the basin (including the Gulf of Suez; cf. Chapter 2.3.1 General circulation system and deep water properties), while the bottom waters at the location of KL17 VL may have been supplied with oxygen by deep water formed in the Gulf of Aqaba. Another explanation could lie in the amount of generated deep and bottom water, which could have been insufficient for the oxygenation of central Red Sea bottom waters, causing longer duration of organic-rich deposition as observed in core KL9. Arz et al. [2003b] proposed that the cause for the termination of the thin *Red Sea sapropel 1b* at around 10.9 ka BP in cores from the northern Red Sea, which cannot be clearly identified in records from the central Red Sea, is the flooding of the Gulf of Suez, which then acted as an additional source of deep water.

Early Holocene (Phase H-IV, 10.5 to 7 ka BP, Figure 38 b)

This phase was in terms of the planktonic foraminifera fauna more similar between KL17 VL in the northern and KL9 in the central Red Sea. The fauna was characterised by an initial abrupt offset

towards high *G. sacculifer* abundances, which occurred earlier in KL17 VL than in KL9, followed by a gradual decline until the recent abundance level of this species was reached at the end of the phase. The early Holocene phase was characterised by considerable changes in the global climate system. Global sea level rose by about 50 m [Fairbanks 1992] and significant alterations in the El Nino Southern Oscillation [Rein et al. 2005] and North Atlantic Oscillation [Rimbu et al. 2003] climatic systems have been recorded. Global climate was in general warmer (Holocene thermal maximum, 10 to 6 ka BP) [COHMAP members 1988; deMenocal et al. 2000] and the insolation differences between summer and winter, a measure for seasonality and thus monsoon strength [Rossignol-Strick 1983], higher than today. The ITCZ migrated further north during summer than at present [Haug et al. 2001; Wanner et al. 2008] and consequently the Red Sea region [Fleitmann et al. 2003a; Fleitmann et al. 2007] and the Sahara [Ritchie et al. 1985] received an increased amount of precipitation. The general picture of an enhanced summer season and with it a stronger SW monsoon is supported by the reconstruction of more intense upwelling conditions in the Arabian Sea [Schulz et al. 1998; Gupta et al. 2003]. Presumably most important for the Red Sea circulation during the early Holocene phase is the lowered sea level, which reduced the amount of inflowing water from the Gulf of Aden and with it the import of nutrients. Superimposed on these conditions, the strengthened/prolonged summer season led to enhanced summer circulation conditions, which further reduced the amount of nutrients reaching the central and northern Red Sea (cf. Chapter 2.3.2 Surface water circulation and properties). The emerging picture of a gradual change from less productive to more productive conditions caused by the rising sea level and the decrease in SW monsoon strength is consistent with the reconstructed pattern of primary productivity, the increase in $\delta^{13}C$ and the Ca/Fe ratio from both cores (Figure 26 and 32); altogether confirming the working hypothesis of a productivity controlled distribution of planktonic foraminifera in the Red Sea.

Without a detailed modelling approach, it is difficult to comment on the fit of the parameters water column stratification and oxygen concentration to the described environmental conditions. Based on the present-day Red Sea circulation system, an intensification/prolongation of summer- at the expense of winter circulation conditions should result in increased stratification in the central Red Sea and by an implied reduction of deep water formation even more so in the northern Red Sea. This estimation does not fit to the stratification reconstructions of KL9 in the central Red Sea (Figure 24), and only partially to those of KL17 VL from the northern Red Sea, where the reconstructed stratification is on average slightly higher than at present day, but the reconstructions of the different methods far from consistent. The effects of the circulation during the early Holocene phase on the oxygen concentrations were twofold: on the one hand the reduced primary productivity led to a decrease in oxygen consumption and on the other hand the reduction of deep water formation caused a general decrease in oxygen concentration in the deeper waters. The reconstructed oxygen concentrations for the northern Red Sea during the early Holocene phase (Figure 30) are indistinguishable from present-

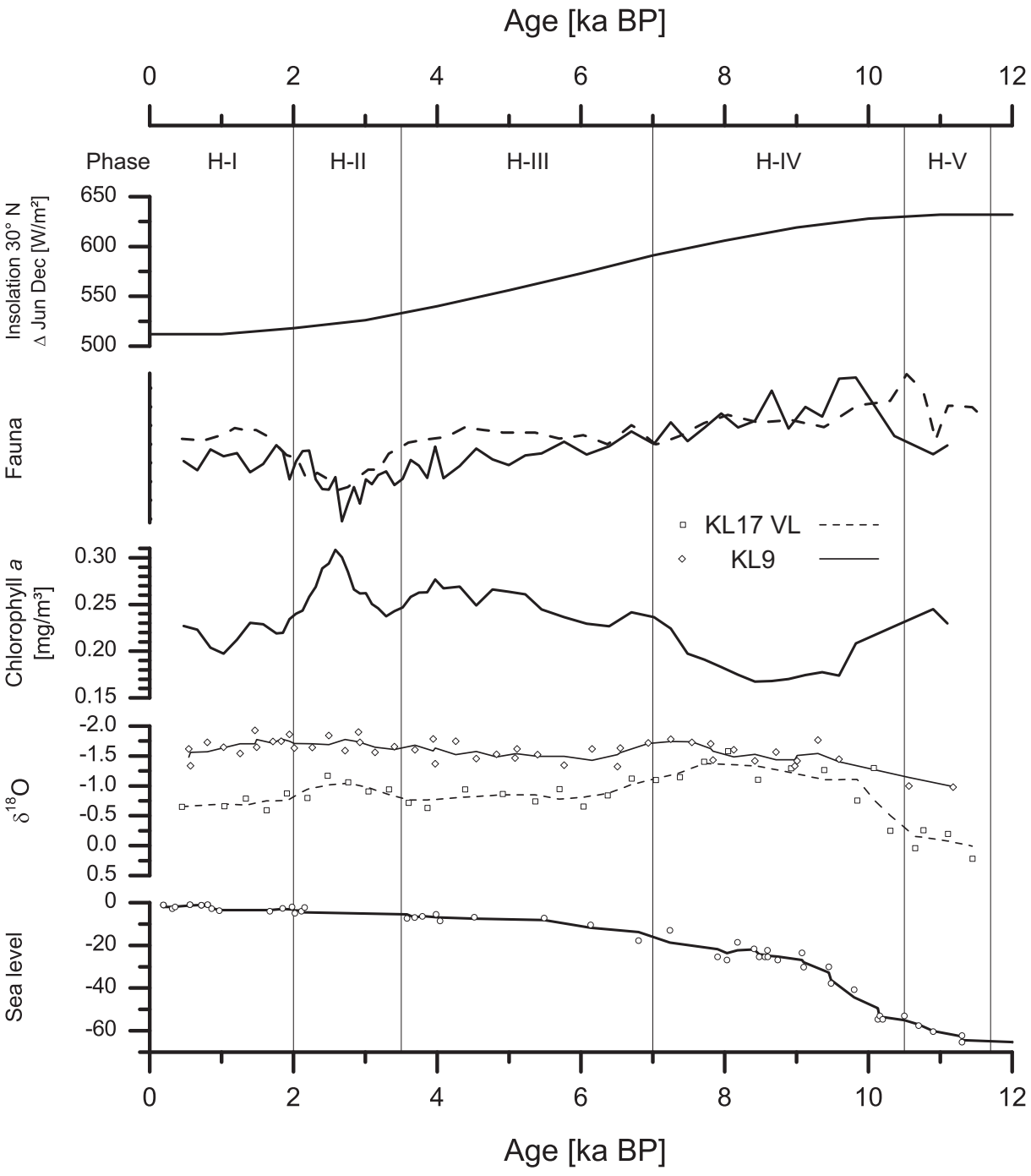

Figure 37 Seasonality index (difference between June and December insolation at 30° N), faunal variation (first component of a PCA of log-transformed faunal data) for KL9 and KL17 VL, composite chlorophyll *a* reconstruction (average of IKM, MAT, WA-PLS and ANN methods) for KL9, oxygen isotopic composition for KL9 and KL17 VL (line is the respective 3-point moving average) and sea level [Fairbanks 1992] (line is the 3-point moving average)

day values and would indicate oxygen saturation in the upper water column, which is not in conflict with the expected conditions. The significant increase of oxygen concentrations reconstructed for the central Red Sea during this phase would indicate that decreased oxygen consumption played a more important role than deep water formation. This however, is disputable as the central Red Sea today is already oligotrophic (0.22 mg Chl *a*/m³) and a further decrease of primary productivity and subsequent

respiration of organic matter can hardly be expected to cause the reconstructed increase of oxygen concentrations of about 1 ml O_2/l. Possible changes in the physical properties of seawater that affect oxygen solubility such as temperature and salinity cannot account for changes in the concentration of dissolved oxygen on this scale (e.g. a temperature difference of 5 °C corresponds to a difference in solubility of 0.25 ml O_2/l in seawater with 35 psu).

Another feature of the early Holocene phase is the distinct change of the $\delta^{18}O$ gradient in the Red Sea. The oxygen isotope values for KL17 VL from the northern Red Sea are lower than at modern times, which is in severe contradiction to the model of Siddall et al. [2004], stating that sea level controls the oxygen isotopic composition of water in the Red Sea. Even under consideration of possible changes in the physical fractionation of oxygen isotopes [Rohling 1999], this phenomenon ultimately cannot be explained without invoking an input of freshwater into the northern Red Sea [Arz et al. 2003a; Trommer et al. 2009a]. A higher humidity for the early Holocene has also been postulated for the whole region on the basis of speleothem records [Bar-Matthews et al. 1999; Bar-Matthews et al. 2000; Fleitmann et al. 2003a; Fleitmann et al. 2007], African lake levels [Gasse and Van Campo 1994; Gasse 2000] and isotopic analyses of terrestrial material [Goodfriend 1999]. The freshwater input into the northern part of the Red Sea during this humid period caused a reduction of surface water salinity, affecting the habitability of the upper water column and was obviously the reason for the meridional asynchrony of the faunal records, the temporally shifted re-establishment of planktonic foraminifera at different latitudes. Yet it did apparently not have any effect on the type of planktonic foraminifera fauna (pronounced *G. sacculifer* dominance) that developed during this phase; another indication for the threshold character of salinity on the distribution of foraminifera species.

Mid-Holocene (Phase H-III, 7 to 3.5 ka BP)

The Mid-Holocene phase was a comparatively stable period and conditions in the Red Sea appear to have been very similar to modern time conditions. The trend of the planktonic foraminifera fauna in the central Red Sea towards a resemblance of a present-day southern Red Sea fauna had slowed down; in the northern Red Sea the faunal composition remained stationary. The abundances of most foraminifera species was similar to those encountered at modern times, only the relative abundances of *G. ruber* were significantly lower. With the establishment of a sea level between 10 m [Fairbanks 1992] and 4 m [Fleming et al. 1998] below present day, post-glacial sea level rise had almost ceased. Seasonality in terms of seasonal insolation differences showed a decreasing trend but was still higher than today, implying a correspondingly stronger summer monsoon [Rossignol-Strick 1983]. A stronger SW monsoon during the late stages of this phase has been reconstructed from varved sediments in the Arabian Sea [Doose-Rolinski et al. 2001; Lückge et al. 2001; von Rad et al. 2006]. The expectation of a pronounced seasonality for this phase is supported by the reconstruction of a stronger seasonal temperature gradient than at present day on basis of the isotopic composition of

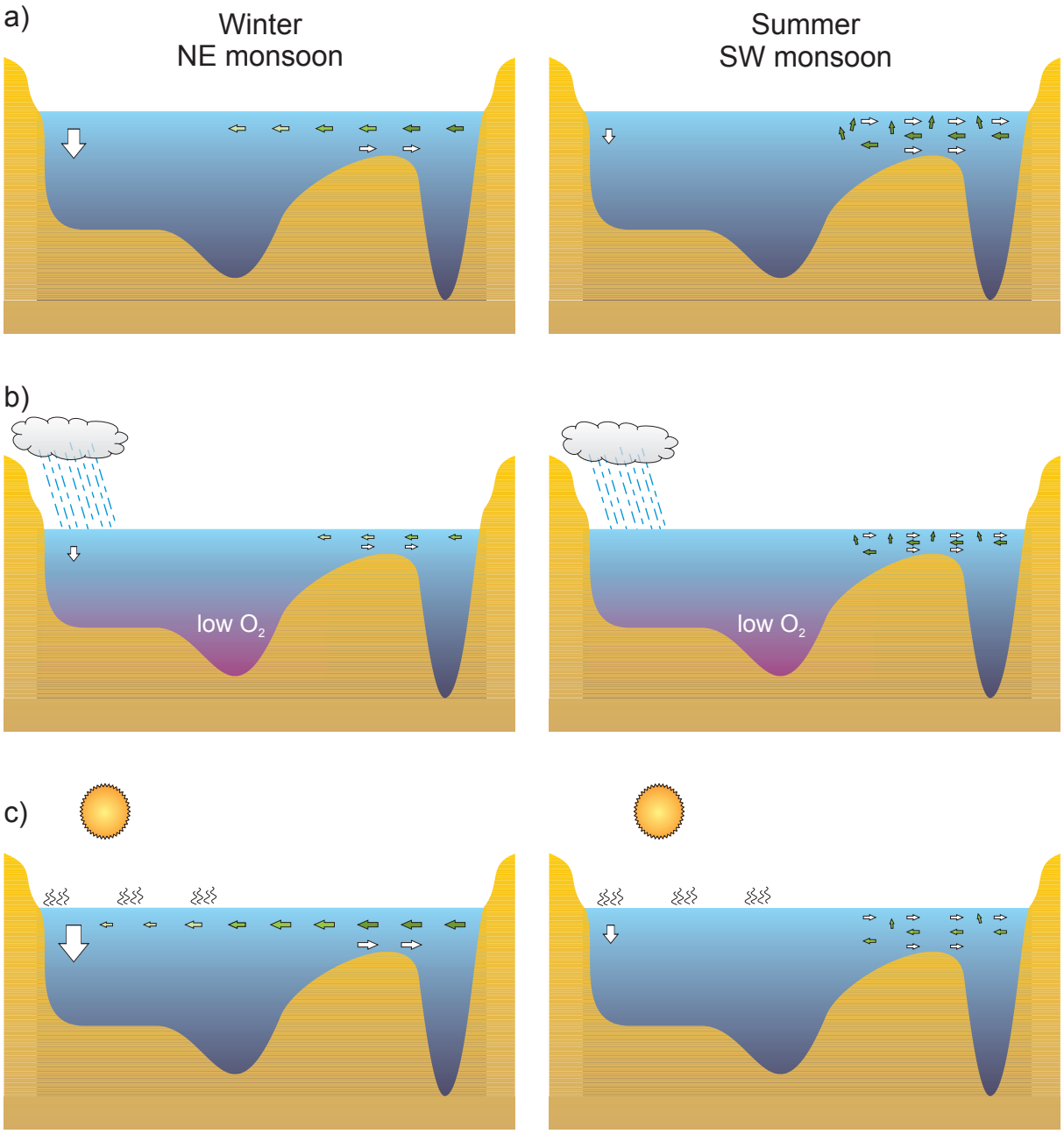

Figure 38 Schemes of circulation system modes of the Red Sea during the Holocene with focus on key elements of the circulation and the pattern of primary productivity. Arrow sizes denote strength of the circulation element, arrow filling (shade of green) denote the fertility, the ability to fuel primary productivity of the circulation element. a) present day mode winter (NE monsoon) and summer (SW monsoon) circulation, erratic smaller arrows denote the patchiness of primary productivity b) early Holocene phase with reduced sea level, local fresh water input in the north and dominant SW monsoon c) faunal shift phase with arid climate, enhanced NE monsoon and weakened SW monsoon.

corals in the northern Red Sea [Moustafa et al. 2000]. The oxygen isotope gradient in the Red Sea was similar to modern times, since the humid period affecting the northern part of the basin had ended at about 6.2 ka BP [Arz et al. 2003a]. In most paleoclimatic studies, the Mid-Holocene phase is inconspicuous and appears as a transient between the humid climate of the early and the arid climate of the late Holocene [Almogi-Labin et al. 1991; Lückge et al. 2001; Fleitmann et al. 2007]. This role of a transition phase with conditions intermediate between the preceding and subsequent phases was

filled well by this time interval; however, its indistinctness makes the identification and interpretation of the small but notable differences to modern times difficult.

Reconstructed primary productivity in the central Red Sea during this phase was slightly higher than at present, a finding that is supported by the carbon isotopic composition. Yet, this reconstruction is not consistent with expectations based on the circulation state that can be assumed for this interval. The stable and same as present-day sea level and the strengthened summer monsoon should have, by the comparable to present input of nutrients into the Red Sea and the dominance of the unproductive season, resulted in a lower primary productivity than today. The circulation system in the Red Sea during the Mid-Holocene must have, at least to a minor degree, been different from the recent one. The main difference in the planktonic foraminifera fauna is the ratio of *G. ruber* to *G. glutinata*, which is at modern times considerably lower than during the Mid-Holocene phase. The differences in this ratio cause the observed differences in the productivity reconstructions, for *G. glutinata* is associated with higher productivity than is *G. ruber* in the recent Red Sea. However, because it is unclear what environmental parameter(s) determine the abundance pattern of *G. ruber* in the present-day Red Sea, the increase in that species abundance cannot be interpreted in terms of the change of any environmental parameter. The same applies for the peak of *G. tenella*, co-occurring with low abundances of *G. siphonifera* at the end of the Mid-Holocene phase. This pattern is reasonably consistent across all cores from the northern and central Red Sea, yet it is again unclear what environmental parameter(s) forced the abundance changes of these species. Thus, on the basis of the available faunal data, the exact differences of the Mid-Holocene phase to the modern time ultimately cannot be determined by this study.

A distinct dry event at 4.2 ka BP, contemporaneous with a volcanic eruption in northern Syria [Weiss et al. 1993], has been inferred from the assemblage composition of thecosomate pteropods [Edelman-Furstenberg et al. 2009] and sediment properties in the northern and central Red Sea [Arz et al. 2006b]. This short-lived event was found mainly in terrestrial or terrestrial-influenced records of high latitude climate [Staubwasser et al. 2003; Marchant and Hooghiemstra 2004; Staubwasser and Weiss 2006] and could to date not be identified in any planktonic foraminifera fauna record from the Red Sea.

Faunal shift (Phase H-II, 3.5 to 2 ka BP, Figure 38 c)

The faunal shift is characterised by extreme changes in the planktonic foraminifera fauna. In all records from the southern and northern Red Sea, the relative abundances of *G. sacculifer* reach uniquely low values, while those of *G. glutinata* and *G. ruber* show distinctive peaks. In the northern Red Sea, the faunal shift is of greater magnitude and the relative abundances of *G. ruber* increase more than those of *G. glutinata*, while in the central Red Sea, the faunal shift is less pronounced and

the increase in relative abundance of these two species is more balanced (Figure 21, 27 and 33). Such capacious changes in the planktonic foraminifera fauna of the Red Sea are certainly forced by the environment, and indeed there is abundant evidence for dramatic and rapid changes in paleoclimate during the faunal shift phase [Mayewski et al. 2004]. Outside of the Red Sea, these significant changes are also manifested in various proxies in marine sediment records from the Mediterranean Sea [Schilman et al. 2001] and the Arabian Sea [Caratini et al. 1994; Bentaleb et al. 1997; von Rad et al. 1999; Doose-Rolinski et al. 2001; Lückge et al. 2001; Jung et al. 2004; von Rad et al. 2006]. The published literature consistently indicates a colder and predominantly more arid climate in the Red Sea region during this time. Millenial scale North Atlantic climate cycles, which propagate cold air from polar to subpolar regions and were found to effect regions as far as the Aegean Sea [Casford et al. 2001; Ehrmann et al. 2007] and the Arabian Sea [Berger and von Rad 2002], peak during the time of the faunal shift phase [O´Brien et al. 1995; Bond et al. 1997]. Episodes of colder climate have been reconstructed for the Mediterranean [Emeis et al. 2000; Rohling et al. 2002; Rimbu et al. 2004] and African regions [Bonnefille et al. 1990; Thompson et al. 2002]. Enhanced aridity have been inferred from pollen and lake levels in western Asia [Gasse and Van Campo 1994; Bryson 1997; Eastwood et al. 2007], speleothem records from Israel and the Arabian peninsula [e.g. Bar-Matthews et al. 1999; Fleitmann et al. 2003a] and vegetation changes in Africa [Petite-Maire et al. 1997; Salzmann and Waller 1998; Kröpelin et al. 2008]. The Indian monsoon system during the faunal shift phase has been found to be opposite to the monsoon system during the early Holocene [Sarkar et al. 2000]; a finding consistent with reports of a minimum in the SW monsoon [Phadtare 2000] and an intensified NE monsoon [Doose-Rolinski et al. 2001; Lückge et al. 2001; von Rad et al. 2006]. The picture of intensified winter conditions in the Red Sea region is perfectly consistent with the reconstructed peak of primary productivity in the central part of the basin. Compared to present day, a strengthened NE monsoon is expected to result in more productive conditions in the central and northern parts of the Red Sea, promoted by the increased transport of Gulf of Aden surface waters to higher latitudes in the basin. The effect of the strengthened winter circulation, in particular the increased deep water formation, on the planktonic foraminifera fauna of the northernmost Red Sea, however, is more difficult to interpret, because the fauna lacks clear analogues in the present day. The productivity reconstructions of KL17 VL during the faunal shift are inconsistent and afflicted with larger uncertainties. Only the WA-PLS transfer function approach reconstructs a significantly higher productivity for this phase. Support for more productive conditions during the faunal shift phase from non-microfossil proxies is sparse. Although $\delta^{13}C$ values in KL17 VL and KL9 are elevated during this phase, KL9 exhibits similar high values during the subsequent modern time phase. $\delta^{15}N$ values measured in KL9 exhibit a local minimum accompanied by increased amounts of total organic carbon in the sediment (Figure 26 and 32). While these patterns all indicate an increased primary productivity, but it must be noted for KL9 that the described proxies show an extremely erratic behaviour during the

faunal shift and modern time phases, which could imply that measurements are affected by edge effects of the core sections related to material alteration during storage.

In contrast to productivity, the reconstructions of the parameters stratification and oxygen concentration are not consistent with intensified winter conditions in the Red Sea. An increased deep water formation in the northern Red Sea would lead to a decreased stratification in the water column and the minimum oxygen concentrations in the almost oxygen saturated upper water layer would stay the same or even increase, due to enhanced mixing and cooling. Instead, the reconstructions of KL17 VL show elevated stratification and a slight reduction of minimum oxygen concentrations. For the central Red Sea it is again difficult to estimate the behaviour of water column stratification under altered circulation conditions without a modelling approach, but the reconstructed decrease in oxygen concentrations of about 0.5 to 1 ml O_2/l in combination with a better aerated water body by the increased formation of deep water would require a substantial increase of grazing intensity and microbial degradation. Nevertheless, a comparable seasonal contrast in minimum oxygen concentrations does exist in the present-day southern Red Sea (cf. Figure 10). The outlined picture of arid and NE monsoon dominated climate for the time around 3 ka BP is in diametral opposition to the reconstruction of a humid time interval by Edelman-Furstenberg at al. [2009], inferred from planktonic foraminifera (7.4 Holocene records of multicorers MC91, MC93 and MC98) and thecosomate pteropod data from the central Red Sea.

Modern time (Phase H-I, 2 ka BP to present time, Figure 38 a)

The beginning of the modern time phase marks the establishment of modern Red Sea circulation conditions. The abundances of planktonic foraminifera species and environmental proxies are stable (the only exceptions are the carbon and nitrogen isotopes of KL9, cf. Chapter 7.2.4 Non-faunal proxy results). Paleoclimatic studies of the Red Sea region reconstruct the return to a more humid climate from the arid conditions of the preceding faunal shift period, on the basis of the re-establishment of fluvial deposition in the Sudan highlands [Mawson and Williams 1984], the resumption of speleothem growth on the Arabian Peninsula [Fleitmann et al. 2007] and pollen data from the Arabian Sea [Caratini et al. 1994]. Marine sediment records from the Mediterranean Sea and the Arabian Sea record the establishment of climatic conditions and circulation patterns, indistinguishable from those at present day, between 1.5 and 2 ka BP [Schilman et al. 2001]

In summary, it can be concluded that the Red Sea, its circulation system and accordingly its fauna is predominantly controlled by changes of sea level. The early Holocene demonstrates that even sea level differences below 30 m to present have a major impact. The later parts of the Holocene records, on the other hand, show that under conditions of a stable and high sea level, the Red Sea is highly sensitive to atmospheric climate forcing linked to variations of the Indian monsoon system. The productivity

reconstructions based on the Holocene records from the central and northern Red Sea are almost perfectly consistent with the established paleoclimatic picture of this interval. Hypothetical reconstructions of other environmental parameters, on the other hand, imply changes, which are difficult to reconcile with the oceanographic scenario of the Holocene. This further supports the concept of a productivity control on the planktonic foraminifera distribution in the Red Sea during times of high and stable sea level.

8 The late Pleistocene

Topic of this chapter is the application of the developed transfer functions for primary productivity to records older than the Holocene. The critical point for the application is clearly the analogy of fauna and environmental conditions and accordingly the focus lies on the identification of analogue intervals, where the transfer functions can produce realistic and reliable reconstructions. A detailed interpretation of the climate for the analysed records will not be attempted, for this is outside the scope of this work.

8.1 Orbital age model

The stratigraphic framework for core KL9 was obtained by correlation of the oxygen isotope record (included in the Appendix) with the orbitally tuned SPECMAP timescale [Imbrie et al. 1984; Imbrie et al. 1990] (Figure 39). Although there exist age models for the Pleistocene, which incorporate many more data points [e.g. Huybers 2006a; Huybers 2006b], the SPECMAP timescale was used during the conduct of this work, to facilitate comparisons with other existing SPECMAP-tuned late Pleistocene faunal records from the Red Sea [e.g. Fenton 1998; Geiselhart 1998; Schmelzer 1998]. Ages for samples between tie-points of the SPECMAP timescale and KL9 (Table 14) were calculated by linear interpolation. Age models for the cores MD921017 and MD921039 were taken from the supplementary material of Fenton at al. [Fenton et al. 2000].

Age [ky BP]	Event	Depth [cm]	Age [ky BP]	Event	Depth [cm]	Age [ky BP]	Event	Depth [cm]
28	3.1	197	183	6.6	609	331	9.3	1070
40.5	3.2	215	194	7.1	651	341	10.2	1100
53	3.3	234	205	7.2	671	349	*	1131
65	4.2	245	216	7.3	681	368	11.1	1261
80	5.1	305	228	7.4	721	375	11.2	1271
87	5.2	327	238	7.5	766	405	11.3	1326
99	5.3	377	249	8.2	812	434	12.2	1441
107	5.4	403	257	8.3	822	461	12.33	1508
122	5.5	447	269	8.4	842	471	12.4	1521
135	6.2	489	287	8.5	902	481	13.11	1571
146	6.3	510	299	8.6	921	491	13.12	1601
151	6.4	542	310	9.1	961	502	13.13	1631
171	6.5	572	320	9.2	1008	514	13.2	1671

Table 14 Isotopic events from the SPECMAP timescale [Imbrie et al. 1984; Imbrie and et al. 1990] used as control points for the age model of KL9. * inserted control point in reference to record of MD921017 [Fenton et al. 2000]

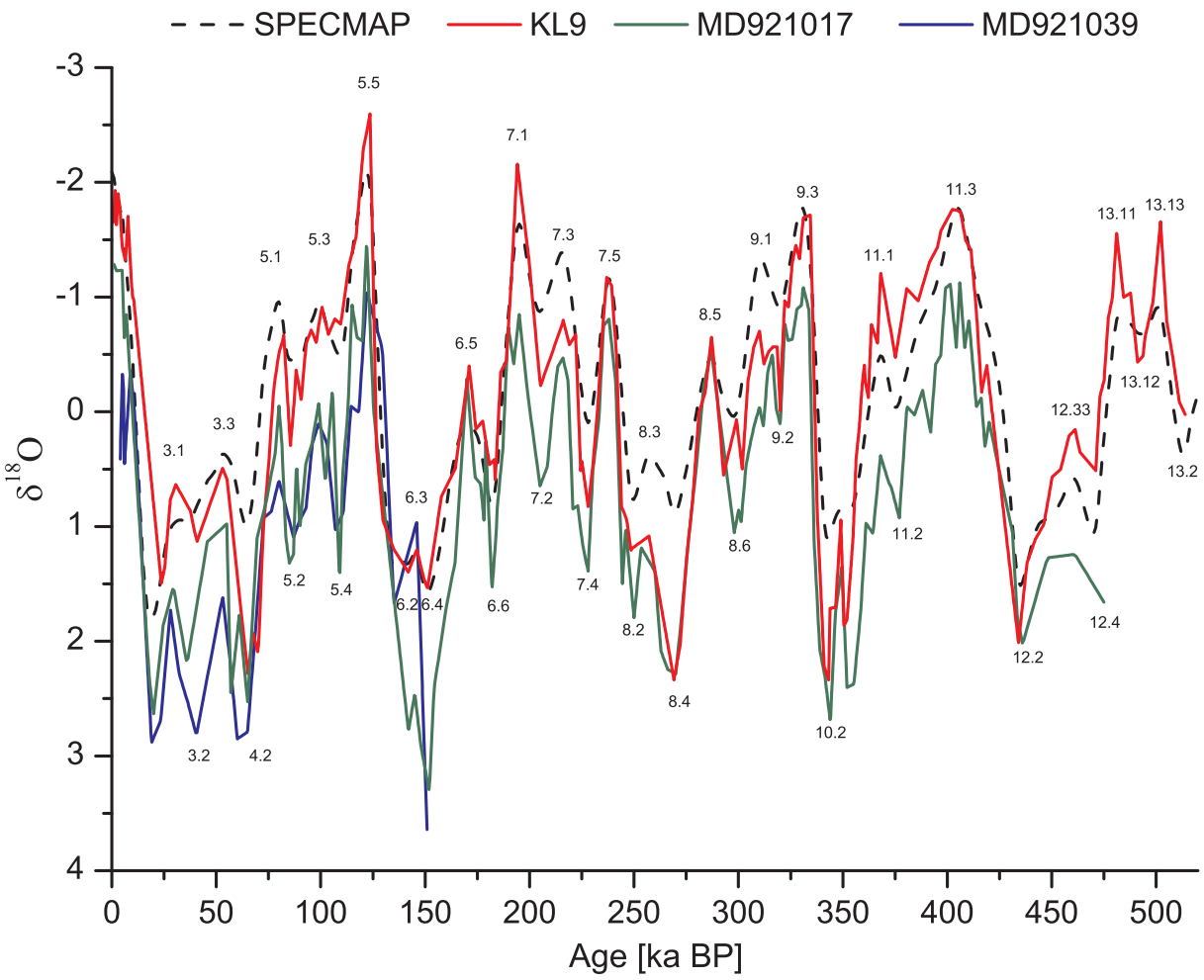

Figure 39 Oxygen isotope records of cores KL9 (this study), MD921017, MD921039 [Fenton et al. 2000] and the SPECMAP record [Imbrie et al. 1984; Imbrie et al. 1990].

8.2 Marine Isotope stage 5e record of KL9

The faunal record that covers MIS 5e in core KL9, (511-387 cm) includes an aplanktonic zone between 499 and 466 cm depth, corresponding to the MIS 6 glacial sea level lowstand, and the entire MIS 5e peak interglacial sea level highstand. The faunal census data were taken from Trommer et al. [in preparation]. Following the working hypothesis on environmental control of the planktonic foraminifera assemblage in the Red Sea, further confirmed by paleoenvironmental reconstructions of Holocene climate variability (cf. Chapter 7.5 Synopsis of Holocene climatic conditions for the Red Sea), only the reconstructions of chlorophyll *a* are presented.

8.2.1 Faunal record

In the first samples with abundant foraminifera after the MIS 6 aplanktonic zone, the absolute abundance of planktonic foraminifera was still very low (Figure 40). The fauna recovered initially slowly and later rapidly to reach maximal values at around 450 cm depth. Between 440 and 405 cm depth, the absolute abundance fluctuated around the overall average before it declined to very low levels at around 392 cm. The end of the record shows a sharp increase of absolute abundance to values close to the earlier maximum. The record of MIS 5 allows the identification of five faunal phases (not to be confused with the faunal phases of the Holocene). The first phase after the MI 5/6 boundary (M5-I) is very similar to the Holocene postglacial phase. The planktonic foraminifera composition changed rapidly until the first stable interglacial assemblages, similar to those present in the modern northern Red Sea were established. In a second phase (M5-II) from 461 to 442 cm, the foraminifera fauna changed gradually and selectively. The abundances of *G. sacculifer* declined from peak values to almost zero, while *G. glutinata* increased in abundance from 0 % to around 30 %. Relative abundances of *G. ruber* and *G. siphonifera* remained unchanged, those of *G. tenella* increased during the late stages of this phase from 5 % to just above 10 %. The following phase (M5-III) between 442 and 413 cm saw little changes in terms of assemblage composition. *G. glutinata* was the dominant species throughout this phase and its abundance showed a unimodal pattern with maximum abundances of 54 % at around 425 cm depth. The abundances of *G. sacculifer* and *G. siphonifera* were generally very low during this phase and both species were not present in several samples. Relative abundances of *G. ruber* were, compared to the preceding or ensuing phase elevated and showed a weak declining trend. *G. tenella* abundances remained on the level attained at the end of the preceding phase. The next phase (M5-IV) between 413 and 393 cm was again characterised by large gradual changes in the species composition. *G. sacculifer* increased in relative abundance at the expense of *G. glutinata* that decreased from 40 % to 10 % relative abundance. *G. ruber* abundances were reduced at the beginning of this phase, but a relative abundance of 25 % was regained at its end. The abundances of *G. siphonifera* had recovered from their low in the preceding phase to a level of 10 %,

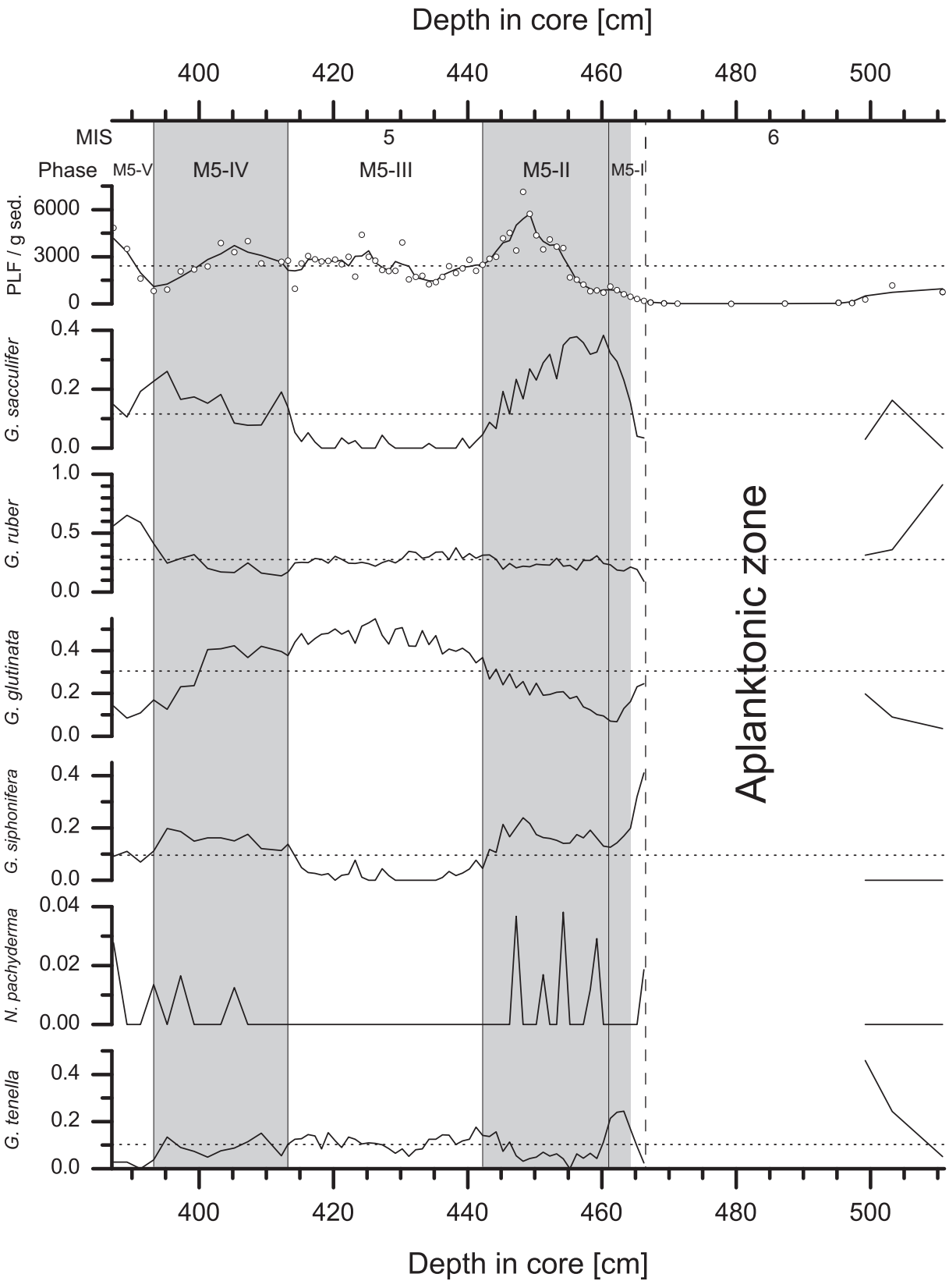

Figure 40 Faunal record of MIS 5e in core KL9. Absolute number of planktonic foraminifera per gram sediment (solid line is the 3-point moving average) and relative abundances of taxonomic units present. Horizontal dotted lines are the averages for the respective variables. Vertical lines represent the boundaries of the described faunal phases. Vertical dashed line indicates the MIS 5/6 boundary. Shaded denote the parts of the record considered as analogous (see Chapter 8.2.2 Analogy situation).

which was later on almost doubled during the course of this phase. Relative abundances of *G. tenella* remained at around 10 %. The last phase (M5-V) is only poorly resolved, but experienced rapid changes in species composition. The decreasing trend of *G. glutinata* continued, but also *G. sacculifer*, *G. siphonifera* and *G. tenella* abundances dropped during this phase. *G. ruber* proliferated and reached relative abundances above 60 %. *N. pachyderma* appeared only sporadically during the whole MIS 5e record and then only with very low abundances, yet is intriguing that it did not occur in the *G. glutinata* dominated phase.

8.2.2 Analogy situation

A substantial portion of the faunal record of MIS 5e is not analogous to the calibration dataset. In the analogy plot (Figure 41) only few samples of these two records can be considered as overlapping. Phase M5-III is due to the high *G. glutinata* abundances on the one hand similar to the modern fauna in the southern Red Sea (component one), but on the other hand for the lack of *G. bulloides* and the Gulf of Aden species group in combination with high abundances of *G. tenella* also very different (component two). The environmental analogy plot (Figure 42) differentiates between two analogue phases of the record. The samples of phase M5-II form the horizontal line in the upper half of the plot, spanning a range of almost 3 ‰ in oxygen isotope values. The younger analogue phase M5-IV is represented by a cluster of samples around the lower 95 % confidence interval with oxygen isotope values

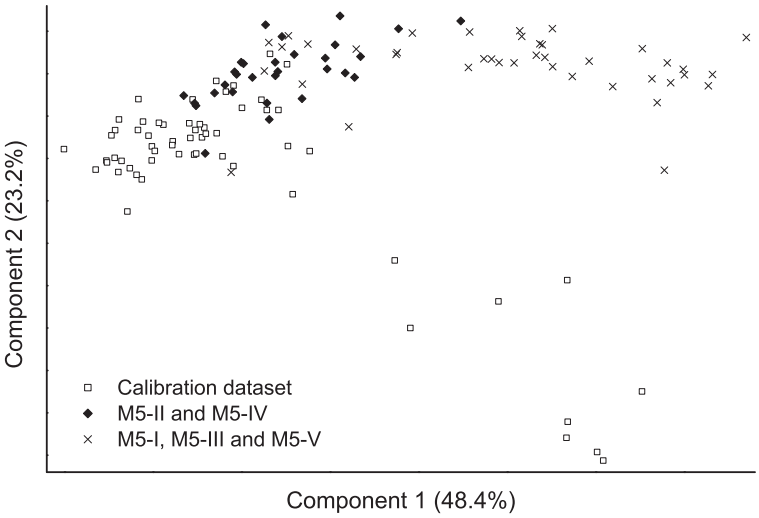

Figure 41 Analogy analysis in form of a scaled plot of a principal component analysis of log-transformed faunal data from of the MIS 5e record of KL9 and the calibration dataset. Phase M5-I includes three samples of MIS 6.

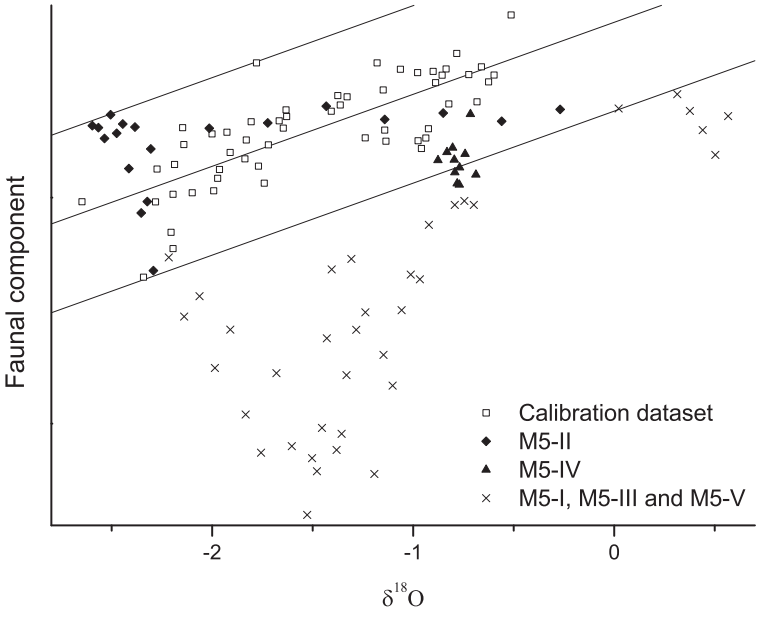

Figure 42 Analogy analysis in form of a cross plot of oxygen isotopes and the first principal component of faunal data from the MIS 5e record of KL9 and the calibration dataset. Solid lines denote the linear fit of the calibration dataset and the boundaries of the 95 % confidence interval. Phase M5-I includes three samples of MIS 6.

of approximately -0.75 ‰. The non-analogue *G. glutinata* dominated phase M5-III lies between these two clusters, with oxygen isotope values from -2 to -1 but faunal component values far outside the range found in the Red Sea at present. Based on these two analogy test approaches, the intervals 464 cm to 442 cm (126.4 to 120.4 ka BP, including phase M5-II) and 413 to 393 cm depth in core (110.5 to 104 ka BP, phase M5-IV) can be considered as analogous to the calibration dataset. The Bray-Curtis dissimilarity measure (Figure 43) supports these conclusions and denotes almost exactly the same phases as analogue; the last sample of phase M5-II and two samples within phase M5-IV exceed the critical dissimilarity value. During these two analogue phases, transfer function reconstructions of chlorophyll *a* could be considered reliable and interpreted in terms of absolute values.

8.2.3 Transfer function reconstructions

The chlorophyll *a* reconstructions show an increasing trend for the older analogue phase (corresponding to M5-II) from 127 to 120 ka BP (Figure 43). Chlorophyll *a* concentrations range from 0.1 to around 0.3 mg/m³ over this interval, which is a change of 50 % in either direction compared to the recent value at the core position. Minor deviations of these generally consistent reconstructions are brought up by IKM with an estimate below zero for the first sample of this phase and the WA-PLS approach, whose estimates are generally higher than those produced by the other methods and attain a value of almost 0.5 mg/m³ at the end of the interval. Sea level reconstructions during this phase reach the highest values within the whole record of KL9 [Rohling et al. 2009] and seasonal insolation differences are high with a decreasing trend (Figure 43). Both these environmental conditions are consistent with the trend of the productivity reconstructions and suggest a situation similar to the early Holocene: low but increasing primary productivity during sea level rise and a weakening of summer circulation conditions.

The younger analogue phase (corresponding to M5-IV) from 110 to 104 ka BP shows a consistent decreasing trend, with chlorophyll *a* concentrations of 0.5 mg/m³ declining to the present-day value of around 0.2 mg/m³. During this interval, the MAT approach exhibits the largest deviations and huge jumps, where reconstructed values change by 0.6 units from one sample to the next. Sea level was constant and lower than at present day during this phase (cf. oxygen isotopic composition), while seasonal insolation differences show an increasing trend. The corresponding change from dominant winter to summer circulation conditions in the Red Sea is again consistent with the trend of the productivity reconstructions, although the reduced sea level contradicts the absolute values of reconstructed productivity, which are much higher than at present day. The reliability of the reconstructions for both of the analogue phases is good (Figure 44), only three samples exceed the critical value for estimate divergence.

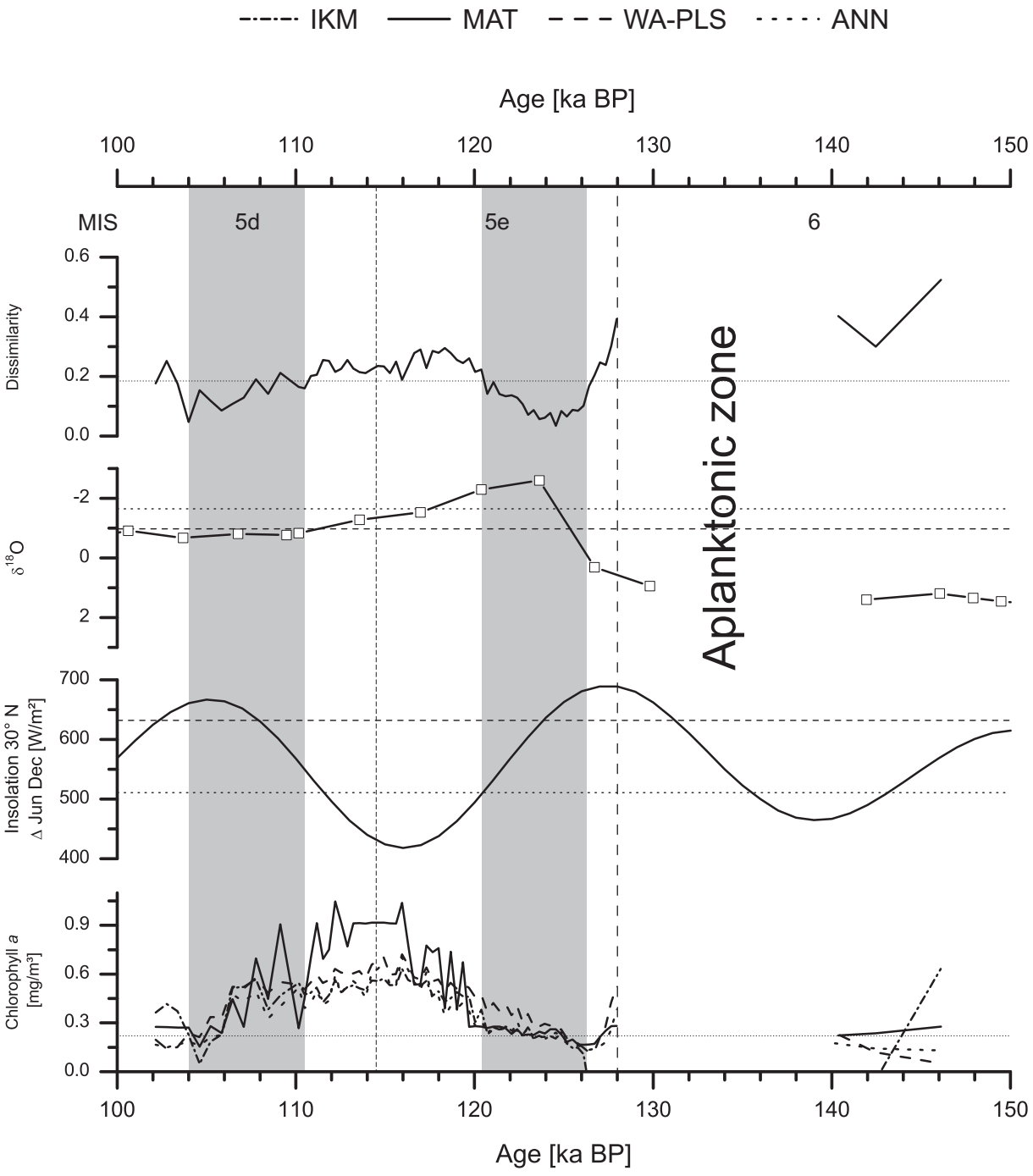

Figure 43 Transfer function chlorophyll *a* reconstruction results and environmental parameters for the MIS 5e record of KL9. The topmost minimal dissimilarity is shown as an indicator of sample analogy, oxygen isotopes as proxy for sea level [Siddall et al. 2004] and the difference between June and December insolation at 30° N as seasonality index. Horizontal dotted lines represent present day values of the respective environmental parameter at the core position. In case of dissimilarity, the dotted line is the critical value of dissimilarity (cf. Chapter 5.6.3 Assessment of uncertainties on reconstructions). Horizontal dashed line represent the respective parameter value during the early Holocene. Vertical dashed lines denote marine isotope stage and substage boundaries. Shaded area indicates the phases considered as analogous.

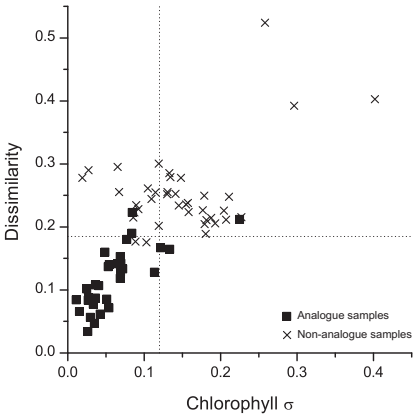

Figure 44 Transfer function reconstruction assessment for the productivity reconstructions of the MIS 5e record of KL9. Dotted lines indicate the defined critical values for dissimilarity and estimate divergence.

For the non-analogue, *G. glutinata* dominated phase, the transfer functions produce productivity reconstructions, which could link the two analogue phases in a convincing way. Except for MAT, which shows the largest deviation and jumps similar to those during the younger analogue phase, the methods follow the *G. glutinata* abundances and yield a unimodal pattern of reconstructed primary productivity. The attained maximal values of chlorophyll *a* concentration are approximately 0.6 mg/m³, only the MAT approach shows two peaks of 1 mg/m³. Sea level decreases over more than the full Holocene range during this phase. Seasonal insolation differences are at a minimum and imply strong winter circulation conditions. While the condition of a very strong winter circulation at a lower sea level is possibly consistent with the reconstruction of greatly increased primary productivity, they are certainly difficult to unite with the general picture of paleoclimate that exists for this time interval. Speleothem studies [Bar-Matthews et al. 2003; Fleitmann et al. 2003b] and modelling approaches [Herold and Lohmann 2009] agree on the reconstruction of a very humid climate with high precipitation during MIS 5e. Because in the recent Red Sea circulation system, high rates of precipitation are connected to summer circulation conditions and low productivity, it is very probable that the non-analogue fauna during MIS 5e/d denote non-analogue circulation conditions. In this MIS 5e circulation mode, the combination of strong winter monsoon and high rates of precipitation result in greatly enhanced primary productivity in the Red Sea.

8.3 Marine Isotope stage 11 record of KL9

The faunal record of core KL9 covering MIS 11 ranges between 1160 to 1466 cm depth and includes an aplanktonic zone between 1378 and 1442 cm, corresponding to the sea level lowstand of MIS 12. K. Braun produced the faunal census data during her diploma theses [Braun 2009], which has been conducted contemporaneously with this study at the geological institute of the University of Tübingen. The foraminifera taxonomy follows exactly the concepts used in the Red Sea calibration dataset and other data in this study. Following the working hypothesis on environmental control of the planktonic foraminifera assemblage in the Red Sea, further confirmed by paleoenvironmental reconstructions of Holocene climate variability (cf. Chapter 7.5 Synopsis of Holocene climatic conditions for the Red Sea), only the reconstructions of chlorophyll *a* are presented.

8.3.1 Faunal record

The absolute abundance of planktonic foraminifera was in general highly variable. The abundances during the interglacial MIS 11 were higher than during the investigated parts of MIS 10 and MIS 12, where they were the lowest (Figure 45). Within MIS 11, two periods of increased foraminifera abundance can be identified between 1270 and 1310 cm and between 1340 and 1375 cm. On basis of trends in the planktonic foraminifera fauna, three phases can be defined within the interval of MIS 11 (M11-I to M11-III). The first phase (M11-I), starting after the aplanktonic zone of MIS12 and reaching up to 1355 cm depth, was characterised by a highly variable abundances of *G. sacculifer* (30 % - 5 %) and *G. ruber* (75 % - 30 %). Relative abundances of *G. glutinata* were higher than any time later in this record and *G. siphonifera* was almost absent from the planktonic foraminifera community. During the second phase (M11-II) from 1355 to around 1300 cm, the relative abundances of the four dominant planktonic foraminifera species were balanced. *G. sacculifer*, *G. ruber*, *G. glutinata* and *G. siphonifera* abundances fluctuated around an average of about 20 %. Abundance of the taxonomic group *N. pachyderma* peaked with abundance values of around 5 % at the beginning and a short way above this second phase. The remainder of the MIS 11, the interval between 1300 and 1220 cm depth, represents the third phase (M11-III). *G. sacculifer* abundances had decreased to a level of around 12 % while *G. ruber* clearly dominated the foraminifera fauna with a relative abundance of around 40 %. Abundances of *G. glutinata* were with 17 % stable, in contrast to those of *G. siphonifera*, which decreased from 18 % to 8 % during this phase. *G. tenella* abundances were with 4 % very low but slightly elevated when compared to the other phases. *G. bulloides* and the Gulf of Aden species group were not found in the MIS 11 record of core KL9. It is interesting to note that foraminifera assemblages of the investigated part of the subsequent MIS 10 were very similar to the last faunal phase of MIS 11, the only notable difference was the continuing increase of the relative

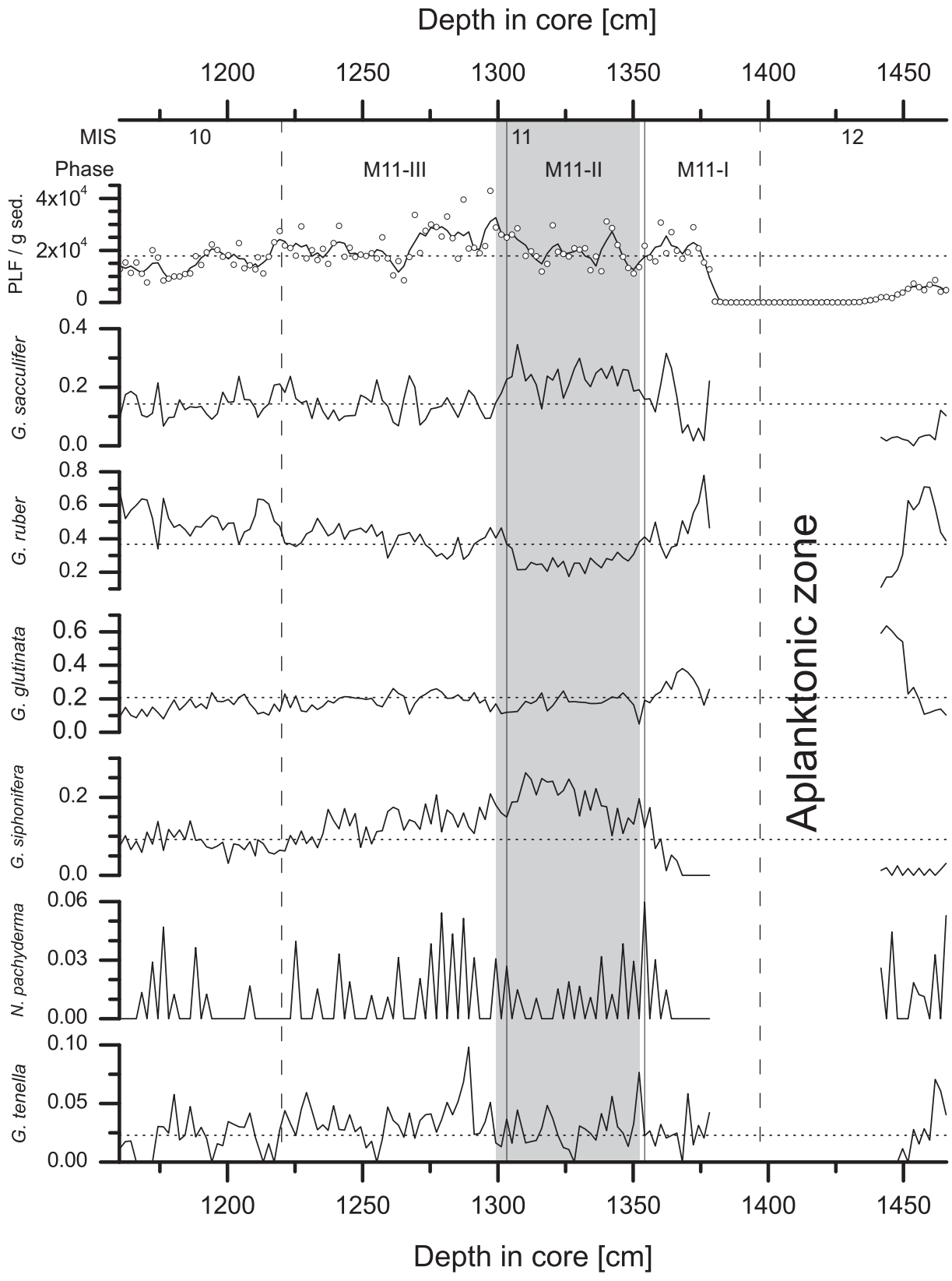

Figure 45 MIS 11 faunal record of KL9. Data from *Braun* [2009]. Absolute number of planktonic foraminifera per gram sediment (solid line is the 3-point moving average) and relative abundances of taxonomic units present. Horizontal dotted lines are the averages for the respective variables. Vertical lines represent boundaries between the described faunal phase boundaries. Vertical dashed lines denote marine isotope stage boundaries. Shaded area denotes the part of the record considered as analogous (see Chapter 8.3.2 Analogy situation).

abundance of *G. ruber* to approximately 50 %. The few counts from MIS 12 give no consistent picture, apart from low *G. sacculifer* and very low *G. siphonifera* abundances.

8.3.2 Analogy situation

The faunal record of MIS 11 can be considered analogous only for a part of the interglacial. The analogy plot (Figure 46) shows that the differences to the calibration dataset are not related to the recent north-south gradient, covered by the first component, but lie in the values of the second component, which in part reflects the *G. ruber* abundances. The area where the two datasets overlap is occupied by samples from the southern and central Red Sea. The analogue samples identified on the basis of the analogy plot are virtually identical to those marked as analogue by the environmental analogy analysis (Figure 47). The majority of samples of the MIS 11 record, particularly those from MIS 10 and MIS 12 plot due to the heavy oxygen isotopic composition far away from the recent faunal gradient in the Red Sea and the few analogue downcore samples cluster with samples from the central Red Sea. The samples with the lowest values of the faunal component originate from MIS 12 and the faunal phase M11-I. Based on these two analogy test approaches, the interval 1299 cm to 1352 cm (390.4 to 411.5 ka BP, corresponding approximately to M11-II) can be considered as analogous to the calibration dataset. The values of the Bray-Curtis similarity measure (Figure 48) are very high for the whole

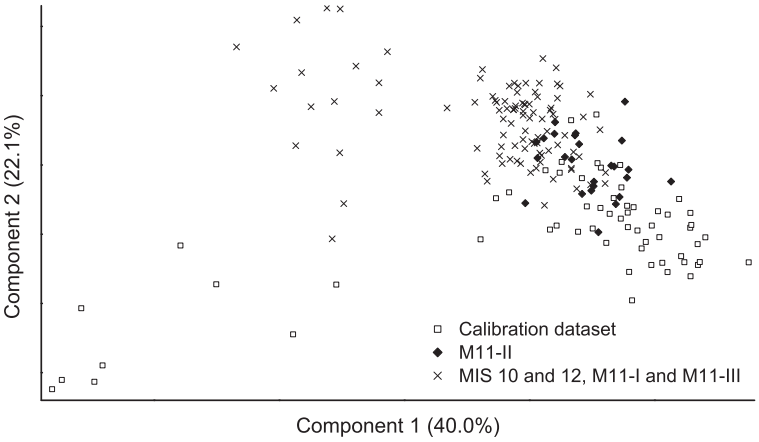

Figure 46 Analogy analysis in form of a scaled plot of a principal component analysis of log-transformed faunal data from the MIS 11 record of KL9 [Braun 2009] and the calibration dataset.

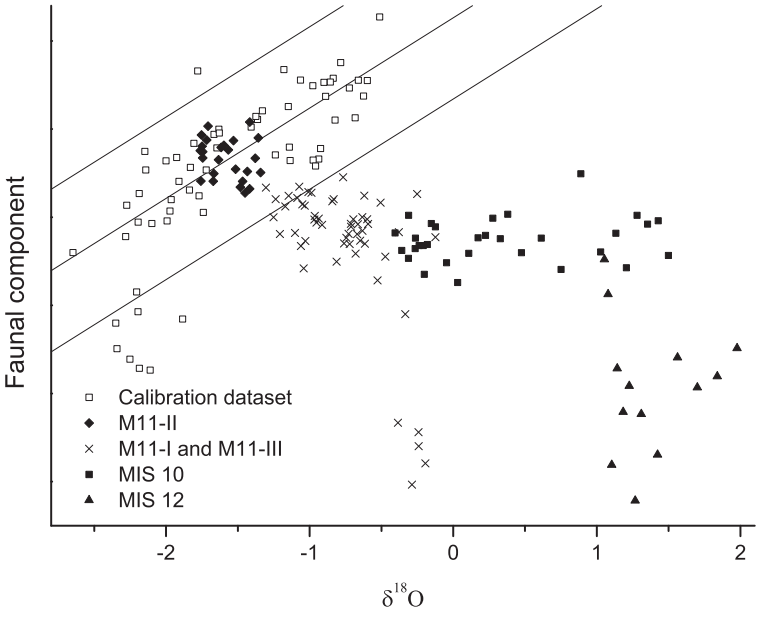

Figure 47 Analogy analysis in form of a cross plot of oxygen isotopes and the first principal component of faunal data from the MIS 11 record of KL9 and the calibration dataset. Solid lines denote the linear fit of the calibration dataset and the boundaries of the 95 % confidence interval.

record and by this approach almost no sample could be considered analogous. The analogue interval identified by the other approaches exhibits average dissimilarity values of approximately 0.24, which is above the threshold value of 0.185 (cf. Chapter 5.6.3 Assessment of uncertainties on reconstructions) and very high compared to the Holocene average of 0.076.

8.3.3 Transfer function reconstructions

The exceptionally long interglacial MIS 11 is a long-standing focus in paleoceanography [e.g. Droxler et al. 2003b]. Its similar orbital climate forcing makes it a potential analogue for today's and future climate without anthropogenic impact [Berger and Wefer 2003; Droxler et al. 2003a]. The scientific community is at issue about the analogy of MIS 11 [Bauch et al. 2000; Hodell et al. 2000; Dickson et al. 2009; McManus et al. 2003; de Abreu et al. 2005] and the specific differences to Holocene and present-day climate [Bowen 2003; Lea et al. 2003]. The identification of only a weak-analogue phase to recent conditions and thus also Holocene conditions between 411 and 390 ka BP is therefore interesting by itself. The estimated chlorophyll *a* concentrations for this analogue phase are highly inconsistent for the different methods (Figure 48). The IKM approach cannot deal with the low analogy and reconstructs negative chlorophyll *a* concentrations for almost the entire phase. The other three methods exhibit a similar pattern in their reconstructions, with close to the present-day primary productivity between 406 to 410 ka BP, followed by two separated productivity peaks at 404 and 399 ka BP and lower productivity from 395 ka BP to the end of the analogue phase at 390 ka BP. The MAT approach produces the most conservative estimates, which diverge from those of WA-PLS and ANN near the end of the analogue phase and do not show the productivity peaks. Although this pattern is only weakly resolved (the second peak is based on one sample), most of its constituent parts are consistent with the prevailing environmental conditions. The close to present-day productivity, reconstructed for the beginning of the analogue phase occur under conditions of a similar to present-day sea level (cf. oxygen isotopes, Figure 48) and a strengthened summer monsoon (cf. insolation seasonality, Figure 48). The first peak in productivity coincides with sea level highstand during MIS 11 and a decreasing trend in summer monsoon strength. The second peak coincides with slightly reduced sea level and a minimum in insolation seasonality, which probably caused a strong winter monsoon and a strong winter circulation mode in the Red Sea. The reconstructions of the two samples between these two peaks cannot be explained by our knowledge of the Red Sea circulation system, since the environmental conditions during this low in the productivity reconstructions must have been intermediate between those during the adjacent peaks and are thus expected to promote primary productivity. The observed change of the foraminifera fauna for these samples is a combination of a decrease of *G. glutinata* and an increase of *G. siphonifera* and *G. tenella* abundances. The consequent decrease of reconstructed productivity is consistent with the expectation from the general paleoenvironmental conditions in the basin, for it coincides with decreasing sea level and increasing

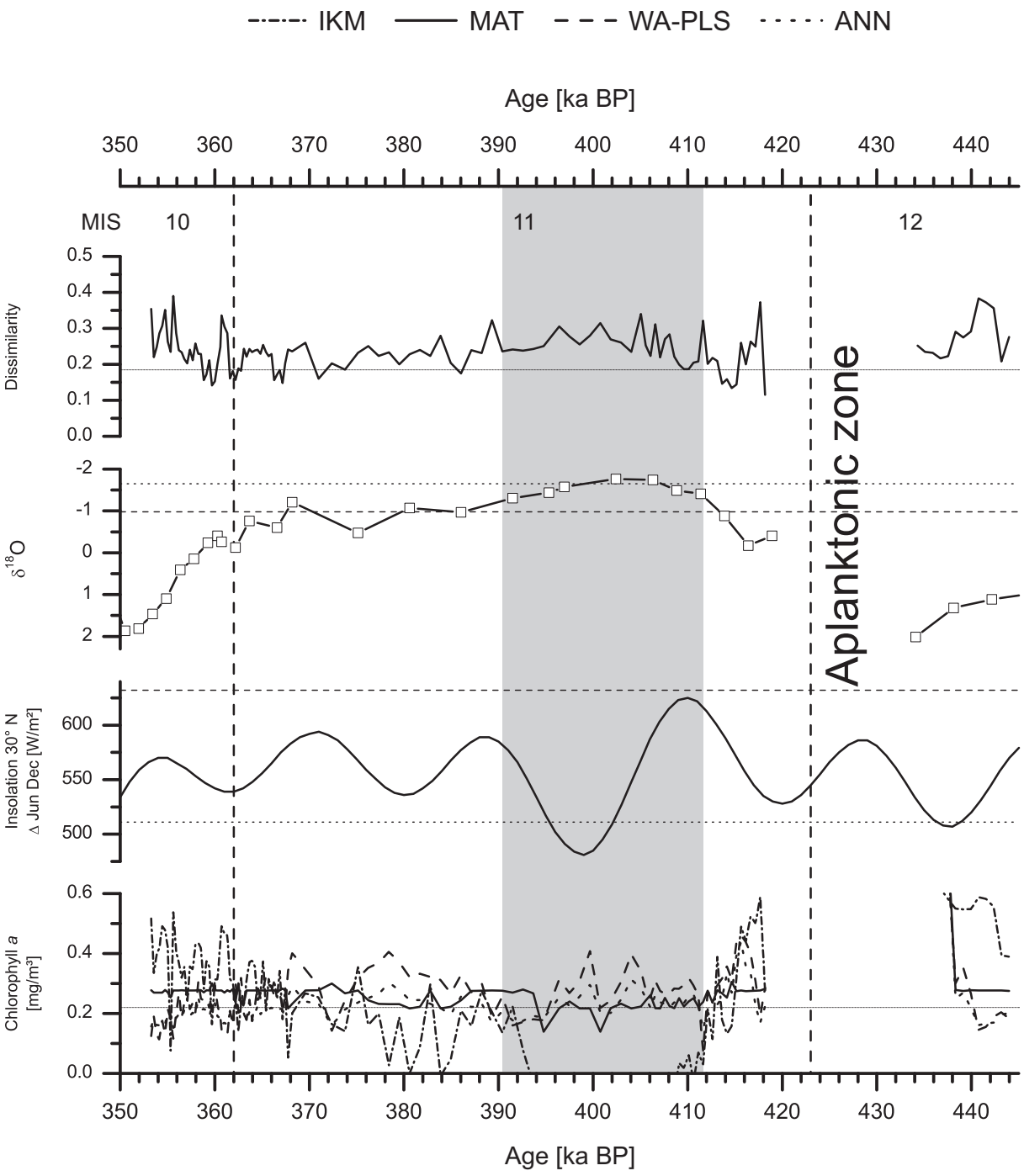

Figure 48 Transfer function chlorophyll *a* reconstruction results and environmental parameters for the MIS 11 record of KL9. The topmost minimal dissimilarity is shown as an indicator of sample analogy, oxygen isotopes as proxy for sea level [Siddall et al. 2004] and the difference between June and December insolation at 30° N as seasonality index. Horizontal dotted lines represent present day values of the respective environmental parameter at the core position. In case of dissimilarity, the dotted line is the critical value of dissimilarity (cf. Chapter 5.6.3 Assessment of uncertainties on reconstructions). Horizontal dashed line represent the respective parameter value during the early Holocene. Vertical dashed lines denote marine isotope stage boundaries. Shaded area indicates the episode considered as analogous.

seasonal insolation difference. According to the set standards for the assessment of transfer function uncertainties the chlorophyll *a* reconstructions of the MIS 11 must be considered unreliable. The inability of the IKM approach to deal with the high abundances of *G. ruber* cause for the majority of the samples of the analogue phase estimate divergences that clearly surpass the critical value (Figure 49). It can be concluded that both analogy analyses and transfer function reconstruction results support the point of view that a subsection of marine isotope stage 11 is analogous to present day and the Holocene. The identified analogue period corresponds to the second half of the MIS 11 optimum (second peak of the 65° N insolation curve), that is for its special boundary conditions by some researchers considered not to be an ideal analogue [Dickson et al. 2009].

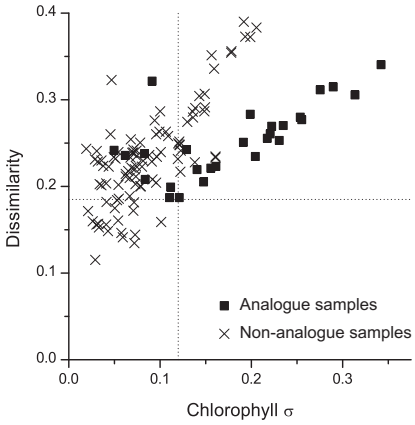

Figure 49 Transfer function reconstruction assessment for the productivity reconstructions of the MIS 11 record of KL9. Dotted lines indicate the defined critical values for dissimilarity and estimate divergence.

8.4 Records of cores MD921017 and MD921039

The cores MD921017 and MD921039 were collected by RV Marion Dufresne in 1992 [Caulet et al. 1992] and have a length of 1540 cm and 750 cm respectively. The faunal census data were produced by M. Fenton during her Ph.D. thesis [Fenton 1998], and were taken from the supplementary material of Fenton at al. [2000]. The census data do not meet the standards of 300 counted individuals per samples, and detection limits of foraminifera species are consequently lower. Due to less than 100 counted individuals per sample, nine samples from MD921017 (157) and thirteen samples from MD921039 (57) were excluded altogether. Based on SEM pictures in the thesis [Fenton 1998], the taxonomy of the faunal records agrees with the one used in this study.

8.4.1 Faunal records

The description of the two long records will focus on glacial/interglacial variations and differences to the discussed records of KL9. The low resolution complicates a comparison with the discussed Holocene data, but it appears that both records capture the faunal shift around 2.6 ka BP, identified in all records discussed in chapter 7. The Holocene. In MD921017, the next-last sample shows the corresponding abundance pattern, while in MD921039 the record seems to end just during the faunal shift. The early Holocene feature of elevated *G. sacculifer* abundances is only exhibited in MD921017. The core tops of both cores were radiocarbon dated to 1.1 ka BP (MD921017; 1 cm depth in core) and 1.4 ka BP (MD921039; 4 cm depth in core).

On a longer timescale, *G. sacculifer* was clearly more abundant during interglacial periods than during glacials and reached peak abundances during the Holocene and MIS 5, a finding consistent with the faunal records of KL9. *G. ruber* is the overall dominant species in both records with peak abundances during glacials. Especially high relative abundances of around 70 % were attained during MIS 4 to 2, a finding consistent with the counts for this period by Schmelzer [1998]. The relative abundance of *G. glutinata* was higher during interglacial periods and lower during glacials, MIS 8 and 7 being an exception with no clear trend for this species. Peak abundances during MIS 11 and 5 are consistent with findings in the corresponding records of KL9. The abundance pattern of *G. siphonifera* is not obvious, the highest relative abundances were attained during the Holocene, MIS 5, 6 and 11, the lowest during MIS 3, 6, 8, 10 and 11. This species almost disappeared during MIS 3, a finding consistent with the counts of Schmelzer [1998]. *N. pachyderma* occurs very rarely in both records and only in two samples of MIS 6 with relative abundances above 1 %. *G. bulloides* occurs slightly more frequently than *N. pachyderma*, but no clear pattern can be extracted from these occurrences. The abundance pattern of *G. tenella* is indistinct, exceptional peaks with relative abundances above 20 % occurred in MIS 8 and at the MIS 10/9 boundary.

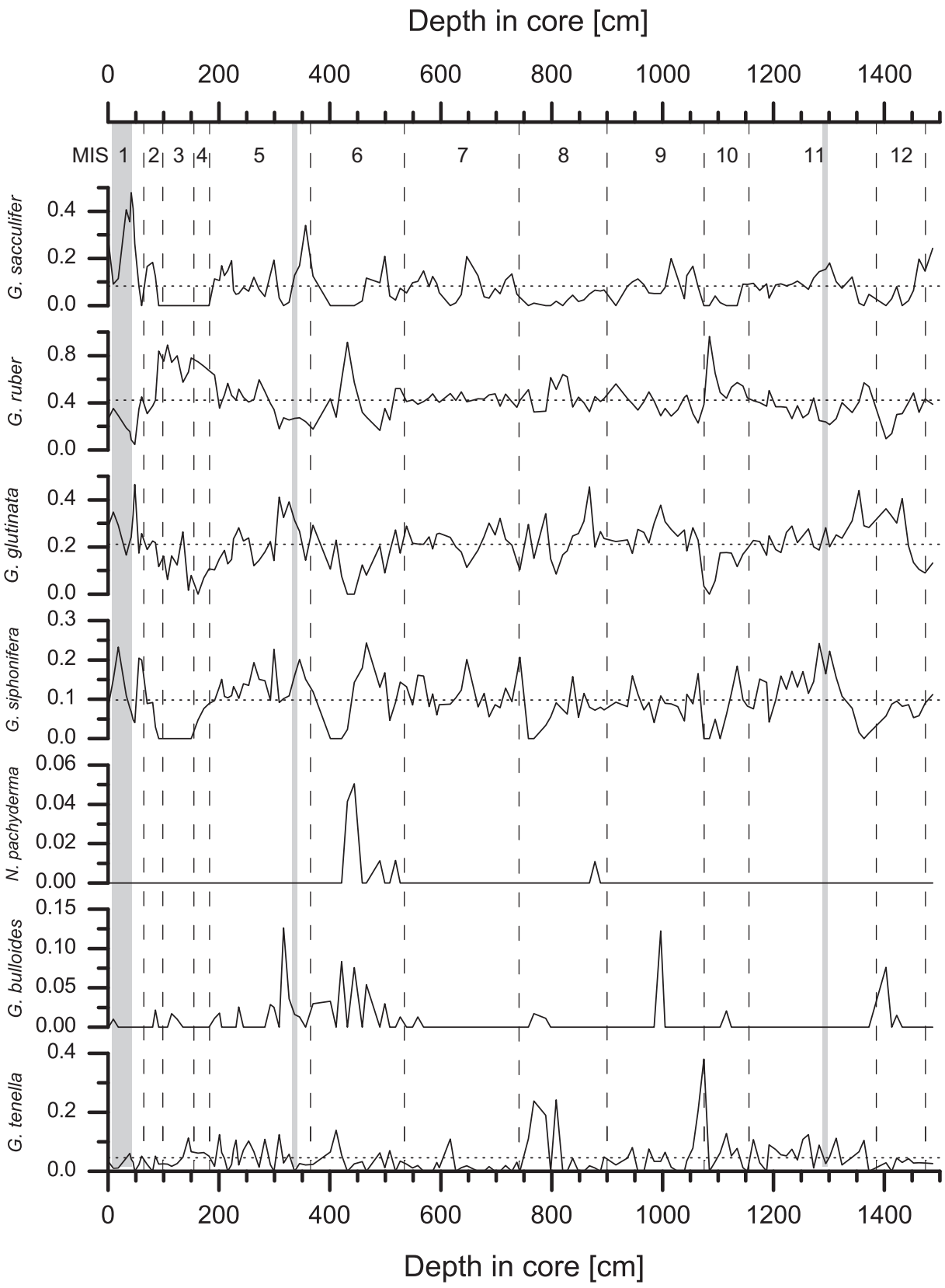

Figure 50 Faunal record of MD921017. Data from *Fenton* [2000]. Horizontal dotted lines are the averages for the taxonomic units. Vertical dashed lines denote marine isotope stage boundaries. Shaded areas denote the parts of the record considered as analogue.

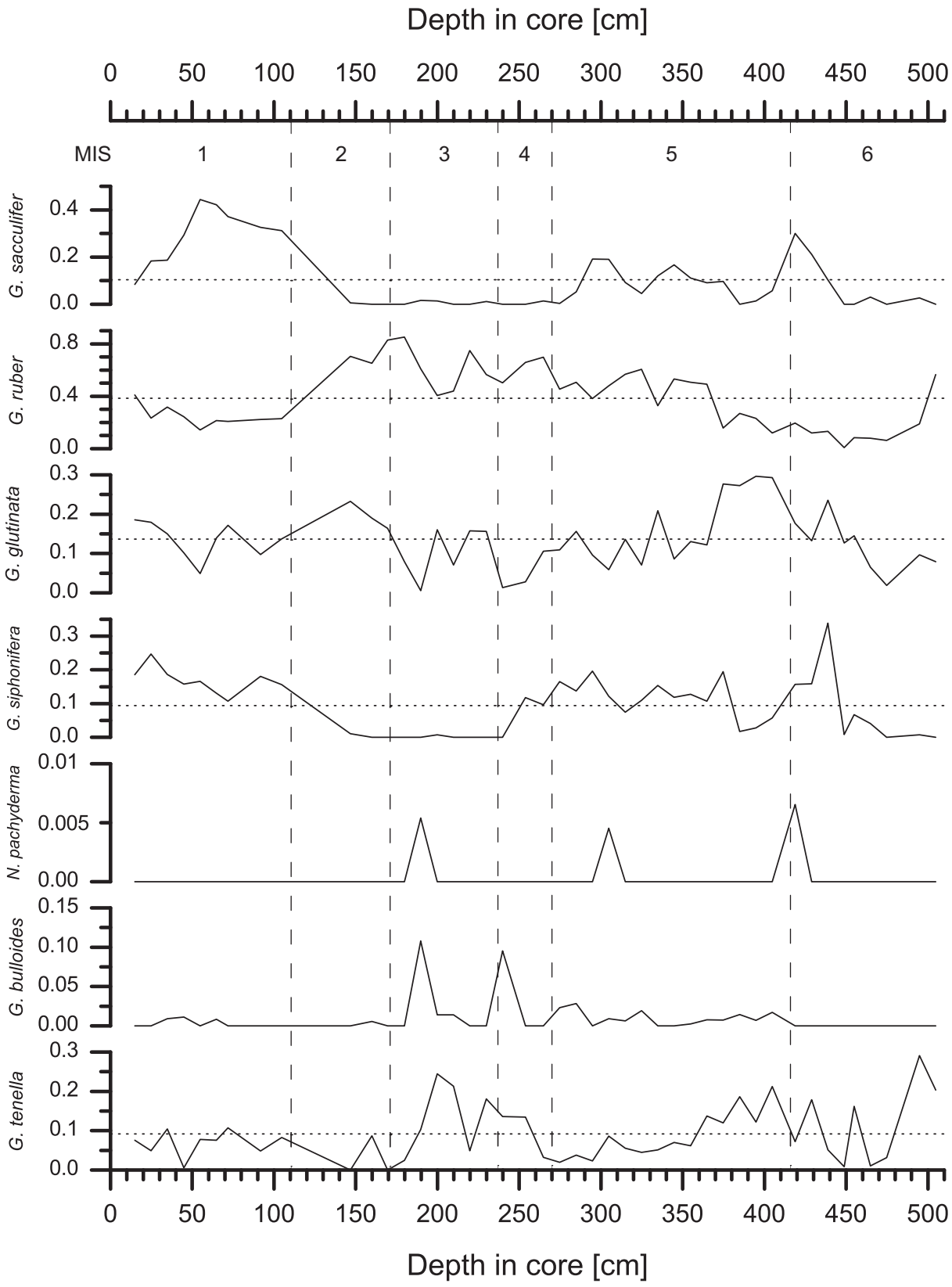

Figure 51 Faunal record of MD921039. Data from *Fenton* [2000]. Horizontal dotted lines are the averages for the taxonomic units. Vertical dashed lines denote marine isotope stage boundaries.

8.4.2 Analogy situation

In the analogy plot (Figure 52), the MD921017 samples plot as a stretched cluster separated from the calibration dataset. Only very few samples from the Gulf of Aden and the southern Red Sea overlap with the downcore samples, although their values for the first PCA component lie within the range of the calibration dataset. The environmental analogy plot (Figure 53) shows a comparable situation, only seven samples of the faunal record of MD921017 plot within the 95 % confidence interval boundaries of the calibration dataset. Five of these are from the Holocene, one from MIS 5 at around 120 ka BP and one from MIS 11 at 404 ka BP. The record of MD921039 is even less analogous than that of MD921017; in the analogy plot (Figure 55) the four most marginal samples of the MD921039 samples only just

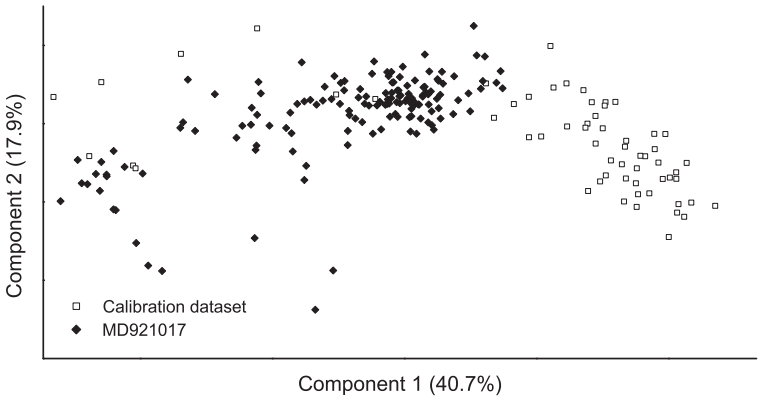

Figure 52 Analogy analysis in form of a scaled plot of a principal component analysis of log-transformed faunal data from the record of MD921017 [Fenton et al. 2000] and the calibration dataset.

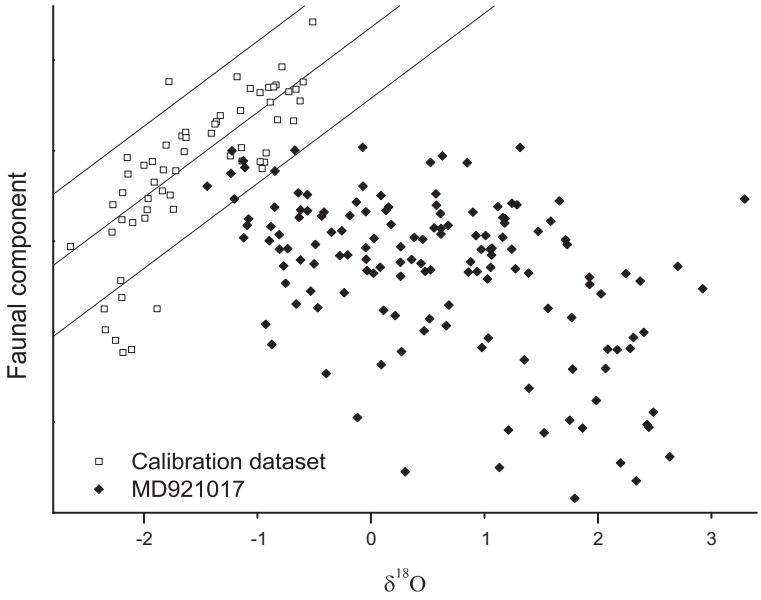

Figure 53 Analogy analysis in form of a cross plot of oxygen isotopes and the first principal component of faunal data from the record of MD921017 [Fenton et al. 2000] and the calibration dataset. Solid lines denote the linear fit of the calibration dataset and the boundaries of the 95 % confidence interval.

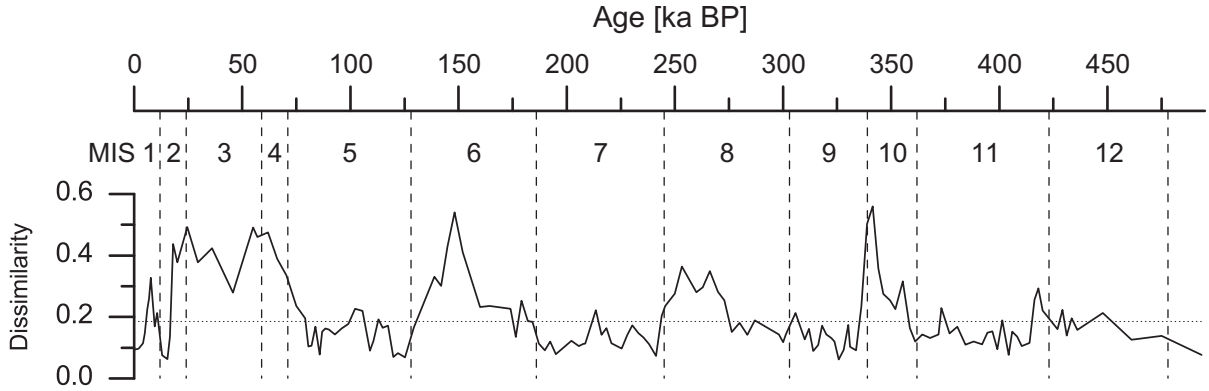

Figure 54 Bray-Curtis dissimilarity of the faunal records of MD921039 [Fenton et al. 2000]. Horizontal dotted line represents the critical value of dissimilarity (cf. Chapter 5.6.3 Assessment of uncertainties on reconstructions). Vertical dashed lines represent marine isotope stage boundaries.

approach the calibration dataset. In the corresponding environmental analogy plot (Figure 56) only a single sample from the Holocene of this record plots within the range of the recent faunal gradient in the Red Sea. Based on these two approaches on the determination of analogy, the records of MD921017 and MD921039 must be regarded as non-analogous.

The Bray-Curtis similarity measure, however, draws a different picture (Figure 57) and the differences in the evaluation of analogy between the approaches come to light. In case of MD921017, the calculated values for similarity for the interglacial samples are mostly below the defined critical value. The similarity record of MD921039 shows acceptable values only for the Holocene and few samples of MIS 5. In the calculation of the Bray-Curtis dissimilarity the census of all species is equally weighted, while the analogy and cross analogy analyses are based on PCA, which put the emphasis on the census data explaining most of the recent faunal gradient in the Red Sea. More specifically, the PCA disregard much of the variance in the census data of

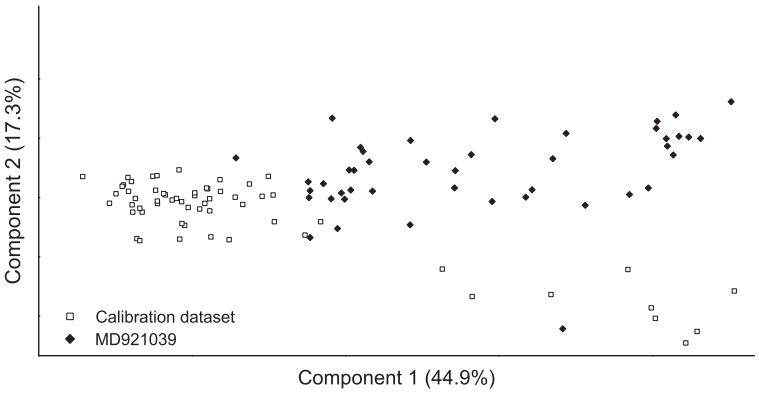

Figure 55 Analogy analysis in form of a scaled plot of a principal component analysis of log-transformed faunal data from the record of MD921039 [Fenton et al. 2000] and the calibration dataset.

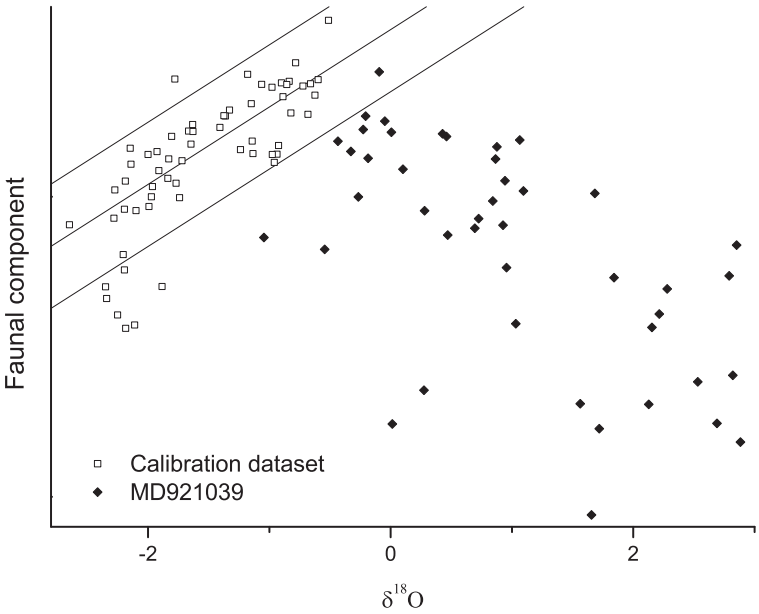

Figure 56 Analogy analysis in form of a cross plot of oxygen isotopes and the first principal component of faunal data from the record of MD921039 [Fenton et al. 2000] and the calibration dataset. Solid lines denote the linear fit of the calibration dataset and the boundaries of the 95 % confidence interval.

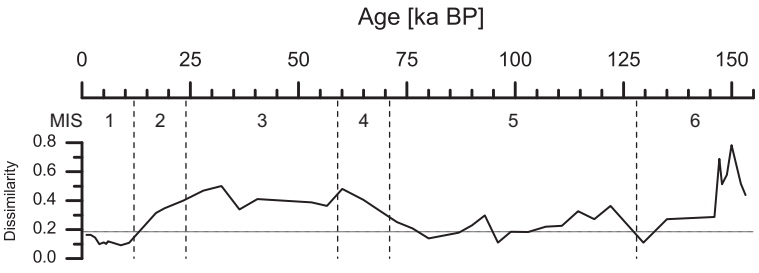

Figure 57 Bray-Curtis dissimilarity of the faunal records of MD921039 [Fenton et al. 2000]. Horizontal dotted line represents the critical value of dissimilarity (cf. Chapter 5.6.3 Assessment of uncertainties on reconstructions). Vertical dashed lines represent marine isotope stage boundaries.

G. ruber and *G. siphonifera*, because both are abundant throughout all samples of the calibration dataset. For this work the records of MD921017 and MD921039 are considered as non-analogous for the major part of their duration and thus no transfer function will be applied on their faunal data.

8.5 Applicability of transfer functions during the late Pleistocene

All records reaching further back in time than the Holocene have demonstrated the high variability of the planktonic foraminifera assemblages in the Red Sea on glacial/interglacial timescales (Figure 58). This variability is by far larger than that of the calibration dataset, which is especially obvious for glacial periods for the foraminifera species *G. sacculifer* and *G. ruber*. Based on the published literature [e.g. Fenton 1998; Schmelzer 1998], the lack of faunal analogy of glacial periods had been expected, but the weakly developed analogy of the interglacial periods had not. While the differences to the records of Fenton [2000] may lie in differing taxonomy and the positioning of cores along the axis of the Red Sea, the finding of non-analogy for large intervals during interglacial periods in KL9 is not a methodological issue. Examples are the low abundance of *G. sacculifer* during MIS 11 or the very high abundances of *G. glutinata* during MIS 5.

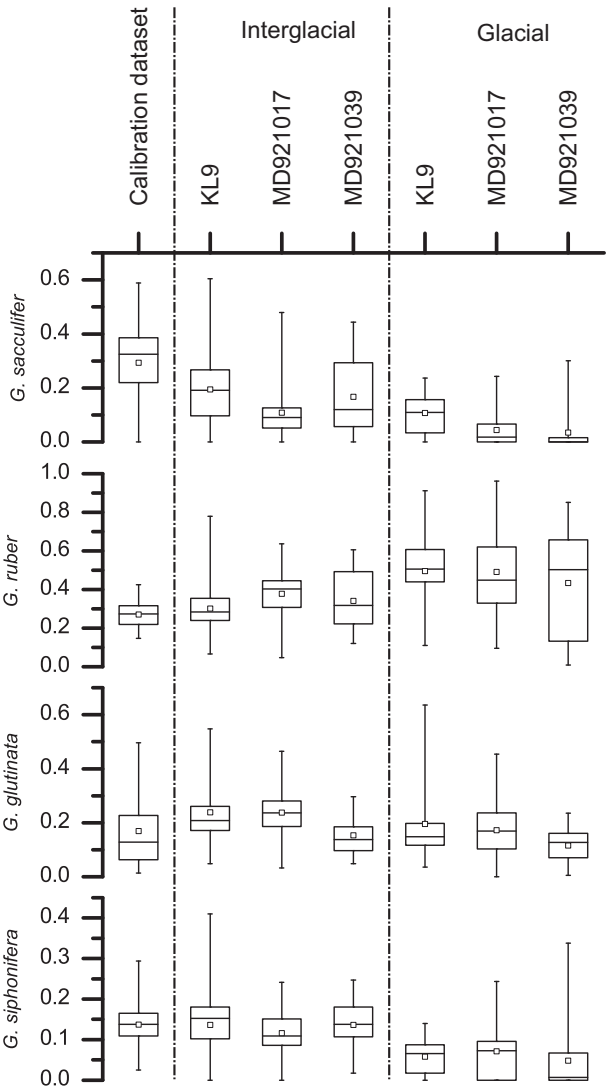

Figure 58 Box plot of the variability of Red Sea faunal records in form of relative abundances of the four dominant species in the calibration dataset (n = 60), interglacial samples (excluding MIS 3) and glacial samples (including MIS3) of cores KL9 (n = 204 and 59), MD921017 (n = 89 and 53) and MD921039 (n = 23 and 21). Boxes represent the 75 %, 25 % quantile and median, squares the mean, bars the minimum and maximum values.

Since the generated calibration dataset covers the full extent of the recent faunal gradient, the addition of further samples would increase the accuracy of any transfer function based on that dataset but would not increase the range of faunal variation covered by it. The ultimate cause for the undesirable analogy situation lies in the variability of the Red Sea circulation system. Its sensitivity to sea level changes and the amplification of climate signals are the reason that the environmental gradient and accordingly also the faunal gradient along the basin axis observable at any time is only a fraction of the total variation observable in the basin on glacial/interglacial timescales at a fixed position. Consequently, the Red Sea is not suited for investigations of paleoenvironmental parameters by use of faunal transfer functions on these timescales. Even under conditions of faunal

analogy, the analogy of the environment, particularly the circulation system is in most cases not given, rendering the quantitative reconstructions unreliable.

This complex of problems could be potentially circumvented by oceanographic modelling. Such a modelling approach, based on estimates of sea level (oxygen isotopes) and monsoon system (insolation seasonality) could validate the corresponding planktonic foraminifera transfer function results during periods of weak analogy and vice versa. A step further could be the extension of the calibration dataset by inclusion of downcore samples (Holocene and/or MIS 3), with the corresponding environmental parameters calculated by an oceanographic model or derived from independent proxies. In a study on the reconstruction of glacial temperatures in the equatorial Atlantic and Pacific oceans, Mix et al. [1999] circumvented the no-analog problem of faunal transfer functions by use of an alternative analogy concept. Instead of focusing on the spatial variation of fauna data in surface samples, they focused on the variation over time in the downcore data to determine analogue conditions and changing environmental forcing. For the Red Sea such an approach is due to the high variability of faunal assemblages in the Red Sea over time and their response to a forcing that is not expressed in any recent surface sample (salinity) unsuited. Such an approach could probably expand the ranges of faunal compositions considered as analogous, but certainly not overcome the principle issue.

Conclusions

The potential of Red Sea planktonic foraminifera assemblage composition as a quantitative proxy for paleoclimate reconstructions has been assessed by this study. Since there is no consensus in the published literature on the environmental parameters that directly control the foraminifera assemblages in the basin, a new surface sediment sample dataset, consistent in taxonomy and methodology, was generated and analysed. This new dataset confirmed the existence of a distinct gradient in foraminifera species distribution along the axis of the Red Sea [Auras-Schudnagies et al. 1989]: *G. sacculifer* being the dominant species in the north, *G. ruber* in the central and *G. glutinata* in the southern part of the basin. The faunal data and database- or satellite-derived data for the environmental parameters temperature, salinity, primary productivity (approximated by chlorophyll *a* concentration), water column stratification and properties of the oxygen minimum zone on the foraminifera fauna were analysed by gradient analysis to determine the controlling factor of the foraminifera distribution. Due to the high intercorrelation of all environmental parameters along the basin axis, no unambiguous identification of the controlling parameter was possible by statistical analysis alone. However, a comparison of the gradient analysis results with published studies on the ecology of planktonic foraminifera allowed the formulation of a working hypothesis that prefers primary productivity as the determinant of the distinct gradient in the planktonic foraminifera assemblages in the Red Sea.

Employing the surface sample dataset for calibration, foraminiferal transfer functions were developed to reconstruct primary productivity conditions from fossil foraminifera assemblages in the Red Sea. To alleviate the suboptimal conditions for transfer function development pertaining to this study, such as the small size of the calibration dataset and the pronounced autocorrelation of environment and fauna, a range of different transfer function methods with very different mathematical approaches was employed. The methods comprised the Imbrie and Kipp method that directly correlates the faunal variance to the environmental parameter, the modern analogue technique that bases on the calculation of similarity between modern and fossil assemblages, the weighted averaging partial least squares method, which assumes that species occupy specific positions along the environmental gradient, and the artificial neural network approach that fits observed faunal data to environmental data in an efficient but rather inscrutable fashion. Due to the correlation among the environmental parameters, the developed transfer functions could estimate all parameters with acceptable accuracy. The average RMSEP of the four different methods for chlorophyll *a* concentration is 0.124 mg/m³, corresponding to 10.3 % of the observed gradient.

The working hypothesis was then tested on two newly generated Holocene faunal records from the central (core KL9) and northern (core KL17 VL) Red Sea. The faunal data was found to be consistent

with previously published Holocene records of the Red Sea and almost entirely analogue to the calibration dataset. For the relatively high uncertainty of radiocarbon dating in basins with restricted water exchange such as the Red Sea, a new generalised age model for the Holocene was developed, which not only included the radiocarbon datings and faunal data generated for this study but also those available in the published literature. The Holocene faunal records document the impact of sea level and the dominant climatic system, the Indian monsoon, on the hydrography of the Red Sea. From the high abundances of the oligotrophic species *G. sacculifer*, the transfer functions reconstruct low productivity for the early Holocene; a consequence of a lowered sea level and a strong SW monsoon. There was also evidence found for a notable input of fresh water into the northern Red Sea during this time, consistent with the findings by Arz et al. [2003a]. Through the Mid-Holocene, the dominance of *G. sacculifer* decreased and species indicating higher primary productivity attained higher relative abundances in the central Red Sea, resulting in the reconstruction of productivity conditions comparable to present day. Between 3.5 and 2 ka BP a dramatic shift in the relative abundances of the dominant planktonic foraminifera taxa occurred throughout the Red Sea. This faunal shift phase exhibits uniquely low abundance levels of *G. sacculifer*, compensated by increased abundances of *G. glutinata* and *G. ruber*. The productivity reconstructions reach a maximum during this phase, which is interpreted as a consequence of enhanced winter circulation due to a strengthened NE monsoon and generally higher aridity in the region. After 2 ka BP, the modern circulation and climatic conditions became established. The reconstructions of paleoproductivity for the Holocene by foraminiferal transfer functions are in excellent agreement with the established picture of paleoclimatic conditions during this time interval, which is in the very basic principle a humid, SW-monsoon dominated early Holocene and an arid, NE-monsoon dominated late Holocene. Transfer functions developed for environmental parameters, such as stratification and oxygen concentration that have in other works been invoked as controlling parameters for the planktonic foraminifera distribution in the Red Sea [e.g. Edelman-Furstenberg et al. 2009], could not be easily reconciled with the existing data on paleoclimate and their implications for the circulation system, confirming the working hypothesis that productivity is the primary control on the distribution of planktonic foraminifera in the Red Sea under conditions analogous to the present.

The developed transfer functions were also applied to longer Red Sea faunal records that include glacial and interglacial periods and records that focus on the interglacials MIS 5e and MIS 11. It became apparent that the analogy of fossil assemblages with the calibration dataset, a vital prerequisite for the application of transfer functions, is not given for the majority of samples from downcore records on that timescale. While this situation had been expected for glacials periods, it had not for long intervals of MIS 5e and MIS 11, which are often considered as analogous to the present. This phenomenon can partially be ascribed to methodological and taxonomical differences to the respective studies, but is ultimately based on the extraordinary variability of the hydrography of the Red Sea on

these timescales. The reconstructions of MIS 5e suggest, under the constraint of partially non-analogue conditions, a considerably higher primary productivity in the Red Sea during that time. A finding that without the invocation of a very different circulation system cannot not easily be reconciled with the picture of humid and SW-monsoon dominated conditions established by paleoclimatic studies. Investigations of MIS 11 showed only a weak analogy of the foraminifera fauna limited to a short interval shortly after the second insolation peak of this interglacial at around 410 ka BP. The reconstructions of primary productivity for this time period are fluctuating, but within realistic ranges compared to present-day conditions.

The planktonic foraminifera fauna in the Red Sea is clearly sensitive to both sea level and monsoon induced changes in circulation. In the past, faunas were often not analogous to present, not only due to a different sea level, but also due to different insolation affecting the monsoon climate system. Where transfer functions based on planktonic foraminifera are applicable, the estimates for paleoproductivity are consistent with other proxies and indicative for the circulation pattern in the Red Sea.

Appendix

Surface samples

Name	Longitude [°E]	Latitude [°N]	depth [m]	type
Cruise RV Meteor 5/2				
MC-71	23.39	36.98	1387	M 1
MC-71A	23.39	36.98	1387	M 1
MC-73	22.92	37.38	1324	M 1
MC-73A	22.92	37.38	1324	M 1
MC-79	22.25	37.78	1521	M 1
MC-79A	22.25	37.78	1521	M 1
MC-85	21.43	37.98	1538	M 1
MC-93	19.99	38.21	934	M 2
MC-94	20.04	38.09	813	M 1
MC-95	19.91	38.01	713	M 1
MC-97	19.76	37.64	600	M 2
MC-98	19.72	37.53	585	M 2
MC-99	19.68	37.48	684	M 2
MC-100	19.64	37.39	786	M 1
MC-101	20.11	38.42	2309	M 1
MC-103	19.09	39.15	1348	M 1
MC-105	18.6	39.06	501	M 2
MC-107	19.13	39.12	1161	M 1
MC-108	19.14	39.05	1657	M 1
MC-109	19.46	38.72	1825	M 3
MC-111	19.46	38.72	1825	M 1
MC-112	19.61	38.73	2831	M 3
MC-113	19.64	38.61	1991	M 1
MC-115	19.1	39.15	1602	M 2
MC-120	12.49	45.71	1315	M 3
MC-124	12.87	47.42	1662	M 3
Cruise RV Valdivia 29				
707KG	21.43	38.1	1985	B 4
710KG	21.45	38.23	1084	B 4
725KG	22.28	37.76	1449	B 4
730KG	24.73	36.94	722	B 4
735KG	24.76	36.59	1070	B 4
745KG	26.76	35.04	1377	B 4
750KG	26.78	35.14	1046	B 4
754KG	26.88	35.43	593	B 4

Name	Longitude [°E]	Latitude [°N]	depth [m]	type
Cruise RV Meteor 44/3				
5832-1	27.05	35.41	628	M 1
5837-1	27.61	34.86	771	M 1
5838-1	27.58	34.74	832	M 1
5839-2	27.58	34.8	803	M 1
5840-1	27.53	34.69	908	M 1
5842-1	27.71	35.05	863	M 1
5843-2	27.88	34.97	529	M 1
5844-1	27.71	34.68	963	M 1
Cruise RV Meteor 31/2 and 31/3				
78 MC 4	27.69	34.6	1018	M 1
80 MC 6	26.29	35.36	1175	M 1
84 MC 2	25.75	34.87	736	M 1
84 MC 3	25.75	35.09	666	M 1
86 MC	25.52	35.61	941	M 1
90 MC 1	24.76	36.23	1185	M 1
92 MC 1	23.31	36.71	1024	M 1
101 MC 1	17.36	40.02	475	M 1
103 MC 3	15.56	41.67	604	M 1
105 MC 1	12.4	44.49	174	M 1
Cruise RV Sonne 121				
SO-75	24.77	36.41	1402	M 1
SO-91	25.85	36.08	1585	M 1
SO-92	25.78	36.1	1726	M 1
SO-98	15.94	41.68	959	M 1
SO-100	15	42.21	826	M 1
SO-103	14.72	42.44	509	M 1
SO-106	12.39	44.17	383	M 1
SO-110	12.25	44.47	740	M 1

type codes

M = multicorer

B = boxcorer

1 = unprocessed before this study / depth interval 0 cm - 0.5 cm

2 = processed before this study / depth interval 0 cm - 0.5 cm

3 = unprocessed before this study / depth interval 0 cm - 1.0 cm

4 = processed before this study / depth interval 0 cm - 1.0 cm

Surface sample faunal dataset

Name	counted specimens	*G. anfracta*	*G. bulloides*	*G. calida*	*G. conglobatus*	*G. conglomerata*	*G. digitata*	*G. falconensis*	*G. glutinata*	*G. hexagonus*	*G. inflata*	*G. menardii*	*G. minuta*	*G. ruber*	*G. rubescens*	*G. sacculifer*	*G. scitula*
MC-71 *	696	0	0	28	0	0	0	0.5	62.1	0	0	0	1.6	243	9	252	0
MC-71A *	496	0	0	2.3	0.6	0	0	0	36.6	0	0	0	0	137	1.7	220	0
MC-73	438	0	0	23	0	0	0	0	29	0	0	0	0	140	5	172	0
MC-73A	314	0	0	9	0	0	0	1	40	0	0	0	0	92	4	119	0
MC-79	354	0	0	18	0	0	0	0	59	0	0	0	0	118	6	102	0
MC-79A	377	0	0	10	0	0	0	0	40	0	0	0	0	113	3	138	0
MC-85	304	0	0	8	0	0	0	0	16	0	0	0	0	53	1	176	0
MC-93 *	359	1.5	0	6.2	0	0	0	0	44	0	0	0	0	114	3.2	118	0
MC-94	499	0	1	26	0	0	0	1	124	0	1	0	0	141	6	108	0
MC-95	320	0	0	7	0	0	0	0	67	0	0	0	1	76	0	91	0
MC-97 *	500	0.8	0	7.2	0	0	0	0	103	0	0	0	0	205	10.3	110	0
MC-98 *	509	0	0	8.5	0	0	0	0	112	0	0	0	0	159	5.5	127	0
MC-99	372	2	0	2	0	0	0	0	82	0	0	0	0	125	2	85	0
MC-100	339	1	1	2	0	0	0	0	71	0	0	0	0	138	3	82	0
MC-101	364	0	0	9	0	0	0	0	75	0	0	0	0	103	4	101	0
MC-103	414	1	6	0	0	0	0	0	80	0	0	0	12	135	3	74	1
MC-105	334	0	0	4	0	0	0	0	92	0	0	0	0	127	8	53	0
MC-107	559	1	0	25	0	0	0	0	113	0	0	0	0	185	14	125	5
MC-108	398	3	0	0	0	0	0	0	93	0	0	0	1	121	9	77	0
MC-109	605	0	0	22	0	0	0	0	117	0	0	0	0	162	12	193	0
MC-111	455	0	0	11	0	0	0	0	96	0	0	0	0	125	2	149	0
MC-112	475	3	0	4	0	0	0	0	110	0	0	0	1	163	0	106	0
MC-113	301	2	0	13	0	0	0	0	60	0	0	0	0	73	0	111	0
MC-115	498	2	0	10	0	0	0	0	134	0	0	0	0	161	11	97	0
MC-120	654	10	145	6	1	0	4	6	199	3	0	34	0	158	6	17	4
MC-124	377	1	94	4	0	0	2	1	144	2	0	9	1	63	0	10	1
707KG	474	0	1	13	3	0	0	0	48	0	0	0	0	137	2	207	0
710KG	320	0	0	0	0	0	0	0	31	0	0	0	0	78	0	138	0
725KG	386	2	0	8	0	0	0	0	50	0	0	0	0	74	4	139	0
730KG	342	0	0	1	0	0	0	0	44	0	0	0	0	92	6	127	0
735KG	353	0	0	3	0	0	0	0	13	0	0	0	0	76	2	181	0
745KG	302	0	0	7	0	0	0	0	19	0	0	0	0	73	5	119	0
750KG	319	2	0	29	0	0	0	0	7	0	0	0	0	90	5	122	0
754KG	320	0	0	1	0	0	0	0	15	0	0	0	0	74	6	109	0
5832-1	304	0	0	16	0	0	0	0	16	0	0	0	0	94	8	86	0
5837-1	326	0	0	3	0	0	0	0	13	0	0	0	0	64	5	137	0
5838-1	394	0	0	34	0	0	0	0	13	0	0	0	0	94	6	160	0
5839-2	403	0	0	7	0	0	0	0	25	0	0	0	0	98	4	126	0
5840-1	343	1	0	9	0	0	0	0	22	0	0	0	0	58	11	143	0
5842-1	326	0	0	5	0	0	0	0	19	0	0	0	0	65	2	132	0
5843-2	391	0	0	4	1	0	0	0	22	0	0	0	0	79	9	142	0
5844-1	354	0	0	9	0	0	0	0	15	0	0	0	0	80	5	139	0
78 MC 4	421	0	0	23	0	0	0	0	6	0	0	0	0	85	1	177	1
80 MC 6	301	0	1	5	1	0	0	0	37	0	0	0	0	80	8	95	0
84 MC 2	319	0	0	23	0	1	0	0	35	0	0	0	0	105	4	110	0
84 MC 3	388	0	2	11	0	0	0	0	39	0	0	0	0	117	12	138	0
86 MC	514	0	0	24	0	0	1	0	38	0	0	0	0	131	3	184	0
90 MC 1	326	0	0	28	0	0	0	0	19	0	0	0	0	66	3	162	0
92 MC 1	346	1	0	6	0	0	0	0	21	0	0	0	1	111	3	130	0
101 MC 1	301	0	3	9	0	0	0	1	98	0	0	0	0	84	4	51	0
103 MC 3	346	5	73	0	0	0	0	0	151	0	0	1	0	57	1	5	0
105 MC 1	368	0	54	4	0	0	0	0	146	0	0	32	0	73	9	6	3
SO-75	326	0	0	0	0	0	0	0	10	0	0	0	0	73	1	138	0
SO-91	330	0	0	7	0	0	0	0	24	0	0	0	0	105	1	103	0
SO-92	425	9	0	12	0	0	0	0	37	0	0	0	1	128	3	119	0
SO-98	411	1	54	2	0	0	0	0	172	0	0	0	0	78	3	20	0
SO-100	314	3	26	7	0	0	0	0	149	0	0	1	0	56	2	7	0
SO-103	301	2	28	0	0	0	0	0	142	0	0	1	0	43	1	2	1
SO-106	323	7	42	6	0	0	0	1	98	0	0	10	3	68	1	4	2
SO-110	340	3	56	5	0	0	1	0	104	0	0	11	0	100	4	5	5

Surface sample faunal dataset (continued)

Name	*G. siphonifera*	*G. tenella*	*G. truncatulinoides*	*G. uvula*	*G. vivans*	*H. digitata*	*H. pelagica*	*N. dutertrei*	*N. incompta*	*N. pachyderma*	*O. universa*	*P. obliquiloculata*	*S. dehiscens*	*T. humilis*	*T. quinqueloba*
MC-71 *	46.1	6.8	0	0	0	0	0	5.3	13.2	25.4	0	0	0	0	3.2
MC-71A *	79.7	2.3	0	0	0	4.1	0	1.2	5.2	4.1	0	0	0	1.2	1.2
MC-73	48	5	0	0	0	1	0	3	5	6	0	0	0	1	1
MC-73A	33	5	0	0	0	0	0	2	2	7	0	0	0	0	0
MC-79	35	3	0	0	1	1	0	3	3	5	0	0	0	0	0
MC-79A	62	1	0	0	0	5	0	1	1	3	0	0	0	0	0
MC-85	37	0	0	0	0	2	0	2	4	5	0	0	0	0	0
MC-93 *	59.4	2.6	0	0	0	2.1	0	2.6	1.9	3.2	0	0	0	0	0
MC-94	45	16	0	0	0	0	0	15	7	8	0	0	0	0	0
MC-95	43	5	0	0	0	5	0	1	8	15	0	0	0	1	1
MC-97 *	46.1	7.4	0	0	0	1.9	0	4	2.1	1.1	0	0	0	0	0
MC-98 *	69.3	5.5	0	0	0	8.3	0	7.6	3.5	3.5	0	0	0	0	0
MC-99	46	7	0	0	0	3	0	6	4	5	0	0	0	3.2	3
MC-100	24	0	0	0	0	3	0	6	2	2	0	0	0	4	4
MC-101	51	1	0	0	1	9	0	4	4	1	0	0	0	0	0
MC-103	32	2	0	0	0	4	0	0	2	6	0	0	0	56	56
MC-105	28	8	0	0	0	0	1	2	6	5	0	0	0	0	0
MC-107	46	7	0	0	0	0	1	11	12	13	0	0	0	1	1
MC-108	29	8	0	0	1	6	0	8	4	7	0	0	0	31	31
MC-109	76	6	0	0	7	0	0	7	0	1	0	0	0	0	0
MC-111	48	1	0	0	0	8	0	5	3	7	0	0	0	0	0
MC-112	57	3	1	0	0	4	1	11	2	2	0	0	0	7	7
MC-113	32	0	0	0	0	0	0	5	2	1	0	0	0	0	0
MC-115	49	11	0	0	0	0	1	7	7	8	0	0	0	0	0
MC-120	24	12	0	0	0	0	12	0	1	2	4	0	3	3	3
MC-124	11	1	0	0	0	1	10	0	1	2	0	0	0	19	19
707KG	51	2	0	0	3	3	0	0	1	3	0	0	0	0	0
710KG	40	7	0	0	0	1	0	2	6	8	0	0	0	9	9
725KG	65	2	0	0	0	2	0	14	7	11	0	0	0	8	8
730KG	41	11	0	0	0	2	0	2	4	11	0	0	0	1	1
735KG	54	5	0	0	0	4	0	3	5	7	0	0	0	0	0
745KG	53	8	0	0	0	3	1	3	5	6	0	0	0	0	0
750KG	17	10	0	0	0	0	0	6	13	18	0	0	0	0	0
754KG	65	21	0	0	0	1	0	5	3	13	0	0	0	7	7
5832-1	37	20	0	0	0	2	0	7	9	9	0	0	0	0	0
5837-1	47	13	0	0	0	4	0	9	14	17	0	0	0	0	0
5838-1	63	9	0	0	0	1	0	9	3	2	0	0	0	0	0
5839-2	52	19	0	0	0	2	0	7	33	30	0	0	0	0	0
5840-1	55	10	0	0	0	2	0	10	10	12	0	0	0	0	0
5842-1	56	5	0	0	0	5	0	6	7	13	0	0	0	11	11
5843-2	58	24	0	0	0	11	0	5	15	21	0	0	0	0	0
5844-1	56	6	0	0	0	2	0	8	19	15	0	0	0	0	0
78 MC 4	99	10	0	0	0	0	0	4	5	10	0	0	0	0	0
80 MC 6	27	16	0	0	0	4	0	6	9	12	0	0	0	0	0
84 MC 2	12	7	0	1	0	0	1	1	13	6	0	0	0	0	0
84 MC 3	19	22	0	0	0	1	0	2	11	14	0	0	0	0	0
86 MC	82	8	0	0	0	13	0	7	9	14	0	0	0	0	0
90 MC 1	30	4	0	0	0	0	0	2	6	6	0	0	0	0	0
92 MC 1	32	4	0	0	0	6	0	4	9	17	0	0	0	0	0
101 MC 1	38	5	0	0	0	0	0	3	3	0	0	0	0	2	2
103 MC 3	33	1	0	0	1	4	0	1	1	0	0	0	0	12	12
105 MC 1	5	3	0	0	0	1	2	5	14	6	0	0	0	5	5
SO-75	42	3	0	0	0	25	0	23	1	9	0	0	0	1	1
SO-91	30	8	0	0	0	5	0	8	17	22	0	0	0	0	0
SO-92	30	5	0	0	0	14	0	10	4	22	0	0	0	30	30
SO-98	54	4	0	0	0	3	4	6	5	5	0	0	0	0	0
SO-100	30	5	0	0	0	0	0	2	6	3	0	0	0	17	17
SO-103	23	5	0	11	0	1	1	4	1	0	0	0	0	35	35
SO-106	5	3	0	1	0	1	9	4	8	13	0	0	0	36	36
SO-110	6	3	0	0	0	1	5	0	11	11	0	0	0	9	9

* the counts of odd,preprosessed sample splits (e.g. 7/8) had to be mathematically grossed up to the count of a complete sample

Faunal data for the Holocene section of KL9

Depth in core [cm]	counted specimens	*G. anfracta*	*G. bulloides*	*G. calida*	*G. conglobatus*	*G. digitata*	*G. glutinata*	*G. inflata*	*G. menardii*	*G. ruber*	*G. rubescens*	*G. sacculifer*	*G. siphonifera*	*G. tenella*	*H. digitata*	*H. pelagica*	*N. dutertrei*	*N. incompta*	*N. pachyderma*	*O. universa*	*T. quinqueloba*
0.25	302	0	0	13	0	0	58	0	0	88	1	82	44	8	2	0	0	2	4	0	0
2.25	411	1	0	1	0	0	77	0	0	131	0	112	69	10	0	0	0	3	1	6	0
4.25	322	0	1	11	0	0	56	0	0	91	2	82	60	8	0	2	0	4	3	2	0
6.25	353	0	1	6	1	0	42	0	0	121	2	116	51	6	3	0	0	1	2	1	0
8.25	301	0	0	7	0	0	48	0	0	87	3	88	49	10	0	0	0	3	4	2	0
10.25	383	0	0	1	0	0	85	0	0	117	2	97	69	7	0	0	0	1	3	0	1
12.25	342	0	0	5	1	0	63	0	0	98	1	92	54	11	2	4	0	4	3	3	1
14.25	305	0	0	6	1	0	42	0	0	85	0	95	50	7	5	2	0	2	3	7	0
15.25	308	0	0	4	0	0	56	0	0	80	3	92	53	11	4	1	0	0	2	2	0
16.25	384	0	0	19	0	0	72	0	0	132	1	73	53	12	0	6	0	5	8	2	1
17.25	316	0	0	3	0	0	64	0	0	92	4	86	58	5	0	1	0	1	0	2	0
18.25	460	0	1	8	0	0	95	0	0	121	2	117	94	11	0	0	0	3	2	5	1
19.25	337	0	0	3	0	0	64	0	0	91	5	92	68	5	0	2	0	1	2	4	0
20.25	304	0	0	0	0	0	81	0	0	83	1	72	51	8	0	1	0	2	2	3	0
21.25	348	0	0	7	0	0	89	0	0	112	3	46	68	11	0	0	0	2	0	10	0
22.25	324	0	0	7	1	0	86	0	0	93	3	57	48	11	2	0	0	2	5	9	0
23.25	329	0	0	8	0	0	87	0	0	90	6	67	54	5	0	1	0	2	3	6	0
24.25	489	0	0	15	0	0	147	0	0	175	4	64	57	17	1	0	0	1	0	7	1
25.25	315	0	0	6	0	0	76	0	0	113	4	33	57	10	0	1	0	5	2	8	0
26.25	312	0	0	9	0	0	71	0	0	99	2	39	57	11	0	2	0	2	9	11	0
27.25	301	0	0	4	0	0	74	0	0	100	1	59	37	18	0	0	0	1	0	7	0
28.25	313	0	0	5	0	0	73	0	0	92	2	71	48	11	1	3	0	1	1	5	0
29.25	308	0	0	3	0	0	70	0	0	97	1	67	48	17	0	0	0	0	2	3	0
30.25	328	0	0	7	0	0	66	0	0	94	3	85	43	15	2	1	0	2	8	2	0
31.25	307	0	0	2	0	0	70	0	0	83	4	74	51	19	0	0	0	1	2	0	1
32.25	350	1	0	8	0	0	75	0	0	98	1	78	41	39	0	0	0	1	2	3	3
33.25	336	0	0	3	0	0	78	0	0	83	1	102	39	23	1	0	0	0	2	3	1
34.25	304	0	0	3	0	0	71	0	0	54	5	100	35	24	1	1	0	1	2	7	0
35.25	338	1	0	6	0	0	84	0	0	73	5	96	45	22	0	0	0	2	1	3	0
36.25	381	0	0	4	0	0	90	0	0	109	6	84	62	11	1	3	0	7	1	3	0
37.25	326	0	0	5	0	0	73	0	0	67	4	99	55	16	0	0	0	2	3	1	1
38.25	341	0	0	6	0	0	97	0	0	80	3	80	47	23	0	0	0	0	4	1	0
40.25	349	0	0	15	0	0	72	0	0	92	1	103	40	15	0	1	0	4	5	1	0
42.25	376	0	0	12	0	0	83	0	0	82	6	95	65	12	2	1	0	3	7	8	0
44.25	315	0	0	2	0	0	65	0	0	81	3	92	53	12	3	1	0	0	1	2	0
46.25	326	0	0	3	0	1	84	0	0	79	3	77	59	13	0	0	1	0	2	2	2
48.25	316	0	0	12	0	0	72	0	0	78	5	78	54	11	1	0	0	0	4	1	0
50.25	391	0	1	16	1	0	75	0	0	99	7	99	61	20	3	0	0	2	4	3	0
52.25	337	1	0	2	1	0	61	0	0	70	5	117	54	12	5	2	0	2	1	3	1
54.25	318	1	0	4	0	0	58	0	0	77	1	109	45	9	7	1	0	1	2	3	0
56.25	345	1	1	12	0	0	55	0	0	86	3	124	45	7	1	0	0	1	2	5	2
58.25	382	1	0	4	0	0	63	0	0	91	4	121	82	6	2	0	0	1	2	4	1
60.25	388	1	0	8	0	0	86	0	0	74	7	127	59	11	2	5	0	4	0	4	0
62.25	327	0	0	3	0	0	45	0	0	66	5	123	58	14	1	2	0	3	2	5	0
64.25	374	0	0	5	0	0	55	0	0	90	2	136	57	19	3	0	0	0	5	2	0
66.25	355	0	0	12	0	0	51	0	1	79	2	135	55	14	0	0	0	3	3	0	0
68.25	321	0	0	3	0	0	38	0	0	63	1	145	54	6	0	3	0	0	1	7	0
70.25	341	0	0	12	0	0	37	0	0	76	1	155	38	15	0	0	0	3	3	1	0
72.25	361	0	0	6	0	0	41	0	0	72	5	149	52	23	1	0	0	1	3	7	1
74.25	364	0	0	7	0	0	31	0	0	55	4	197	50	7	2	1	0	1	1	8	0
76.25	324	0	0	3	1	0	44	0	0	54	5	170	35	2	0	1	0	2	1	6	0
78.25	422	0	0	9	0	0	54	0	0	58	2	201	53	23	0	0	0	4	6	9	3
80.25	385	0	0	7	0	0	50	0	0	55	0	195	41	17	2	0	0	5	4	9	0
82.25	345	0	0	6	0	0	40	0	0	33	5	182	48	16	0	0	0	1	5	6	3
84.25	442	0	0	5	1	0	57	0	0	29	1	264	45	5	0	5	0	2	1	27	0
86.25	350	0	1	5	0	0	84	0	0	41	4	155	35	8	0	0	0	4	4	9	0
88.25	335	1	1	6	0	0	64	0	0	71	4	120	40	11	0	0	0	4	4	5	4
89.0	331	0	1	3	0	0	58	0	0	79	1	102	58	19	1	1	1	1	2	4	0

Faunal data for the Holocene section of KL17 VL

Depth in core [cm]	counted specimens	*G. anfracta*	*G. bulloides*	*G. calida*	*G. glutinata*	*G. minuta*	*G. ruber*	*G. rubescens*	*G. sacculifer*	*G. siphonifera*	*G. tenella*	*H. digitata*	*H. pelagica*	*N. dutertrei*	*N. incompta*	*N. pachyderma*	*O. riedeli*	*O. universa*	*T. quinqueloba*
0.5	386	0	0	3	9	2	114	0	153	83	12	0	3	0	0	2	0	4	1
2.5	307	1	0	13	14	1	73	4	104	79	16	0	0	0	0	2	0	0	0
4.5	331	0	0	18	10	3	77	3	108	82	20	0	1	0	0	9	0	0	0
5.5	377	0	0	12	12	2	75	2	144	113	11	0	2	0	0	1	0	3	0
6.5	310	0	0	9	9	3	69	0	112	90	8	0	0	0	0	4	0	4	2
7.5	365	0	0	10	14	0	70	3	139	109	14	0	0	0	0	0	0	6	0
8.5	317	0	0	26	12	0	74	2	87	94	10	0	4	0	0	0	0	8	0
9.5	326	0	0	4	16	2	86	3	88	103	14	0	0	0	0	0	0	10	0
10.5	434	0	0	30	22	2	135	7	81	106	32	0	0	0	0	6	0	11	2
11.5	415	0	0	21	20	2	145	3	79	102	29	0	1	0	0	3	0	10	0
12.5	329	0	0	6	28	0	110	8	15	121	22	0	0	1	0	0	0	18	0
13.5	329	1	0	23	22	2	93	1	16	107	42	0	0	0	0	2	1	19	0
14.5	367	0	0	19	29	4	124	3	22	104	31	0	0	0	0	8	0	23	0
15.5	307	0	0	11	28	1	116	2	14	80	31	0	0	0	0	1	0	23	0
16.5	322	1	0	1	27	2	116	0	23	71	57	0	1	0	0	0	0	23	0
17.5	373	0	0	9	24	3	128	4	28	95	58	0	0	0	0	3	0	20	1
18.5	306	0	0	17	22	1	88	6	46	51	52	0	1	0	0	5	0	15	2
19.5	390	0	0	11	28	3	140	1	73	78	39	0	1	0	0	2	0	14	0
20.5	436	1	1	1	25	0	118	1	138	97	35	0	0	0	0	0	0	17	2
21.5	304	0	0	6	16	1	64	1	129	46	34	0	0	0	0	4	0	3	0
22.5	418	1	0	7	29	2	61	6	170	77	52	0	1	0	0	5	0	6	1
24.5	350	1	0	14	21	1	51	6	130	64	59	0	0	0	0	2	0	0	1
26.5	311	0	0	1	17	0	51	1	131	74	32	0	0	0	0	0	0	2	2
28.5	346	0	0	5	20	2	42	6	150	96	19	0	0	0	0	2	0	4	0
30.5	345	0	0	6	19	2	51	2	123	113	25	0	0	0	0	0	0	3	1
32.5	320	0	0	13	19	4	42	7	120	75	20	0	1	0	1	9	0	8	1
36.5	411	0	0	4	22	1	66	4	167	117	16	1	3	0	0	2	0	8	0
40.5	399	0	0	12	34	2	46	5	170	73	40	0	3	0	2	3	0	7	2
44.5	338	1	0	6	32	2	34	14	121	84	34	0	1	0	0	0	0	9	0
48.5	305	0	0	4	26	6	50	2	117	71	9	0	3	0	0	5	0	11	1
52.5	343	0	0	8	19	3	43	2	145	106	9	0	0	0	0	3	0	5	0
56.5	387	0	0	1	31	2	69	3	143	100	22	0	2	0	0	6	0	1	7
60.5	394	0	0	9	27	1	60	1	183	92	16	0	2	0	0	2	0	1	0
64.5	397	0	0	5	17	4	44	1	201	89	16	0	1	0	1	1	0	2	6
68.5	316	0	0	7	8	0	39	3	162	76	12	0	2	0	0	1	0	6	0
72.5	461	0	0	9	12	0	67	2	236	93	29	0	0	0	0	2	0	10	1
76.5	520	1	0	6	11	2	68	5	311	83	20	0	4	0	0	3	0	4	2
80.5	365	0	0	2	6	1	63	2	202	50	27	0	1	0	0	2	0	6	3
84.5	328	0	0	6	4	2	25	2	202	38	38	0	2	0	0	2	0	4	3
88.5	411	0	0	6	8	1	29	1	243	86	25	0	0	0	2	0	0	4	6
90.5	307	0	0	6	6	0	4	0	242	33	6	0	0	0	0	2	0	8	0
92.5	422	0	0	1	15	5	10	1	269	71	8	0	0	0	0	5	0	27	1
93.5	304	0	0	3	53	3	14	2	161	32	19	0	0	0	0	3	0	13	1
94.5	348	0	0	10	19	2	13	0	225	55	15	0	0	0	0	1	0	4	4
96.5	374	0	0	6	13	1	24	0	240	74	4	0	0	0	0	3	0	8	1
97.5	308	0	0	9	31	3	14	0	170	53	2	0	0	0	0	5	0	7	1

Appendix

Oxygen and carbon iostope data for the cores KL9 and KL17 VL

KL9		
depth [cm]	$\delta^{18}O$	$\delta^{13}C$
1.25	-1.620	1.604
11.25	-1.930	1.712
15.25	-1.749	1.255
17.25	-1.630	1.087
27.25	-1.899	1.445
37.25	-1.783	1.251
47.25	-1.467	1.528
57.25	-1.321	1.424
67.25	-1.704	1.064
77.25	-1.334	1.114
87.25	-0.998	0.574
90.25	-0.979	1.136
170.75	1.496	0.885
180.75	1.356	1.050
200.75	0.633	0.846
210.75	0.862	0.981
215.25	1.138	1.279
235.25	0.449	0.504
245.25	2.314	0.738
255.25	1.918	0.556
265.25	2.117	1.053
275.25	1.007	1.242
285.25	0.459	1.157
295.25	-0.209	1.063
305.25	-0.524	1.704
310.25	-0.607	1.330
312.25	-0.667	1.374
322.25	0.295	1.249
332.25	-0.363	1.007
342.25	-0.108	0.963
352.25	-0.596	1.066
362.25	-0.713	1.226
372.25	-0.604	1.289
382.25	-0.912	1.017
392.25	-0.675	0.990
402.25	-0.809	1.134
410.25	-0.765	1.238
412.25	-0.832	0.962
422.25	-1.283	1.035
432.25	-1.527	1.298
442.25	-2.293	0.762
452.25	-2.596	0.314
462.25	0.313	1.254
472.25	0.946	0.656
502.25	1.398	0.454
510.25	1.194	0.624
522.25	1.347	0.857
532.25	1.459	0.905
542.25	1.535	0.720
552.25	0.738	0.861
562.25	0.491	0.797
572.25	-0.401	1.075
582.25	0.149	0.595
592.25	0.081	0.246
602.25	0.461	0.848
609.25	0.418	1.010
611.25	0.593	0.989

KL9		
depth [cm]	$\delta^{18}O$	$\delta^{13}C$
621.25	-0.347	1.417
631.25	-0.440	1.468
641.25	-1.203	1.516
651.25	-2.159	1.359
661.25	-1.338	1.118
671.25	-0.228	1.204
681.25	-0.799	1.414
691.25	-0.585	1.281
701.25	-0.671	1.192
709.25	0.513	0.998
711.25	0.433	1.086
721.25	0.827	1.114
731.25	0.472	0.751
741.25	-0.018	1.144
751.25	-0.651	1.344
761.25	-1.171	1.317
771.25	-1.099	1.174
781.25	-0.480	1.440
791.25	0.825	0.876
801.25	0.936	0.853
810.25	1.207	1.056
812.25	1.189	1.071
822.25	1.083	0.950
832.25	1.712	0.848
842.25	2.338	0.922
852.25	2.037	1.145
862.25	1.291	0.979
872.25	0.769	1.153
882.25	0.009	1.364
892.25	-0.170	1.141
902.25	-0.649	0.982
909.25	0.238	1.296
911.25	0.552	1.302
921.25	0.069	0.901
931.25	0.499	1.175
941.25	-0.267	0.853
951.25	-0.563	1.269
961.25	-0.703	1.059
971.25	-0.416	1.106
981.25	-0.520	0.987
991.25	-0.565	0.996
1001.25	-0.566	1.113
1008.25	-0.007	1.397
1010.25	-0.311	1.151
1020.25	-0.966	0.914
1030.25	-0.914	1.308
1040.25	-1.292	0.790
1050.25	-1.451	1.164
1060.25	-1.333	0.948
1070.25	-1.691	0.770
1080.25	-1.714	0.442
1090.25	0.891	0.624
1100.25	2.221	0.653
1108.25	2.338	0.726
1111.25	-0.406	0.797
1121.25	-0.240	1.243
1131.25	0.147	1.312

KL9		
depth [cm]	$\delta^{18}O$	$\delta^{13}C$
1141.25	0.406	1.102
1151.25	1.095	1.206
1161.25	1.464	1.139
1171.25	1.812	1.253
1181.25	1.863	0.709
1191.25	0.943	0.711
1201.25	1.705	0.411
1208.25	1.714	0.579
1211.25	-0.266	0.864
1221.25	-0.124	1.527
1231.25	-0.760	1.413
1251.25	-0.599	1.090
1261.25	-1.207	1.077
1271.25	-0.473	1.125
1281.25	-1.072	1.272
1291.25	-0.967	1.137
1301.25	-1.304	1.615
1308.25	-1.435	1.009
1311.25	-1.579	1.046
1321.25	-1.764	1.212
1331.25	-1.743	0.865
1341.25	-1.491	0.782
1351.25	-1.410	0.235
1361.25	-0.884	0.739
1371.25	-0.171	0.689
1381.25	-0.404	0.584
1441.25	2.012	0.915
1451.25	1.320	0.685
1461.25	1.111	0.645
1471.25	0.983	0.603
1481.25	0.568	0.770
1491.25	0.502	1.183
1501.25	0.210	0.759
1508.25	0.156	0.679
1511.25	0.352	0.806
1521.25	0.514	1.372
1531.25	-0.132	1.493
1541.25	-0.274	1.320
1551.25	-0.815	0.933
1561.25	-0.998	0.788
1571.25	-1.555	1.479
1581.25	-0.998	1.408
1591.25	-1.035	1.295
1601.25	-0.433	1.650
1608.25	-0.484	1.427
1611.25	-0.658	1.396
1621.25	-0.953	0.924
1631.25	-1.658	1.074
1641.25	-0.788	1.206
1651.25	-0.463	0.904
1661.25	-0.086	1.268
1671.25	0.031	1.420
1681.25	-0.281	1.009
1691.25	-0.348	0.695
1701.25	-0.620	1.148
1708.25	-0.674	1.301

KL17 VL		
depth [cm]	$\delta^{18}O$	$\delta^{13}C$
0.5	-0.649	0.753
4.5	-0.658	0.566
6.5	-0.789	0.320
8.5	-0.593	0.759
10.5	-0.875	0.257
12.5	-0.799	0.438
14.5	-1.169	0.656
16.5	-1.062	1.193
18.5	-0.908	0.692
20.5	-0.940	0.881
22.5	-0.718	0.867
24.5	-0.631	0.542
28.5	-0.941	0.553
32.5	-0.866	0.696
36.5	-0.741	-0.126
40.5	-0.946	0.601
44.5	-0.655	0.427
48.5	-0.842	0.894
52.5	-1.124	0.624
56.5	-1.098	0.753
60.5	-1.146	0.368
64.5	-1.402	0.329
68.5	-1.581	0.660
72.5	-1.104	0.661
76.5	-1.292	0.246
80.5	-1.267	0.489
84.5	-0.753	-0.148
86.5	-1.301	0.566
88.5	-0.250	0.360
91.5	0.040	-0.344
92.5	-0.257	-0.058
94.5	-0.197	0.072
96.5	0.219	-0.140
128.5	-0.596	0.941
132.5	-0.750	0.753
136.5	-0.728	0.591

Acknowledgements

First of all, I am most indebted to my parents for giving me the possibility to attain my education, through their care and support.

I wish to thank my supervisor Michal Kucera, who allowed a very high degree of freedom in terms of thinking and tried methods. I am also grateful to Gerhard Schmiedl for accepting the task of second supervisor. Christoph Hemleben is thanked for provided access to material and hard to find data. Eelco Rohling and Hartmut Schulz were a source of advice and often provided helpful answers for mind preying questions on short notice.

I wish to thank Ralf Aurahs, Nadia Al-Sabouni, Petra Heinz, Lea Numberger, Franziska Simmank, Kerstin Braun, Wolfram Schinko, Ulrike van Raden and Tobias Moller for being the nice colleagues they are and have been. I am grateful to Peter Fittkau for assistance with the SEM and countless cigarettes. I thank Margret Bayer and Anne Ulmer for countless smaller and bigger organisational things and Wolfgang Kürner for the construction of many useful tools and parts that made the work easier and faster. Libuse Rammersdorfer was always helpful in the search for literature and with bibliographical questions. Alexander Floria, Sofie Jehle, Valentina Cruz and Kerstin Schiele are thanked for help in processing of the samples.

I want to thank my abroad colleagues Marcel van der Meer, Jeroen Groeneveld, Ralf Schiebel, Babette Hoogakker and Stefan Schouten for their cooperation, helpful suggestions, constructive discussions and general advice. Ellen Hopmans, Michiel Kienhuis, Guy Rothwell and Kathrine Grant are especially thanked for the measurement of samples or the help therewith. I appreciate the hopefully continuing cooperation with our colleagues Eli Biton and Hezi Gildor during the late stages of the work.

Lastly and by no means least I want to thank Gabriele Trommer for turning the three years of work in the RedStar project into a very good time.

References

Aitchison, J. (1999):
"Logratio and natural laws in compositional data analysis" Mathematical Geology 31(5): 563-580.

Aitchison, J., C. Barcelo-Vidal, J. A. Martin-Fernandez and V. Pawlowsky-Glahn (2000):
"Logratio analysis and compositional distance" Mathematical Geology 32(3): 271-275.

Almogi-Labin, A. (1982):
"Stratigraphic and paleoceanographic significance of late quaternary pteropods from deep-sea cores in the Gulf of Aqaba (Elat) and northernmost Red Sea" Marine Micropaleontology 7: 53-72.

Almogi-Labin, A. (1984):
"Population dynamics of planktic foraminifera and pteropoda - Gulf of Aqaba, Red Sea" Proceedings of the Koninklijke Nederlands Akademie van Westenschappen Series B 87: 481-511.

Almogi-Labin, A., B. Lux and J. C. Duplessy (1986):
"Quaternary paleoceanography, pteropod preservation and stable- isotope record of the Red Sea" Palaeogeography, Palaeoclimatology, Palaeoecology 57(2-4): 195-211.

Almogi-Labin, A., Ch. Hemleben, D. Meischner and H. Erlenkeuser (1991):
"Paleoenvironmental events during the last 13,000 years in the central Red Sea as recorded by pteropoda" Paleoceanography 6(1): 83-98.

Almogi-Labin, A., Ch. Hemleben and D. Meischner (1998):
"Carbonate preservation and climatic changes in the central Red Sea during the last 380 kyr as recorded by pteropods" Marine Micropaleontology 33: 87-107.

Amante, C. and B. W. Eakins (2008):
"ETOPO1 1 Arc-Minute Global Relief Model: Procedures, Data Sources and Analysis" National Geophysical Data Center, National Environmental Satellite, Data and Information Service, National Oceanic and Atmospheric Adminstration, U.S. Department of Commerce, Boulder, Colorado, USA. http://www.ngdc.noaa.gov/mgg/global/global.html

Anand, P., H. Elderfield and M. H. Conte (2003):
"Calibration of Mg/Ca thermometry in planktonic foraminifera from a sediment trap time series" Paleoceanography, DOI: 10.1029/2002PA000846.

Arz, H. W., F. Lamy, J. Pätzold, P. J. Müller and M. Prins (2003a):
"Mediterranean moisture source for an Early-Holocene humid period in the northern Red Sea" Science 300: 118-121.

Arz, H. W., J. Pätzold, P. J. Müller and M. O. Moammar (2003b):
"Influence of Northern Hemisphere climate and global sea level rise on the restricted Red Sea marine environment during termination I" Paleoceanography, DOI: 10.1029/2002PA000864.

Arz, H. W., F. Lamy, A. Ganopolski, N. Nowaczyk and J. Pätzold (2006a):
"Dominant Northern Hemisphere climate control over millennial-scale glacial sea-level variability" Quaternary Science Reviews, DOI: 10.1016/j.quascirev.2006.07.016.

Arz, H. W., F. Lamy and J. Pätzold (2006b):
"A pronounced dry event recorded around 4.2 ka in brine sediments from the northern Red Sea" Quaternary Research 66(3): 432-441.

Auras-Schudnagies, A., D. Kroon, G. Ganssen, Ch. Hemleben and J. E. Van Hinte (1989):
"Distributional pattern of planktonic foraminifers and pteropods in surface waters and top core sediments of the Red Sea, and adjacent areas controlled by the monsoonal regime and other ecological factors" Deep-Sea Research 36(10): 1515-1533.

Austin, M. P. (1985):
"Continuum concept, ordination methods, and niche theory" Annual Review of Ecology and Systematics 16: 39-61.

Badawi, A. (1997):
"Planktonic foraminifera as paleoecological indicators in the northern Red Sea" M.Sc. thesis, Oceanography department, Faculty of Science, Alexandria University, Alexandria, Egypt.

Badawi, A. (2003):
"Reconstruction of late Quaternary paleoceanography of the Red Sea: Evidence from benthic foraminifera" Tübinger Mikropaläontologische Mitteilungen Nr. 28, University of Tübingen, Tübingen, Germany.

Badawi, A., G. Schmiedl and Ch. Hemleben (2005):
"Impact of late Quaternary environmental changes on deep-sea benthic foraminiferal faunas of the Red Sea" Marine Micropaleontology 58(1): 13-30.

Bar-Matthews, M., A. Ayalon, A. Kaufman and G. J. Wasserburg (1999):
"The Eastern Mediterranean paleoclimate as a reflection of regional events: Soreq cave, Israel" Earth and Planetary Science Letters 166: 85-95.

Bar-Matthews, M., A. Ayalon and A. Kaufman (2000):
"Timing and hydrological conditions of Sapropel events in the Eastern Mediterranean, as evident from speleothems, Soreq cave, Israel" Chemical Geology 169: 145-156.

Bar-Matthews, M., A. Ayalon, M. Gilmour, A. Matthews and C. J. Hawkesworth (2003):
"Sea–land oxygen isotopic relationships from planktonic foraminifera and speleothems in the Eastern Mediterranean region and their implication for paleorainfall during interglacial intervals" Geochimica et Cosmochimica Acta 67(17): 3181-3199.

Bauch, H. A., H. Erlenkeuser, J. P. Helmke and U. Struck (2000):
"A paleoclimatic evaluation of marine oxygen isotope stage 11 in the high-northern Atlantic (Nordic seas)" Global and Planetary Change 24: 27-39.

Bayer, H.-J., Z. El-Isa, H. Hotzl, J. Mechie, C. Prodehl and G. Saffarini (1989):
"Large tectonic and lithospheric structures of the Red Sea region" Journal of African Earth Sciences 8(2-4): 565-587.

Bé, A. W. H. and R. W. Gilmer (1977):
"A zoogeographic and taxonomic overview of euthecosomatous pteropoda" in A. T. S. Ramsay "Oceanic Micropaleontology", Vol. 1, London, Academic Press, pp. 733-808.

Bé, A. W. H. and W. H. Hutson (1977):
"Ecology of planktonic foraminifera and biogeographic patterns of live and fossil assemblages in the Indian Ocean" Micropaleontology 23: 369-414.

Bé, A. W. H. (1980):
"Gametogenic calcification in a spinose planktonic foraminifer, *Globigerinoides sacculifer* (Brady)" Marine Micropaleontology 5: 283-310.

Beckmann, W. (1984):
"Mesozooplankton distribution on a transect from the Gulf of Aden to the central Red Sea during the winter monsoon" Oceanologica Acta 7(1): 87-102.

Behrenfeld, M. J. and P. G. Falkowski (1997):
"Photosynthetic rates derived from satellite-based chlorophyll concentration" Limnology and Oceanography 42(1): 1-20.

Bentaleb, I., C. Caratini, M. Fontugne, M. T. Morzadec-Kerfourn, J. P. Pascal and C. Tissot (1997):
"Monsoon regime variations during the late Holocene in southwestern India" in H. N. Dalfes, G. Kukla and H. Weiss " North Atlantic Treaty Organization Advanced Science Institute Series I, Vol. 49, Third millenium BC climate change and Old World collapse" Berlin, Springer-Verlag, pp. 475-488.

Berger, W. H., R. C. Finkel, J. S. Killingley and V. Marchig (1983):
"Glacial-Holocene transition in deep-sea sediments: manganese-spike in the east-equatorial Pacific" Nature 303: 231-233.

Berger, W. H. and U. von Rad (2002):
"Decadal to millennial cyclicity in varves and turbidites from the Arabian Sea: hypothesis of tidal origin" Global and Planetary Change 34: 313-325.

Berger, W. H. and G. Wefer (2003):
"On the dynamics of the ice ages: Stage-11 paradox, mid-Brunhes climate shift, and 100-ky cycle" in A. W. Droxler, R. Z. Poore and L. H. Burckle "Earth's climate and orbital eccentricity: the marine isotope stage 11 question" Geophysical Monograph Series 137, Washington, District of Columbia, American Geophysical Union, pp. 41-59.

References

Berggren, W. A. and A. Boersma, (1969):
"Late Pleistocene and Holocene Planktonic Foraminifera from the Red Sea" in E. T. Degens and D. A. Ross "Hot Brines and Recent Heavy Metal Deposits in the Red Sea" Berlin, Springer-Verlag, pp. 282-298.

Bernhard, J. M. and B. K. S. Gupta (1999):
"Foraminifera of oxygen-depleted environments" in B. K. S. Gupta "Modern Foraminifera" Dordrecht, Kluwer Academic Publishers, pp. 201-216.

Bijma, J., W. W. Faber Jr and Ch. Hemleben (1990):
"Temperature and salinity limits for growth and survival of some planktonic foraminifers in laboratory cultures" Journal of Foraminiferal Research 20(2): 95-116.

Bijma, J., Ch. Hemleben, H. Oberhänsli and M. Spindler (1992):
"The effects on increased water fertility on tropical spinose planktonic foraminifers in laboratory cultures" Journal of Foraminiferal Research 22(3): 242-256.

Bijma, J. and Ch. Hemleben (1994):
"Population dynamics of the planktic foraminifer *Globigerinoides sacculifer* (Brady) from the central Red Sea" Deep-Sea Research I 41(3): 485-510.

BioComp Systems, Inc. (1997):
"Neurogenetic Optimizer" Neural network development system, version 2.6.142, BioComp Systems, Inc., Minneapolis, Minnesota, USA.
http://www.biocompsystems.com/products/ngo/index.htm

Birks, H. J. B., J. M. Line, S. Juggins, A. C. Stevenson and C. J. F. Ter Braak (1990):
"Diatoms and pH reconstruction"
Philosophical Transactions of the Royal Society of London B 327(1240): 263-278.

Birks, H. J. B., (1995):
"Quantitative paleoenvironmental reconstructions" in D. Maddy and J. S. Brew "Statistical Modelling of Quaternary Science Data" Cambridge, Quaternary Reseach Association, pp. 161-254.

Biton, E. (2006):
"The Red Sea during the Last Glacial Maximum" M.Sc. thesis, Department of Environmental Science and Energy Research, Weizmann Institute of Science, Rehovot, Israel.

Biton, E., H. Gildor and W. R. Peltier (2008):
"Red Sea during the Last Glacial Maximum: Implications for sea level reconstruction"
Paleoceanography DOI: 10.1029/2007PA001431.

Bond, G., W. Showers, M. Cheseby, R. Lotti, P. Almasi, P. deMenocal, P. Priore, H. Cullen, I. Hajdas and G. Bonani (1997):
"A pervasive millennial-scale cycle in North Atlantic Holocene and glacial climates"
Science 278: 1257-1265.

Bonnefille, R., J. C. Roeland and J. Guiot (1990):
"Temperature and rainfall estimates for the past 40,000 years in equatorial Africa" Nature 346: 347-349.

Bosworth, W., P. Huchon and K. McClay (2005):
"The Red Sea and Gulf of Aden basins" Journal of African Earth Sciences 43(1-3): 334-378.

Bowen, D. Q. (2003):
"Uncertainty in oxygen isotope stage 11 sea-level: an estimate of ~13 ± 2 m from Great Britain" in A. W. Droxler, R. Z. Poore and L. H. Burckle "Earth's climate and orbital eccentricity: the marine isotope stage 11 question" Geophysical Monograph Series 137, Washington, District of Columbia, American Geophysical Union, pp. 131-144.

Brachert, T. C. (1999):
"Non-skeletal carbonate production and stromatolite growth within a Pleistocene deep ocean (Last Glacial Maximum, Red Sea)" Facies 40: 211-228.

Brassell, S. C., G. Eglinton, I. T. Marlowe, U. Pflaumann and M. Sarnthein (1986):
"Molecular stratigraphy: a new tool for climatic assessment" Nature 320: 129-133.

Braun, K. (2009):
"Red Sea planktonic foraminifera faunas of MIS 11 - comparison to the Holocene and paleo-environmental implications" Diploma thesis. Institute of Geosciences, University of Tübingen, Tübingen, Germany.

Bray, J. R. and J. T. Curtis (1957):
"An ordination of the upland forest communities of Southern Wisconsin" Ecological Monographs 27: 325-349.

Brummer, G.-J. A. and D. Kroon (1988):
"Planktonic foraminifers as tracers of cean-climate history" Amsterdam, Free University Press.

Bryson, R. A. (1997):
"Proxy indications of Holocene winter rains in southwest Asia compared with simulated rainfall" in H. N. Dalfes, G. Kukla and H. Weiss "NATO ASI Series, Vol. I 49, Third millenium BC climate change and Old World collapse" Berlin, Springer-Verlag, pp.465-473.

Calvert, S. E., B. Nielsen and M. R. Fontugne (1992):
"Evidence from nitrogen isotope ratios for enhanced productivity during formation of eastern Mediterranean sapropels" Nature 359: 223-225.

Caratini, C., I. Bentaleb, M. Fontugne, M. T. Morzadec-Kerfourn, J. P. Pascal and C. Tissot (1994):
"A less humid climate since ca. 3500 yr B.P. from marine cores off Karwar, western India" Palaeogeography, Palaeoclimatology, Palaeoecology 109: 371-384.

Casford, J. S. L., R. Abu-Zied, E. J. Rohling, S. Cooke, K. P. Boessenkool, H. Brinkhues, C. De Vries, G. Wefer, M. Geraga, G. Papatheodorou, I. Croudace, J. Thomson and V. Lykousis (2001):
"Mediterranean climate variability during the Holocene" Mediterranean Marine Science 2/1: 45-55.

Casford, J. S. L., R. H. Abu-Zied, E. J. Rohling, S. Cooke, C. Fontanier, M. Leng, A. Millard and J. Thomson (2007):
"A stratigraphically controlled multiproxy chronostratigraphy for the eastern Mediterranean" Paleoceanography, DOI: 10.1029/2007PA001422.

Cattell, R. B. (1966):
"The scree test for the number of factors" Multivariate Behaviorial Research 1: 245-276.

Caulet, J. P., P. Celment and P. J. Giannesini (1992):
"GEOCORES: Inventèire informatise des roches et sèdiments marins conservès au Museum National d'Histoire Naturelle" Bulitin Museum National d'Histoire Naturelle Vol. 14, section C(No. 1): 93-136.

Cayre, O., L. Beaufort and E. Vincent (1999):
"Paleoproductivity in the equatorial Indian Ocean for the last 260,000 yr: A transfer function based on planktonic foraminifera" Quaternary Science Reviews 18(6): 839-857.

Cember, R. P. (1988):
"On the sources, formation and circulation of Red Sea deep water" Journal of Geophysical Research 93(C7): 8175-8191.

Chave, K. E. (1954):
"Aspects of biochemistry of magnesium: 1.Calcareous marine organisms" Journal of Geology 62: 266-283.

Chen, M. T. and W. L. Prell (1998):
"Faunal distribution patterns of planktonic foraminifers in surface sediments of the low-latitude Pacific" Palaeogeography, Palaeoclimatology, Palaeoecology 137(1-2): 55-77.

Clifford, M., C. Horton, J. Schmitz and L. H. Kantha (1997):
"An oceanographic nowcast/forecast system for the Red Sea" Journal of Geophysical Research 102: 25,101-25,122.

COHMAP members (1988):
"Climatic changes of the last 18,000 years: observations and model simulations" Science 241(4869): 1043-1052.

Conte, M. H., M.-A. Sicre, C. Rühlemann, J. C. Weber, S. Schulte, D. Schulz-Bull and T. Blanz (2006):
"Global temperature calibration of the alkenone unsaturation index ($U^{K'}_{37}$) in surface waters and comparison with surface sediments" Geochemistry, Geophysics, Geosystems 7(2): Q02005 1-22.

References

Croudace, I. W., A. Rindby and R. G. Rothwell (2006):
"ITRAX: description and evaluation of a new multi-function X-ray core scanner" in R. G. Rothwell "New Techniques in Sediment Core Analysis" London, Geological Society, Special Publications, pp. 51-63.

da Silva, A., C. Young and S. Levitus (1994):
"Atlas of Surface Marine Data 1994, Volume 1: Algorithms and Procedures" U.S. Department of Commerce, National Oceanic and Atmospheric Administration, National Environmental Satellite, Data, and Information Service. http://iridl.ldeo.columbia.edu/SOURCES/.DASILVA/

Darling, K. F., M. Kucera, D. Kroon and C. M. Wade (2006):
"A resolution for the coiling direction paradox in *Neogloboquadrina pachyderma*" Paleoceanography, DOI: 10.1029/2005PA001189.

de Abreu, C., F. F. Abrantes, N. J. Shackleton, P. C. Tzedakis, J. F. McManus, D. W. Oppo and M. A. Hall (2005):
"Ocean climate variability in the eastern North Atlantic during interglacial marine isotope stage 11: A partial analogue to the Holocene?" Paleoceanography, DOI:10.1029/2004PA001091.

De Lange, G. J., J. Thomson, A. Reitz, C. P. Slomp, M. S. Principato, E. Erba and C. Corselli (2008):
"Synchronous basin-wide formation and redox-controlled preservation of a Mediterranean sapropel" Nature Geoscience 1(9): 606-610.

de Vernal, A., F. Eynaud, M. Henry, C. Hillaire-Marcel, L. Londeix, S. Mangin, J. Matthiessen, F. Marret, T. Radi, A. Rochon, S. Solignac and J. L. Turon (2005):
"Reconstruction of sea-surface conditions at middle to high latitudes of the Northern Hemisphere during the Last Glacial Maximum (LGM) based on dinoflagellate cyst assemblages" Quaternary Science Reviews 24(7-9): 897-924.

Degens, E. T. and D. A. Ross (1969):
"Hot brines and recent heavy metal deposits in the Red Sea" New York, Springer Verlag.

DeLong, E. F. (1992):
"Archaea in coastal marine environments" Proceedings of the National Academy of Sciences, USA 89: 5685-5689.

deMenocal, P., J. Ortiz, T. Guilderson and M. Sarnthein (2000):
"Coherent high- and low-latitude climate variability during the Holocene warm period" Science 288: 2198-2202.

Dickson, A. J., C. J. Beer, C. Dempsey, M. A. Maslin, J. A. Bendle, E. L. McClymont and R. D. Pancost (2009):
"Oceanic forcing of the Marine Isotope Stage 11 interglacial" Nature Geoscience 2(6): 427-432.

Doose-Rolinski, H., U. Rogalla, G. Scheeder, A. Lückge and U. von Rad (2001):
"High-resolution temperature and evaporation changes during the late Holocene in the northeastern Arabian Sea" Paleoceanography 16(4): 357-367.

Droxler, A. W., R. B. Alley, W. R. Howard, R. Z. Poore and L. H. Burckle (2003a):
"Unique and exceptionally long interglacial Marine Isotope Stage 11: Window into earth warm future climate" in A. W. Droxler, R. Z. Poore and L. H. Burckle "Earth's climate and orbital eccentricity: the marine isotope stage 11 question" Geophysical Monograph Series 137, Washington, District of Columbia, American Geophysical Union, pp. 1-14.

Droxler, A. W., R. Z. Poore and L. H. Burckle (2003b):
"Earth's climate and orbital eccentricity: the marine isotope stage 11 question" Geophysical Monograph 137, Washington, District of Columbia, American Geophysical Union.

Dryden, A. L. J. (1931):
"Accuracy in percentage representation of heavy mineral frequencies" Proceedings of the National Academy of Sciences, USA 17(5): 233-238.

Duplessy, J. C., L. Labeyrie, A. Juilletleclerc, F. Maitre, J. Duprat and M. Sarnthein (1991):
"Surface salinity reconstruction of the North-Atlantic ccean during the last glacial maximum" Oceanologica Acta 14(4): 311-324.

Eastwood, W. J., M. J. Leng, N. Roberts and B. Davis (2007):
"Holocene climate change in the eastern Mediterranean region: a comparison of stable isotope and pollen data from Lake Gölhisar, southwest Turkey" Journal of Quaternary Science 22(4): 327-341.

Edelman-Furstenberg, Y., M. Scherbacher, Ch. Hemleben and A. Almogi-Labin (2001):
"Deep-Sea benthic foraminifera from the central Red Sea"
Journal of Foraminiferal Research 31(1): 48-59.

Edelman-Furstenberg, Y., A. Almogi-Labin and Ch. Hemleben (2009):
"Palaeoceanographic evolution of the central Red Sea during the late Holocene"
The Holocene 19(1): 117-127.

Edelman, Y. (1996):
"Reconstruction of paleocenographic settings during the late Holocene in the central Red Sea"
M.Sc. thesis, Institute of Earth Sciences, Hebrew University, Jerusalem, Israel.

Ehrmann, W., G. Schmiedl, Y. Hamann, T. Kuhnt, Ch. Hemleben and W. Siebel (2007):
"Clay minerals in the late glacial and Holocene sediments of the northern and southern Red Sea"
Palaeogeography, Palaeoclimatology, Palaeoecology 249: 36-57.

Emeis, K.-C., U. Struck, H.-M. Schulz, R. Rosenberg, S. Bernasconi, H. Erlenkeuser,
T. Sakamoto and F. Martinez-Ruiz (2000):
"Temperature and salinity variations of Mediterranean Sea surface waters over the last 16,000 years from records of planktonic stable oxygen isotopes and alkenone unsaturation ratios"
Palaeogeography, Palaeoclimatology, Palaeoecology 158: 259-280.

Emiliani, C. (1955):
"Pleistocene temperatures" Journal of Geology 63: 538-578.

Erez, J. and S. Honjo (1981):
"Comparison of isotopic composition of planktonic foraminifera in plankton tows, sediment traps and sediments" Paleogeography, Paleoclimatology, Paleoecology (33): 129-156.

Eshel, G., M. A. Cane and M. B. Blumenthal (1994):
"Modes of subsurface, intermediate, and deep water renewal in the Red Sea"
Journal of Geophysical Research 99: 15,941-15,952.

Eshel, G. and N. H. Naik (1997):
"Climatological coastal jet collision, intermediate water formation, and the general circulation of the Red Sea" American Meteorological Society 27: 1233-1257.

Eshel, G. and N. Heavens (2007):
"Climatological evaporation seasonality in the northern Red Sea"
Paleoceanography, DOI: 10.1029/2006PA001365.

Fairbanks, R. G., M. Sverdlove, R. Free, P. H. Wiebe and A. W. H. Bé (1982):
"Vertical distribution and isotopic fractionation of living planktonic foraminifera from the Panama Basin" Nature 298: 841-844.

Fairbanks, R. G. (1992):
"Barbados Sea Level and Th/U ^{14}C Calibration" National Oceanic and Atmospheric Administration / National Geophysical Data Center Paleoclimatology Program, Boulder, Colorado, USA,

Farmer, E. C., A. Kaplan, P. B. de Menocal and J. Lynch-Stieglitz (2007):
"Corroborating ecological depth preferences of planktonic foraminifera in the tropical Atlantic with the stable oxygen isotope ratios of core top specimens" Paleoceanography, DOI: 10.1029/2006PA001361.

Feldman, G. C. and C. R. McClain (2006):
"Ocean Color Web, Merged SeaWIFS/Aquamodis Chlorophyll *a* concentration" National Aeronautics and Space Administration Goddard Space Flight Center, Washington, District of Columbia, USA.
http://oceancolor.gsfc.nasa.gov/

Fenton, M. (1998):
"Late quaternary history of Red Sea outflow" Ph.D. thesis. School of ocean and earth science, University Southampton, Southampton, United Kingdom.

Fenton, M., S. Geiselhart, E. J. Rohling and Ch. Hemleben (2000):
"Aplanktonic zones in the Red Sea" Marine Micropaleontology 40: 277-294.

Ferguson, J. E., G. M. Henderson, M. Kucera and R. E. M. Rickaby (2008):
"Systematic change of foraminiferal Mg/Ca ratios across a strong salinity gradient"
Earth and Planetary Science Letters 265: 153-166.

Fleitmann, D., S. J. Burns, M. Mudelsee, U. Neff, J. Kramers, A. Mangini and A. Matter (2003a):
"Holocene forcing of the Indian monsoon recorded in a stalagmite from Southern Oman"
Science 300(5626): 1737-1739.

Fleitmann, D., S. J. Burns, U. Neff, A. Mangini and A. Matter (2003b):
"Changing moisture sources over the last 330,000 years in Northern Oman from fluid-inclusion evidence in speleothems" Quaternary Research 60: 223-232.

Fleitmann, D., S. J. Burns, A. Mangini, M. Mudelsee, J. Kramers, I. Villa, U. Neff, A. A. Al-Subbary, A. Buettner, D. Hippler and A. Matter (2007):
"Holocene ITCZ and Indian monsoon dynamics recorded in stalagmites from Oman and Yemen (Socotra)" Quaternary Science Reviews 26: 170-188.

Fleming, K., P. Johnston, D. Zwartz, Y. Yokoyama, K. Lambeck and J. Chappell (1998):
"Refining the eustatic sea-level curve since the Last Glacial Maximum using far- and intermediate-field sites" Earth and Planetary Science Letters 163: 327-342.

Froelich, P. N., G. P. Klinkhammer, M. L. Bender, N. A. Luedtke, G. R. Heath, D. Cullen, P. Dauphin, D. Hammond, B. Hartman and V. Maynard (1979):
"Early oxidation of organic matter in pelagic sediments of the eastern equatorial Atlantic: suboxic diagenesis" Geochimica et Cosmochimica Acta 43: 1075-1090.

Ganssen, G. and D. Kroon (1991):
"Evidence for Red Sea surface circulation from oxygen isotopes of modern surface waters and planktonic foraminiferal tests" Paleoceanography 6(1): 73-82.

Gasse, F. and E. Van Campo (1994):
"Abrupt post-glacial climate events in West Asia and North Africa monsoon domains"
Earth and Planetary Science Letters 126: 435-456.

Gasse, F. (2000):
"Hydrological changes in the last African tropics since the Last Glacial Maximum"
Quaternary Science Reviews 19: 189-211.

Geiselhart, S. (1998):
"Late Quaternary paleoceanographic and paleoclimatologic history of the Red Sea during the last 380.000 years: Evidence from stable isotopes and faunal assemblages" Tübinger Mikropaläontologische Mitteilungen Nr. 17, University of Tübingen, Tübingen, Germany.

Gersonde, R., X. Crosta, A. Abelmann and L. Armand (2005):
"Sea-surface temperature and sea lee distribution of the Southern Ocean at the EPILOG Last Glacial Maximum - A circum-Antarctic view based on siliceous microfossil records"
Quaternary Science Reviews 24(7-9): 869-896.

Girdler, R. W. and P. Styles (1974):
"Two stage Red Sea floor spreading" Nature 247: 7-11.

Golden Software, Inc. (2004):
"Surfer 8" Surface mapping system, version 8.05, Golden Sofware, Inc., Golden, Colorado, USA.
http://www.goldensoftware.com

Goodfriend, G. A. (1999):
"Terrestrial stable isotope records of Late Quaternary paleoclimates in the eastern Mediterranean region" Quaternary Science Reviews 18(4-5): 501-513.

Grace, S. F. (1930):
"The influence of friction on the tidal motion of the Gulf of Suez" Monthly Notices, Royal Astronomical Society, Geophysical Supplement 2: 273-296.

Groeneveld, J., M. Raitzsch, M. Siccha, G. Trommer, Ch. Hemleben and M. Kucera (2008):
"Salinity influence on planktonic foraminiferal Mg/Ca: A case study from the Red Sea"
Geochimica et Cosmochimica Acta 72(12): A330-A330.

Gupta, A. K., D. M. Anderson and J. T. Overpeck (2003):
"Abrupt changes in the Asian southwest monsoon during the Holocene and their links to the North Alantic Ocean" Nature 421(6921): 354-357.

Guttman, L. (1954):
"Some necessary conditions for common factor analysis" Psychometrika 19: 149-161.

Halicz, E. and Z. Reiss (1981):
"Paleoecological relations of foraminifera in a desert-enclosed sea - The Gulf of Aqaba (Elat), Red Sea" Marine Ecology 2(1): 15-34.

Haug, G. H., K. A. Hughen, D. M. Sigman, L. C. Peterson and U. Röhl (2001):
"Southward migration of the intertropical convergence zone through the Holocene" Science 293: 1304-1308.

Hayes, A., M. Kucera, N. Kallel, L. Sbaffi and E. J. Rohling (2005):
"Glacial Mediterranean sea surface temperatures based on planktonic foraminiferal assemblages" Quaternary Science Reviews 24(7-9 special issue): 999-1016.

Hemleben, Ch., M. Spindler and O. R. Anderson (1989):
"Modern Planktonic Foraminifera" New York, Springer-Verlag.

Hemleben, Ch., W. Roether and P. Stoffers (1995):
"Östliches Mittelmeer, Rotes Meer, Arabisches Meer Cruise No. 31, 30 December 1994 - 22 March 1995" Meteor-Berichte, Institut für Meereskunde der Universität Hamburg, Hamburg, Germany. http://www.dfg-ozean.de/de/berichte/fs_meteor

Hemleben, Ch., D. Meischner, R. Zahn, A. Almogi-Labin, H. Erlenkeuser and B. Hiller (1996):
"Three hundred eighty thousand year long stable isotope and faunal records from the Red Sea: Influence of global sea level change on hydrography" Paleoceanography 11(2): 147-156.

Herold, M. and G. Lohmann (2009):
"Eemian tropical and subtropical African moisture transport: an isotope modelling study" Climate Dynamics DOI:10.1007/s00382-008-0515-2.

Hodell, D. A., C. D. Charles and U. S. Ninnemann (2000):
"Comparison of interglacial stages in the South Atlantic sector of the southern ocean for the past 450 kyr: implifications for Marine Isotope Stage (MIS) 11" Global and Planetary Change 24(1): 7-26.

Hoogakker, B. A. A., G. P. Klinkhammer, H. Elderfield, E. J. Rohling and C. Hayward (2009):
"Mg/Ca paleothermometry in high salinity environments" Earth and Planetary Science Letters 284: 583-589

Hughen, K. A., M. G. L. Baillie, E. Bard, J. W. Beck, C. J. H. Bertrand, P. G. Blackwell, C. E. Buck, G. S. Burr, K. B. Cutler, P. E. Damon, R. L. Edwards, R. G. Fairbanks, M. Friedrich, T. P. Guilderson, B. Kromer, G. McCormac, S. Manning, C. B. Ramsey, P. J. Reimer, R. W. Reimer, S. Remmele, J. R. Southon, M. Stuiver, S. Talamo, F. W. Taylor, J. van der Plicht and C. E. Weyhenmeyer (2004):
"Marine04 marine radiocarbon age calibration, 0-26 cal kyr BP" Radiocarbon 46(3): 1059-1086.

Hutchinson, G. E. (1957):
"Concluding remarks" Cold Spring Harbor Symposia on Quantitative Biology 22(2): 415-427.

Hutson, W. H. (1977):
"Transfer functions under no-analog conditions: Experiments with Indian Ocean planktonic foraminifera" Quaternary Research 8: 355-367.

Hutson, W. H. (1980):
"The Agulhas Current during the late Pleistocene: Analysis of modern faunal analogs" Science 207: 64-66.

Huybers, P. (2006a):
"Early pleistocene glacial cycles and the integrated summer insolation forcing" Science 313(5786): 508-511.

Huybers, P. (2006b):
"Pleistocene depth-derived age model and composite $\delta^{18}O$ record" International Geosphere-Biosphere Programme PAGES / World Data Center for Paleoclimatology, National Oceanic and Atmospheric Administration / National Climatic Data Center Paleoclimatology Program, Boulder Colorado, USA.

References

Imbrie, J. and N. G. Kipp (1971):
"A new micropaleontological method for quantitative paleoclimatology: application to a late pleistocene caribbean core" in K. K. Turekian "Late Cenozoic Glacial Ages" New Haven, Yale University Press, pp. 71-81.

Imbrie, J., J. D. Hayes, D. G. Martinson, A. McIntyre, A. C. Mix, J. J. Morley, N. G. Pisias, W. L. Prell and N. J. Shackleton, (1984):
"The orbital theory of Pleistocene climate: support from a revised chronology of the $\delta^{18}O$ record" in A. L. Berger et al. "Milankovitch and Climate" Dordrecht, Reidel Publishing Company, pp. 269-305.

Imbrie, J., A. Duffy et al., Brown University (1990):
"SPECMAP Archive" National Oceanic and Atmospheric Administration / National Geophysical Data Center Paleoclimatology Program, Boulder Colorado, USA.

Ishikawa, S. and M. Oda (2007):
"Reconstruction of Indian monsoon variability over the past 230,000 years: Planktic foraminiferal evidence from the NW Arabian Sea open-ocean upwelling area"
Marine Micropaleontology 63(3-4): 143-154.

Ivanova, E., R. Schiebel, A. D. Singh, G. Schmiedl, H. S. Niebler and Ch. Hemleben (2003):
"Primary production in the Arabian Sea during the last 135 000 years" Palaeogeography, Palaeoclimatology, Palaeoecology 197(1-2): 61-82.

Ivanova, E. V. (1985):
"Late Quaternary biostratigraphy and paleotemperatures of the Red Sea and the Gulf of Aden based on planktonic foraminifera and pteropods" Marine Micropaleontology 9(4): 335-364.

Janowiak, J. E. and P. Xie (1999):
"CAMS_OPI: A global satellite-rain gauge merged product for real-time precipitation monitoring applications" Journal of Climate 12: 3335-3342.

Juggins, S. (2007):
"C2" Software for ecological and palaeoecological data analysis and visualisation.
Newcastle University, Newcastle upon Tyne, United Kingdom.
http://www.staff.ncl.ac.uk/staff/stephen.juggins/software.htm

Jung, S. J. A., G. R. Davies, G. M. Ganssen and D. Kroon (2004):
"Stepwise Holocene aridification in NE Africa deduced from dust-borne radiogenic isotope records"
Earth and Planetary Science Letters 221: 27-37.

Kim, J.-H., S. Schouten, E. C. Hopmans, B. Donner and J. S. Sinninghe Damsté (2008):
"Global sediment core-top calibration of the TEX_{86} paleothermometer in the ocean"
Geochimica et Cosmochimica Acta 72(4): 1154-1173.

Kröpelin, S., D. Verschuren, A.-M. Lezine, H. Eggermont, C. Cocquyt, P. Francus, J.-P. Cazet, M. Fagot, B. Rumes, J. M. Russell, F. Darius, D. J. Conley, M. Schuster, H. von Suchodoletz and D. R. Engstrom (2008):
"Climate-driven ecosystem succession in the Sahara: The past 6000 years" Science 320: 765-768.

Kucera, M., A. Rosell-Mele, R. Schneider, C. Waelbroeck and M. Weinelt (2005a):
"Multiproxy approach for the reconstruction of the glacial ocean surface (MARGO)"
Quaternary Science Reviews 24: 813-819.

Kucera, M., M. Weinelt, T. Kiefer, U. Pflaumann, A. Hayes, M. Weinelt, M.-T. Chen, A. C. Mix, T. T. Barrows, E. Cortijo, J. Duprat, S. Juggins and C. Waelbroeck (2005b):
"Reconstruction of sea-surface temperatures from assemblages of planktonic foraminifera: multi-technique approach based on geographically constrained calibration data sets and its application to glacial Atlantic and Pacific Oceans" Quaternary Science Reviews 24: 951-998.

Kuroyanagi, A. and H. Kawahata (2004):
"Vertical distribution of living planktonic foraminifera in the seas around Japan"
Marine Micropaleontology 53(1-2): 173-196.

Lampert, W. and U. Sommer (1993):
"Limnoökologie" Stuttgart, Thieme Verlag.

Larrasoana, J. C., A. P. Roberts, E. J. Rohling, M. Winklhofer and R. Wehausen (2003):
"Three million years of monsoon variability over the northern Sahara"
Climate Dynamics 21(7-8): 689-698.

Lea, D. W., D. K. Pak and H. J. Spero (2003):
"Sea surface temperatures in the Western Equatorial Pacific during Marine Isotope Stage 11" in A. W. Droxler, R. Z. Poore and L. H. Burckle "Earth's climate and orbital eccentricity: The Marine Isotope Stage 11 question" Geophysical Monograph 137, Washington, District of Columbia, American Geophysical Union, pp. 147-156.

Lee, J. J. and O. R. Anderson, (1991):
"Symbiosis in foraminifera" in J. J. Lee and O. R. Anderson "Biology of foraminifera" London, United Kingdom, Academic Press, pp. 157-220.

Legge, H. L., J. Mutterlose and H. W. Arz (2006):
"Climatic changes in the northern Red Sea during the last 22,000 years as recorded by calcareous nannofossils" Paleoceanography DOI: 10.1029/2005PA001142.

Legge, H. L., J. Mutterlose, H. W. Arz and J. Pätzold (2008):
"Nannoplankton successions in the northern Red Sea during the last glaciation (60 to 14.5 ka BP): Reactions to climate change" Earth and Planetary Science Letters 270(3-4): 271-279.

Leps, J. and P. Smilauer (2003):
"Multivariate Analysis of Ecological Data using CANOCO" Cambridge, Cambridge University Press.

Levitus, S. and National Oceanographic Data Center:
World Ocean Atlas 2001 [electronic resource]: objectively analyzed fields and statistics / prepared by the Ocean Climate Laboratory, National Oceanographic Data Center; editor S. Levitus.
http://www.nodc.noaa.gov/OC5/WOA01/pr_woa01.html

Lisitzin, E. (1965):
"The mean sea level of the world ocean"
Commentationes Physico Mathematicae - Helsingfors 30(7): 30-35.

Locke, S. and R. C. Thunell (1988):
"Paleoceanographic record of the last glacial/interglacial cycle in the Red Sea and Gulf of Aden"
Palaeogeography, Palaeoclimatology, Palaeoecology 64: 163-187.

Lohmann, G. P. (1995):
"A model for variation in the chemistry of planktonic foraminifera due to secondary calcification and selective dissolution" Paleoceanography 10(3): 445-457.

Lombard, F., L. Labeyrie, E. Michel, H. J. Spero and D. W. Lea (2009):
"Modelling the temperature dependent growth rates of planktic foraminifera"
Marine Micropaleontology 70(1-2): 1-7.

Loncaric, N., F. J. C. Peeters, D. Kroon and G. J. A. Brummer (2006):
"Oxygen isotope ecology of recent planktic foraminifera at the central Walvis Ridge (SE Atlantic)"
Paleoceanography, DOI: 10.1029/2005PA001207.

Lückge, A., H. Doose-Rolinski, A. A. Khan, H. Schulz and U. von Rad (2001):
"Monsoonal variability in the northeastern Arabian Sea during the past 5000 years: geochemical evidence from laminated sediments"
Palaeogeography, Palaeoclimatology, Palaeoecology 167(3-4): 273-286.

Lyberis, N. (1988):
"Tectonic evolution of the Gulf of Suez and the Gulf of Aqaba" Tectonophysics 153: 209-220.

Meteorological Assimilation Data Ingest System (MADIS)
National Oceanic and Atmospheric Administration / Forecast Systems Laboratory.
http://www.madis.noaa.gov

Malmgren, B. A. and U. Nordlund (1997):
"Application of artificial neural networks to paleoceanographic data"
Palaeogeography, Palaeoclimatology, Palaeoecology 136(1-4): 359-373.

Malmgren, B. A., M. Kucera, J. Nyberg and C. Waelbroeck (2001):
"Comparison of statistical and artificial neural network techniques for estimating past sea surface temperatures from planktonic foraminifer census data" Paleoceanography 16(5): 520-530.

Manasrah, R., M. Badran, H. U. Lass and W. Fennel (2004):
"Circulation and winter deep-water formation in the northern Red Sea" Oceanologia 46(1): 5-23.

Marchant, R. and H. Hooghiemstra (2004):
"Rapid environmental change in African and South American tropics around 4000 years before present: a review" Earth-Science Reviews 66(3-4): 217-260.

Marlowe, I. T., J. C. Green, A. C. Neal, S. C. Brassell, G. Eglinton and P. A. Course (1984):
"Long-chain (n-C37- C39) alkenones in the Prymnesiophyceae. Distribution of alkenones and other lipids and their taxonomic significance" British Phycological Journal 19: 203-216.

Mawson, R. and M. A. J. Williams (1984):
"A wetter climate in eastern Sudan 2,000 years ago?" Nature 309: 49-51.

Mayewski, P. A., E. J. Rohling, J. C. Stager, W. Karlèn, K. A. Maasch, L. D. Meeker, E. A. Meyerson, F. Gasse, S. van Kreveld, K. Holmgren, L.-T. J., G. Rosqvist, F. Rack, M. Staubwasser, R. R. Schneider and E. J. Steig (2004):
"Holocene climate variability" Quaternary Research 62: 243-255.

McManus, J., D. Oppo, J. Cullen and S. Healey, (2003):
"Marine isotope stage 11 (MIS 11): Analog for Holocene and future climate?" in A. W. Droxler, R. Z. Poore and L. H. Burckle "Earth's climate and orbital eccentricity: The Marine Isotope Stage 11 question" Geophysical Monograph 137, Washington, District of Columbia, American Geophysical Union, pp. 69-85.

Mix, A. C., A. E. Morey, N. G. Pisias and S. W. Hostetler (1999):
"Foraminiferal faunal estimates of paleotemperature: Circumventing the no-analog problem yields cool ice age tropics" Paleoceanography 14(3): 350-359.

Morcos, S. A. (1970):
"Physical and chemical oceanography of the Red Sea"
Oceanography and Marine Biology: an annual review 8: 73-202.

Morey, A. E., A. C. Mix and N. G. Pisias (2005):
"Planktonic foraminiferal assemblages preserved in surface sediments correspond to multiple environment variables" Quaternary Science Reviews 24: 925-950.

Moustafa, Y. A., J. Pätzold, Y. Loya and G. Wefer (2000):
"Mid-Holocene stable isotope record of corals from the northern Red Sea"
International Journal of Earth Sciences 88: 742-751.

Müller, P. J., G. Kirst, G. Ruhland, I. von Storch and A. Rosell-Melé (1998):
"Calibration of the alkenone paleotemperature index $U^{K'}_{37}$ based on core-tops from the eastern South Atlantic and the global ocean (60° N-60° S)" Geochimica et Cosmochimica Acta 62(10): 1757-1772.

Murray, S. P. and W. Johns (1997):
"Direct observations of seasonal exchange through the Bab el Mandab Strait"
Geophysical Research Letters 24(21): 2557-2560.

Naidu, P. D. and B. A. Malmgren (1996):
"A high-resolution record of late quaternary upwelling along the Oman Margin, Arabian Sea based on planktonic foraminifera" Paleoceanography 11(1): 129-140.

Naqvi, W. A. and R. G. Fairbanks (1996):
"A 27,000 year record of Red Sea outflow: Implication for timing of post-glacial monsoon intensification" Geophysical Research Letters 23(12): 1501-1504.

Nellen, W., B. W., W. Roether, D. Schnack, H. Thiel, H. Weikert and B. Zeitschel (1996):
"MINDIK (Band II), Reise Nr. 5, 2.Januar-24.September 1987" Meteor-Berichte, Universität Hamburg, Hamburg, Germany. http://www.dfg-ozean.de/de/berichte/fs_meteor

Neumann, A. C. and D. A. McGill (1962):
"Circulation of the Red Sea in early summer" Deep-Sea Research 8: 223-235.

National Oceanographic Data Center (Levitus):
World Ocean Atlas 1994, U.S. Department of Commerce, National Oceanic and Atmospheric Administration, National Environmental Satellite, Data, and Information Service http://www.cdc.noaa.gov/data/gridded/data.nodc.woa94.html

Nürnberg, D., J. Bijma and Ch. Hemleben (1996):
"Assessing the reliability of magnesium in foraminiferal calcite as a proxy for water mass temperatures" Geochimica et Cosmochimica Acta 60(5): 803-814.

O´Brien, S. R., P. A. Mayewski, L. D. Meeker, D. A. Meese, M. S. Twickler and S. I. Whitlow (1995):
"Complexity of Holocene climate as reconstructed from a Greenland ice core" Science 270: 1962-1964.

Ocean Productivity Homepage
Online database, Oregon state University. http://www.science.oregonstate.edu/ocean.productivity/

Ortiz, J. D., A. C. Mix and R. W. Collier (1995):
"Environmental control of living symbiotic and asymbiotic foraminifera of the California Current" Paleoceanography 10(6): 987-1009.

Parker, F. L. (1962):
"Planktonic foraminiferal species in Pacific sediments" Micropaleontology 8(2): 219-254.

Patzert, W. C. (1974):
"Wind-induced reversal in Red Sea circulation" Deep-Sea Research 21: 109-121.

Pedgley, D. E. (1974):
"An outline of the weather and climate of the Red Sea"
L'oceanographie physique de la Mer Rouge, CNEXO: 9-27.

Peeters, F. J. C. and G.-J. A. Brummer, (2002):
"The seasonal and vertical distribution of living planktic foraminifera in the NW Arabian Sea" in P. D. Clift, D. Kroon, C. Gaedicke and J. Craig "The tectonic and climatic evolution of the Arabian Sea region" Geological Society Special Publications, pp. 463-497.

Petite-Maire, N., L. Beufort and N. Page, (1997):
"Holocene climate change and man in the present day Sahara desert" in H. N. Dalfes, G. Kukla and H. Weiss "North Atlantic Treaty Organization Advanced Science Institute Series I, Vol. 49, Third millenium BC climate change and Old World collapse" Berlin Heidelberg, Springer-Verlag, pp. 297-308.

Phadtare, N. R. (2000):
"Sharp decrease in summer monsoon strength 4000-3500 cal yr B.P. in the central Higher Himalaya of India based on pollen evidence from Alpine peat" Quaternary Research 53: 122-129.

Pollard, A. M. and S. P. E. Blockley (2006):
"Some numerical considerations on the geochemical analysis of distal microtephra" Applied Geochemistry 21: 1692-1714.

Prell, W. L., (1985):
"The stability of low-latitude sea-surface temperatures: An evaluation of the CLIMAP reconstruction with emphasis on the positive SST anomalies" Report TR025, U.S. Department of Energy, pp. 1-60.

Prell, W. L. (2003):
"The Brown University Foraminiferal Database (BFD)" http://www.pangaea.de/.

Pujol, C. and C. Vergnaud Grazzini (1994):
"Distribution patterns of live planktic foraminifers as related to regional hydrography and productive systems of the Mediterranean Sea" Marine Micropaleontology 25: 187-217.

Quadfasel, D. and H. Baudner (1993):
"Gyre-scale circulation cells in the Red Sea" Oceanologica Acta 16(3): 221-229.

Ravelo, A. C., R. G. Fairbanks and S. G. H. Philander (1990):
"Reconstructing tropical Atlantic hydrography using planktonic foraminifera and an ocean model" Paleocenaopgraphy 5(3): 409-431.

Reimer, P. J. and R. W. Reimer (2001):
"A marine reservoir correction database and on-line interface" Radiocarbon 43(2A): 461-463.

Rein, B., A. Lückge, L. Reinhardt, F. Sirocko, A. Wolf and W. C. Dullo (2005):
"El Niño variability off Peru during the last 20,000 years"
Paleoceanography, DOI: 10.1029/2004PA001099.

Reiss, Z., E. Halicz and L. Perelis (1974):
"Planktonic foraminifera from recent sediments in the Gulf of Elat"
Israel Journal of Earth Sciences 23: 69-105.

Reiss, Z., B. Luz, A. Almogi-Labin, E. Halicz, A. Winter and M. Wolf (1980):
"Late quaternary paleoceanography of the Gulf of Aqaba (Elat), Red Sea"
Quaternary Research 14: 294-308.

Revets, S. A. (2004):
"On confidence intervals from micropalaeontological counts"
Journal of Micropalaeontology 23(1): 61-65.

Rimbu, N., G. Lohmann, J. H. Kim, H. W. Arz and R. Schneider (2003):
"Arctic/North Atlantic Oscillation signature in Holocene sea surface temperature trends as obtained from alkenone data" Geophysical Research Letters, DOI: 10.1029/2002GL06570.

Rimbu, N., G. Lohmann, S. J. Lorenz, J. H. Kim and R. R. Schneider (2004):
"Holocene climate variability as derived from alkenone sea surface temperature and coupled ocean-atmosphere model experiments" Climate Dynamics 23: 215-227.

Ritchie, J. C., C. H. Eyles and C. V. Haynes (1985):
"Sediment and pollen evidence for an early to mid-Holocene humid period in the eastern Sahara"
Nature 314: 352-355.

Roeser, H. A. (1975):
"A detailed magnetic survey of the southern Red Sea" Geologisches Jahrbuch D 13: 131-153.

Rohling, E. J. (1994):
"Glacial conditions in the Red Sea" Paleoceanography 9(5): 653-660.

Rohling, E. J., M. Fenton, F. J. Jorissen, P. Bertrand, G. Ganssen and J. P. Caulet (1998):
"Magnitudes of sea-level lowstands of the past 500,000 years" Nature 394(6689): 162-165.

Rohling, E. J. (1999):
"Environmental control on Mediterranean salinity and $\delta^{18}O$" Paleoceanography 14(6): 706-715.

Rohling, E. J., P. A. Mayewski, R. H. Abu-Zied, J. S. L. Casford and A. Hayes (2002):
"Holocene atmosphere-ocean interactions: records from Greenland and the Aegean Sea"
Climate Dynamics 18: 587-593.

Rohling, E. J., M. Sprovieri, T. Cane, J. S. L. Casford, S. Cooke, I. Bouloubassi, K. C. Emeis, R. Schiebel, M. Rogerson and A. Hayes (2004):
"Reconstructing past planktic foraminiferal habitats using stable isotope data: a case history for Mediterranean sapropel S5" Marine Micropaleontology 50(1-2): 89-123.

Rohling, E. J., K. Grant, Ch. Hemleben, M. Kucera, A. P. Roberts, I. Schmeltzer, H. Schulz, M. Siccha, M. Siddall and G. Trommer (2008a):
"New constraints on the timing of sea level fluctuations during early to middle marine isotope stage 3"
Paleoceanography, DOI: 10.1029/2008PA001617.

Rohling, E. J., K. Grant, Ch. Hemleben, M. Siddall, B. A. A. Hoogakker, M. Bolshaw and M. Kucera (2008b):
"High rates of sea-level rise during the last interglacial period" Nature Geoscience 1(1): 38-42.

Rohling, E. J., K. Grant, M. Bolshaw, A. P. Roberts, M. Siddall, Ch. Hemleben and M. Kucera (2009):
"Antarctic temperature and global sea level closely coupled over the past five glacial cycles"
Nature Geoscience 2: 500-504.

Rosell-Melé, A. and E. L. McClymont, (2007):
"Biomarkers as paleoceanographic proxies" in C. Hillaire-Marcel and A. De Vernal "Proxies in late Cenozoic paleoceanography" Amsterdam, Elsevier, pp. 441-490.

Rossignol-Strick, M. (1983):
"African monsoons, and immediate climate response to orbital insolation" Nature 304: 46-49.

Rothwell, R. G., B. Hoogakker, J. Thomson, I. W. Croudace and M. Frenz, (2006):
"Turbidite emplacement on the southern Balearic Abyssal Plain (western Mediterranean Sea) during Marine Isotope Stages 1-3: an application of ITRAX XRF scanning of sediment cores to lithostratigraphic analysis" in R. G. Rothwell "New techniques in sediment core analysis" London, Geological Society, Special Publications, pp. 79-98.

Salzmann, U. and M. Waller (1998):
"The Holocene vegetational history of the Nigerian Sahel based on multiple pollen profiles" Review of Palaeobotany and Palynology 100: 39-72.

Sarkar, A., R. Ramesh, B. L. K. Somayajulu, R. Agnihotri, A. J. T. Jull and G. S. Burr (2000):
"High resolution Holocene monsoon record from the eastern Arabian Sea" Earth and Planetary Science Letters 177: 209-218.

Schiebel, R., J. J. Waniek, M. Bork and Ch. Hemleben (2001):
"Planktic foraminiferal production stimulated by chlorophyll redistribution and entrainment of nutrients" Deep-Sea Research I 48: 721-740.

Schiebel, R., A. Zeltner, U. F. Treppke, J. J. Waniek, J. Bollmann, T. Rixen and Ch. Hemleben (2004):
"Distribution of diatoms, coccolithophores and planktic foraminifers along a trophic gradient during SW monsoon in the Arabian Sea" Marine Micropaleontology 51: 345-371.

Schilman, B., M. Bar-Matthews, A. Almogi-Labin and B. Luz (2001):
"Global climate instability reflected by Eastern Mediterranean marine records during the late Holocene" Palaeogeography, Palaeoclimatology, Palaeoecology 176: 157-176.

Schlitzer, R. (2007):
"Ocean Data View" version 3.3.2, Alfred-Wegener-Institut für Polar- und Meeresforschung, Bremerhaven, Germany. http://www.odv.awi.de

Schluter, D. (2000):
"The ecology of adaptive radiation" Oxford, Oxford University Press.

Schmelzer, I. (1998):
"High-frequency event-stratigraphy and paleoceanography of the Red Sea" Ph.D. thesis. Institute of Geosciences, University of Tübingen, Tübingen, Germany.

Schouten, S., E. C. Hopmans, E. Schefuss and J. S. Sinninghe Damsté (2002):
"Distributional variations in marine crenarchaeotal membrane lipids: a new tool for reconstructing ancient sea water temperatures?" Earth and Planetary Science Letters 204: 265-274.

Schouten, S., E. C. Hopmans, A. Forster, Y. van Breugel, M. M. M. Kuypers and J. S. Sinninghe Damsté (2003):
"Extremely high sea-surface temperatures at low latitudes during the middle Cretaceous as revealed by archaeal membrane lipids" Geology 31(12): 1069-1072.

Schulz, H., U. von Rad and H. Erlenkeuser (1998):
"Correlation between Arabian Sea and Greenland climate oscillations of the past 110,000 years" Nature 393: 54-57.

Schulz, H., U. von Rad and V. Ittekkot, (2002):
"Planktic foraminifera, particle flux and oceanic productivity off Pakistan, NE Arabian Sea: modern analogues and application to the paleoclimatic record" in P. D. Clift, D. Kroon, C. Gaedicke and J. Craig "The tectonic and climatic evolution of the Arabian Sea region" Geological Society Special Publications, pp. 499-516.

Seppa, H., H. J. B. Birks, A. Odland, A. Poska and S. Veski (2004):
"A modern pollen-climate calibration set from northern Europe: developing and testing a tool for palaeoclimatological reconstructions" Journal Of Biogeography 31(2): 251-267.

Shackleton, N. J. (1987):
"Oxygen isotopes, ice volume and sea level" Quaternary Science Reviews 6: 183-190.

Siddall, M., E. J. Rohling, A. Almogi-Labin, Ch. Hemleben, D. Meischner, I. Schmelzer and D. A. Smeed (2003):
"Sea-level fluctuations during the last glacial cycle" Nature 423: 853-858.

Siddall, M., D. A. Smeed, Ch. Hemleben, E. J. Rohling, I. Schmelzer and W. Peltier (2004):
"Understanding the Red Sea response to sea level" Earth and Planetary Science Letters 225: 421-434.

References

Sikes, E. L., J. W. Farrington and L. D. Keigwin (1991):
"Use of the alkenone unsaturation ratio $U^{K'}_{37}$ to determine past sea surface temperatures: core-top SST calibrations and methodology considerations" Earth and Planetary Science Letters 104(1): 36-47.

Singh, A. D., D. Kroon and R. S. Ganeshram (2006):
"Millennial scale variations in productivity and OMZ intensity in the Eastern Arabian Sea"
Journal of the Geological Society of India 68(3): 369-377.

Sinninghe Damsté, J. S., S. Schouten, E. C. Hopmans, A. C. T. van Duin and J. A. J. Geenevasen (2002):
"Crenarchaeol: the characteristic core glycerol dibiphytanyl glycerol tetraether membrane lipid of cosmopolitan pelagic crenarchaeota" Journal of Lipid Research 43(10): 1641-1651.

Smeed, D. A. (1997):
"Seasonal variation of the flow in the strait of Bab al Mandab" Oceanologica Acta 20(6): 773-781.

Sofianos, S. S. and W. E. Johns (2002):
"An Oceanic General Circulation Model (OGCM) investigation of the Red Sea circulation:
1. Exchange between the Red Sea and the Indian Ocean"
Journal of Geophysical Research, DOI: 10.1029/2001JC001184.

Sofianos, S. S., W. E. Johns and S. P. Murray (2002):
"Heat and freshwater budgets in the Red Sea from direct observations at Bab el Mandeb"
Deep-Sea Research II 49(7-8): 1323-1340.

Sofianos, S. S. and W. E. Johns (2003):
"An Oceanic General Circulation Model (OGCM) investigation of the Red Sea circulation:
2. Three-dimensional circulation in the Red Sea"
Journal of Geophysical Research, DOI: 10.1029/2001JC001185.

Sofianos, S. S. and W. E. Johns (2007):
"Observations of the summer Red Sea circulation"
Journal of Geophysical Research , DOI: 10.1029/2006JC003886.

Souvermezoglou, E., N. Metzl and A. Poisson (1989):
"Red Sea budgets of salinity, nutrients and carbon calculated in the Strait of Bab-El-Mandab during the summer and winter seasons" Journal of Marine Research 47: 441-456.

Spero, H. J., K. M. Mielke, E. M. Kalve, D. W. Lea and D. K. Pak (2003):
"Multispecies approach to reconstructing eastern equatorial Pacific thermocline hydrography during the past 360 kyr" Paleoceanography, DOI: 10.1029/2002PA000814.

Spindler, M., Ch. Hemleben, J. B. Salomons and L. P. Smit (1984):
"Feeding behaviour of some planctonic Foraminifers in laboratory cultures"
Journal of Foraminiferal Research 14(4): 237-249.

Staubwasser, M., F. Sirocko, P. M. Grootes and M. Segl (2003):
"Climate change at 4.2 ka BP termination of the Indus valley civilization and Holocene south Asian monsoon variability" Geophysical Research Letters 30(8): 1425, DOI:10.1029/2002GL016822.

Staubwasser, M. and H. Weiss (2006):
"Holocene climate and cultural evolution in late prehistoric-early historic West Asia"
Quaternary Research 66: 372-387.

Stein, M., A. Almogi-Labin, S. L. Goldstein, Ch. Hemleben and A. Starinsky (2007):
"Late Quaternary changes in desert dust inputs to the Red Sea and Gulf of Aden from $^{87}Sr/^{86}Sr$ ratios in deep sea cores" Earth and Planetary Science Letters 261: 104-119.

Steph, S., M. Regenberg, R. Tiedemann, S. Mulitza and D. Nürnberg (2009):
"Stable isotopes of planktonic foraminifera from tropical Atlantic/Caribbean core-tops: Implications for reconstructing upper ocean stratification" Marine Micropaleontology 71(1-2): 1-19.

Stuiver, M. and P. J. Reimer (1993):
"Extended ^{14}C Data Base and revised Calib 3.0 14C age calibration program"
Radiocarbon 35(1): 215-230.

Struck, U., K. C. Emeis, M. Voss, M. D. Krom and G. H. Rau (2001):
"Biological productivity during sapropel S5 formation in the Eastern Mediterranean Sea: Evidence from stable isotopes of nitrogen and carbon" Geochimica et Cosmochimica Acta 65(19): 3249-3266.

Telford, R. J., C. Andersson, H. J. B. Birks and S. Juggins (2004):
"Biases in the estimation of transfer function prediction errors"
Paleoceanography, DOI: 10.1029/2004PA001072.

Telford, R. J. and H. J. B. Birks (2005):
"The secret assumption of transfer funtions: problems with spatial autocorrelation in evaluating model performance" Quaternary Science Reviews 24(20-21): 2173-2179.

ter Braak, C. J. F. and I. C. Prentice (1988):
"A theory of gradient analysis" Advances in Ecological Research 18: 271-317.

ter Braak, C. J. F. and S. Juggins (1993):
"Weighted averaging partial least squares regression (WA-PLS): an improved method for reconstructing environmental variables from species assemblages" Hydrobiologia 269/270: 485-502.

ter Braak, C. J. F. and P. Smilauer (1997):
"Canoco for Windows" version 4.54, Biometris – Plant Research International, Wageningen, The Netherlands. http://www.pri.wur.nl/UK/

Thiede, J. (1975):
"Distribution of foraminifera in coastal waters of an upwelling area" Nature 253: 712-714.

Thompson, L. G., E. Mosley-Thompson, M. E. Davis, K. A. Henderson, H. H. Brecher, V. S. Zagorodnov, T. A. Mashiotta, P.-N. Lin, V. N. Mikhalenko, D. R. Hardy and J. Beer (2002):
"Kilimanjaro ice core records: Evidence of Holocene climate change in tropical Africa"
Science 298: 589-593.

Thunell, R. C., S. M. Locke and D. F. Williams (1988):
"Glacio-eustatic sea-level control on Red Sea salinity" Nature 334: 601-604.

Thunell, R. C. and D. F. Williams (1989):
"Glacial-Holocene salinity changes in the Mediterranean-Sea - Hydrographic and depositional effects"
Nature 338(6215): 493-496.

Tragou, E. and C. Garrett (1997):
"The shallow thermohaline circulation of the Red Sea" Deep-Sea Research I 44: 1355-1376.

Tribovillard, N., T. J. Algeo, T. Lyons and A. Riboulleau (2006):
"Trace metals as paleoredox and paleoproductivity proxies: An update"
Chemical Geology 232(1-2): 12-32.

Trommer, G., M. Siccha, H. Schulz, Ch. Hemleben, E. J. Rohling, K. Grant, M. T. J. van der Meer, S. Schouten and M. Kucera (2009a):
"Millenial scale variability in Red Sea circulation in response to Holocene insolation forcing"
Paleoceanography, submitted.

Trommer, G., M. Siccha, M. T. J. van der Meer, S. Schouten, J. S. Sinninghe Damsté, H. Schulz, Ch. Hemleben and M. Kucera (2009b):
"Distribution of Crenarchaeota tetraether membrane lipids in surface sediments from the Red Sea"
Organic Geochemistry 40: 724-731.

Trommer, G., M. Siccha, M. T. J. van der Meer, S. Schouten and M. Kucera (in preparation):
"Amplitude of climate varibability in the Red Sea during the next-last glacial termination and during the peak intergalcial MIS 5e".

von Rad, U., M. Schaaf, K. H. Michels, H. Schulz, W. H. Berger and F. Sirocko (1999):
"A 5000-yr record of climate change in varved sediments from the oxygen minimum zone off Pakistan, northeastern Arabian Sea" Quaternary Research 51(1): 39-53.

von Rad, U., A. Lückge, W. H. Berger and H. Doose-Rolinski (2006):
"Annual to millennial monsoonal cyclicity recorded in Holocene varved sediments from the NE Arabian Sea" Journal of the Geological Society of India 68(3): 353-368.

Wanner, H., J. Beer, J. Bütikofer, T. J. Crowley, U. Cubasch, J. Flückiger, H. Goosse, M. Grosjean, F. Joos, J. O. Kaplan, M. Küttel, S. A. Müller, I. C. Prentice, O. Solomina, T. F. Stocker, P. Tarasov, M. Wagner and M. Widmann (2008):
"Mid- to Late Holocene climate change: an overview" Quaternary Science Reviews 27: 1791-1828.

Watkins, J. M., A. C. Mix and J. Wilson (1996):
"Living planktic foraminifera: Tracers of circulation and productivity regimes in the central equatorial Pacific" Deep-Sea Research II 43(4-6): 1257-1282.

Watkins, J. M. and A. C. Mix (1998):
"Testing the effects of tropical temperature, productivity, and mixed-layer-depth on foraminiferal transfer functions" Paleoceanography 13(1): 96-105.

Weikert, H. (1982):
"The vertical distribution of zooplankton in relation to habitat zones in the area of the Atlantis II Deep, central Red Sea" Marine Ecology Progress Series 8: 129-143.

Weikert, H., (1987):
"Plankton and the pelagic environment" in F. J. Edwards and S. M. Head "Red Sea (key environments)" New York, Pergamon Press, pp. 90-111.

Weiss, H., M. A. Courty, W. Wetterstrom, F. Guichard, L. Senior, R. Meadow and A. Curnow (1993):
"The genesis and collapse of 3rd millennium north Mesopotamian civilization"
Science 261(5124): 995-1004.

Werner, F. and K. Lange (1975):
"A bathymetric survey of the sill area between the Red Sea and the Gulf of Aden"
Geologisches Jahrbuch D 13: 125-130.

Winter, A., Z. Reiss and B. Luz (1979):
"Distribution of living coccolithophore assemblages in the Gulf of Elat (Aqaba)"
Marine Micropaleontology 4: 197-223.

Winter, A. (1982):
"Paleoenvironmental interpretation of Quaternary coccolith assemblages from the Gulf of Aqaba (Elat), Red Sea" Revista Española de Micropaleontología 14: 291-314.

Woelk, S. and D. Quadfasel (1996):
"Renewal of deep water in the Red Sea during 1982-1987"
Journal of Geophysical Research 101(C8): 18155-18165.

Zaric, S., B. Donner, G. Fischer, S. Mulitza and G. Wefer (2005):
"Sensitivity of planktic foraminifera to sea surface temperature and export production as derived from sediment trap data" Marine Micropaleontology 55: 75-105.